HOKKAIDO UNIVERSITY

Title	Taxonomy and evolution of marine benthic dinoflagellates from sub-tropical Japan
Author(s)	PINTO, Sohail Keegan
Degree Grantor	北海道大学
Degree Name	博士(理学)
Dissertation Number	甲第12819号
Issue Date	2017-06-30
DOI	https://doi.org/10.14943/doctoral.k12819
Doc URL	https://hdl.handle.net/2115/70880
Type	doctoral thesis
File Information	Sohail_Keegan_PINTO.pdf



Hokkaido University Collection of Scholarly and Academic Papers : HUSCAP

Taxonomy and evolution of marine benthic dinoflagellates from sub-tropical Japan

(日本の亜熱帯域の海産底生性渦鞭毛藻類の分類および進化に関する研究)

Sohail Keegan PINTO

Department of Natural History Sciences

Graduate School of Science

Hokkaido University

June 2017

Abstract

Dinoflagellates are a groups of protists defined by their unique heterokont flagellation and possessing a unique eukaryotic nucleus – the dinokaryon. They are cosmopolitan organisms, found in freshwater, brackish and marine aquatic environments around the world. Of about 2500 extant dinoflagellate species, about 78% are marine planktonic representatives, while only 8% are known to be benthic. Benthic dinoflagellates have been studied intermittently since the 1920s; research picked up in the last decades of the 20th century and since 2000, modern techniques have been utilised in the study of benthic dinoflagellates. Studies of benthic habitats revealed that the species presence and diversity greatly differed from that of the planktonic habitats. Benthic habitats include beach sand, intertidal flats, sub-tidal areas and tide pools; seaweed, seagrass and corals (as epibionts); and stony areas (as epiliths). Benthic dinoflagellates are also of great economic and ecological importance, as about 30% of the known species have been shown to be conclusively or potentially toxic. The phylogenetic positions of number of benthic dinoflagellates have been revealed by recent molecular works. However, it is obvious that we still do not know the phylogenetic positions of many of the benthic species and also further taxonomic studies are required to unravel further biodiversity of marine benthic dinoflagellates.

In the preliminary study by our laboratory, it was revealed that a wide variety of species are present on the seabed at about 30 – 50 m deep off Mageshima Island, Kagoshima Prefecture, subtropical Japan and it was suggested that this region might be unexploited habitat for benthic dinoflagellates and further detailed study is obviously needed to further exploit species diversity. Therefore, I have studied benthic dinoflagellates from this region using the culture strains isolated from this habitat. For the purpose of comparison, I have also studied marine benthic dinoflagellates from shallow intertidal area in Okinawa Island. The aims of this study are: 1) to discover new species of benthic dinoflagellates from this deep-water region as well as from shallow-water region, 2) to observe their morphology in detail, using light, scanning electron and transmission electron

microscopy, 3) to unveil phylogenetic positions of each species using molecular techniques, and finally, 4) to discuss their evolutionary scenario based on phylogeny and character evolution.

In the first chapter of my thesis, I described thirteen strains of dinoflagellates that belong to the genus *Testudodinium*, which included only three species at the time of establishment. I described the external and internal morphology of these strains and have also calculated their phylogeny with respect to the partial SSU rDNA gene sequences of the previously described species. I revealed that these thirteen strains, in combination with the three previous described species in the genus, were divided into three groups, i.e. magnum group, corrugatum group and maedaense group. I establish that all of the four strains belonging to the magnum group represented four novel species. Two of the three strains belonging to the corrugatum group represented two novel species, while the third was identified as a previously described species *Testudodinium corrugatum*. The remaining six strains are morphologically indistinguishable from *T. maedanse*, leading me to classify them as such. I reported a unique internal structure, the internal prop, which spans the depth of the cell, for the first time, and demonstrated that this novel structure was quite common within the genus.

In the second chapter, I described two novel species that are morphologically very similar to *Testudodinium* and to the athecate benthic dinoflagellate genus *Amphidinium*. I examined external and internal morphologies and calculated the phylogeny of these species with respect to the partial SSU rDNA and partial LSU D1 – D3 rDNA gene sequences of previously described species. The phylogenetic trees indicate that there are no supported relationships between these two novel species and either *Testudodinium* or *Amphidinium*. Based on morphological comparisons, it was obvious that these two species are new species. However, the phylogenetic affinities of these two species were not clearly determined due to poor resolution and, therefore, it was not possible to determine whether these two species should be accommodated in each autonomous genus or classify these species in a novel genus. It should be noted that this is a clear example of the existence of convergent evolution of the morphology in the single-celled organisms. I also

described the presence of internal props in one of the two species, similar but not identical to those found in *Testudodinium*.

In the third chapter, I described two novel benthic species of the genus *Heterocapsa*. *Heterocapsa* is a well-studied genus, consisting of eighteen species and one sub-species; the criteria for the determination and delineation of species are well-defined. Based on a combination of internal and external morphology and phylogeny calculated from the ITS-5.8S gene sequences, the two species I described do not belong to any of the currently accepted taxonomic groups. Hence I established them as new species, increasing the number of recorded benthic *Heterocapsa* species from one to three. I also described the internal morphology of a *Heterocapsa* cyst for the first time, and report the presence of some unique variations of standard organelles.

In the fourth chapter, I made the first report *Prorocentrum* cf. *elegans* from sub-tropical Japan. This species is known from two other locations in the world, and its external morphology is well-known. The external morphology of the species I described agreed with the previous descriptions. Additionally, in the phylogenetic tree, the SSU rDNA gene sequence was adjacent to the sequence reported for *P. elegans*. The internal structure of *P. elegans* is so far unknown; I report the internal structure in some detail, and indicate the presence of a grana-like lamellae within the chloroplasts. Based on the combination of morphological and phylogenetic data, and taking into account the limited data in the original description of *P. elegans*, I identified my species as *Prorocentrum* cf. *elegans*.

In the fifth chapter, I described a novel small peridiniod dinoflagellate. I described the internal and external morphology of the cell, and calculate the phylogeny of the partial SSU rDNA and LSU D1-D3 rDNA. I noted the similarities and differences to other peridiniod species such as *Peridiniopsis borgei*, *Palatinus apiculatus* and *Parvodinium umbonatum*. As the phylogenetic tree only demonstrates support for a relationship between *Peridiniopsis borgei* and the novel species, I

compared the ultrastructure of the two in order to establish that the novel species does not belong to *Peridiniopsis* and that a new genus should be erected to accommodate it.

In conclusion, over the course of research towards my doctoral thesis, I have described a total of nineteen strains, with eight of them being identified as previously described species and the other eleven described as novel species. This work contributed to increase our knowledge of the benthic dinoflagellate species in sub-tropical regions, including deep water habitat and revealed evolutionary scenario of each species.

Acknowledgements

First and foremost, I would like to express my deepest gratitude to Professor Takeo Horiguchi, who guided me throughout my thesis, from the time I began applying. It is only with his most able guidance that I have made it so far, and there are no words to express the entirety of my gratefulness.

I am also immensely grateful to Professor Kazuhiro Kogame, who was part of the Advisory Committee, and one of the reviewers of my thesis. His input has been invaluable.

I also thank Professor Hiroshi Kajihara, who reviewed my thesis, pointing out areas that I could improve upon.

I am extremely grateful to Professor Kevin Wakeman, who also reviewed my thesis. His input over the last year has been a considerable boon.

I would also like to extend my warmest appreciation to the members of the Laboratory of Phycology II, both past and present; Haruka Yamaguchi, Norico Yamada, Ryo Onuma, Clark Gen, Toshio Kubotsu, Sou Ohtsu, Fred Santiañez, Akito Ikeda, Suttikarn Sutti (Nui), Masakazu Hoshino, João Kieffer e Silva, Jin Sungmin, Mahmutjan Dawut Maria Emilia Croce, Koh Yokouchi, Eriko Sasagawa, Aya Kosako, and others, without whose presence and assistance this would have been a much harder path to walk.

I am also grateful the Professor Ryuta Terada and the members of the Marine Botany Lab (Kagoshima University) for the collection of the samples used in my thesis, and for hosting me in 2014 during a sample collection and teaching me how to collect samples.

I am equally grateful to Professor Taizo Motomura, Professor Chikako Nagasato, Professor Atsuko Tanaka (University of the Ryukyus) and the staff and members of the Muroran Marine Station (Field Science Centre Hokkaido University) who conducted a course on transmission electron microscopy in 2015, and cleared many of the doubts I had about the technique.

I am indebted to the Hokkaido University, which funded supported me throughout the course of my doctoral research via the Hokkaido University President’s Scholarship.

A huge thank-you to all the friends I made during the course of my stay in Sapporo. You made the time I spent outside the university enormous fun.

I am deeply grateful to my two best friends, Vedrana and Shivani. They have always supported me through thick and thin, encouraging me whenever I felt overwhelmed.

And finally, I would like to express my gratitude to my family. They may not quite understand what I have chosen to study, but they are behind me all the way.

Table of contents

Abstract i

Acknowledgements v

Table of Contents vii

Introduction 1

Chapter 1. Species diversity and evolution of the benthic marine dinoflagellate genus *Testudodinium* 7

Introduction 8

Materials and Methods 9

Results 12

Discussion 32

Chapter 2. *Testudodinium*-like species – convergent evolution? 40

Introduction 41

Materials and Methods 42

Results 46

Discussion 50

Chapter 3. Two new psammophilic species of the *Heterocapsa* 54

Introduction 55

Materials and Methods 56

Results 59

Discussion 63

Chapter 4. Ultrastructure and phylogenetic position of a benthic marine dinoflagellate, *Prorocentrum* cf. *elegans* Faust 67

Introduction 68

Materials and Methods 69

Results 72

Discussion 75

Chapter 5. A taxonomic study on a new marine benthic thecate peridiniod dinoflagellate 77

Introduction 78

Materials and Methods 79

Results 83

Discussion 85

References 88

Introduction

Dinoflagellates are a group of flagellate protists that in their entirety constitute the phylum Dinophyta. Together with the ciliates and the apicomplexans, they form the alveolates, which in turn is a member of the SAR supergroup, which is comprised of the stramenopiles, alveolates and Rhizaria (hence the name) (Adl *et al.*, 2012). Dinoflagellates are common in all ecosystems. They have a wide variety of nutrition: phototrophic, heterotrophic and mixotrophic; as such, they are members of both the phytoplankton and zooplankton of marine and freshwater ecosystems (Hoppenrath, 2016; Hoppenrath and Saldarriaga, 2012). They are morphologically diverse and genetically unique, and are most known for as the causative agent in harmful algal blooms (see Hallegraeff, 1993; Taylor, 1985), paralytic shellfish poisoning, neurotoxic shellfish poisoning, diarrhoeic shellfish poisoning and ciguatera fish poisoning (see Bagnis *et al.*, 1980; Clark, 1968; Dale and Yentsch, 1978; Yentsch, 1984); additionally, some dinoflagellates are parasitic (Hoppenrath, 2016; Horiguchi, 2015; Taylor, 1985). Their greatest significance, however, is as marine primary producers in the phytoplankton. *Symbiodinium* spp., a genus of dinoflagellates, play a key role in the survival of coral reefs and other marine invertebrates, such as sea anemone, and jellyfish, as symbiotic partners (see Baker, 2003; Hoppenrath and Saldarriaga, 2012; LaJeunesse and Thornhill, 2011; Rouzé et al., 2017).

Dinoflagellates are distinct from other eukaryotes primarily due to the structure of their flagella and their dinokaryotic nucleus – the dinokaryon (Fig. 1 a). The dinokaryotic nucleus contains large number of thick chromosomes, which are condensed throughout cell cycle and devoid of substantial amount of histones and thus lacking nucleosomes. All species possess a conventionally structured longitudinal flagellum and a ribbon-like transverse flagellum. In the dinokont dinoflagellates, a transverse groove termed the cingulum divides the cell into an episome and a hyposome; the transverse flagellum is situated in this groove. A longitudinal groove termed the sulcus defines the ventral surface of the cell; the longitudinal flagellum arises from here (Fig. 1 b). In prorocentroids the flagellation is that of desmokont: the typical longitudinal and transverse

flagella arise from the periflagellar area, and are not associated with grooves (Fig. 1 c). As befitting members of the Alveolata, all dinoflagellates possess alveolar vesicles, which are termed as amphiesmal vesicles in dinoflagellates. The outer plasma membrane and underlain amphiesmal vesicles together form the amphiesma. Traditionally, the dinoflagellates have been classified into two groups based on the presence or absence of thecal plates, i.e. thecate (armoured) dinoflagellates and athecate (unarmoured) dinoflagellates or naked dinoflagellates. In thecate dinoflagellates, the cellulose thecal plates formed within these amphiesmal vesicles, are arranged in a specific pattern and thus the thecal plate arrangement has been extensively used as a taxonomic marker within thecate dinoflagellates (Fensome *et al.*, 1993; Hoppenrath and Saldarriaga, 2012). Those dinoflagellates without thecal plates are called athecate dinoflagellates (Fig. 1 b). The athecate dinoflagellates are covered with many small amphiesmal vesicles. The amphiesma may be underlain by a pellicle (Hoppenrath, 2016). Organelles found in the dinoflagellates include mitochondria; chloroplasts that typically contain chlorophylls a/c and a unique xanthophyll, peridinin, is enclosed by three membranes, and often associated with pyrenoids (Dodge and Crawford, 1971; Schnepf and Elbrächter, 1999); extrusomes such as trichocysts, mucocysts and nematocysts; pusules; and eyespots in a diversity that is unique (Dodge, 1971, 1984; Dodge and Crawford, 1969; Hayakawa et al., 2015; Hoppenrath, 2016). The presence of certain ultrastructures is limited to certain groups of dinoflagellates, and thus serves as a taxonomic character; for example, the occelloids in warnowiids (Gavelis et al., 2015; Hoppenrath et al., 2009)

Due to their ecological importance the planktonic dinoflagellates have continuously studied from the time of their discovery (for eg., Claparède and Lachmann, 1859; Ehrenberg, 1830, 1834; Kofoid and Swezy, 1921; von Stein, 1883). There are also a number of marine benthic dinoflagellates that live in depths up to 30 m or more. They are present in a variety of habitats: in beach sediment and in the intertidal and sub-tidal zones, inhabiting the interstices of the sediment; as epibionts on seaweed, seagrass and coral; and rarely, epilithic, on submerged rocks (Hoppenrath

et al., 2014). It is notable that benthic dinoflagellates are reported from mostly marine habitats, at present (Hoppenrath *et al.*, 2014), as opposed to planktonic species that are present in all aquatic habitats. These have been less studied, with the first reports being from the early 20th century (e.g., Balech, 1956; Herdman, 1924; Lebour, 1917). Interest in benthic dinoflagellates experienced a resurgence from the 1980s, with the description of a number of new species and advanced techniques, including scanning electron microscopy, being to obtain detailed descriptions of the dinoflagellates (see Faust, 1993a, 1993b, 1997; Horiguchi, 1995a; Horiguchi and Pienaar, 1994a; Larsen and Patterson, 1990; Saunders and Dodge, 1984); since 2000, significant progress has been made in this area and molecular investigations have complimented traditional morphological studies. Many of the athecate dinoflagellate genera were shown to be polyphyletic on the basis of partial LSU rDNA sequences; as a result, existing genus definitions were emended and new genera were erected. Examples of genera that were thus emended include *Gymnodinium* F. Stein emend. Hansen and Moestrup (Daugbjerg *et al.*, 2000), *Gyrodinium* Kofoid and Swezy emend. Hansen and Moestrup (Daugbjerg *et al.*, 2000) and *Amphidinium* Claparède and Lachmann emend. Flø Jørgensen, Murry and Daugbjerg (Flø Jørgensen *et al.*, 2004a). Benthic dinoflagellates have been reported from numerous areas around the world such as Australia (Larsen and Patterson, 1990; Murray and Patterson, 2002; Watanabe *et al.*, 2014), Malaysia (Al-Has and Mohammad Noor, 2011), Germany (Hoppenrath, 2002),Greece (Aligizaki *et al.*, 2009), Japan (Horiguchi, 1995b; Horiguchi and Kubo, 1997; Horiguchi et al., 2012; Tamura et al., 2005; Watanabe et al., 2014; Yamada et al., 2013), Belize (Faust, 1993a, 1993b, 1997; Faust et al., 2008), Canada (Hoppenrath et al., 2004; Sparmann et al., 2008), Palau (Horiguchi and Sukigara, 2005), France (Chomérat and Couté, 2008; Chomérat et al., 2009, 2011; Nézan and Chomérat, 2011),South Africa (Horiguchi and Pienaar, 1988, 1991, 1994b), and the USA (Tester *et al.*, 2013). Gómez (2012) provided an exhaustive list of all the extant dinoflagellates reported at the time, including planktonic and benthic species. Until quite recently, it was thought that photosynthetic dinoflagellates could not be found at

depths below 30 m, primarily due to a lack of illumination (Taylor, 1985; Taylor *et al.*, 2007). However, more recent reports have shown that photosynthetic dinoflagellates are abundant at depths of up to 50 m, albeit in specific geographical locations (Tester *et al.*, 2013; Yamada *et al.*, 2013). An extremely comprehensive review of benthic dinoflagellates, listing 189 species belonging to 45 genera, was published by Hoppenrath *et al.* (2014).

Taxonomy of the dinoflagellates is a field that is still in development; the most recent review and revisions were by Hoppenrath (2016). Current methods seek to correlate morphological distinctions with phylogenetic variation (Fensome *et al.*, 1993; Hoppenrath, 2016). However, there are instances where only the phylogenetic analyses can reveal different species and taxonomic groups, as in the case of *Symbiodinium* (Baker, 2003; LaJeunesse and Thornhill, 2011; Rouzé *et al.*, 2017), athough some morphologically defined species have been described (Hansen and Daugbjerg, 2009). As the morphology is extremely diverse, DNA sequences have come to assume great importance in elucidating the taxonomy and evolutionary history of dinoflagellates. The SSU rDNA, LSU rDNA, ITS, mtDNA cox1 and cox3, and chlDNA rbcL DNA sequences are utilised in phylogentic analyses, but their value varies in different genera and more distant evolutionary relationships have low or no support (Daugbjerg *et al.*, 2000; Flø Jørgensen *et al.*, 2004a; Hoppenrath, 2016; Penna *et al.*, 2014). The most recent development in the field of dinoflagellate phylogeny is the use of transcriptomes to help elucidate the evolution of dinoflagellates (Janouškovec *et al.*, 2017); this has provided a robust phylogeny that is integrated with morphological data to present a framework for the evolution of all dinoflagellates.

A number of benthic dinoflagellate species have been reported from Japan (Horiguchi *et al.*, 2012; Tamura *et al.*, 2005; Watanabe *et al.*, 2014; Yamada *et al.*, 2013), including novel species. In the preliminary study by our laboratory, it was revealed that a wide variety of species are present on the seabed at about 30 – 50 m deep off Mageshima Island, Kagoshima Prefecture, subtropical Japan and it was suggested that this region might be unexploited habitat for benthic dinoflagellates and

further detailed study is obviously needed to exploit further species diversity. Therefore, I have studied benthic dinoflagellates from this region using the culture strains isolated from this habitat. For the purpose of comparison, I have also studied marine benthic dinoflagellates from shallow intertidal area in Okinawa Island. The aims of this study are: 1) to discover new species of benthic dinoflagellates from this deep-water region as well as from shallow-water region, 2) to observe their morphology in detail, using light, scanning electron and transmission electron microscopy, 3) to unveil phylogenetic positions of each species using molecular techniques, and finally, 4) to discuss their evolutionary scenario based on phylogeny and character evolution. With morphological and phylogenetic data, I shall show that we are far from cognizant of the diversity of benthic dinoflagellates even in this relatively small location of the Earth.

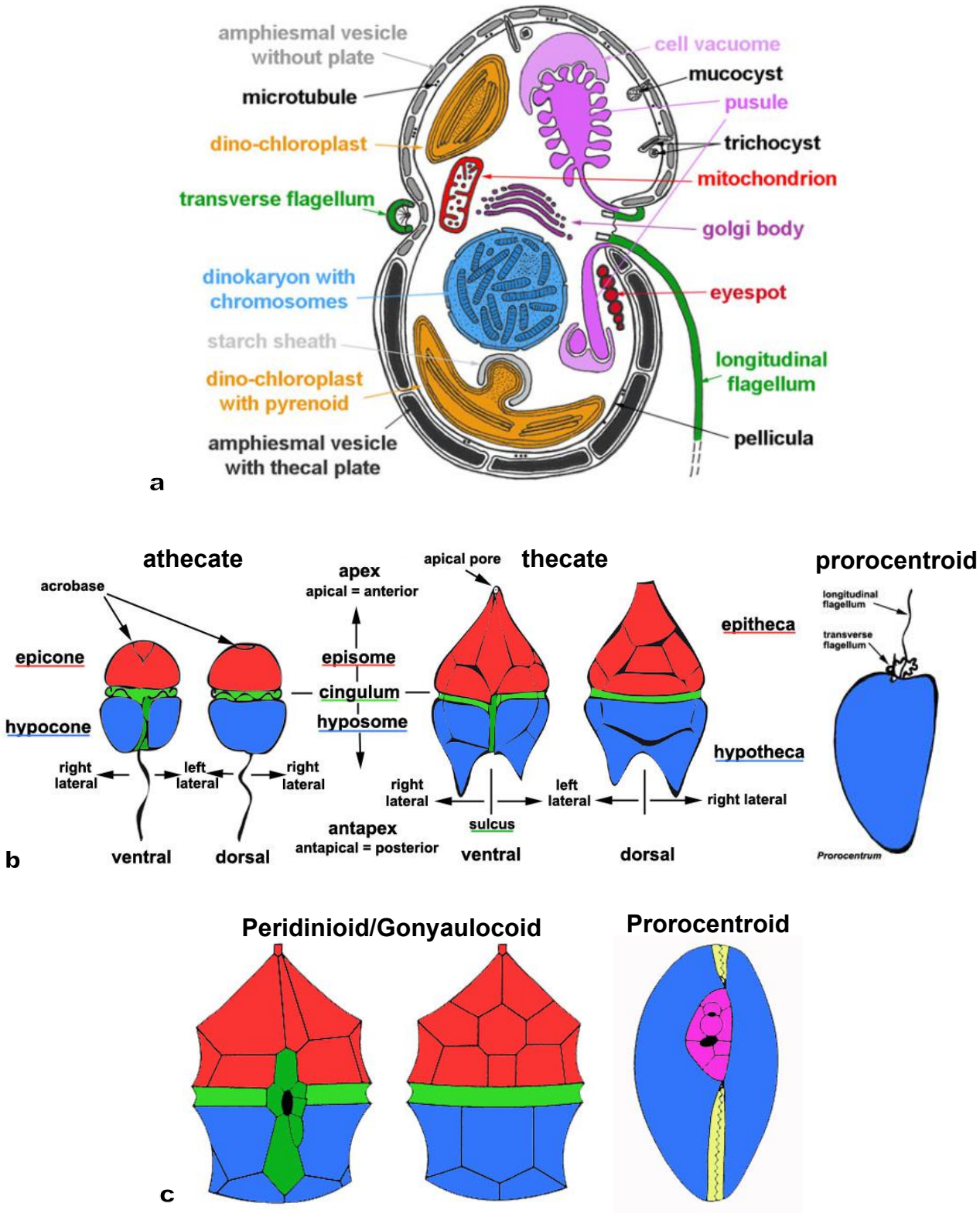


Fig. 1. General morphology of dinoflagellate cells.
a. Schematic representation of the ultrastructural features of a typical dinoflagellate cell (from Hoppenrath et al., 2016).
b. Schematic representation of the external morphology and the orientation of dinokont and desmokont cells. Red, epitheca; green, cingulum and sulcus; blue, hypotheca; (from Hoppenrath and Saldarriaga, 2012)
c. Schematic representation of the tabulation in thecate dinoflagellates; Red, epitheca; green, cingulum and sulcus; blue, hypotheca; purple, periflagellar area (from Hoppenrath and Saldarriaga, 2012)

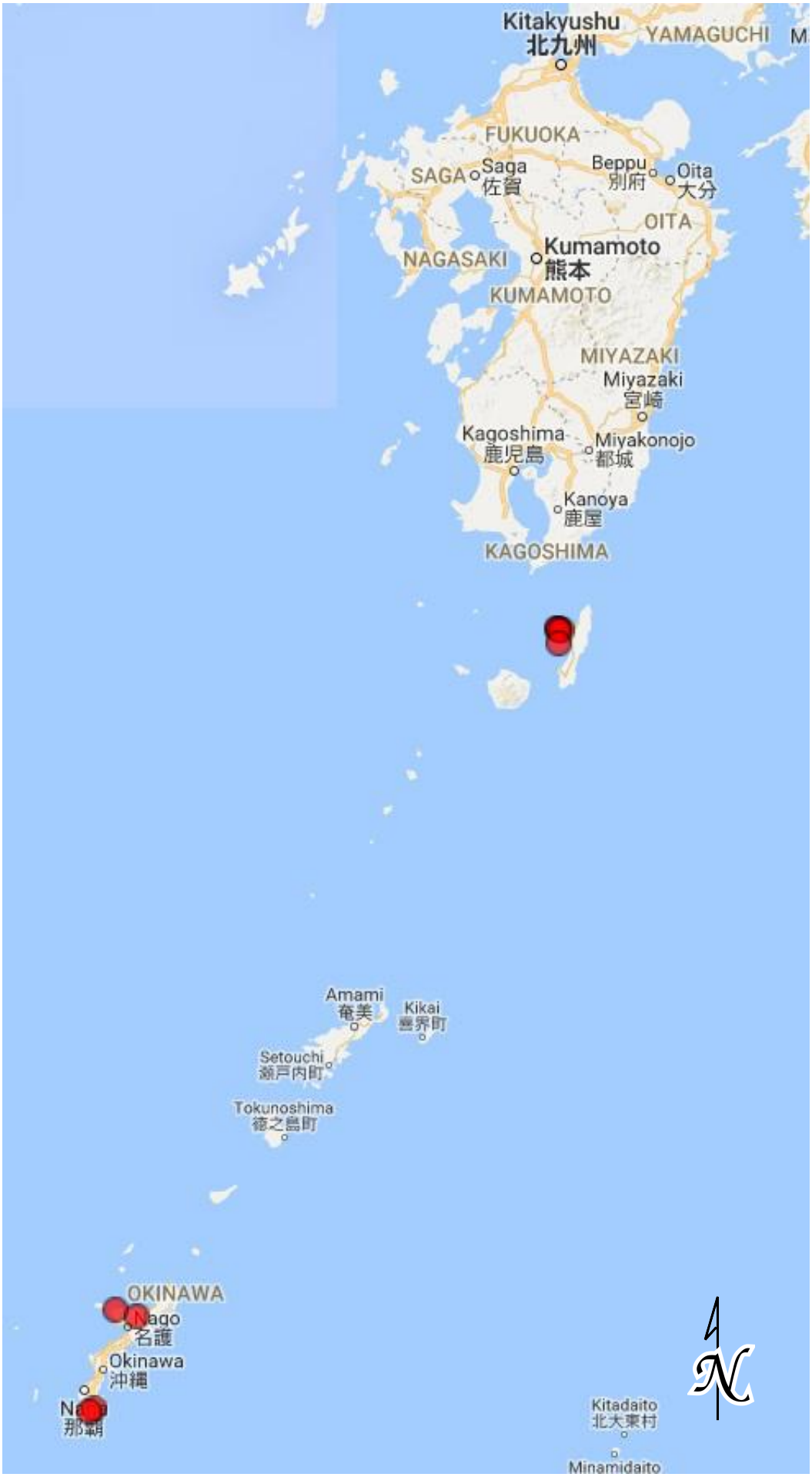


Fig. 2. Sampling locations in Kagoshima and Okinawa Prefectures, Japan. Refer to Table 1 for more information.



Fig. 3. Detail of the sampling area off Mageshima Island (a) and around Okinawa Island (b). The strains collected at each location are noted.

Table 1. List of strains used in this study

Strain Number	Species	Collection location	Collection co-ordinates	Depth	Date
HG229	*Testudodinium magnum*	Mageshima, Kagoshima	30˚41.800'N 130˚52.200'E	30 m	30 May 2012
HG230	*Testudodinium* sp.	Mageshima, Kagoshima	30˚41.800'N 130˚52.200'E	30 m	30 May 2012
HG272	*Testudodinium* sp.	Sumuide, Okinawa #35	26.668910N 128.022917E	< 1m	28 April 2013
HG273	*Testudodinium maedaense*	Bise, Okinawa #33	26.702710N 127.879637E	< 1m	27 April 2013
HG275	*Testudodinium* sp.	Bise, Okinawa #17	26.702710N 127.879637E	< 1m	25 April 2013
HG276	*Testudodinium maedaense*	Bise, Okinawa #17	26.702710N 127.879637E	< 1m	25 April 2013
HG278	*Testudodinium maedaense*	Hanashiro, Okinawa #11	26.114388N 127˚743748E	< 1m	23 April 2013
HG288	*Testudodinium maedaense*	Hanashiro, Okinawa #10	26.114388N 127˚743748E	< 1m	23 April 2013
HG291	*Testudodinium maedaense*	Sumuide, Okinawa #36	26.668910N 128.022917E	< 1m	28 April 2013
HG297	*Testudodinium maedaense*	Sumuide, Okinawa #36	26.668910N 128.022917E	< 1m	28 April 2013
HG304	*Testudodinium* sp.	Mageshima, Kagoshima #1	30˚41.850’N 130˚50.546E	34m	30 July 2013
HG312	*Testudodinium* sp.	Sumuide, Okinawa #36	26.668910N 128.022917E	< 1m	28 April 2013
NY050	*Testudodinium corrugatum*	Okinawa	Co-ordinates not available	ND	ND
HG310	*Amphidinium* sp. *sensu lato*	Mageshima, Kagoshima #1	30˚41.850’N 130˚50.546E	34m	30 July 2013
HG345	*Amphidinium* sp. *sensu lato*	Mageshima, Kagoshima #1	30˚42.252'N 130˚50.730E	25.0 m	19 August 2014
HG333	*Heterocapsa* sp.	Mageshima, Kagoshima #10	30˚41.272'N 130˚50.751'E	35 m	30 April 2014
HG341	*Heterocapsa* sp.	Mageshima, Kagoshima #12	30˚37.223'N 130˚51.067E	56.4 m	19 August 2014
HG277	*Prorocentrum* cf. *elegans*	Bise, Okinawa #31	26.702710N 127.879637E	< 1m	27 April 2013
HG152	Unknown (small peridiniod)	Odo, Okinawa	26.090055N 127.708909E	< 1m	11 April 2011

Table 2. PCR and sequencing primers used in this study

Target	Name	Direction	Sequence	Source
18S rDNA	SR1	Sense	TACCTGGTTGATCCTGCCAG	Nakayama *et al.* (1996)
	SR2TAK	Sense	CATTCAAATTTCTGMCCTATC	Takano and Horiguchi (2004)
	SR4	Sense	AGCCGCGGTAATTCCAGCT	Nakayama *et al.* (1996)
	SR4R	Anti-sense	CTGGCACCAGACTTGCCCT	Nakayama *et al.* (1996)
	SR5TAK	Anti-sense	ACTACGAGCTTTTTAACYGC	Takano and Horiguchi (2004)
	SR6	Sense	GTCAGAGGTGAAATTCTTGG	Nakayama *et al.* (1996)
	SR7TAK	Anti-sense	TCCWTGGCAAATGCTTTCGC	Takano and Horiguchi (2004)
	SR8TAK	Sense	GGATTGACAGATTGAKAGCT	Takano and Horiguchi (2004)
	SR9	Anti-sense	AACTAAGAACGGCATGCAC	Nakayama *et al.* (1996)
	SR11	Anti-sense	CGCTTACTAGGAATTCCTCG	Nakayama *et al.* (1996)
	SR12b	Sense	CGGAAACCTTGTTACGACTTCTCC	Takano and Horiguchi (2004)
ITS	SR12cF	Sense	TAGAGGAAGGAGAAGTCGTAA	Takano and Horiguchi (2005)
	25F1R	Anti-sense	ATATGCTTAAATTCAGCGG	Takano and Horiguchi (2005)
28S rDNA	D1RF1	Sense	ACCCGCTGAATTTAAGCATA	Takano and Horiguchi (2005)
	25R1*	Anti-sense	CCTTGGTCCGTGTTTCAAGA	Takano and Horiguchi (2005)
	305F-27	Sense	CGATAGCAAACAAGTACCATGAG	Yamada *et al.* (unpublished)
	852R-70	Anti-sense	CGAACGATTTGCACGTCAG	Yamada *et al.* (unpublished)
	D3A	Sense	GACCCGTCTTGAAACACGGA	Takano and Horiguchi (2005)
	28-1483R	Anti-sense	GCTACTACCACCAAGATCTGC	Takano and Horiguchi (2005)

Chapter 1

Species diversity and evolution of the benthic marine dinoflagellate genus *Testudodinium*

Introduction

The genus *Amphidinium* Claparède & Lachmann was described as consisting of athecate dinoflagellates with an episome that is one-third or less of the total cell length in size (Claparède and Lachmann, 1859; Kofoid and Swezy, 1921; Steidinger and Tangen, 1997). This encompassed approximately 200 morphologically dissimilar species. A cladistic analysis of morphological and structural features combined with the analysis of partial LSU rDNA sequences showed that this classification was polyphyletic, and led to the redefinition of *Amphidinium sensu stricto* (Flø Jørgensen *et al.*, 2004a). This new, stringent definition reduced the number of species to around 20, including the type species *A. operculatum* Claparède & Lachmann (Flø Jørgensen *et al.*, 2004a). This monophyletic group shares the primary defining character of a minute and left-deflected episome. *A. testudo* was included in *Amphidinium sensu stricto* solely on the basis of the morphological and structural features (Flø Jørgensen *et al.*, 2004a). Later, on the basis of SSU rDNA sequence analysis, *A. testudo*, along with two related taxa, was demonstrated to form a clade distinct from the typical *Amphidinium* clade including the type species (i.e. distinct from *Amphidinium sensu stricto*) (Horiguchi *et al.*, 2012). Thus, the genus *Testudodinium* was established, with *T. testudo* (Herdman) Horiguchi, Tamura, Katsumata & A.Yamaguchi as the type species (Horiguchi *et al.*, 2012). *A. corrugatum* Larsen & Patterson was also demonstrated to belong to this genus, and a new combination, *T. corrugatum* (Larsen & Patterson) Horiguchi, Tamura & A.Yamaguchi, was made (Horiguchi *et al.*, 2012). In addition, a novel species was also included in the genus, described as *T. maedaense* Katsumata & Horiguchi (Horiguchi *et al.*, 2012). Morphologically, the genus *Testudodinium* resembles the members of the genus *Amphidinium sensu stricto* in having a small rounded episome with a large hyposome, but can be clearly distinguished by the latter by possessing a longitudinal furrow on the ventral side of the episome (Horiguchi *et al.*, 2012).

During the course of my study on benthic marine dinoflagellates, a number of culture strains of *Testudodinium* spp. were established. Their variations suggested the presence of further species diversity within the genus. To explore the biodiversity of the members of the genus, I have studied these strains by means of light, scanning electron and transmission electron microscopy together with molecular phylogeny of the SSU rDNA gene. In this chapter, I will report six new species within the genus *Testudodinium* and explore character evolution within the genus.

Materials and methods

Sampling and culture

Sand samples were collected either from deep seafloor or shallow sandy beaches (Table 1, Fig. 3). In case of the samples from the sea floor, off Mageshima Island, Kagoshima Prefecture, Japan. A Smith-McIntyre bottom sampler (Rigosha, Tokyo, Japan) was used. The samples were collected during the cruise of Nansei-Maru vessel of Kagoshima University. In case of shallow sandy beaches, the sand samples were directly collected by hand using 50 ml centrifuge tubes (Becton Dickinson, Franklin Lakes, NJ, USA). The sand samples were sent to the laboratory of Phycology at the Faculty of Science, Hokkaido University, where dinoflagellate cells were isolated. A spoonful of the sand sample was taken in a plastic cup containing autoclaved seawater supplemented with Daigo IMK medium (Nihon Pharmaceutical Co., Tokyo, Japan) for enrichment. 0.1% Germanium dioxide (Sigma-Aldrich Japan, Tokyo) was also added to prevent growth of diatoms. This was cultured at 25°C and with an illumination of 50 µmol photons m^{-2} s^{-1} with 16:8 light:dark regime. Dinoflagellate cells found were isolated using drawn capillary Pasteur pipettes under an inverted microscope (Olympus CX41, Tokyo, Japan) and a clonal culture was established. The culture strains (Table 1) were maintained in IMK-supplemented seawater under the same conditions described above.

Light- and scanning electron microscopy

For light microscopic observations, living cells were observed using a Carl Zeiss Axioskop 2 microscope equipped with Nomarski interference optics (Carl Zeiss Japan, Tokyo) and the fluorescent microscopic observations were made using the same microscope with filter set No. 15. Photographs were taken using a Leica MC-120HD digital camera (Leica Microsystems, Germany). For scanning electron microscopy, the cells were fixed dehydrated and critical point dried according to the protocol described by Yamada *et al*. (2013). Cells were collected by centrifugation (2000 rpm) and the cell pellet was fixed in 1% OsO_4 made up in culture medium for 20 min at room temperature. After rinsing first in sterilized filtered seawater and then twice in distilled water, for 10 min in each wash, a drop of water containing cells was placed on a poly-L-lysine coated SEM glass plate and the cells were allowed to settle for 10 min. The cells were then gradually dehydrated by introducing the SEM plate to each of an increasing series of ethanol concentrations (25%, 30%, 50%, 70%, 80%, 90% and 95%) for 10 min each, followed by two washes in 100% ethanol, each for 30min. Finally critical-point dried (HITACHI HCP-2, Tokyo, Japan) samples were sputter-coated with gold for 180 seconds at 40 mA (HITACHI E-1045) and viewed with a SEM (S-3000N, HITACHI). Contrast of the images was edited using Adobe Photoshop CS5.

Transmission electron microscopy

To collect cells, after removing excess culture medium, the attached cells at the bottom of Petri dish were harvested by sweeping gently by a sterilized paint brush. The collected cells were transferred into 15 ml plastic tubes and centrifuged at 40 × g for 10 min. The cell pellet was re-suspended in 150 µl culture medium and 50 µl of 4% OsO_4 made up in distilled water was added and fixed for 1 hour at room temperature. The following protocol was the same as chemical fixation protocol

described by Yamada *et al*. (2013) except that fixation was made only with 1% osmium tetroxide (OsO_4) instead of a cocktail of glutaraldehyde and OsO_4. Sections were cut using a diamond knife on an ultramicrotome (Diatome, Biel, Switzerland). Sections were picked up on formvar coated one-slot grids and these were viewed with a transmission electron microscope (H-7650, HITACHI, Tokyo). Contrast of the images was edited using Adobe Photoshop CS5. For counting of props, high-magnification images were assembled in Adobe Illustrator CS5 into the entire cell section, and manually counted.

DNA extraction and polymerase chain reaction (PCR) amplification

The following protocols were applied as standard method in my study. Approximately 10 cells from each culture strain were used to extract DNA using the QuickExtract™ FFPE DNA extraction kit (Epicentre, Tokyo, Japan) according to the recommended protocol. The primers used to amplify the SSU DNA are shown in the Table 2. For the first round of PCR, primers SR1 and SR12b were used. The PCR amplification process consisted of an initial denaturation cycle of at 94°C for 5 min, followed by 35 cycles of denaturation at 94°C for 30 s, annealing at 50°C for 30 s and extension at 72°C for 90 s. The final extension cycle was at 72°C for 7 min. For the second round of PCR, the following primer sets were used: SR1 and SR4R or SR5TAK; SR2TAK and SR7TAK; SR4 and SR9; SR6 and SR11; and SR8TAK and SR12b (Table 2). The PCR amplification conditions were the same as described earlier. The PCR products were purified and sequenced with ABI PRISM Big Dye Terminator (Perkin-Elmer, USA). The purified sequence reaction products were run on a DNA autosequencer ABI PRISM310 Genetic Analyser (Perkin-Elmer). Both sense and anti-sense strands were sequenced.

Sequence analyses

The sequences were aligned manually, based on the published secondary structure of the SSU rRNA molecule, using alveolate taxa available at the rRNA server (no longer available). 3041 aligned sites (sequences augmented by the gaps from the rRNA secondary structure) were used for the analyses. *Perkinsus marinus* (Mackin, Owen & Collier) Levine (Perkinsozoa) was used as an out-group for the SSU rDNA analyses. The aligned sequences were analysed by the ML method using PAUP* version 4.0a152 (Swofford, 2001) and the Bayesian method using MrBayes 3.2.1 (Huelsenbeck and Ronquist, 2001; Ronquist and Huelsenbeck, 2003). The selected model was TIM2 + I + G model. The heuristic search for the ML analysis was performed with the following options: a TBR branch-swapping algorithm and the Kimura 2-parameter NJ tree as the starting tree. The parameters used for the analysis were as follows: assumed nucleotide frequencies A = 0.24653, C = 0.20191, G = 0.26409, and T = 0.28746; substitution rate matrix with A<>C = 1.33229, A<>G = 4.32595, A<>T = 1.59843, C<>G = 0.685529, C<>T = 8.56599, G<>T = 1.0000; proportion of sites assumed to be invariable = 0.310574; rates for variable sites assumed to follow a gamma distribution with shape parameter = 0.590508, and number of rate categories = 4. For the Bayesian analysis, GTR + I + G was selected as the best evolutionary model by MrModeltest 2.3 (Nylander *et al.*, 2004). Markov chain Monte Carlo iterations were carried out until 2,500,000 generations, when the average standard deviations of split frequencies fell below 0.01, indicating the convergence of the iterations.

Results

Species descriptions

Testudodinium magnum Pinto, Terada & Horiguchi (Magnum group)

(Figures 4 – 9)

Diagnosis: Sessile (non-motile) cell dorso-ventrally compressed, circular in ventral view, 37.5–55 µm long, 27.5–52.5 µm wide; episome conical and symmetric with a longitudinal furrow on its ventral side, completely concealed by hyposome; hyposome large, circular, with a rugose dorsal surface; sulcus shallow and broad. Motile cell ovoid in ventral view, dorso-ventrally compressed, 25–40 µm long, 17.5–27.5 µm wide; episome tongue-shaped with longitudinal furrow on its ventral side, tip of episome slightly projected from confinement of upper part of hyposome; hyposome large, ovoid, with a rugose dorsal surface. Chloroplast yellow-brown, peripheral, radiating from a central pyrenoid, granular chloroplast portions connected to each other forming a chloroplast network; thylakoids mostly trilamellar, ocassionally bilamellar; pyrenoid single, starch-sheathed, its matrix traversed by several thylakoids, located in the centre of the cell; nucleus located below the pyrenoid; many internal props spanning the thickness of the cell.

Holotype: SAP115075, collected on 30 May 2012, deposited as SEM stub (cells from this stub are illustrated in Figs 10 – 13) in the Faculty of Science Herbarium, Hokkaido University.

Type locality: 30°41.800' N 130°52.200' E; marine, benthic, sand-dwelling; 30 m deep; off Mageshima Island, Kagoshima Prefecture, Japan.

Etymology: '*magnum*' refers to the large size of the dinoflagellate.

Light and scanning electron microscopy

The sessile cells were rounded to sub-circular in ventral view and were strongly dorso-ventrally flattened (Fig. 4 a; Fig. 5 a, b). The cells were 37.5–55 µm (mean = 45.6 µm, *n* = 50) long and 27.5–52.5 µm (mean = 43.0 µm, *n* = 50) wide. The ventral surface was flat to slightly concave (Fig. 5 b), while the dorsal side was convex and possessed a pebbled appearance (Fig. 5 a). The rugose surface was due to the presence of numerous (between 100 and 200) small nodules (*n* = 12) (Fig. 5 a). There was no apparent pattern to the distribution of these nodules. The episome was very small and completely embedded in the hyposome in the sessile cells. (Fig. 4 a; Fig 5 b). The episome was

narrow at its base and widened at the tip, was symmetric, and had a longitudinal furrow in the middle of its ventral surface (Fig. 5 b, c). The episome appeared to be connected to the hyposome on the right of the furrow and formed the furrow by curling clockwise (Fig. 5 b). The cingulum encircled the episome, but both ends of cingulum were interrupted on the ventral side by the connection between episome and hyposome (Fig. 4 a; Fig. 5 b). The sulcus was broad and shallow, and could not easily be distinguished (Fig. 5 b). The hyposome was large and circular (Fig. 4 a; Fig. 5 a, b). The longitudinal flagellum arose from near the centre of the cell (Fig. 5 b). There was a single pyrenoid that was almost central in location (Fig. 4 a, b). The nucleus was found just below the pyrenoid and appeared kidney-shaped (Fig. 4 a). The granular yellow-brown chloroplast portions were peripheral (Fig. 4 a). While the granular chloroplasts appeared to be multiple discrete entities (Fig. 4 a), they were connected to each other forming a single network (Fig. 4 b). Figure 4 b shows granular chloroplast portions closely placed each other and between the separated granular chloroplast portions there was a narrow process to connect these chloroplast portions.

The life cycle of this dinoflagellate consisted of cells with two distinct forms: the dominant sessile form (Fig. 4 a, b, d; Fig. 5 a – c) and the rare motile form (Fig. 4 a; Fig. 5 d). The cell division took place in non-motile forms by longitudinal fission (Fig. 4 d). The motile form was ovoid in shape (Fig. 4 a; Fig. 5 d) and was occasionally seen in young cultures, but almost never in older cultures. The cells were 25–40 µm (mean = 33.5 µm, n = 15) long and 17.5–27.5 µm (mean = 23.3 µm, n = 15) wide. The tip of the episome of the motile form was tongue-shaped with a longitudinal furrow (Fig. 4 c) and the tip of the episome could be observed in the dorsal view of the cell (Fig. 5 d). The dorsal surface of the hyposome possessed the rugose nature characteristic of the species (Fig. 5 d). The nodules on the dorsal surface of the hyposome had no apparent pattern, but the depressions between the nodules appeared to form a cross-hatched pattern that followed the contour of the hyposome (Fig. 5 d).

Transmission electron microscopy

Figure 6 shows general arrangement of the organelles in *Testudodinium magnum*. The cell contained a typical large dinokaryotic nucleus containing many thick chromosomes, which was situated in the posterior of the cell (Fig. 6). The nuclear membrane was a double membrane, with simple nuclear pores (Fig. 7 a). Typical mitochondria were observed (Fig. 7 b). Each of the granular chloroplast portions were lenticular or elongated irregular shape and were connected to each other by narrow areas and processes, forming a network (Fig. 6 a). They possessed the groups of three thylakoid lamellae typical to dinoflagellates (Fig. 8 a). Occasionally, chloroplasts with two thylakoid lamellae were observed; in one instance both two- and three-thylakoid lamellae were observed within the same chloroplast. (Fig. 8 a, inset). The granular chloroplast portions were mostly peripheral (Fig. 6), but at least part of them radiated outwards from the pyrenoid (Fig. 6 a). The circular pyrenoid was surrounded by a starch sheath consisting of starch granules of various sizes (Fig. a; Fig. 8 b). The pyrenoid matrix was traversed by variously curved multiple thylakoid lamellae that were randomly distributed (Fig. 8 b). The dinoflagellate also contained accumulation bodies and a large number of electron-opaque bodies that might be lipid granules (Fig. 6). The pusule consisted of an elongated tube-like chamber and surrounding variously shaped pusular vesicles (Fig. 8 c) It was a pusule with a collecting chamber. The amphiesmal vesicles were small, polygonal and did not contain any plate-like structure. (Fig. 8 d, e). They were underlain by a continuous electron translucent layer (Fig. 8 e) homologous to the electron opaque layer underlying the amphiesma described by Horiguchi *et al*. (2012). This layer, at least in part, was accompanied by cytoskeletal microtubules (Fig. 8 e). Trichocysts (Fig. 8 d) are typical of dinoflagellates and a group of trichocysts were observed (Fig. 8 d).

The most fascinating feature of this species were the props distributed throughout the cell (Fig. 9). They spanned the thickness of the cell (Fig. 9 a, c, d). My preliminary survey revealed about 100 props per cell (n = 3). The prop became wider toward both ends and the base was

connected to the electron translucent layer of amphiesma. The distinction between the prop and electron translucent layer could be clearly observed (Fig. 9 c, d). The props passed through protoplasm (Fig. 9 a, b). They even penetrated the nucleus (Fig. 9 b, e). They were fibrous in nature (Fig. 9 c, d), although their chemical composition was still to be investigated.

Testudodinium sp. HG272 (Magnum group)

(Figures 10 – 14)

Diagnosis: Cell ovoid to elongate in ventral view, dorso-ventrally compressed, 20–32.5 µm long, 16.5–32.5 µm wide; episome tongue-shaped with longitudinal furrow on its ventral side, tip of episome slightly projected from confinement of upper part of hyposome; hyposome large, ovoid, with a rugose dorsal surface. Chloroplasts elongated, yellow-brown, peripheral; lamellae with three-thylakoid bands; pyrenoid single, starch-sheathed, its matrix traversed by cytoplamic invaginations, located in the centre of the cell; nucleus located below the pyrenoid; many internal props spanning the thickness of the cell.

Type locality: 26.668910N 128.022917E; marine, sand-dwelling; <1 m deep; Sumuide, Okinawa Prefecture, Japan.

Light and Scanning electron microscopy

The cells were ovoid in ventral view and were strongly dorso-ventrally flattened (Fig. 10). The cells were 20–32.5 µm (mean = 23.8 ± 2.40 µm, *n* = 50) long and 16.25–32.5 µm (mean = 22.0 ± 3.62 µm, *n* = 50) wide. The dorsal side was convex and possessed a pebbled appearance (Fig. 10 c), while the ventral surface was flat to slightly concave (Fig. 10 d). The rugose surface was due to the presence of numerous (about 50, *n* = 4) small nodules. There was no apparent pattern to the distribution of these nodules. The episome was very small and partially embedded in the hyposome (Fig. 10 b). The episome was oblong, symmetric, and had a longitudinal furrow in the middle of its

ventral surface (Fig. 10 b, d). The episome appeared to be connected to the hyposome on the right of the furrow and formed the furrow by curling clockwise (Fig. 10 d). The cingulum encircled the episome, but both ends of cingulum were interrupted on the ventral side by the connection between episome and hyposome – an incomplete cingulum (Fig. 10 b, d). The sulcus was broad and shallow (Fig. 10 d). The hyposome was large and ovoid (Fig. 10 b-d). The longitudinal flagellum arose from just above the centre of the cell (Fig. 10 d). Chloroplasts were elongated, yellow-brown and peripherally located. There was a single pyrenoid that was central in location (Fig. 10 a). The nucleus was found just below the pyrenoid (Fig. 10 a).

Transmission electron microscopy

Figure 11 shows the general arrangement of organelles in the cell. The cell contained a typical large dinokaryotic nucleus containing many thick chromosomes, which was situated in the posterior of the cell (Fig. 11). A large nucleolus was present (Fig. 13 c). The nuclear membrane was a double membrane, with simple nuclear pores (Fig. 13 a). Typical mitochondria (Fig. 12 c) and Golgi apparatus (Fig. 12 e) were observed. The chloroplasts were elongated (Fig. 12 b) and distributed around the pyrenoid and in the periphery of the cell, some of them connected to the pyrenoid (Fig. 11). They possessed lamellae each consisting of three thylakoid bands (Fig. 12 b) typical to dinoflagellates. The pyrenoid was surrounded by a starch sheath consisting of starch granules of various sizes (Fig. 12 a). The pyrenoid matrix was traversed by variously curved thylakoids (Fig. 12 a). The pusule consisted of a tube-like chamber and surrounding variously shaped pusular vesicles (Fig. 12 d): It was a pusule with a collecting chamber. The amphiesmal vesicles were small and contained a fibrous material (Fig. 13 b). They were underlain by a continuous electron translucent layer similar to the layer underlying the amphiesma in *T. magnum* (Fig. 13 b). Trichocysts typical of dinoflagellates were observed (Fig. 12 f, g).

Internal props similar to those in *T. magnum* were distributed throughout the cell (Fig. 13 c, d). They appeared to span the thickness of the cell. The prop became wider toward both ends and the base was connected to the electron translucent layer of amphiesma (Fig. 13 c, d). The distinction between the prop and electron translucent layer could be clearly observed (Fig. 13 d). The props passed through the nucleus (Fig. 13 c) and the protoplasm (Fig. 13 d). They were fibrous in nature (Fig. 13 d).

Testudodinium sp. HG275 (Magnusm group)

(Figures 14 – 16)

Diagnosis: Cell ovoid in ventral view, dorso-ventrally compressed, 20–27.5 µm long, 13.75–21.25 µm wide; episome tongue-shaped with longitudinal furrow on its ventral side, tip of episome slightly projected from confinement of upper part of hyposome; hyposome large, ovoid, with a rugose dorsal surface. Chloroplasts elongated, yellow-brown, peripheral; thylakoids trilamellar; pyrenoid single, starch-sheathed, its matrix traversed by cytoplamic invaginations, located in the centre of the cell; nucleus located below the pyrenoid; many internal props spanning the thickness of the cell.

Type locality: 26.702710N 127.879637E; marine, sand-dwelling; <1 m; Bise, Okinawa Prefecture, Japan.

Light and Scanning electron microscopy

The cells were ovoid in ventral view and were dorso-ventrally flattened (Fig. 14). The cells were 20–27.5 µm (mean = 23.4 ± 2.21 µm, n = 50) long and 13.75–21.25 µm (mean = 17.05 ± 2.14 µm, n = 50) wide. The dorsal side was convex and possessed a pebbled appearance (Fig. 14 c), while the ventral surface was flat to slightly concave (Fig. 14 d, e). The rugose surface was due to the presence of numerous tiny nodules (Fig. 14 c). There was no apparent pattern to the distribution of

these nodules. The episome was small and partially embedded in the hyposome (Fig. 14). The episome was narrow at the base and wide at the apex, slightly asymmetric, and had a longitudinal furrow in the middle of its ventral surface (Fig. 14 b, d, e). The episome appeared to be connected to the hyposome on the right of the furrow and formed the furrow by curling clockwise (Fig. 14 d). The cingulum encircled the episome, but both ends of cingulum were interrupted on the ventral side by the connection between episome and hyposome – an incomplete cingulum (Fig. 14 b, d, e). The sulcus was broad and shallow (Fig. 14 d). The hyposome was large, ovoid and slightly asymmetric (Fig. 14 a-d). There was a single pyrenoid that was central in location (Fig. 14 a, b). The nucleus was found just below the pyrenoid (Fig. 14 b).

Transmission electron microscopy

Figure 15 shows the general arrangement of organelles in the cell. The cell contained a typical large dinokaryotic nucleus containing many thick chromosomes, which was situated in the posterior of the cell (Fig. 15; Fig. 16 a). The nuclear membrane was a double membrane (Fig. 16 b). Typical mitochondria (Fig. 16 g) and Golgi apparatus (Fig. 16 f) were observed. The chloroplasts were elongated (Fig. 15) and distributed around the periphery of the cell (Fig. 15). They possessed lamellae consisting of three thylakoid bands (Fig. 16 e) typical to dinoflagellates. The asymmetrically-shaped pyrenoid was surrounded by a starch sheath consisting of starch granules of various sizes (Fig. 16 d). Inclusions in the pyrenoid matrix were not observed. The amphiesmal vesicles were small and contained a fibrous material (Fig. 16 g). They were underlain by a continuous electron translucent layer (Fig. 16 g) similar to the layer underlying the amphiesma in *T. magnum*.

Internal props similar to those in *T. magnum* were distributed throughout the cell, spanning the thickness of the cell. They were most easily observed near the periphery of the cell (Fig. 16 c). They were easily recognised where they passed through the nucleus or adjacent to it (Fig. 16 b).

Testudodinium sp. HG312 (Magnum group)

(Figures 17 – 19)

Diagnosis: Cell ovoid to ellipsoid in ventral view, dorso-ventrally compressed, 22.5–30 µm long, 20–27.5 µm wide; episome tongue-shaped with longitudinal furrow on its ventral side, tip of episome slightly projected from confinement of upper part of hyposome; hyposome large, ovoid, with a rugose dorsal surface. Chloroplasts elongated, yellow-brown, peripheral; thylakoids trilamellar; pyrenoid single, starch-sheathed, its matrix traversed by cytoplamic invaginations, located in the centre of the cell; nucleus located below the pyrenoid; many internal props spanning the thickness of the cell.

Type locality: 26.668910N 128.022917E; marine, sand-dwelling; <1 m; Sumuide, Okinawa Prefecture, Japan.

Light and Scanning electron microscopy

The cells were ovoid to ellipsoid in ventral view and were strongly dorso-ventrally flattened (Fig. 17). The cells were 22.5–30 µm (mean = 26.0 ± 2.85 µm, *n* = 25) long and 20–27.5 µm (mean = 23.75 ± 3.06 µm, *n* = 25) wide. The dorsal side was convex and possessed a pebbled appearance (Fig. 17 a, c), while the ventral surface was flat to slightly convex (Fig. 17 d). The rugose surface was due to the presence of numerous (50 to 100) small nodules (*n* = 6). There was no apparent pattern to the distribution of these nodules. The episome was small and partially embedded in the hyposome (Fig. 17 b, d). The episome was ovate, symmetric, and had a longitudinal furrow in the middle of its ventral surface (Figs. 17, b, d). The episome appeared to be connected to the hyposome on the right of the furrow and formed the furrow by curling clockwise (Fig. 17 d). The cingulum encircled the episome, but both ends of cingulum were interrupted on the ventral side by the connection between episome and hyposome – an incomplete cingulum (Fig. 17 b, d). The sulcus

could not be distinguished. The hyposome was large and ovoid (Fig. 17). There was a single pyrenoid that was central in location (Fig. 17 a). The kidney-shaped nucleus was found just below the pyrenoid (Fig. 17 a).

Transmission electron microscopy

Figure 18 shows the general arrangement of organelles in the cell. The cell contained a typical large dinokaryotic nucleus containing many thick chromosomes, which was situated in the posterior of the cell (Fig. 18; Fig. 19 a). Typical mitochondria (Fig. 19 d) and Golgi apparatus (Fig. 19 e) were observed. The chloroplasts were oval to elongated (Fig. 18) and distributed around the pyrenoid and in the periphery of the cell (Fig. 18). They possessed lamellae that consisted of three thylakoid bands (Fig. 19 d), typical to dinoflagellates. The pyrenoid was surrounded by a starch sheath consisting of starch granules of various sizes (Fig. 19 b). The pyrenoid matrix was traversed by variously curved thylakoid bands (Fig. 19 b). The pusule consisted of a central chamber surrounded by pusular vesicles – a simple pusule. The amphiesmal vesicles were small and contained neither fibrous material nor plate-like structures (Fig. 19 d). They were underlain by a continuous electron transparent layer (Fig. 19 d) homologous to the electron translucent layer underlying the amphiesma in *T. magnum*. Trichocysts typical of dinoflagellates were observed (Fig. 19 d).

Internal props similar to those in *T. magnum* were distributed throughout the cell. They spanned the thickness of the cell (Fig. 19 c). The prop became wider toward both ends and the base was connected to the electron translucent layer of amphiesma (Fig. 19 c). The distinction between the prop and electron translucent layer could be clearly observed (Fig. 19 c). The props passed through the protoplasm (Fig. 19 c). They were fibrous in nature (Fig. 19 c).

Testudodinium sp. HG230 (Corrugatum group)

(Figures 20 – 22)

Diagnosis: Cell dorso-ventrally compressed, sub-circular in ventral view, 22.5–32.5 µm long, 15–27.5 µm wide; episome conical and symmetric with a longitudinal furrow on its ventral side; hyposome large, ovoid to sub-circular, with a corrugated dorsal surface possessing 6-8 ribs; sulcus shallow and broad. Chloroplast yellow-brown, peripheral, radiating from a central pyrenoid, granular chloroplast portions connected to each other forming a chloroplast network; pyrenoid starch-sheathed, located in the centre of the cell; nucleus located below the pyrenoid.
Type locality: 30°41.800'N 130°52.200'E; marine, benthic, sand-dwelling; 30 m; seabed off Mageshima, Kagoshima Prefecture, Japan.

Light and Scanning electron microscopy

The cells were ovoid to sub-circular in ventral view (Fig. 20), 22.5-32.5 µm (mean = 26.875 ± 2.32 µm, n = 50) long and 15-27.5 µm (mean = 21.5 ± 2.68 µm, n = 50). The ventral surface of the hyposome was flat (Fig. 20 d) and the dorsal surface was corrugated (Fig. 20 a, c). The corrugated nature was due to six to eight (*n* = 10) longitudinal dorsal ribs (Fig. 20 a, c). The episome was small, tongue-shaped and partly embedded in the hyposome (Fig. 20 b, d). It was narrow at the base and widened at the tip, was symmetric, and had a longitudinal furrow on the middle of its ventral surface (Fig. 20 b, d). The episome appeared to be connected to the hyposome on the right of the furrow and formed the furrow by curling clockwise (Fig. 20 d). The cingulum encircled the episome, but both ends of cingulum were interrupted on the ventral side by the connection between episome and hyposome (Fig. 20 d) – an incomplete cingulum. The sulcus was broad, shallow and could not easily be distinguished (Fig. 20 d). The longitudinal flagellum arose from the centre of the cell (Fig. 20 b, d). The pyrenoid could not be distinguished under the light microscope. The chloroplasts were golden-brown and discrete (Fig. 20 a, b).

Transmission electron microscopy

Figure 21 shows the general arrangement of organelles in the cell. The cell contained a typical large dinokaryotic nucleus containing many thick chromosomes, which was situated in the posterior of the cell (Fig. 21). Typical mitochondria (Fig. 22 d) and Golgi apparatus (Fig. 22 e) were observed. The chloroplasts were elongated (Fig. 22 c) and distributed around the periphery of the cell (Fig. 21). They possessed lamellae that consisted of three thylakoid bands (Fig. 22 c), typical to dinoflagellates. The pyrenoid complex was composed of pyrenoid matrices at the ends of individual chloroplasts, and did not appear to be surrounded by a starch sheath (Fig. 22 f). The matrices of the individual pyrenoids were homogeneous (Fig. 22 f). The amphiesmal vesicles were small and contained neither fibrous material nor plate-like structures (Fig. 22 a). They were underlain by a continuous electron transparent layer (Fig. 22 a) homologous to the electron opaque layer underlying the amphiesma in *T. corrugatum* (Horiguchi *et al.*, 2012). Trichocysts typical of dinoflagellates were observed (Fig. 22 a, b).

Testudodinium sp. HG304 (Corrugatum group)

(Figures 23 – 26)

Diagnosis: Cell dorso-ventrally compressed, sub-circular in ventral view, 23.75–27.5 µm long, 17.5–25 µm wide; episome conical and symmetric with a longitudinal furrow on its ventral side; hyposome large, ovoid to sub-circular, with a corrugated dorsal surface possessing 10-14 ribs; sulcus shallow and broad. Chloroplast yellow-brown, peripheral, radiating from a central pyrenoid, granular chloroplast portions connected to each other forming a chloroplast network; pyrenoid starch-sheathed, located in the centre of the cell; nucleus located below the pyrenoid.
Type locality: 30°41.850 N 130°50.546 E; marine, benthic, sand-dwelling; 34 m; seabed off Mageshima, Kagoshima Prefecture, Japan.

Light and Scanning electron microscopy

The cells were ovoid to sub-circular in ventral view (Fig. 23), 23.75–27.5 µm (mean = 25.875 ± 1.44 µm, n = 25) long and 17.5-25 µm (mean = 22.375 ± 2.66 µm, n = 25). The ventral surface of the hyposome was flat to slightly convex (Fig. 23 d, e) and the dorsal surface was corrugated (Fig. 23 c), with a girdle around the cell. The corrugated nature was due to 10 to 14 (*n* = 13) longitudinal dorsal ribs (Fig. 23 c). The episome was small, tongue-shaped and embedded in the hyposome (Fig. 23 b, d, e). It was narrow at the base and widened at the tip, was symmetric, and had a longitudinal furrow on the middle of its ventral surface (Fig. 23 d, e). The episome appeared to be connected to the hyposome on the right of the furrow and formed the furrow by curling clockwise (Fig. 23 d, e). The cingulum encircled the episome, but both ends of cingulum were interrupted on the ventral side by the connection between episome and hyposome (Fig. 23 b, d) – an incomplete cingulum. The sulcus was broad, shallow and could not easily be distinguished (Fig. 23 b). The longitudinal flagellum arose from the centre of the cell (Fig. 23 d) and the transverse flagellum was within the cingulum (Fig. 23 e). There was a single pyrenoid that was central in location (Fig. 23 a). The nucleus was situated below the pyrenoid (Fig. 23 a). The chloroplasts were golden-brown and discrete (Fig. 23 a, b).

Transmission electron microscopy

Figure 24 shows the general arrangement of organelles in the cell. The cell contained a typical large dinokaryotic nucleus containing many thick chromosomes, which was situated in the posterior of the cell (Fig. 24; Fig. 25 a). Typical mitochondria (Fig. 25 c) and Golgi apparatus (Fig. 25 d) were observed. Electron opaque inclusions that may be lipid granules were observed posterior to the nucleus (Fig. 24). The chloroplasts were elongated (Fig. 25 g) and distributed around the pyrenoid and the periphery of the cell (Fig. 24). They possessed lamellae with three thylakoid bands (Fig. 25 g) typical to dinoflagellates. The pyrenoid complex was composed of multiple discrete pyrenoid matrices, and was surrounded by starch granules of varying sizes (Fig. 25 b). The matrices of the

individual pyrenoids were homogeneous (Fig. 25 b). The pusule consisted of a central chamber and surrounding variously shaped pusular vesicles (Fig. 25 e): It was a pusule with a collecting chamber. The amphiesmal vesicles were small and contained fibrous material (Fig. 25 f). They were underlain by a continuous electron transparent layer (Fig. 25 f) homologous to the electron opaque layer underlying the amphiesma in *T. corrugatum* (Horiguchi *et al.*, 2012). Trichocysts typical of dinoflagellates were observed (Fig. 25 g).

Internal props similar to those in T. magnum were distributed throughout the cell (Fig. 26 a). They spanned the thickness of the cell (Fig. 26). The prop became wider toward both ends and the base was connected to the electron translucent layer of amphiesma (Fig. 26 b). The distinction between the prop and electron translucent layer could be clearly observed (Fig. 26 b). The props passed through the protoplasm (Fig. 26). They were fibrous in nature (Fig. 26 b).

Testudodinium corrugatum NY050 (Corrugatum group)

(Figure 27)

Light and Scanning electron microscopy

The cells were ovoid in ventral view (Fig. 27), 22.5–31.25 µm (mean = 27.5 ± 2.57 µm, n = 25) long and 17.5-30 µm (mean = 23.875 ± 3.46 µm, n = 25). The ventral surface of the hyposome was flat to slightly concave (Fig. 27 c, e) and the dorsal surface was corrugated (Fig. 27 a, d). The corrugated nature was due to eight to ten (n = 7) longitudinal dorsal ribs (Fig. 27 a, d). The episome was small, tongue-shaped and embedded in the hyposome (Fig. 27 b, c). It was narrow at the base and widened at the tip, was symmetric, and had a longitudinal furrow on the middle of its ventral surface (Fig. 27 c). The episome appeared to be connected to the hyposome on the right of the furrow and formed the furrow by curling clockwise (Fig. 27 c). The cingulum encircled the episome, but both ends of cingulum were interrupted on the ventral side by the connection between episome and hyposome (Fig. 27 c) – an incomplete cingulum. The sulcus was broad, shallow and

could not easily be distinguished (Fig. 27 c). The longitudinal flagellum arose from the centre of the cell (Fig. 27 c). There was a single pyrenoid that was central in location (Fig. 27 a). The oval nucleus was situated immediately below the pyrenoid (Fig. 27 a). The chloroplasts were golden-brown and appeared reticulate (Fig. 27 a, b).

Testudodinium maedaense HG273 (Maedaense group)

(Figure 28)

Light and Scanning electron microscopy

The cell is oval in ventral view and dorso-ventrally flattened (Fig. 28). The cells are 16.25–27.5 µm (mean = 23.075 ± 2.61 µm, n = 50) long and 11.25–21.25 µm (mean = 17.025 ± 2.47 µm, n = 50) wide. The ventral surface of the hyposome was flat to slightly concave (Fig. 28 d) and the dorsal surface was smooth (Fig. 28 c). The episome was small, tongue-shaped and partially embedded in the hyposome (Fig. 28). It was narrow at the base and widened at the tip, was asymmetric, and had a longitudinal furrow on the middle of its ventral surface (Fig. 28 d); the tip of the episome deflected to the dorsal side (Fig. 28 c, d). The episome appeared to be connected to the hyposome on the right of the furrow and formed the furrow by curling clockwise (Fig. 28 d). The cingulum encircled the episome, but both ends of cingulum were interrupted on the ventral side by the connection between episome and hyposome (Fig. 28 d) – an incomplete cingulum. The sulcus could not be distinguished. The longitudinal flagellum arose from the centre of the cell (Fig. 28 d). There was a single pyrenoid that was central in location (Fig. 28 a, b). The nucleus was situated immediately below the pyrenoid (Fig. 28 b). The chloroplasts were golden-brown and appeared discrete (Fig. 28 a, b).

Testudodinium maedaense HG276 (Maedaense group)

(Figures 29 – 32)

Light and Scanning electron microscopy

The cell is oval in ventral view and dorso-ventrally flattened (Fig. 29). The cells are 17.5–27.5 µm (mean = 23.85 ± 2.78 µm, n = 50) long and 12.5–22.5 µm (mean = 17.975 ± 2.68 µm, n = 50) wide. The ventral surface of the hyposome was flat to slightly concave (Fig. 29 d) and the dorsal surface was smooth (Fig. 29 c). The episome was small, tongue-shaped and partially embedded in the hyposome (Fig. 29 c, d). It was narrow at the base and widened at the tip, was asymmetric, and had a longitudinal furrow on the middle of its ventral surface (Fig. 29 d); the tip of the episome deflected to the dorsal side (Fig. 29 c, d). The episome appeared to be connected to the hyposome on the right of the furrow and formed the furrow by curling clockwise (Fig. 29 d). The cingulum encircled the episome, but both ends of cingulum were interrupted on the ventral side by the connection between episome and hyposome (Fig. 29 d) – an incomplete cingulum. The sulcus was shallow (Fig. 29 d). There was a single pyrenoid that was central in location (Fig. 29 a). The nucleus was situated immediately below the pyrenoid (Fig. 29 a). The chloroplasts were golden-brown and appeared discrete (Fig. 29 a, b).

Transmission electron microscopy

Figure 30 shows the ultrastructure and arrangement of organelles within a cell. A large dinokaryotic nucleus containing many thick chromosomes is located near the posterior of the cell (Fig. 30). The nuclear membrane was a double membrane, with simple nuclear pores (Fig. 31 e). Typical mitochondria (Fig. 31 b) and Golgi apparatus (Fig. 31 f) were observed. Few electron opaque inclusions that may be lipid granules were observed. (Fig. 30). The chloroplasts were elongated (Fig. 31 d) and distributed around the pyrenoid and the periphery of the cell (Fig. 30). They possessed lamellae with three thylakoid bands (Fig. 31 c) typical to dinoflagellates. The pyrenoid possessed intrusions of cytoplasmic processes, and was surrounded by starch granules of varying sizes (Fig. 31 a). The amphiesmal vesicles were small, polygonal and contained fibrous material

(Fig. 31 g, h). They were underlain by a continuous electron transparent layer (Fig. 31 g) homologous to the electron opaque layer underlying the amphiesma in *T. maedaense* (Horiguchi *et al.*, 2012). Trichocysts typical of dinoflagellates were observed (Fig. 31 d).

Internal props similar to those in *T. magnum* were distributed throughout the cell (Fig. 32 a). They spanned the thickness of the cell (not shown). The prop became wider toward both ends and the base was connected to the electron translucent layer of amphiesma (Fig. 32 c). The distinction between the prop and electron translucent layer could be clearly observed (Fig. 32 c). The props passed through the nucleus (Fig. 32 a) and the protoplasm (Fig. 32 b, c). They were fibrous in nature (Fig. 32 c).

Testudodinium maedaense HG278 (Maedaense group)

(Figure 33)

Light and Scanning electron microscopy

The cell is oval in ventral view and dorso-ventrally flattened (Fig. 33). The cells are 17.5–22.5 µm (mean = 20.125 ± 2.16 µm, n = 25) long and 12.5–17.5 µm (mean = 15.5 ± 2.06 µm, n = 25) wide. The ventral surface of the hyposome was flat to slightly concave (Fig. 33 d) and the dorsal surface was smooth (Fig. 33 c). The episome was small, tongue-shaped and partially embedded in the hyposome (Fig. 33 c, d). It was narrow at the base and widened at the tip, was asymmetric, and had a longitudinal furrow on the middle of its ventral surface (Fig. 33 d); the tip of the episome deflected to the dorsal side (Fig. 33 c, d). The episome appeared to be connected to the hyposome on the right of the furrow and formed the furrow by curling clockwise (Fig. 33 d). The cingulum encircled the episome, but both ends of cingulum were interrupted on the ventral side by the connection between episome and hyposome (Fig. 33 d) – an incomplete cingulum. The sulcus was shallow (Fig. 33 d). There was a single pyrenoid that was central in location (Fig. 33 a). The

nucleus was situated immediately below the pyrenoid (Fig. 33 a). The chloroplasts were golden-brown and appeared discrete (Fig. 33 a, b).

Testudodinium maedaense HG288 (Maedaense group)

(Figure 34)

Light and Scanning electron microscopy

The cell is oval in ventral view and dorso-ventrally flattened (Fig. 34). The cells are 20–25 µm (mean = 22.75 ± 1.93 µm, n = 25) long and 13.75–22.5 µm (mean = 18.0 ± 2.51 µm, n = 25) wide. The ventral surface of the hyposome was flat to slightly concave (Fig. 34 d) and the dorsal surface was smooth (Fig. 34 c). The episome was small, tongue-shaped and partially embedded in the hyposome (Fig. 34 b, d). It was narrow at the base and widened at the tip, was asymmetric, and had a longitudinal furrow on the middle of its ventral surface (Fig. 34 b, d); the tip of the episome deflected to the dorsal side (Fig. 34 c, d). The episome appeared to be connected to the hyposome on the right of the furrow and formed the furrow by curling clockwise (Fig. 34 d). The cingulum encircled the episome, but both ends of cingulum were interrupted on the ventral side by the connection between episome and hyposome (Fig. 34 d) – an incomplete cingulum. The sulcus was broad and shallow (Fig. 34 d), and the longitudinal flagellum was situated within it (Fig. 34 b) There was a single pyrenoid that was central in location (Fig. 34 a, b). The nucleus was situated immediately below the pyrenoid (Fig. 34 a). The chloroplasts were golden-brown (Fig. 34 a, b).

Testudodinium maedaense HG291 (Maedaense group)

(Figures 35 – 37)

Light and Scanning electron microscopy

The cell is oval in ventral view and dorso-ventrally flattened (Fig. 35). The cells are 17.5–27.5 µm (mean = 23.625 ± 2.79 µm, *n* = 25) long and 13.75–21.25 µm (mean = 16.75 ± 2.51 µm, *n* = 25)

wide. The ventral surface of the hyposome was flat to slightly convex (Fig. 35 d) and the dorsal surface was smooth (Fig. 35 c). The episome was small, tongue-shaped and partially embedded in the hyposome (Fig. 35). It was narrow at the base and widened at the tip, was asymmetric, and had a longitudinal furrow on the middle of its ventral surface (Fig. 35 b, d); the tip of the episome deflected to the dorsal side (Fig. 35 c, d). The episome appeared to be connected to the hyposome on the right of the furrow and formed the furrow by curling clockwise (Fig. 35 d). The cingulum encircled the episome, but both ends of cingulum were interrupted on the ventral side by the connection between episome and hyposome (Fig. 35 d) – an incomplete cingulum. There was a single pyrenoid that was central in location (Fig. 35 a). The nucleus was not visible under the light microscope. The chloroplasts were golden-brown (Fig. 35 a, b).

Transmission electron microscopy

Figure 36 shows the ultrastructure and arrangement of organelles within a cell. A large dinokaryotic nucleus containing many thick chromosomes is located near the posterior of the cell (Fig. 36). The nuclear membrane was a double membrane, with simple nuclear pores (Fig. 37 h). Typical mitochondria (Fig. 37 b) and Golgi apparatus (Fig. 37 d) were observed. A single electron opaque inclusion abutting the nucleus that may be a lipid granule was observed (Fig. 36). The chloroplasts were elongated (Fig. 36 a) and distributed around the pyrenoid and the periphery of the cell (Fig. 36 a). They possessed thylakoids with three lamellae (Fig. 37 g) typical to dinoflagellates. The pyrenoid matrix was homogeneous, and was surrounded by starch granules of varying sizes (Fig. 37 a). The amphiesmal vesicles were small and contained fibrous material (Fig. 37 e). They were underlain by a continuous electron transparent layer (Fig. 37 e) homologous to the electron opaque layer underlying the amphiesma in *T. maedaense* (Horiguchi *et al.*, 2012). Trichocysts typical of dinoflagellates were observed (Fig. 37 f).

Internal props similar to those in *T. magnum* were distributed throughout the cell. They spanned the thickness of the cell (Fig. 37 i). The distinction between the prop and electron translucent layer could be clearly observed (Fig. 37 i). The props passed through the nucleus (Fig. 37 h) and the protoplasm (Fig. 37 i). They were fibrous in nature (Fig. 37 i).

Testudodinium maedaense HG297 (Maedaense group)

(Figure 38)

Light and Scanning electron microscopy

The cell is oval in ventral view and dorso-ventrally flattened (Fig. 38). The cells are 20–27.5 µm (mean = 22.5 ± 2.28 µm, n = 25) long and 15–20 µm (mean = 16.625 ± 1.95 µm, n = 25) wide. The ventral surface of the hyposome was flat to slightly concave (Fig. 38 d) and the dorsal surface was smooth (Fig. 38 c). The episome was small, tongue-shaped and partially embedded in the hyposome (Fig. 38 b, d). It was narrow at the base and widened at the tip, was asymmetric, and had a longitudinal furrow on the middle of its ventral surface (Fig. 38 d); the tip of the episome deflected to the dorsal side (Fig. 38 c, d). The episome appeared to be connected to the hyposome on the right of the furrow and formed the furrow by curling clockwise (Fig. 38 d). The cingulum encircled the episome, but both ends of cingulum were interrupted on the ventral side by the connection between episome and hyposome (Fig. 38 d) – an incomplete cingulum. The sulcus was shallow (Fig. 38 d). There was a single pyrenoid that was off-centre in location (Fig. 38 a). The nucleus was situated below the pyrenoid (Fig. 38 a). The chloroplasts were golden-brown and appeared discrete (Fig. 38 a, b).

Phylogenetic analysis

The phylogenetic position of the thirteen *Testudodinium* strains were analysed by ML and Bayesian analyses based on the partial SSU rDNA sequences. The ML tree is presented in Fig. 39, with the

posterior probability (PP) indices of Bayesian analysis and the bootstrap values (BT) of the ML method. The trees by both methods were mostly congruent. All the described strains fell within the *Testudodinium* clade containing the three previously described species of *Testudodinium*; this grouping had maximum support from both the ML and Bayesian inferences (BT/PP = 100%/1.0). Furthermore, the strains divided into three sub-clades: magnum group, corrugatum group and maedaense group. Two of these sub-clades contained previously described species – *T. maedaense* and *T. corrugatum*, respectively, while the third – which contained *T. magnum* – was sister clade to the maedaense clade. The type species of the genus, *T. testudo* was located sister to *T. corrugatum*-subclade. Support for the relationships between individual strains was robust within the corrugatum and magnum sub-clades; within the maedaense sub-clade, support was generally low.

Discussion

In this chapter I describe thirteen strains, all belonging to the genus *Testudodinium*. They share the distinctive features of the genus: a small tongue-shaped episome with a longitudinal furrow on the ventral surface, embedded in a large hyposome. The phylogenetic tree also supports the inclusion of all the strains within the genus *Testudodinium*. Of the 13 strains, *Testudodinium magnum* has been described as a new species (Pinto et al., 2016). The other 12 can be divided into three groups based on the nature of the dorsal surface of the hyposome, which can be determined by observation under the light microscope. Each group contains three of the four recognised species: the magnum group, containing *T. magnum* and additional three novel species, all distinguished by a rugose dorsal hyposome; the corrugatum group, containing *T. corrugatum*, with two novel species, all distinguished by dorsal ribs on the hyposome; and the maedaense group, containing the original *T. maedaense* and six strains that are also representaives of *T. maedaense*, all possessing a smooth hyposome. None of the strains in this study bore any resemblance to *T. testudo*, the type species.

All the 13 strains described in this chapter are similar to the members of *Amphidinium sensu stricto*, as are the previously described other members of *Testudodinium*; the resemblance is so close that – in the absence of sequence data – the recorded species at the time were considered part of *Amphidinium s. s.* when the genus was redefined and the description emended (Flø Jørgensen *et al.*, 2004a). However, all the strains can be distinguished from species of *Amphidinium s. s.* by possession of a longitudinal furrow in the ventral side of the episome (Figs 5 a, 10 d, 14 d, 17 d, 20 d, 23 d, 27 d, 28 d, 29 d, 33 d, 34 d, 35 d, 38 d) as in other species of *Testudodinium* (Horiguchi *et al.*, 2012). The cingulum of the strains is similar to the previously described species in encircling the episome, but being interrupted on the ventral surface – an incomplete cingulum, in short (Horiguchi *et al.*, 2012). The sulcus of the strains is broad and shallow and falls within the genus diagnosis (Horiguchi *et al.*, 2012); however, it can not always be distinguished. The differences between the strains and species are listed in Table 3.

The strain HG229 has been described as a new species of *Testudodinium*, *T. magnum* (Pinto et al., 2016); the other strains within the magnum group – HG272, HG275, and HG312 – are also regarded as new species. All the four strains are distinguished by having a rugose dorsal hyposome with numerous nodules, as compared to the smooth hyposome of *T. testudo* and *T. maedaense*, and the dorsal ridges of the corrugated hyposome of *T. corrugatum* (Horiguchi *et al.*, 2012; Larsen and Patterson, 1990). *T. magnum* is distinguished from congeners primarily by its large size; the other members are closer in size to the previously described species, but are sufficiently distinctive from each other that I consider them separate species. HG272 is different from other members of the magnum group in being much smaller than the other members; the number of nodules on the dorsal hyposome is smaller. HG275 and HG312 are morphologically similar, possessing similar cell sizes. However, under SEM, HG275 is distinguished in possessing numerous tiny nodules on the dorsal surface of the hyposome, whereas the nodules on all the other members are larger and well-defined. One of the characteristic features in *T. magnum* is that it possesses a sessile form in its life cycle,

which is different in morphology. This dimorphism is unknown in other species of *Testudodinium*. However, a similar life cycle pattern was previously reported in the genus *Togula* (Flø Jørgensen *et al.*, 2004b). Like *Togula*, cell division in *Testudodinium magnum* occurs in the sessile cells, but it lacks any structure similar to the hyaline sheath described in *Togula brittanica* and *Togula jolla* (Flø Jørgensen *et al.*, 2004b).

Testudodinum corrugatum currently has two described strains: HG163 and TM85 (Horiguchi *et al.*, 2012). In this work I described three strains similar to this species, one of which – NY050 – is a new representative of the species, while the other two are considered new species. It has been established that the number of dorsal ribs cannot be used as a diagnostic feature (Horiguchi *et al.*, 2012), and my observations confirm this. However, an examination of the SEM images in Horiguchi *et al.* (2012) combined with the observations of *T. corrugatum* NY050 have showed that *T. corrugatum* can be distinguished from the two new species by the presence of a girdle similar to that of *T. testudo*. HG304 and HG230 are also distinguished from *T. corrugatum* in possessing faintly defined dorsal ribs, whereas the latter possesses well-defined dorsal ribs. HG304 and HG230 cannot be easily distinguished from each other on the basis of morphology alone; however, the dorsal ribs can be observed in HG230 under LM, while they are rarely visible in HG304.

The six strains in the maedaense group examined in this study are morphologically indistinguishable from *Testudodinium maedaense* either by light or by scanning electron microscopy. Morphometrically, the cell dimension overlap each other such that they are also no help in establishing delineations. On the basis of LM and SEM data, these strains appear to represent the species *T. maedaense*, and are considered as such.

The strains and species of *Testudodinium* possess morphologically varied types of pyrenoids that are not common within the groups indicated by external morphology. The pyrenoid in *T. magnum*, HG272, and HG312 is more or less circular, surrounded by a starch sheath comprised of

numerous starch granules, and the pyrenoid matrix is traversed by randomly distributed thylakoid lamellae. In HG275 and HG291, the pyrenoid is similar, but the matrix is homogeneous and any inclusions are absent. In *T. testudo*, the pyrenoid matrix is located at the proximal portion of elongated chloroplasts and an aggregation of pyrenoid matrices forms a pyrenoid complex. The pyrenoid matrix itself is not traversed by thylakoid bands (Horiguchi *et al.*, 2012); this feature is shared by HG 230, but the starch sheath is absent. The pyrenoid of *T. maedaense* is surrounded by thick starch sheaths, and the pyrenoid interior is invaded by branched cytoplasmic tubules of various thickness (Horiguchi *et al.*, 2012). The pyrenoid matrix of *T. corrugatum* is invaded by membranous structures. Although it seems to be one body, it may be an aggregation of individual pyrenoids (Horiguchi *et al.*, 2012). This aggregation is seen in HG276 and HG304, the pyrenoid complex in the latter being composed of globules of pyrenoid matrix. Thus, the type of pyrenoid in *Testudodinium* is species-specific and has little value as a generic feature; however, it is of great value in delineating species where the morphological data from LM and SEM is insufficient, as in the case HG304 and HG230.

The ultrastructure of the other organelles does not provide any basis for the delineation between species; the structures are very similar across all the strains and species examined. The nuclear membrane of *T. magnum*, HG272, HG276, and HG291 (Figs 16, 41, 113, 141) has simple nuclear pores. The more complex nuclear pore chambers seen in *Gymnodinium* (Daugbjerg et al., 2000; Dodge and Crawford, 1969) were not observed in any of the cells. The chloroplasts possess thylakoids comprised of three lamellae, but chloroplasts possessing thylakoids with two lamellae are also observed in *T. magnum*. The simultaneous existence of double-thylakoid and triple-thylakoid chloroplasts in the other members of *Testudodinium* is undocumented; however, double- (and quadri-) thylakoids occasionally occur in dinoflagellates (Schnepf and Elbrächter, 1999). The pusule of *T. magnum*, HG272 and HG304 consists of an elongated tube-like chamber and surrounding variously-shaped pusule vesicles. This is most similar morphologically to the pusule

with the collecting chamber which branches from the flagellar canal as described by Dodge (Dodge, 1972); however, the association of the pusule with the flagellar canal could not be determined for any of these. The types of pusules in the three previously described species and the remaining strains are unknown (Horiguchi *et al.*, 2012).

Figure 40 presents a schematic representation of character evolution in *Testudodinium*. *Testudodinium* is easily identifiable by the minute episome possessing a ventral groove or furrow; thus this is most probably the oldest common character in the genus – a synapomorphy. The next major split appears to be the development of a hyaline girdle encircling the cell, which split the genus into two lineages. The lineage that developed the girdle further splits into *T. testudo*, where the dorsal hypotheca remained smooth, and the corrugatum lineage, where the dorsal hypotheca developed dorsal ribs; the lineage without the girdle split into the magnum lineage, where the dorsal hypotheca developed nodules, thus becoming rugose, and the maedaense lineage, where the dorsal hypotheca remained smooth. From this observation, it is possible that the ancestor species had a smooth hypotheca in addition to the ventral groove on the episome. Between the testudo-corrugatum split and the present day, *T. testudo* appears to have developed a pyrenoid complex formed from the aggregation of pyrenoids in the distal portions of numerous chloroplasts. The corrugatum lineage split into three branches. The *T. corrugatum* branch developed a simple, or possibly complex, pyrenoid that possesses membranous structures in the pyrenoid matrix, and the dorsal ribs became well-defined. The HG230 branch developed faintly defined dorsal ribs and a pyrenoid complex similar to that of *T. testudo*, but lacking a starch sheath. The HG304 branch went a completely different route, gaining internal props, and a pyrenoid complex composed of globular pyrenoid matrices. The dorsal ribs in this branch remained faintly defined. HG272 appears to retain the ancestral characteristics of the magnum branch – a rugose dorsal hyposome, internal props, a single, circular pyrenoid whose matrix is traversed by thylakoids. This branch further split to give rise to *T. magnum*, which is set apart by its comparatively massive size and by its dimorphic life

cycle. The other two species in this lineage are morphologically similar, but HG275 has diverged the most, with minute nodules on the dorsal hyposome, and a single, asymmetrically shaped pyrenoid with a homogeneous matrix. Finally, the maedaense lineage appears to have diverged the most, although the lack of internal ultrastructure data limits the inferences that may be drawn. Of the three strains from which the internal ultrastructure is known, two – HG276 and HG291 – possess internal props while *T. maedaense* does not. Further, the pyrenoid in all three are dissimilar: *T. maedaense* has a pyrenoid complex with a matrix invaded by cytoplasmic tubules, HG276 a pyrenoid similar to that of *T. corrugatum*, and HG297 a single circular pyrenoid with a homogeneous matrix. The appearance of the internal props across three of the four lineages of *Testudodinium* could possibly be attributed to sympleisiomorphy – it may be an ancestral trait shared by two or more taxa that have a common ancestor. Thus, the possible ancestral characters of the genus are a small cell size, a minute episome with a ventral groove, and internal props.

The characteristics of the amphiesma also vary slightly among the different *Testudodinium* species. In the original description, the amphiesmal vesicle is described as being underlain by a continuous electron-opaque layer (Horiguchi *et al.*, 2012); this continuous layer is present in all seven of the strains observed under transmission electron microscopy. The only variation is in the nature of the layer: it is either electron-transparent or electron-translucent. This may be an artefact of fixation. The amphiesmal vesicles of *T. magnum* are polygonal, small and electron transparent. In this respect they are most similar to the amphiesmal vesicles of *T. testudo*, which are small and contain no obvious structures (Horiguchi *et al.*, 2012). In contrast, the amphiesmal vesicles of *T. maedaense* contain fibrous materials, while those of *T. corrugatum* each contain a thin, plate-like structure (Horiguchi *et al.*, 2012).

It was first described that *Testudodinium magnum* possesses a unique internal structure, the props, that were previously unknown from any other dinoflagellate (Pinto et al., 2016). Internal siliceous skeletons were discovered in the dinoflagellates *Actiniscus pentasterias* (Ehernberg)

Ehrenberg (Hansen, 1993) and *Dicroerisma psilonereiella* Taylor & Cattell (Gómez, 2008), but their structures are very different from props of *T. magnum*. The props extend from the dorsum to the ventrum; they are fibrous in nature but the composition and function are currently unknown and under investigation. Another athecate dinoflagellate, *Bispinodinium angelaceum*, was described from similar depth and location; it possesses a pair of fibrous structures termed the spinoid apparatus (Yamada *et al.*, 2013). This apparatus extends from the apex to the antapex of the cell, in contrast with the dorso-ventral props of *T. magnum*. Any relation between the two structures is not apparent, and due to their differences, I posit that they are unrelated. While these are some of the deepest reported athecate dinoflagellates, *Gambierdiscus carolinianus*, a thecate dinoflagellate, was reported from 45.7 m (Tester *et al.*, 2013), a full 10 m deeper than *T. magnum*; this corresponds to an increase in pressure of 100 kPa. No internal structures similar to either the spinoid apparatus or the internal props were reported from *Gambierdiscus*; its thecal plates may provide sufficient resistance to the water pressure to obviate the need for such adaptations. However, when discussing the relationship between habitat depth (pressure) and morphological features, one must be very cautious: samples from similar depths as those from which *Bispinodinium angelaceum* and *Testudodinium magnum* were isolated, also contained dinoflagellate species, e.g. *Amphidinium operculatum, A. gibbosum* and *A. steinii* (Horiguchi personal observations, 2012). These latter species have been reported from shallow habitats (Horiguchi et al., 2012; Murray et al., 2004), and no special morphological features such as props or spinoid apparatus were reported. Any hypothesis regarding the role of the props is compounded by the fact that props are present in other *Testudodinium* strains. All the members of the magnum group possess props, which thus can be used as a diagnostic feature in combination with the rugose hyposome; however, all the these species were isolated from the intertidal region, making it unlikely that this was an evolution for mitigating the effects of pressure or size. Props are also observed in the two strains of *Testudodinium maedaense*, which were also isolated from the intertidal zone. While props were not

described in the original description of *T. maedaense*, their appearance in two morphologically and phylogenetically similar strains led me to rexamine the negatives of the images in the original report. They revealed that *T. maedaense* does possess props which were not noticed in the original description. Most remarkably, props were also observed in HG304, which is part of the corrugatum group, and is phylogenetically more distant. This species is, however, a benthic species isolated from a depth of 34 m. Thus, the function of the internal props is currently a mystery.

Our molecular tree shows that, from an evolutionary standpoint, the *Testudodinium* clade is divided into two sub-clades: One consisting of *T. testudo* and the corrugatum sub-clade, and the other the maedanese and magnum sub-clades. The latter is intriguing in light of the vast morphological differences between *T. maedaense and T. magnum*. The case for a total of four species within the magnum sub-clade and two novel species in the corrugatum sub-clade on the basis of morphology is warranted by the high support for this within each sub-clade. Within the maedaense sub-clade, support for any split is low, contributing to the complexity of delineation based on morphological characters.

The discovery of props in Testudodinium maedaense leads to the emendation of the species diagnosis, as follows:

Testudodinium maedaense Katsumata and Horiguchi emend. Pinto and Horiguchi

Cell dorsoventrally compressed, ovoidal in ventral view, 20.0–27.5 µm long, 15.0–20.0 µm wide; tongue-shaped episome bearing a longitudinal striation on ventral side; elongated and ellipsoidal hyposome with rounded anterior end. Chloroplasts many, yellow-brown, some connected with a central pyrenoid; pyrenoid single, central; sulcus short, shallow, in centre of cell; many internal props spanning the thickness of the cell.

Holotype: Figure 13, Horiguchi *et al.* (2012).

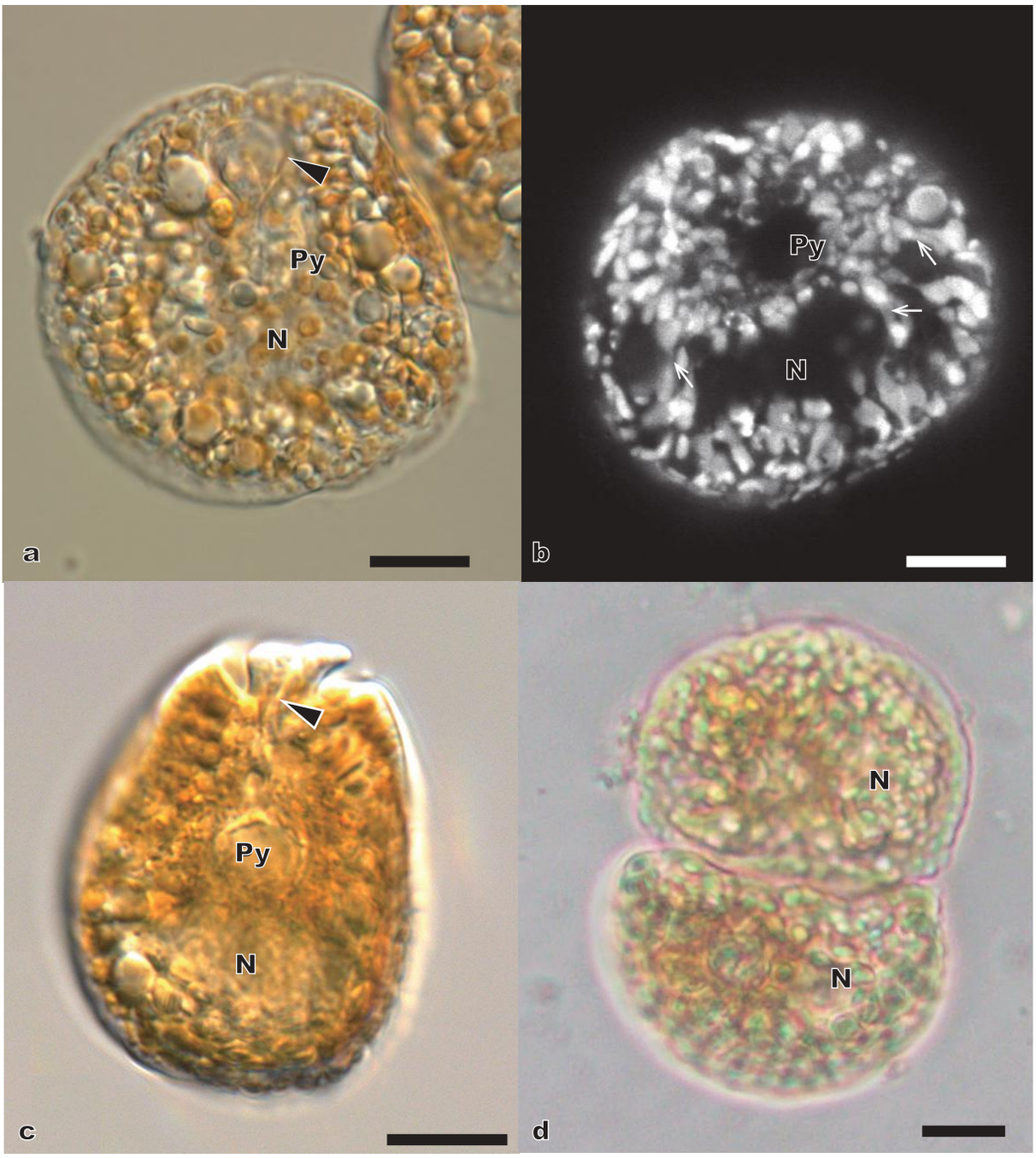


Fig. 4. *Testudodinium magnum* sp. nov. Light and fluorescence microscopy.
a. Typical sessile cell. The episome (arrowhead) is completely embedded in the hyposome. The pyrenoid (Py) is central, and the kidney-shaped nucleus (N) is situated directly below it.
b. Fluorescent microscopy showing distribution of chloroplasts in the cell. The granular chloroplast portions seem to be connected to each other, forming a network and some of the chloroplast portions are connected to each other by narrow, elongated processes (arrows). N: nucleus, Py: pyrenoid.
c. Typical motile cell. The cell shape is ovoid and the episome is tongue-shaped with a longitudinal furrow (arrowhead). N: nucleus, Py: pyrenoid.
d. Dividing cells. The cells divide in the sessile form, in a plane passing through the centre of the cell. N: nucleus.
Scale bar = 10 µm.

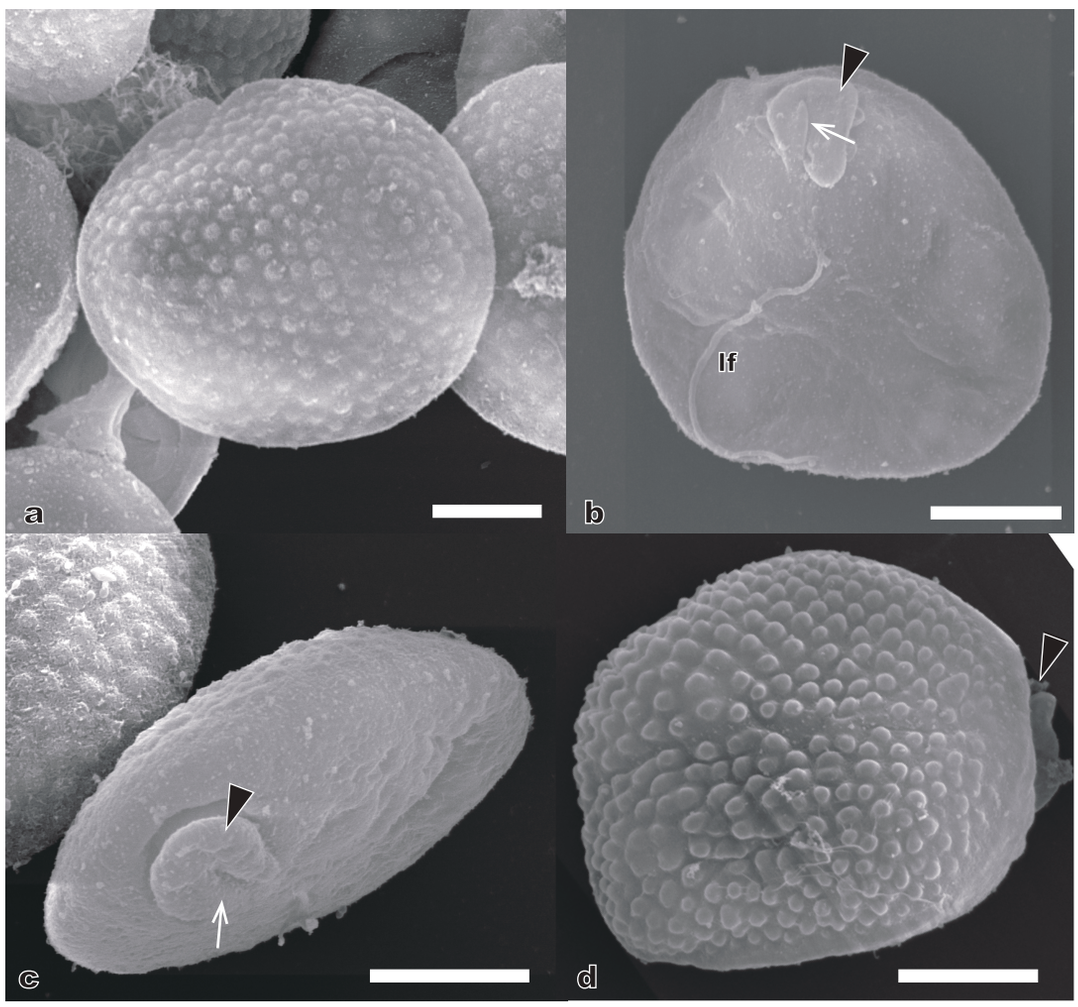


Fig. 5. *Testudodinium magnum* sp. nov. Scanning electron microscopy, based on the holotype SEM stub (SAP115075).
a. Dorsal view of the sessile cell. The episome is not visible. The dorsal surface of the hyposome has a pebbled appearance due to the presence of nodules.
b. Ventral view of the sessile cell. The episome (arrowhead) is embedded in the hyposome. It possesses the characteristic longitudinal furrow (arrow). The sulcus is not clearly visible, but the longitudinal flagellum (lf) arises from the centre of the cell.
c. Apical view of the sessile cell. The hyposome and episome (arrowhead) are separated by an incomplete cingulum. The longitudinal furrow (arrow) is visible in the ventral part of the episome, but the shape of sulcus is obscure.
d. Dorsal view of the motile cell. The tip of the episome is visible (arrowhead). The depressions between the nodules appear to form a cross-hatched pattern.
Scale bar = 10 µm.

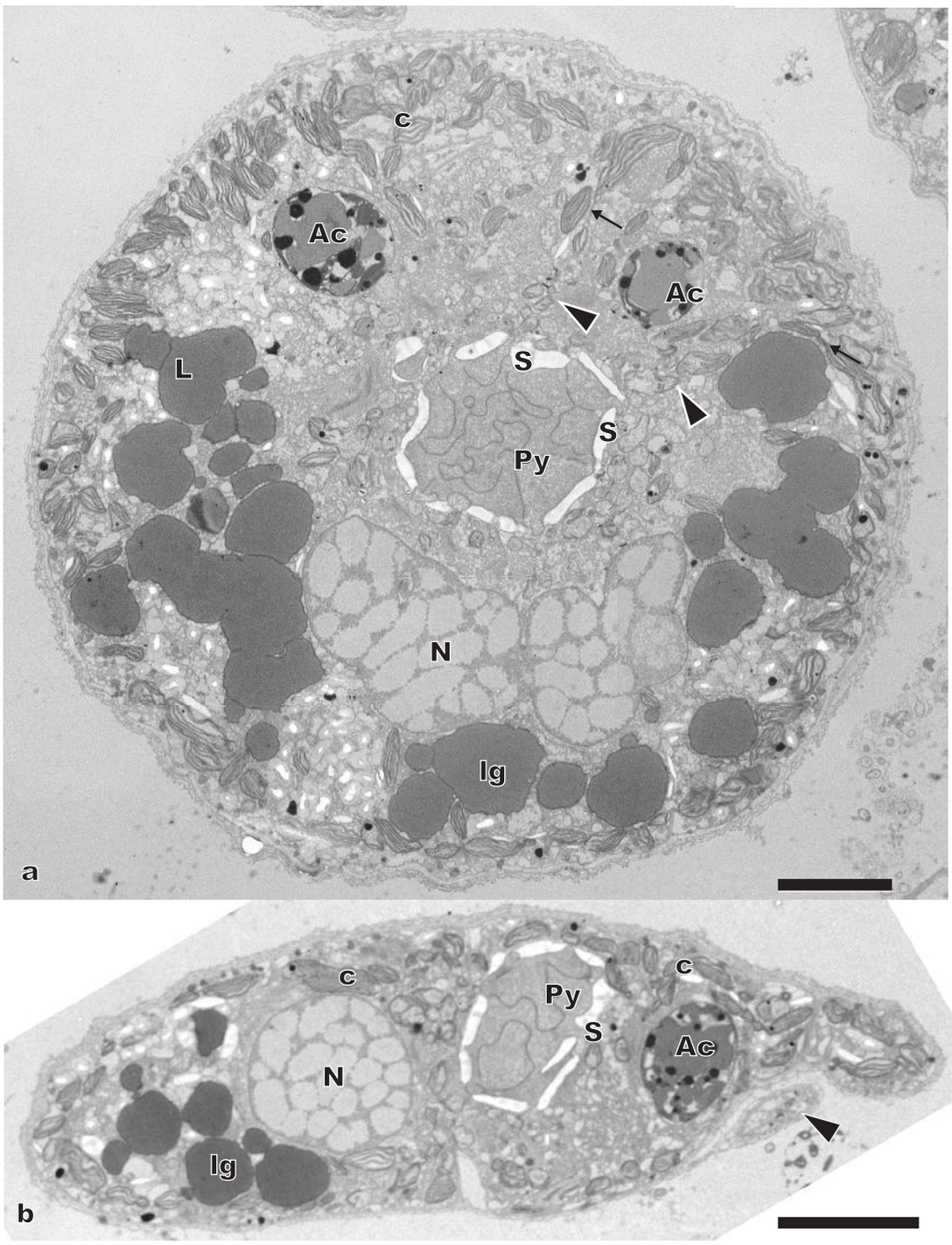


Fig. 6. *Testudodinium magnum* sp. nov. Transmission electron micrographs.
a. Longitudinal section through the cell. The pyrenoid (Py) is central, surrounded by a prominent starch sheath composed of multiple starch granules (S). The nucleus (N) is below the pyrenoid and appears to be lobed. Most of the granular chloroplast portions (c) are peripheral, but some of them radiate outwards from the pyrenoid (arrowheads). They are connected to each other by narrow areas and processes (arrows). Also present are electron-opaque lipid granules (lg) and accumulation bodies (Ac). Scale bar = 10 µm.
b. Longitudinal section through the cell in right-side view, showing dorsoventrally compressed nature of the cell. A part of episome (arrowhead) is visible. The pyrenoid (Py) and the nucleus (N) are visible. The chloroplasts (c) are peripheral. Also present are electron-opaque lipid granules (lg) and accumulation body (Ac). Scale bar = 10 µm.

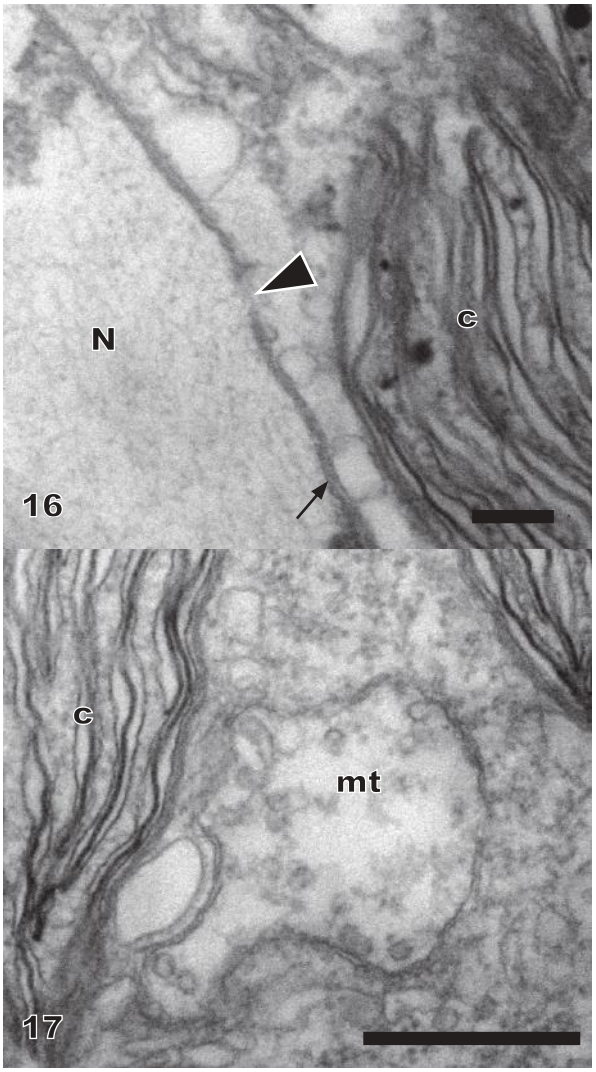


Fig. 7. *Testudodinium magnum* sp. nov. Transmission electron microscopy.
a. High magnification image of the nuclear membrane showing the typical double-membrane (arrow) and a simple nuclear pore (arrowhead). N: nucleus. Scale bar = 200 nm.
b. Typical dinoflagellate mitochondrion (mt) with tubular cristae. c: chloroplast. Scale bar = 500 nm.

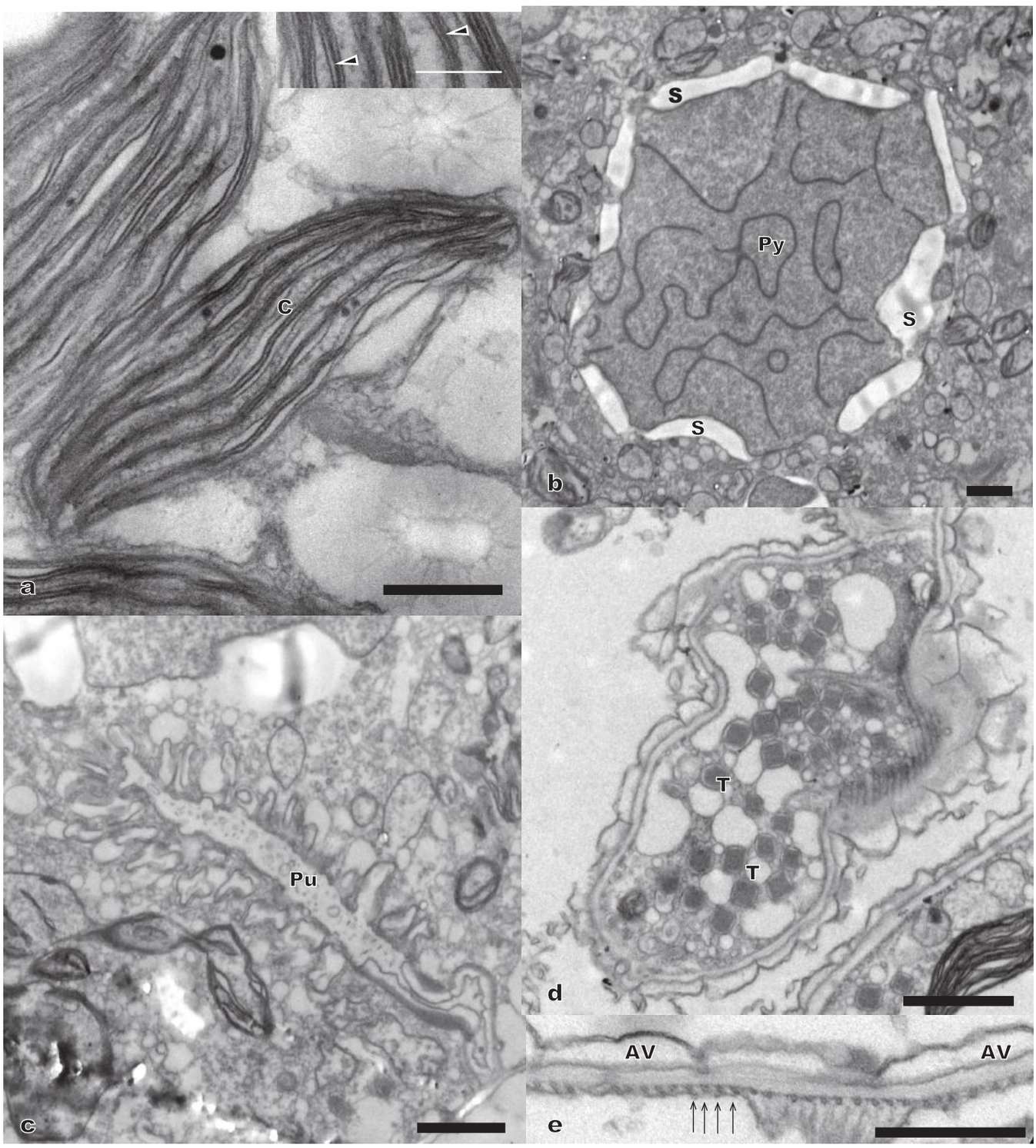


Fig. 8. *Testudodinium magnum* sp. nov. Transmission electron microscopy.
a. Close up of chloroplast (c). The chloroplast profiles contain lamellae comprised of three thylakoid bands. Scale bar = 500 nm. Inset, a part of a chloroplast with lamellae comprised of three and two (arrowheads) thylakoid bands. Scale bar = 100 nm.
b. Pyrenoid (Py) surrounded by multiple starch granules (S) and its matrix is traversed by variously curved thylakoids. Scale bar = 2 µm.
c. Pusule (Pu) consisting of tubular chamber and surrounding pusule vesicles. Scale bar = 1 µm.
d. Tangential section, showing a group of trichocysts (T) and small and polygonal nature of each amphiesmal vesicle. Scale bar = 1 µm.
e. Close-up of amphiesma. The amphiesmal vesicle (AV) is underlain by continuous electron opaque layer and immediately below, there are cytoskeletal microtubules (arrows point some of them). Scale bar = 500 nm.



Fig. 9. *Testudodinium magnum* sp. nov. Transmission electron microscopy, showing detail of props.
a. Lateral section through a cell showing the props (arrowheads). N: nucleus, Py: pyrenoid. Scale bar = 1 µm.
b. Part of nucleus (N), showing that a prop (arrowhead) penetrates into nucleus. Scale bar = 1 µm.
c. A single prop (arrowhead), connecting the dorsum and ventrum of the cell. Scale bar = 1 µm.
d. Close-up of a short prop (arrowhead) at the edge of the cell. The fibrous nature of the props is clearly visible. The both ends of the prop are connected to the continuous electron-translucent layer, but a distinction (arrow) can be seen at the junctions, suggesting both structures are not continuous. T: trichocyst. Scale bar = 1 µm.
e. The transverse section of a prop (arrowhead), penetrating the nucleus (N). Scale bar = 1 µm.

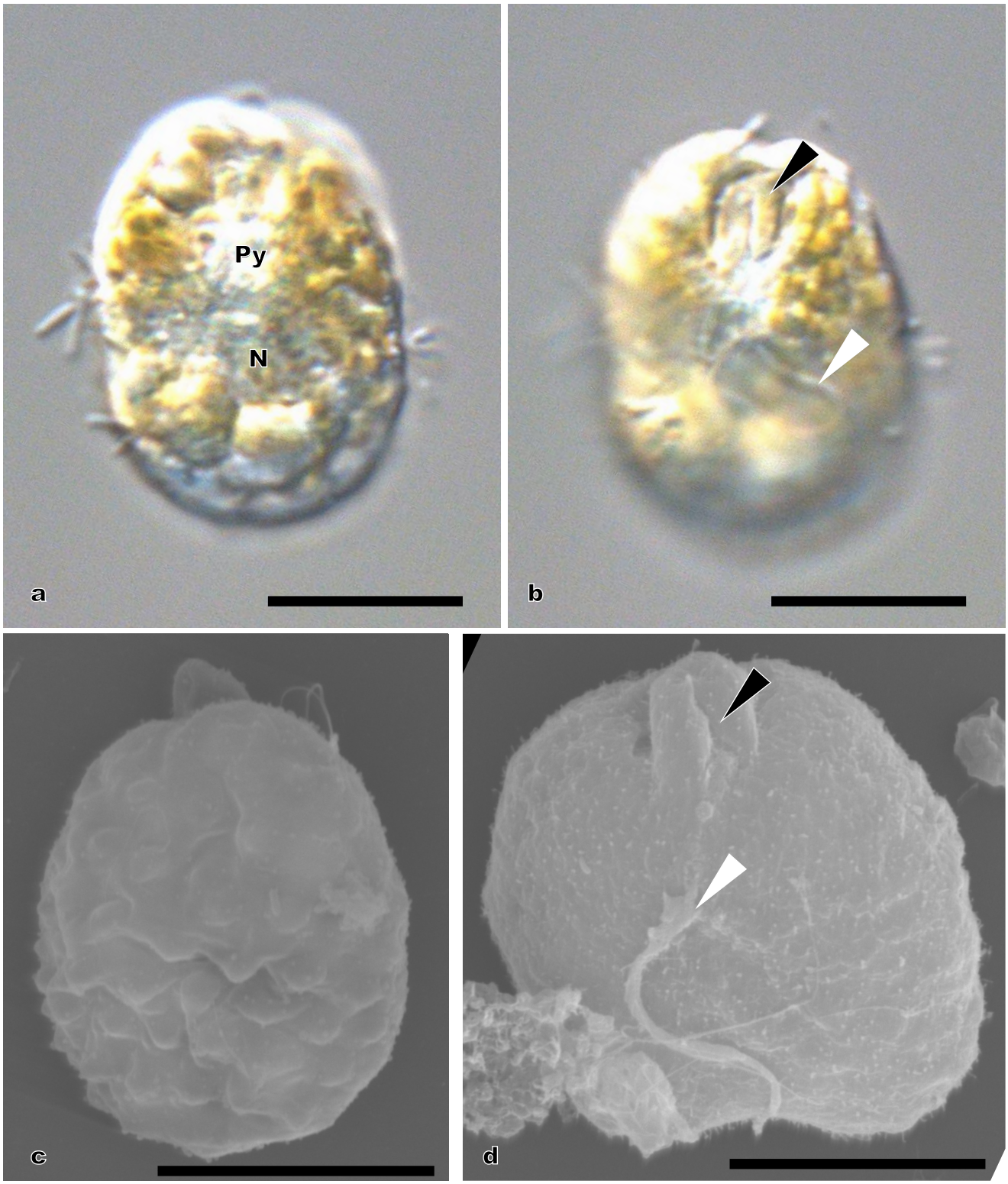


Fig. 10. *Testudodinium* sp. HG272. Light and scanning electron micrographs.
a. Dorsal view of a single cell. The pyrenoid (Py) is central, and the nucleus (N) is below it.
b. Ventral view of a single cell. The episome (solid arrowhead) has the longitudinal furrow characteristic of *Testudodinium*. The longitudinal flagellum (open arrowhead) is also seen.
c. Dorsal view of a sigle cell. The rugose dorsal hypotheca is typical of the magnum sub-clade.
d. Ventral view of a single cell. The episome (solid arrowhead) has the longitudinal furrow characteristic of *Testudodinium*. The longitudinal flagellum (open arrowhead) arises from the centre of the cell.
Scale bar = 10 µm.

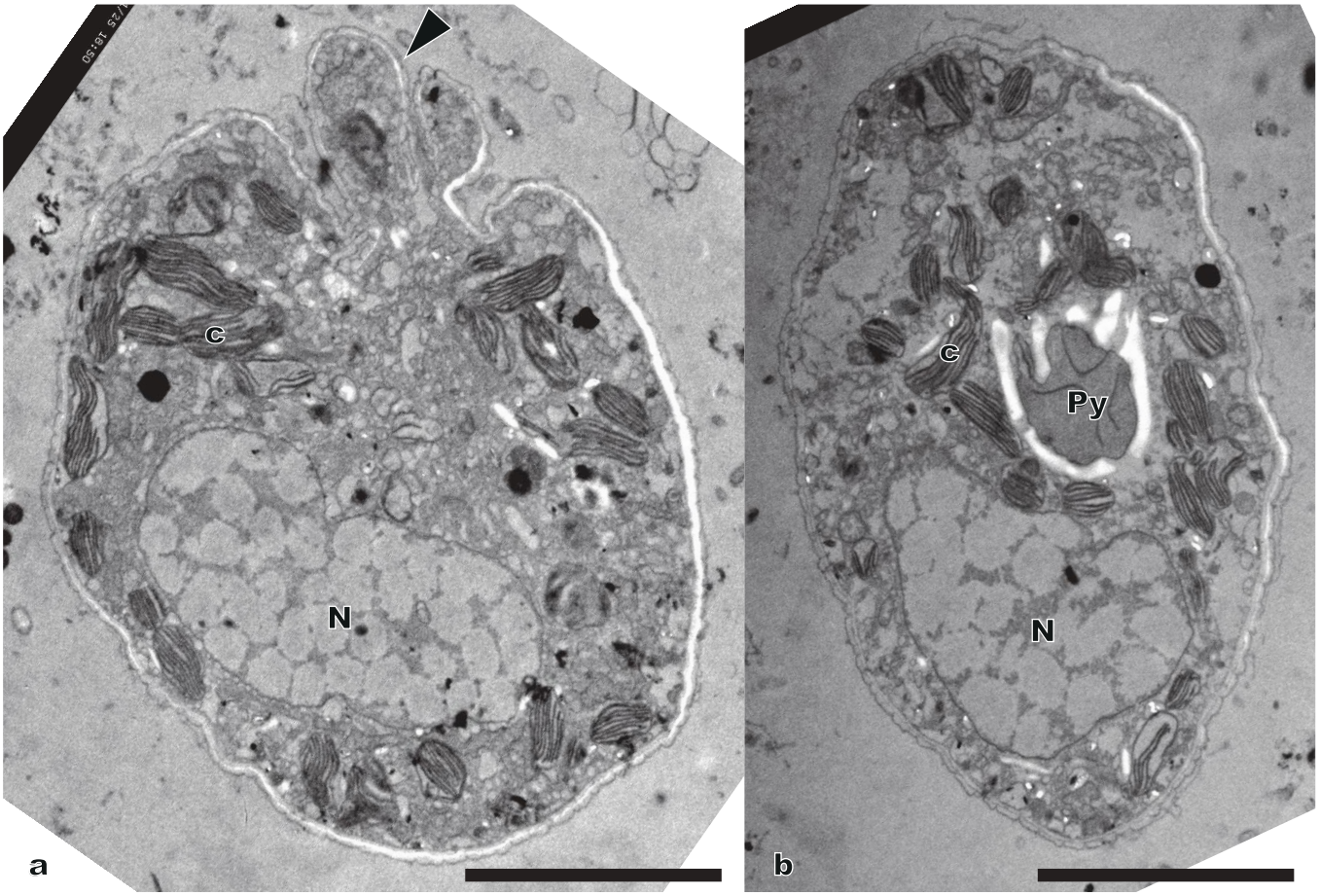


Fig. 11. *Testudodinium* sp. HG272. Transmission electron micrographs.
a. Longitudinal section of a cell in a lateral plane, showing the large posterior nucleus (N) and elongated chloroplasts (c) towards the periphery. The section passes through the episome (arrowhead), and the furrow can be seen at its apex.
b. Longitudinal section of a cell in a dorso-ventral plane. The pyrenoid (Py) is slightly above the centre of the cell, and the nucleus (N) is posterior. The elongated chloroplasts (c) surround the pyrenoid (Py) and are also found in the periphery of the cell.
Scale bar = 5 µm.

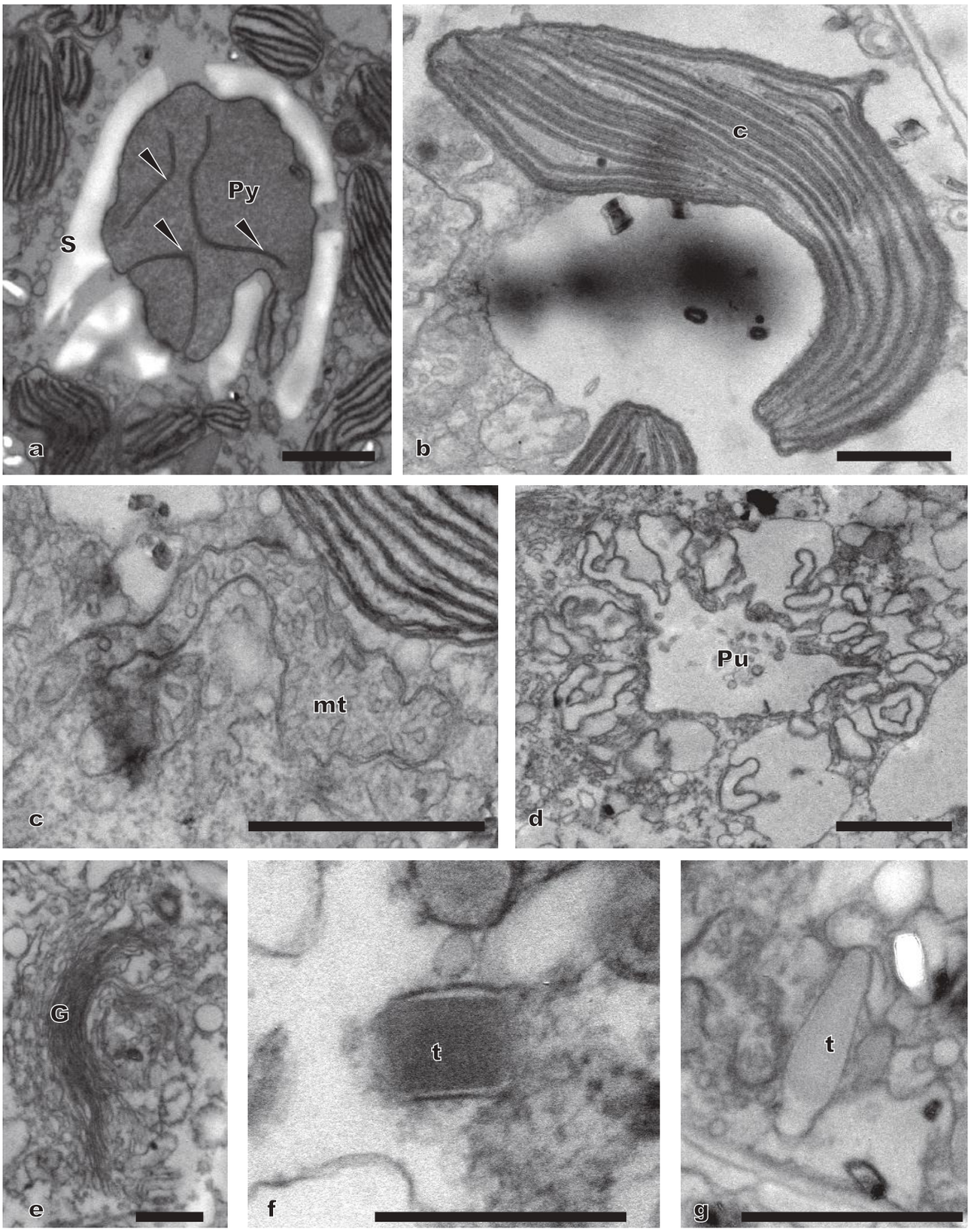


Fig. 12. *Testudodinium* sp. HG272. Transmission electron microscopy.
a. Pyrenoid (Py) surrounded by starch sheath (S); matrix containing thylakoid lamellae (arrowheads). Scale bar = 1 µm.
b. Elongate chloroplast (c) with thylakoids of three lamellae. Scale bar = 100 nm.
c. Typical dinoflagellate mitochodrion (mt). Scale bar = 1 µm.
d. Pusule (Pu) with central tubule surrounded by collecting vacuoles. Scale bar = 1 µm.
e. Golgi apparatus (G). Scale bar = 500 nm.
f. Trichocyst (t) in cross-section. Scale bar = 500 nm.
g. Trichocyst (t) in longitudinal section. Scale bar = 1 µm.

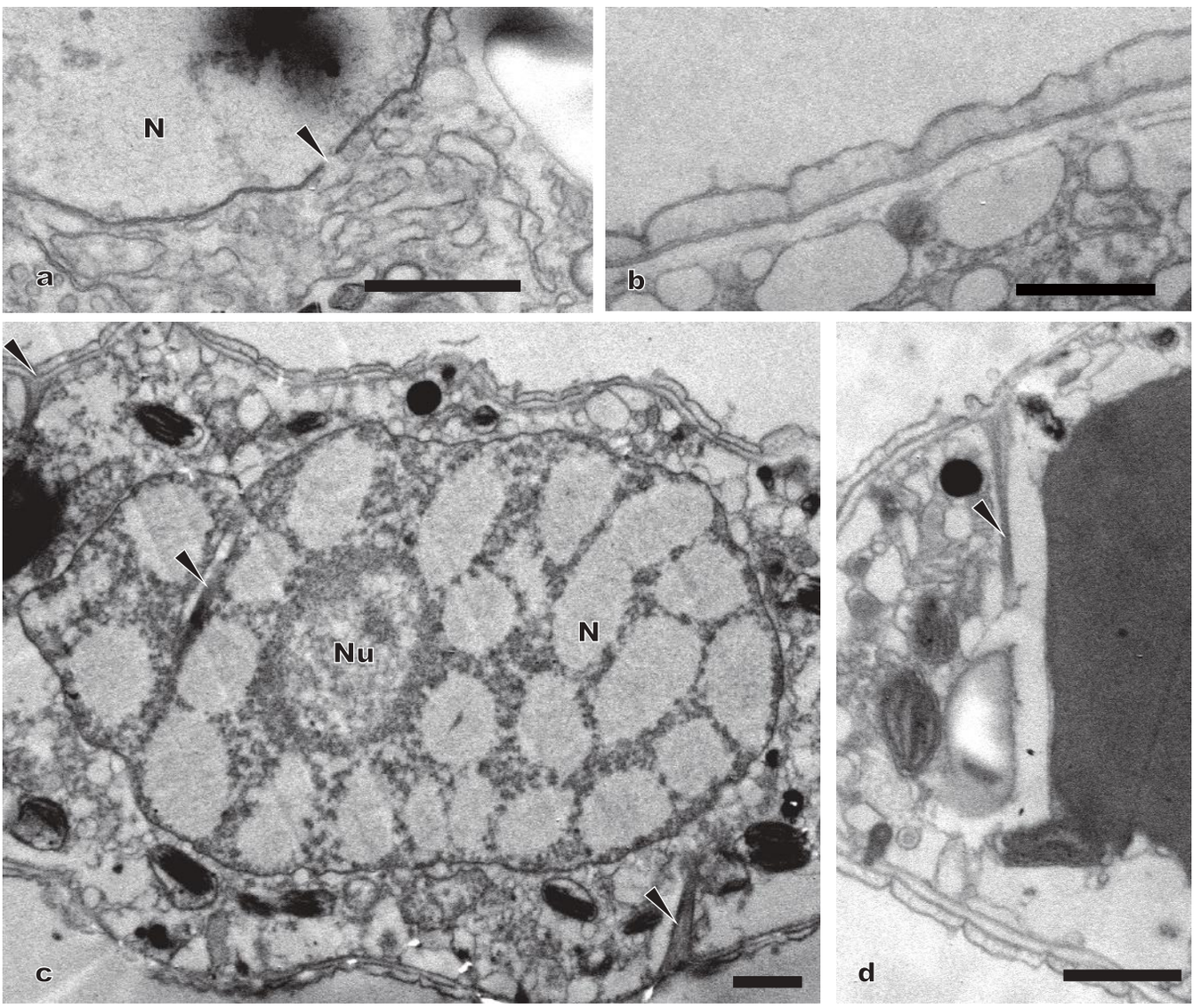


Fig. 13. *Testudodinium* sp. HG272. Transmission electron microscopy.
a. Nuclear envelope with a simple nuclear pore (arrowhead). N: nucleus. Scale bar = 100 nm.
b. Amphiesma showing individual amphiesmal vesicles underlain by a continuous electron-transparent layer. Scale bar = 500 nm.
c. Portion of a transverse section through a single cell, showing the internal props (arrowheads). One is observed passing through the nucleus. N: nucleus, Nu: nucleolus. Scale bar = 1 µm.
d. Portion of a transverse section through a single cell, showing an internal prop (arrowhead) near the margin of the cell. Scale bar = 1 µm.

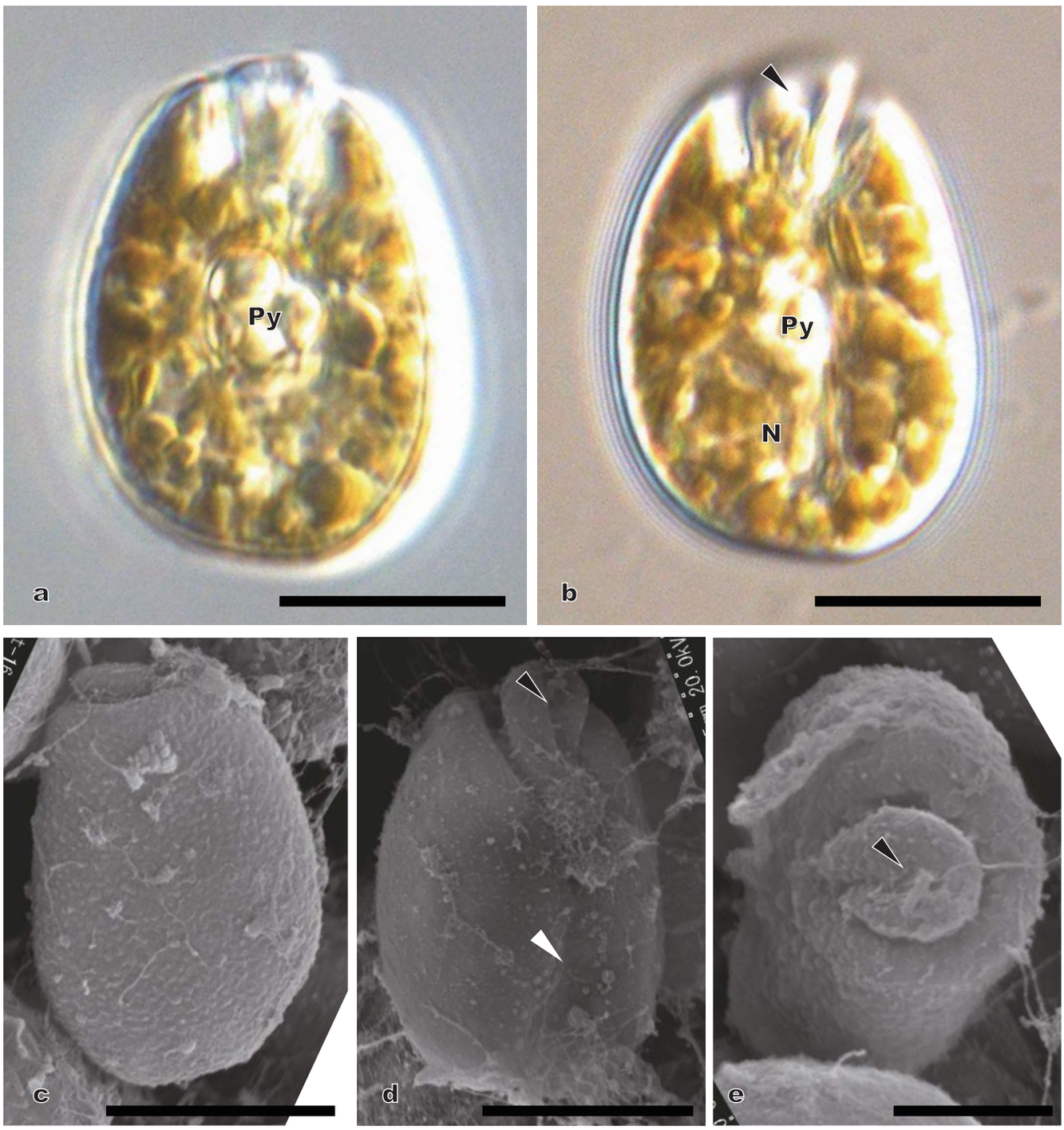


Fig. 14. *Testudodinium* sp. HG275. Light and scanning electron micrographs.
a. Dorsal view. The pyrenoid (Py) is centrally located. Scale bar = 10 µm.
b. Ventral view. The pyrenoid (Py) is centrally located, the nucleus (N) is posterior, and the episome possesses the characteristic ventral furrow (solid arrowhead). Scale bar = 10 µm
c. Dorsal view. The dorsal surface possesses numerous small nodules typical of the magnum subclade. Scale bar = 10 µm.
d. Ventral view. The sulcus is broad and shallow (open arrowhead) and the episome possesses the typical ventral furrow (solid arowhead). Scale bar = 10 µm.
e. Apical view. The external structure of the episome and the location of the furrow are depicted. Scale bar = 5 µm.



Fig. 15. *Testudodinium* sp. HG275. Transmission electron micrograph. Longitudinal section of the entire cell in a lateral plane. The nucleus (N) is posterior. The pyrenoid (Py) is surronded by a continuous starch steath (S) and, in this instance, is atypically situated to one side of the nucleus. Chloroplasts (c) are elongate and are located in the periphery of the cell. Scale bar = 5 μm

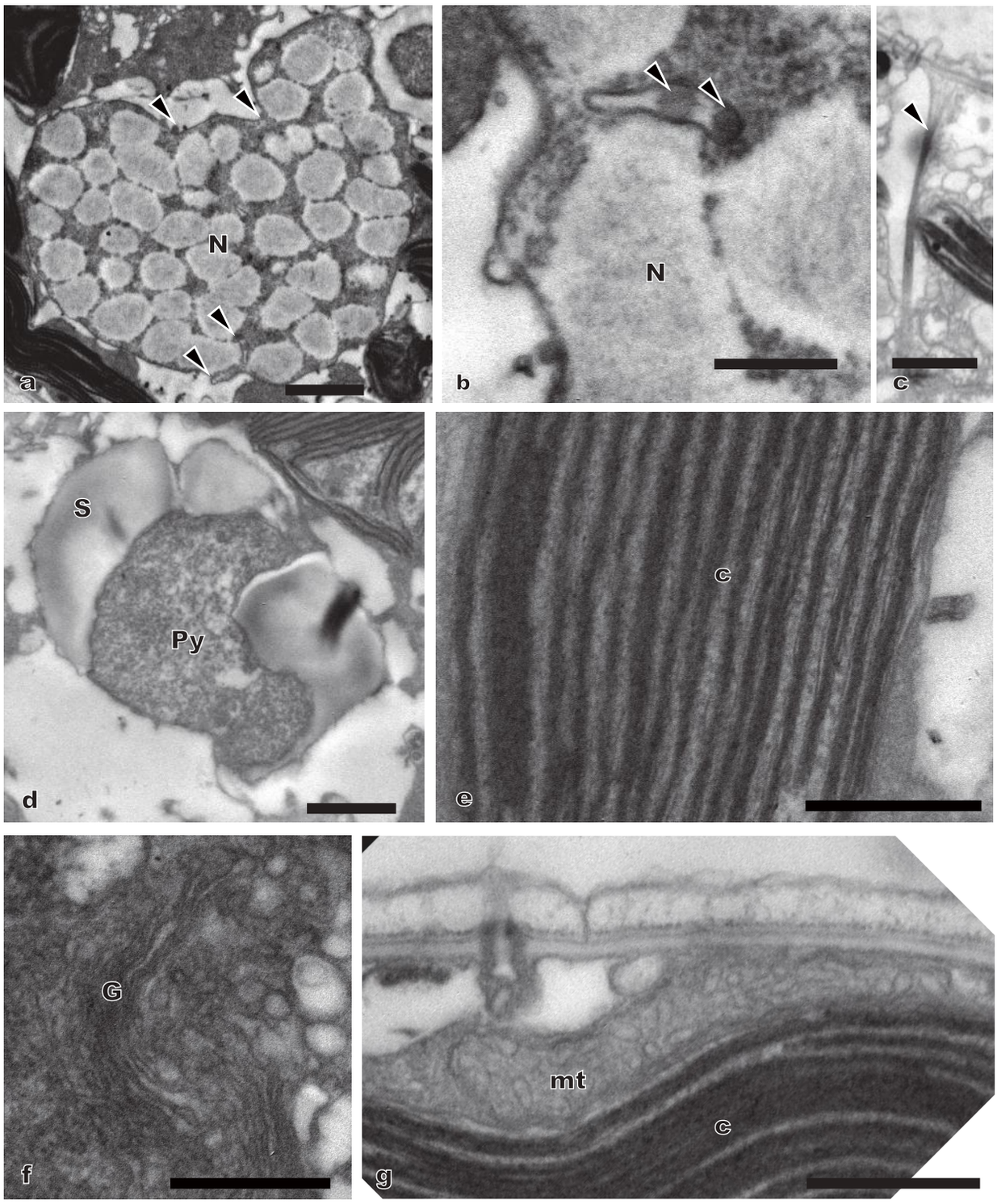


Fig. 16. *Testudodinium* sp. HG275. Transmission electron micrographs.
a. Section of a typical dinoflagellate nucleus (N). Arrowheads indicate props around and within the nucleus. Scale bar = 2 µm.
b. Enlarged section of the nucleus (N) showing props (arrowheads) passing through the nucleus. Scale bar = 500 nm.
c. Portion of an internal prop (arrowhead) attached to the basal layer. Scale bar = 1 µm.
d. Pyrenoid (Py) surrounded by a starch sheath (S). Scale bar = 1 µm
e. Portion of a chloroplast (c) showing the thylakoids with three lamellae. Scale bar = 500 nm
f. Golgi apparatus (G). Scale bar = 500 nm.
g. Typical mitochondrion (mt) and the amphiesma showing amphiesmal vesicles underlain by a continuous electron-translucent layer. c: chloroplast. Scale bar = 500 nm.

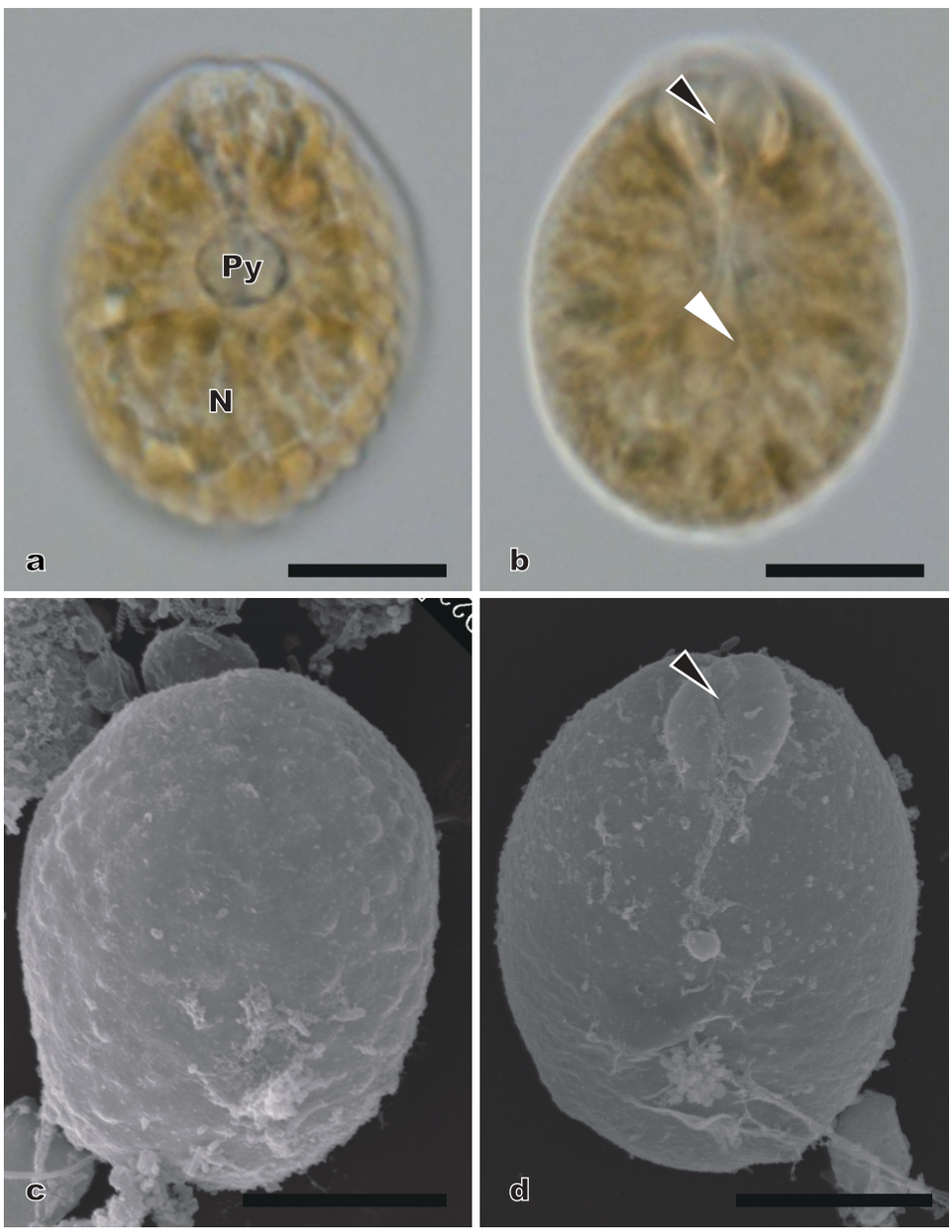


Fig. 17. *Testudodinium* sp. HG312. Light and scanning electron micrographs.
a. Dorsal view. The pyrenoid (Py) is centrally located, and the nucleus is (N) posterior. The rugose nature of the dorsal surface of the hyposome is visible.
b. Ventral view. The episome possesses the typical ventral furrow (solid arrowhead). The longitudinal flagellum (open arrowhead) is also seen.
c. Dorsal view. The rugose dorsal surface of the hyposome is typical of the magnum sub-clade.
d. Ventral view. The episome possesses the ventral furrow typical to the genus. The sulcus is not distinguishable.
Scale bar = 10 µm.

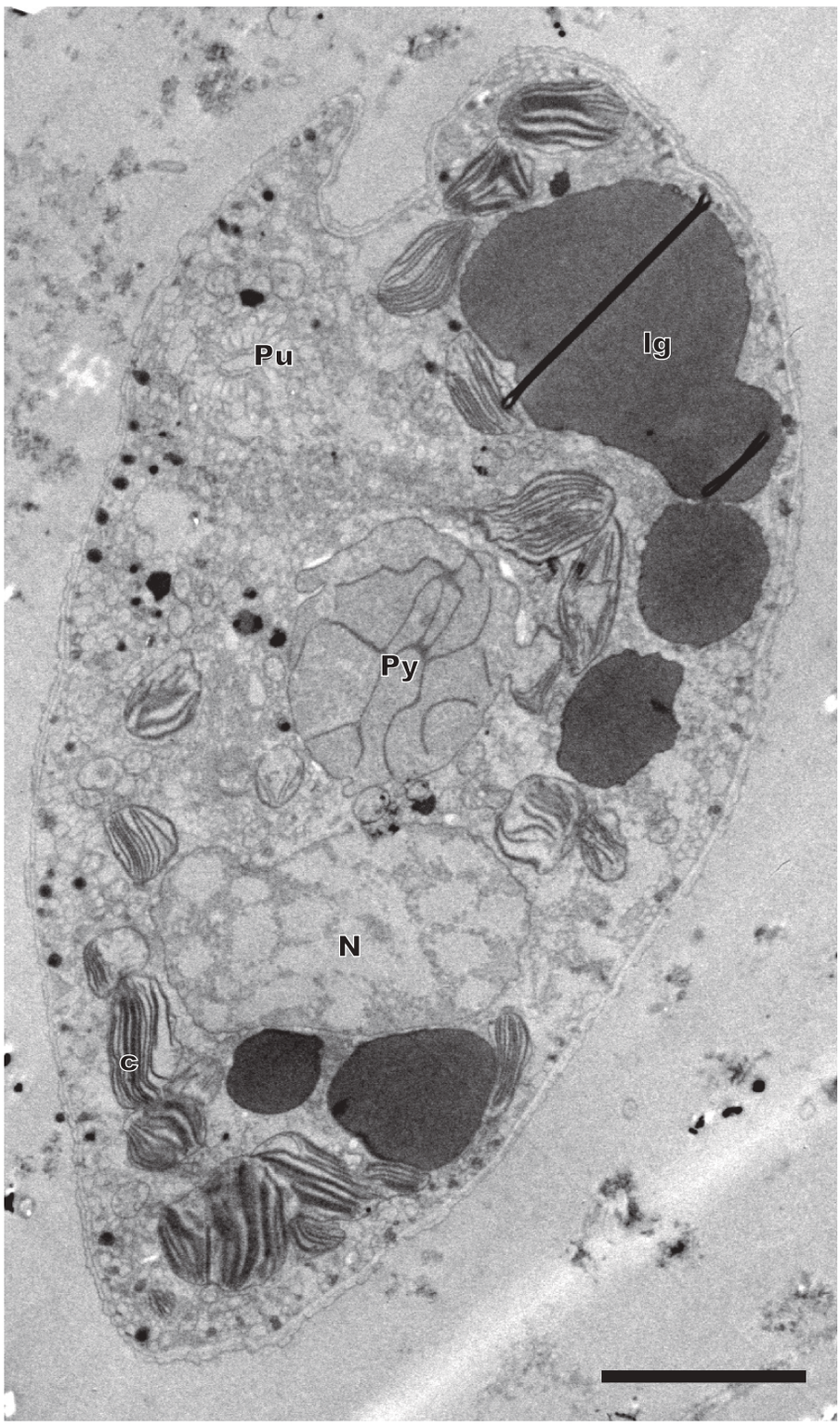


Fig. 18. *Testudodinium* sp. HG312. Transmission electron microscopy. Longitudinal section through a cell in a dorso-ventral plane. The pyrenoid (Py) is centrally located. The nucleus (N) is posterior. Chloroplasts (c) surround the pyrenoid and are also forund in the periphery of the cell. Electron-opaque inclusions that may be lipid granules (lg) are also present. A pusule (Pu) with central tubule surrounded by collecting vacuoles is also present. Scale bar = 5 μm.

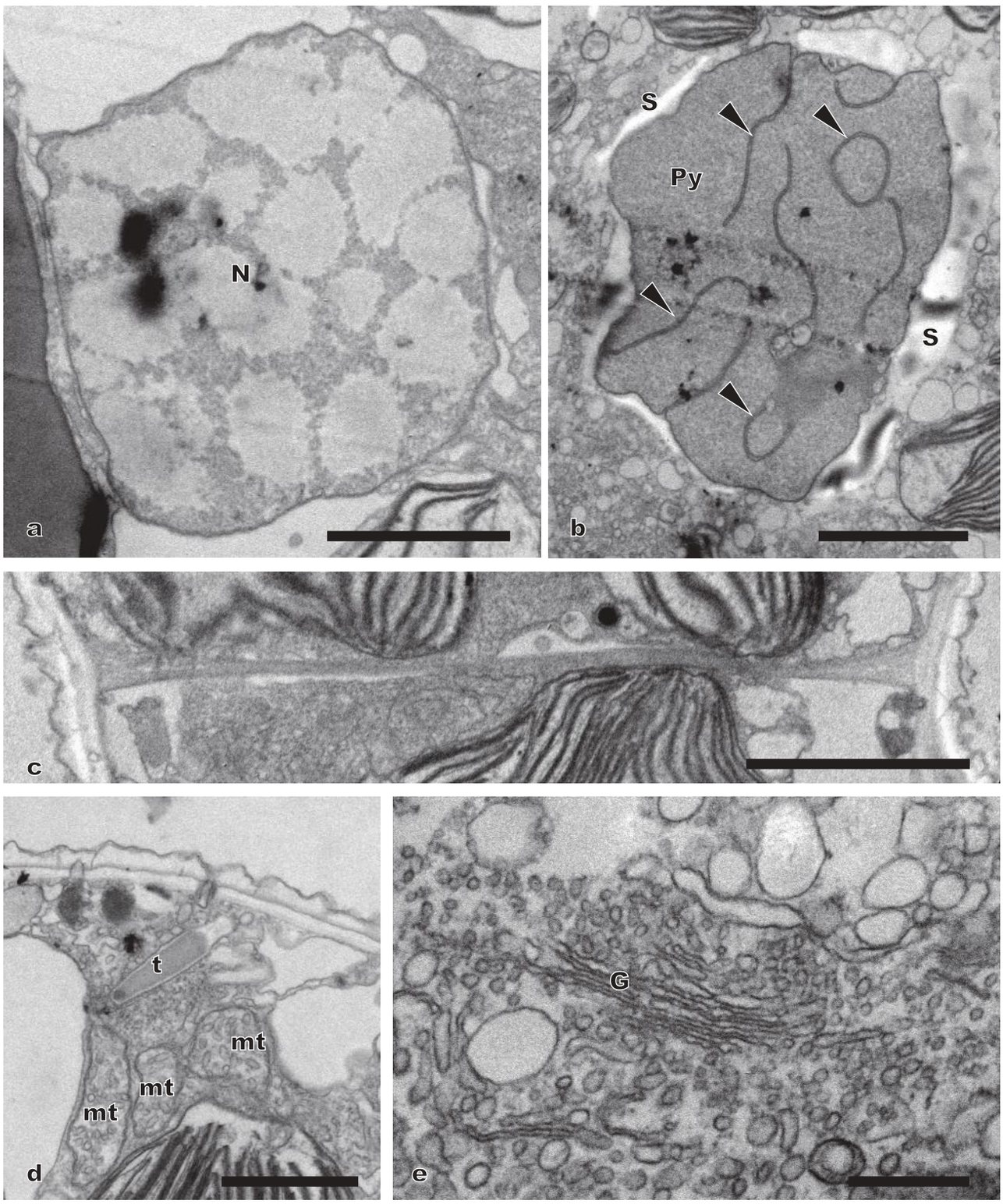


Fig. 19. *Testudodinium* sp. HG312. Transmission electron microscopy.
a. Typical dinoflagellate nucleus (N). Scale bar = 2µm.
b. Pyrenoid (Py) surrounded by a thin starch sheath (S). The pyrenoid matrix contains loose thylakoid lamellae (arrowheads). Scale bar = 2 µm.
c. Internal prop spanning the thickness of the cell. It is fibrous and distinct. Scale bar = 2 µm.
d. Trichocyst (t), mitochondria (mt), and the amphiesma. The amphiesmal vesicles are underlain by a continuous electron-transparent layer. Scale bar = 1 µm.
e. Golgi apparatus (G). Scale bar = 500 nm.

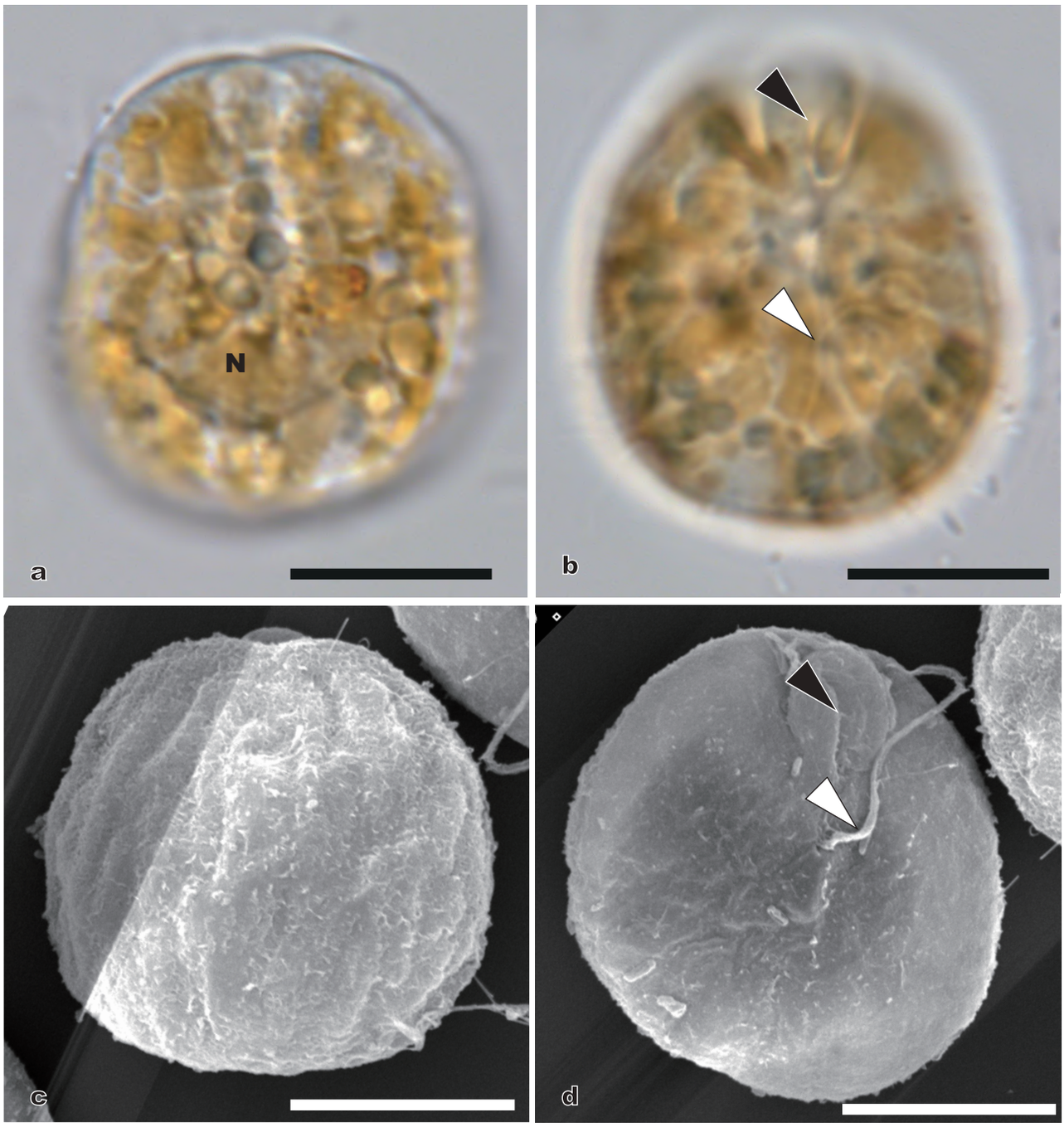


Fig. 20. *Testudodinium* sp. HG230. Light and scanning electron micrographs.
a. Dorsal view. The dorsal ribs on the hyposome is typical for the corrugatum sub-clade. The nucleus (N) is posterior. The pyrenoid is not visible.
b. Ventral view. The episome possesses the ventral furrow (solid arrowhead) typical of the genus. The longitudinal flagellum (open arrowhead) is also present.
c. Dorsal view. The dorsal ribs are present but are not well defined.
d. Ventral view. The ventral furrow on the episome (solid arrowhead) is typical of the genus. The longitudinal flagellum (open arrowhead) is present and arises from the centre of the cell. Traces of the transverse flagellum are present around the episome. The sulcus cannot be distinguished.
Scale bar =10 μm.

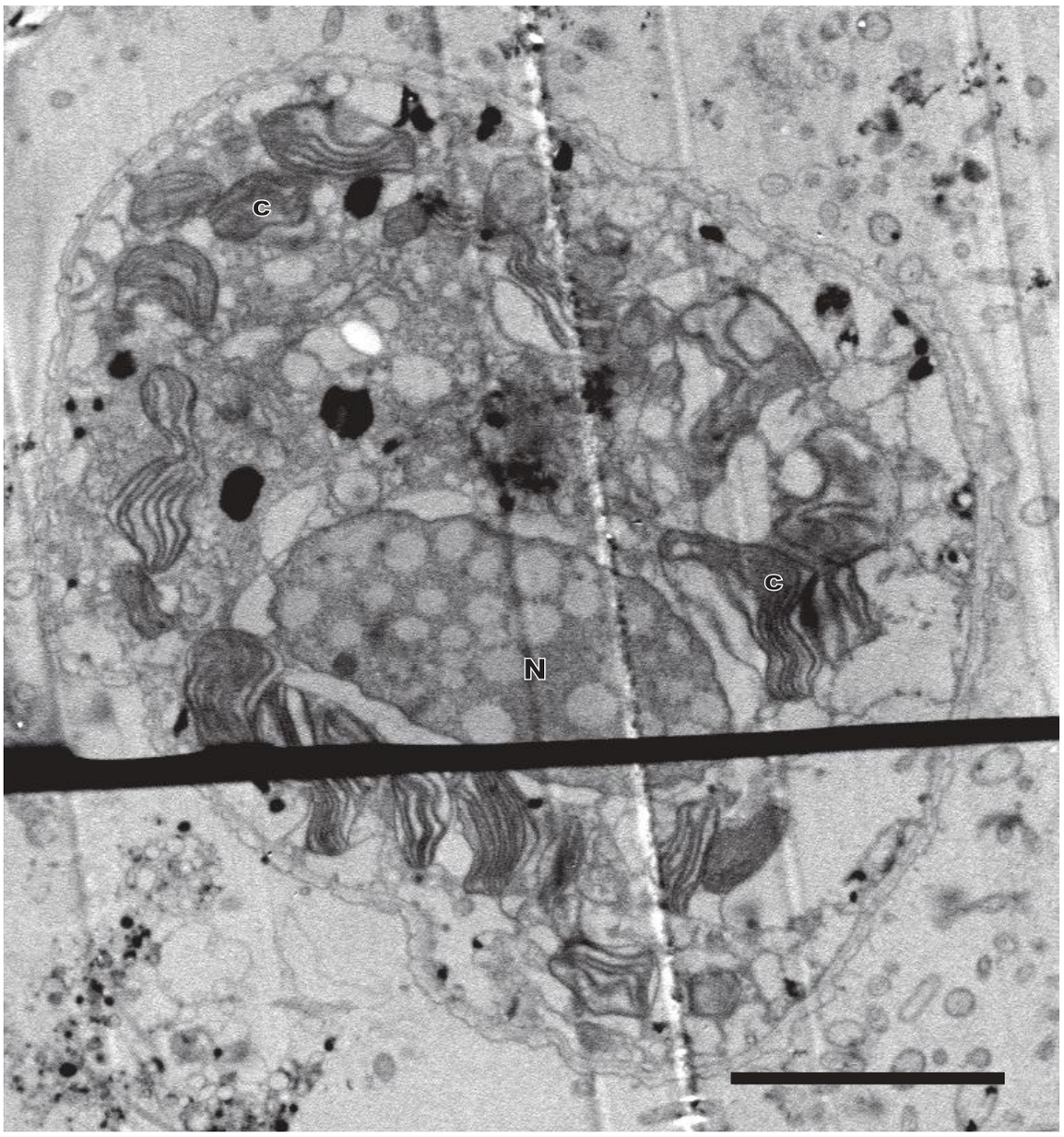


Fig. 21. *Testudodinium* sp. HG230. Transmission electron micrograph. Longitudinal section. The nucleus (N) is posterior. The chloroplasts (c) are elongated and towards the periphery of the cell. Scale bar = 5 μm.

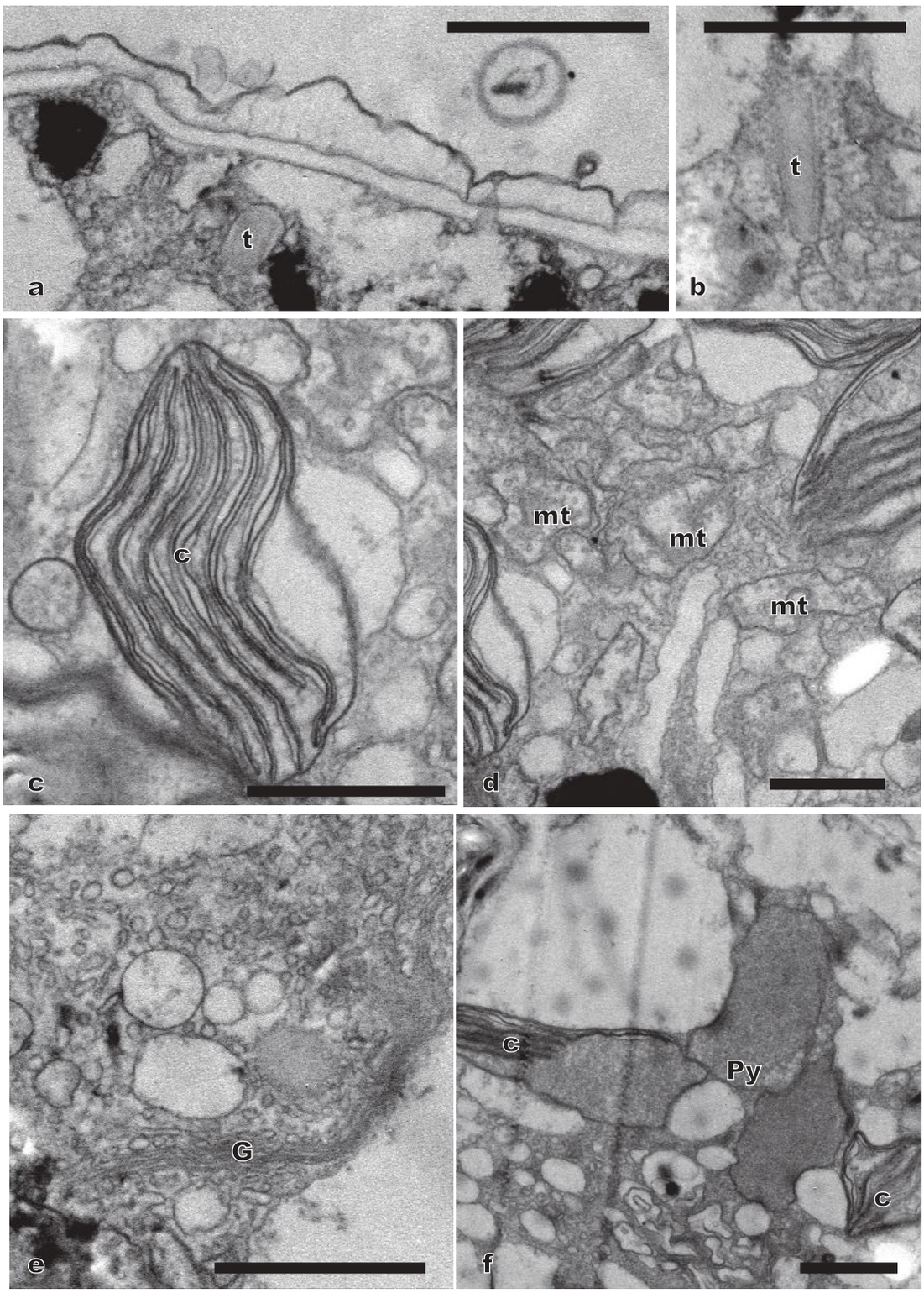


Fig. 22. *Testudodinium* sp. HG230. Transmission electron micrographs.
a. Trichocyst (t) and amphiesma. The amphiesmal vesicles are underlain by a continuous electron-transparent layer.
b. Trichocyst (t), longitudinal section.
c. Elongate chloroplast (c) with thylakoids with three lamellae.
d. Mitochondria (mt).
e. Golgi apparatus (G).
f. Pyreniod complex (Py), composed of pyrenoids of the ends of multiple chloroplasts (c).
Scale bar = 1 μm.

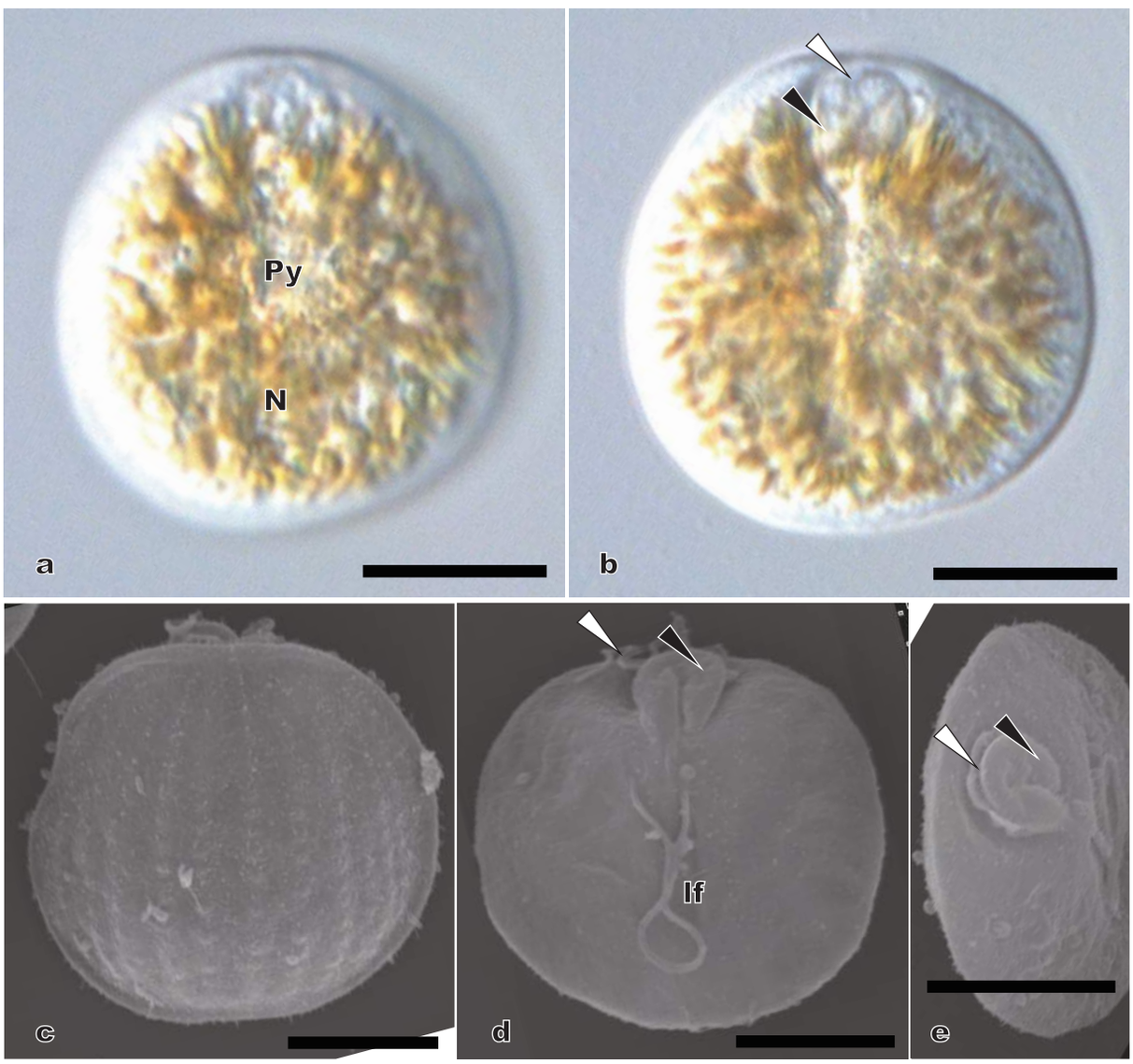


Fig. 23. *Testudodinium* sp. HG304. Light and scanning electron micrographs.
a. Dorsal view. The pyrenoid (Py) is central and the nucleus (N) posterior.
b. Ventral view. The ventral furrow on the episome (solid arrowhead) typical to the genus is not visible. The transverse flagellum (open arrowhead) is present in the cingulum.
c. Dorsal view. The dorsal ribs on the hyposome are typical of the corrugatum sub-clade.
d. Ventral view. The ventral furrow on the episome (solid arrowhead) is typical to the genus. The transverse flagellum (open arrowhead) and the longitudinal flagellum (lf) are present.
e. Apical view. The positions of the episome (solid arrowhead), transverse flagellum (open arrowhead), and hyposome relative to each other are depicted.
Scale bar = 10 µm.

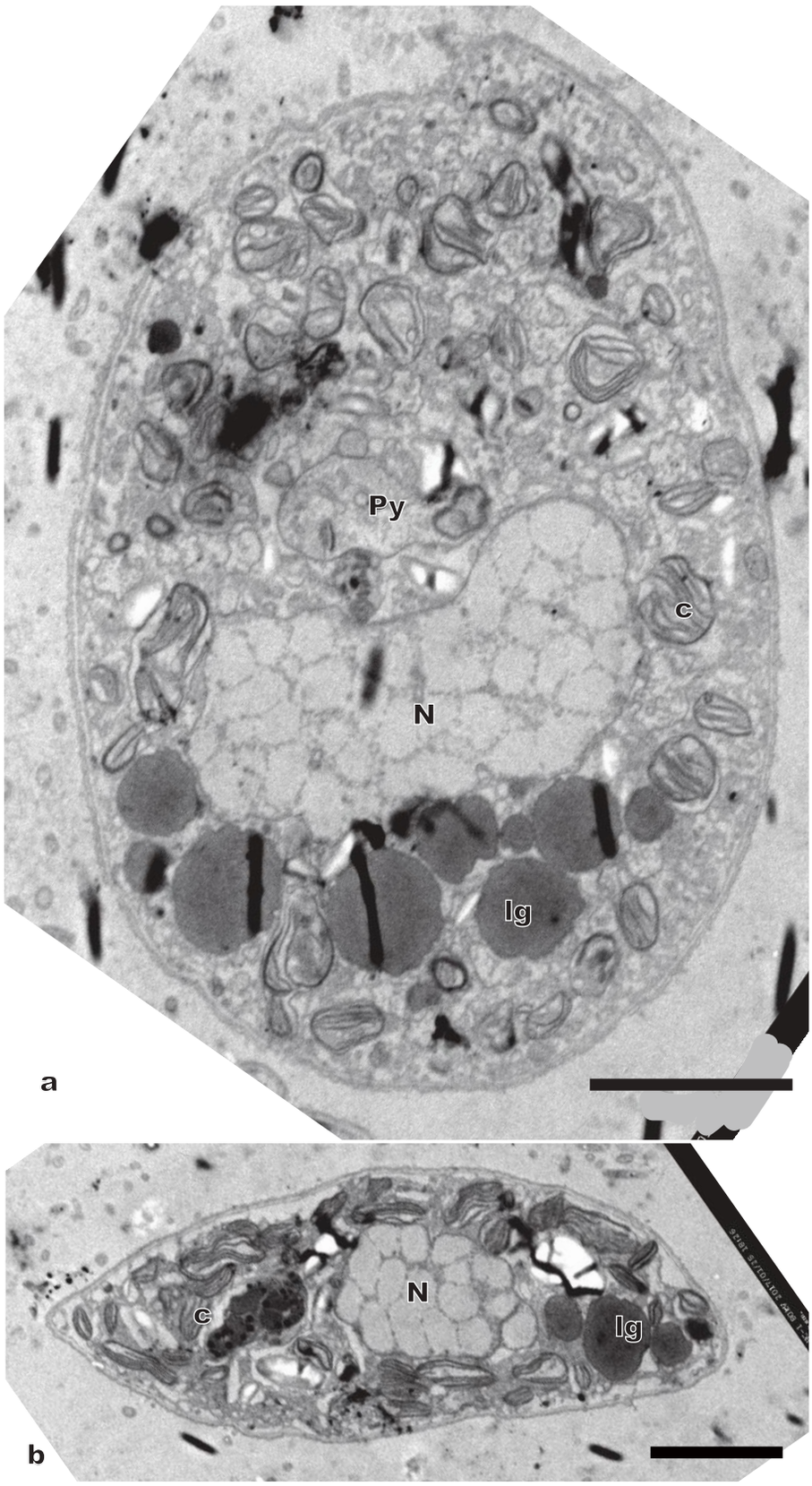


Fig. 24. *Testudodinium* sp. HG304. Transmission electron micrographs.
a. Longitudinal section in a lateral plane. The pyrenoid (Py) is central, the nucleus (N) is posterior, the choloroplasts (c) surround the pyrenoid and are peripheral. Lipid granules (lg) are found posterior to the nucleus.
b. Longitudinal section in a dorso-ventral plane. The nucleus (N) appears more central, with chloroplasts (c) peripheral and lipid granules (lg) posterior.
Scale bar = 5 μm.

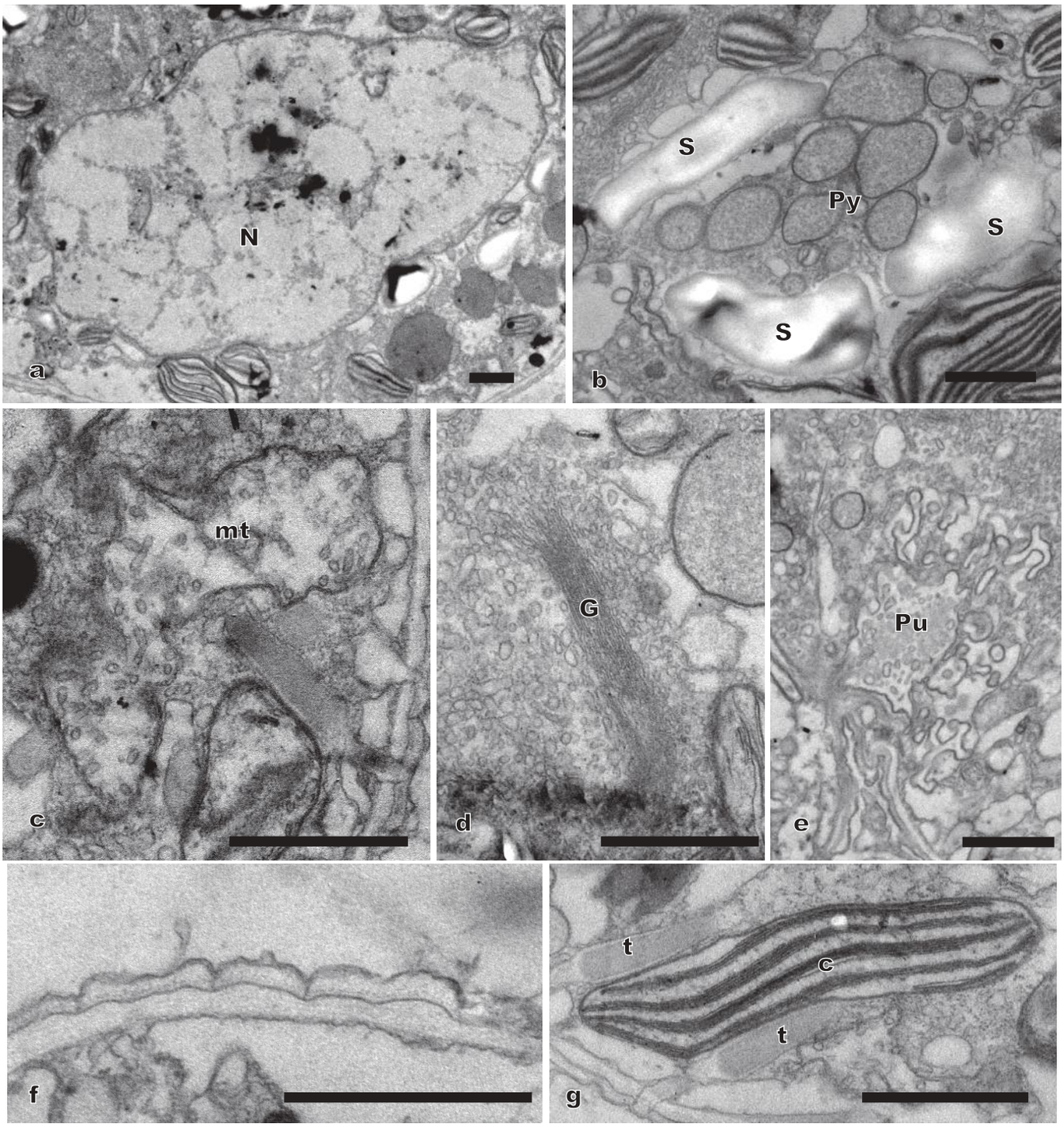


Fig. 25. *Testudodinium* sp. HG304. Transmission electron micrographs.
a. Typical dinoflagellate nucleus (N).
b. Pyrenoid complex (Py), composed of numerous pyrenoids, surrounded by a starch sheath (S).
c. Mitochondrion (mt).
d. Golgi apparatus (G).
e. Pusule (Pu) comprised of a central collecting tubule and collecting vesicles.
f. Amphiesma. The amphiesmal vesicles are underlain by a continuous, electron-transparent layer.
g. Elongate chloroplasts (c) with thylakoids of three lamellae, and trichocysts (t).
Scale bar = 1 μm.

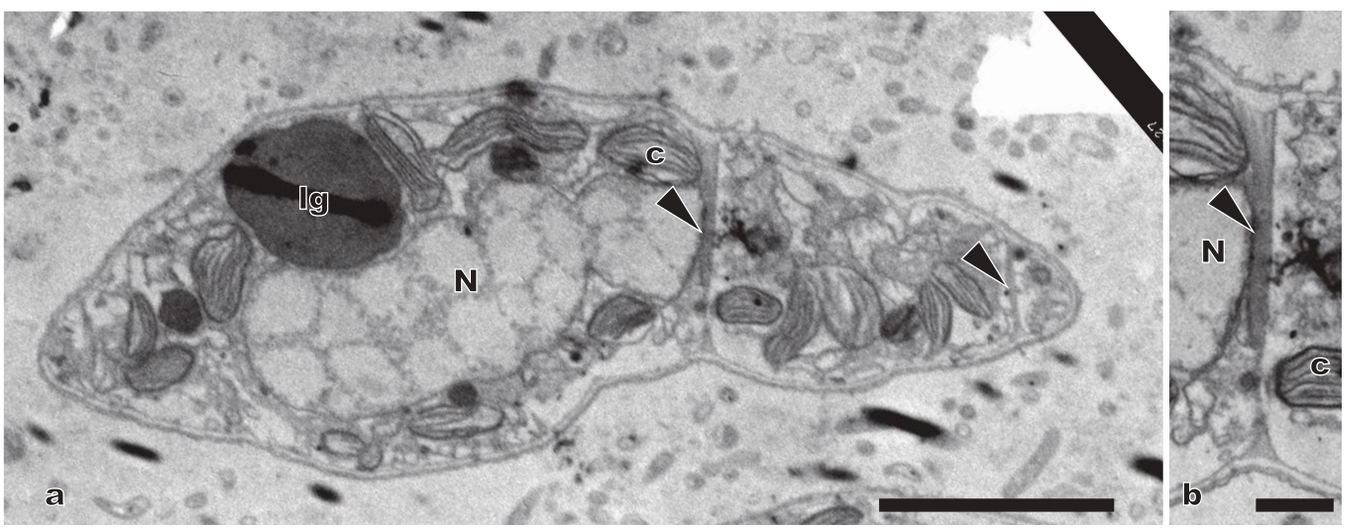


Fig. 26. *Testudodinium* sp. HG304. Transmission electron micrographs.

a. Longitudinal section through a dorso-ventral plane showing internal props (arrowheads) spanning the thickness of the cell. Scale bar = 5 µm.

b. Close-up of a single prop (arrowhead). It is fibrous in nature, and is separated from the continuous layer underlying the amphiesma by a distinction. Scale bar = 1 µm

N: nucleus, c: chloroplast, lg: lipid granules.

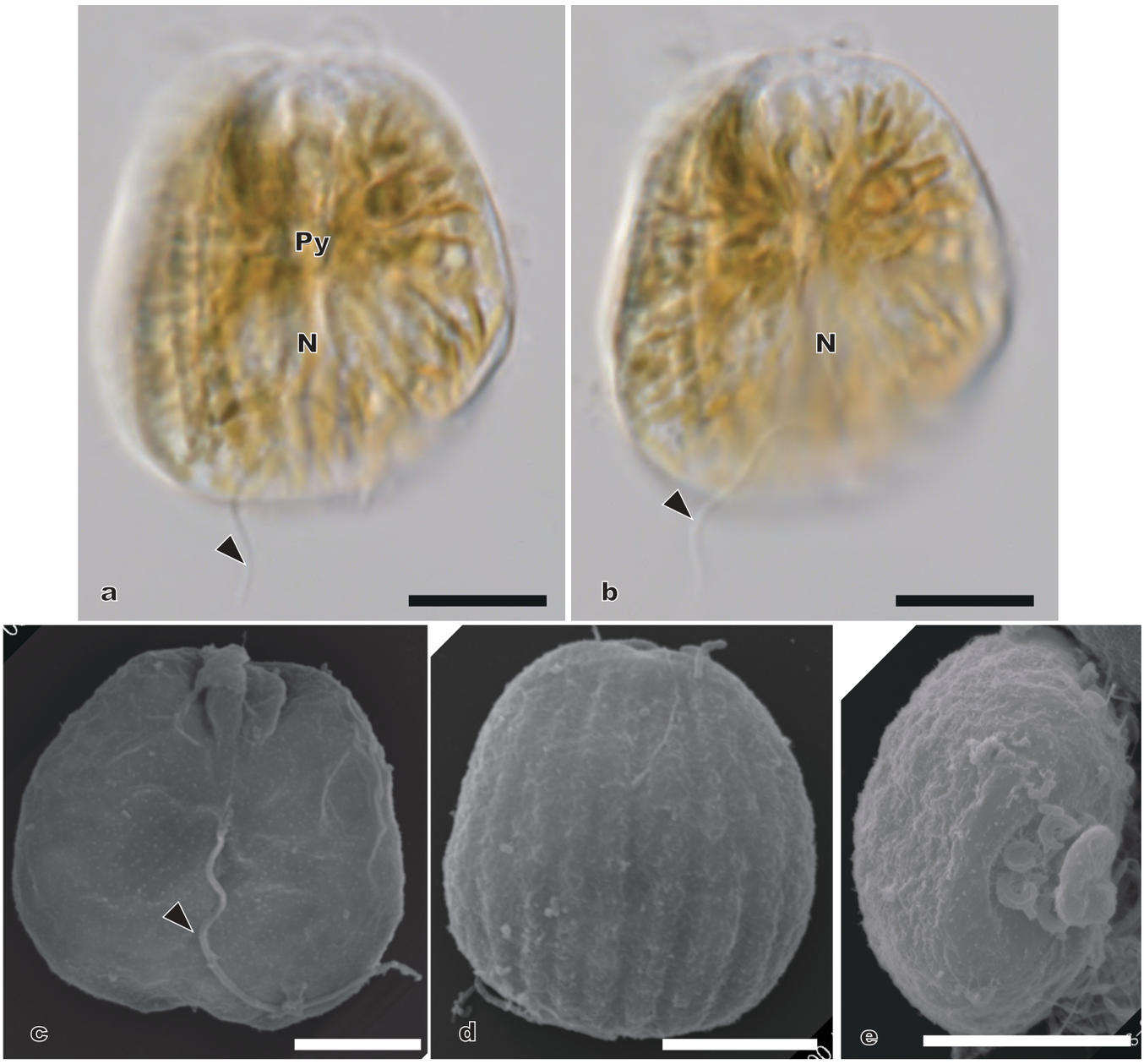


Fig. 27. *Testudodinium corrugatum* NY050. Light and scanning electron mirographs.
a. Dorsal view. The pyrenoid (Py) is central and the nucleus (N) posterior. The dorsal ribs are the identifying feature of *T. corrugatum*. The longitudinal flagellum (arrowhead) is present in this focal plane.
b. Ventral view. The episome is small and symmetrical. The longitudinal flagellum (arrowhead) is present. N: nucleus.
c. Ventral view. The episome possesses the ventral furrow typical of the genus. The longitudinal flagellum (arrowhead) arises from the centre of the cell.
d. Dorsal view. The dorsal ribs on the hyposome are currently the identifying feature of *Testudodinium corrugatum*.
e. Apical view. The transverse flagellum is situated within the cingulum, between the episome and the hyposome.
Scale bar = 10 μm.

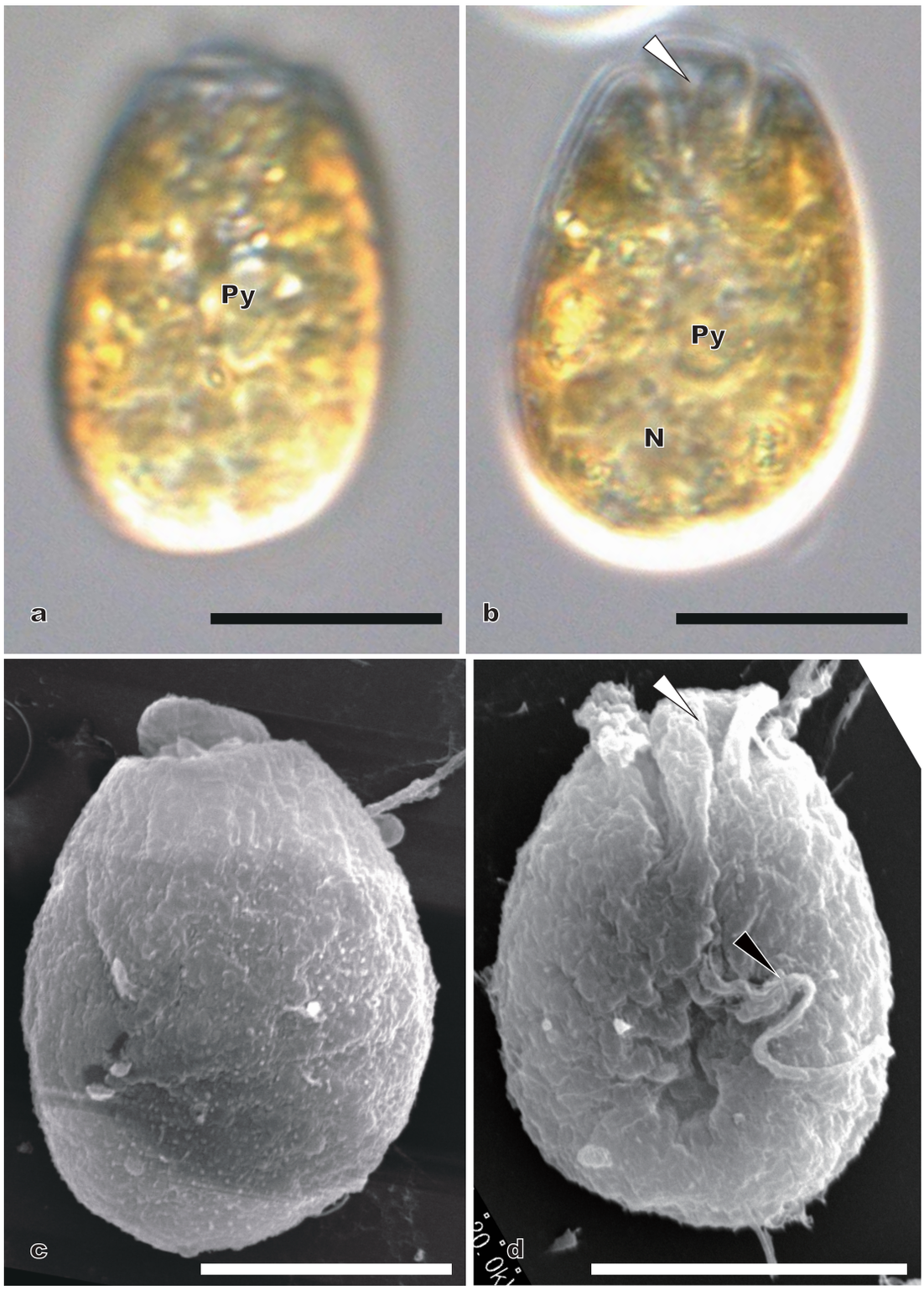


Fig. 28. *Testudodinium* cf. *maedaense* HG273. Light and scanning electron micrography.
a. Dorsal view. The pyrenoid (Py) is central. The dorsal surface of the hyposome is smooth.
b. Ventral view. The episome possesses the ventral furrow (open arrowhead) that is typical of the genus. The nucleus (N) is posterior. Py: pyrenoid.
c. Dorsal view. The dorsal surface of the hyposome is smooth and the sac-like shape of the cell is typical of the maedaense sub-clade.
d. Ventral view. The episome possess the ventral furrow (open arrowhead) that is typical of the genus. The longitudinal flagellum (solid arrowhead) arises from the centre of the cell.
Scale bar = 10 µm.

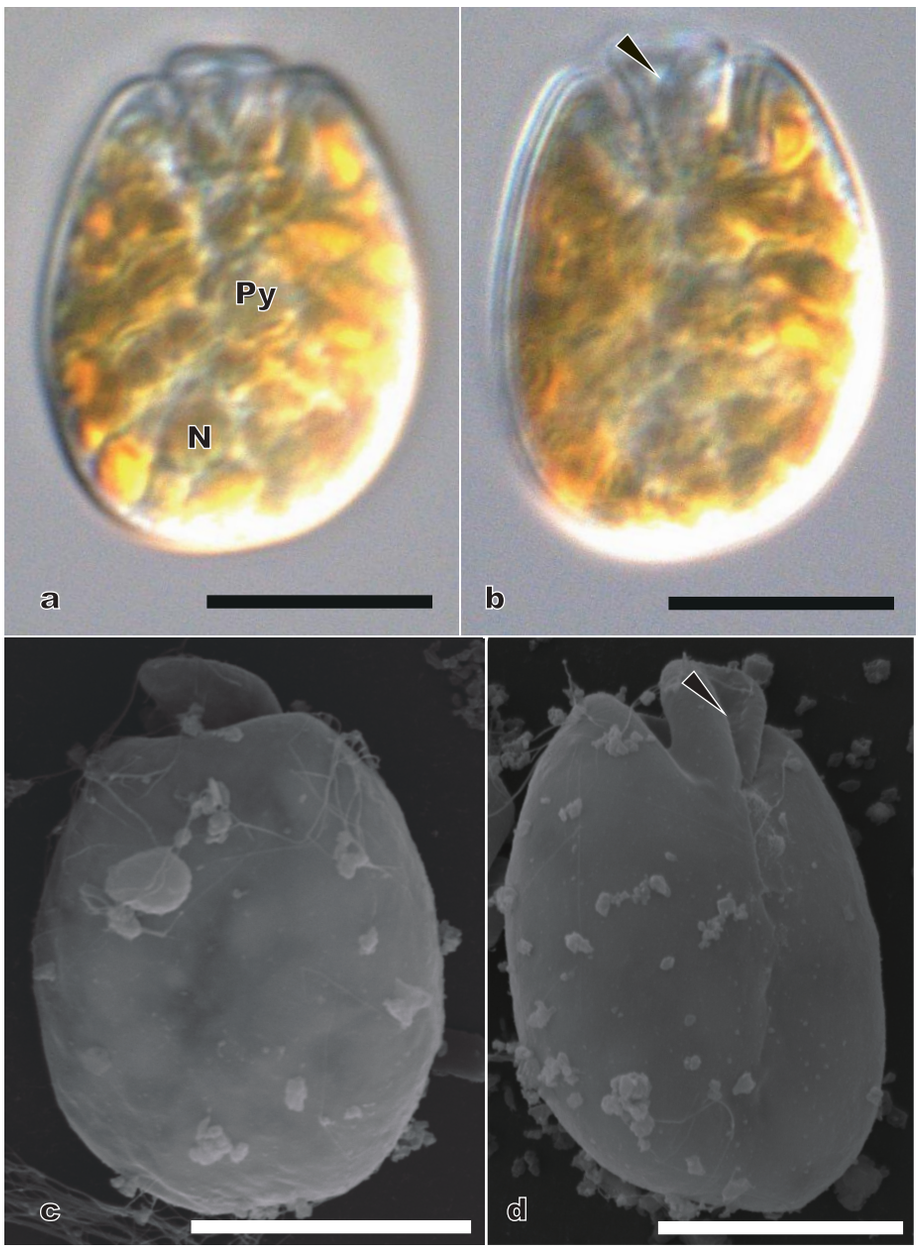


Fig. 29. *Testudodinium* cf. *maedaense* HG276. Light and scanning electron micrography.
a. Dorsal view. The pyrenoid (Py) is central and the nucleus (N) is posterior. The dorsal surface of the hyposome is smooth.
b. Ventral view. The episome possesses the ventral furrow (arrowhead) that is typical of the genus.
c. Dorsal view. The dorsal surface of the hyposome is smooth and the sac-like shape of the cell is typical of the maedaense sub-clade.
d. Ventral view. The episome possess the ventral furrow (arrowhead) that is typical of the genus. The sulcus is present but indistinct.
Scale bar = 10 µm.

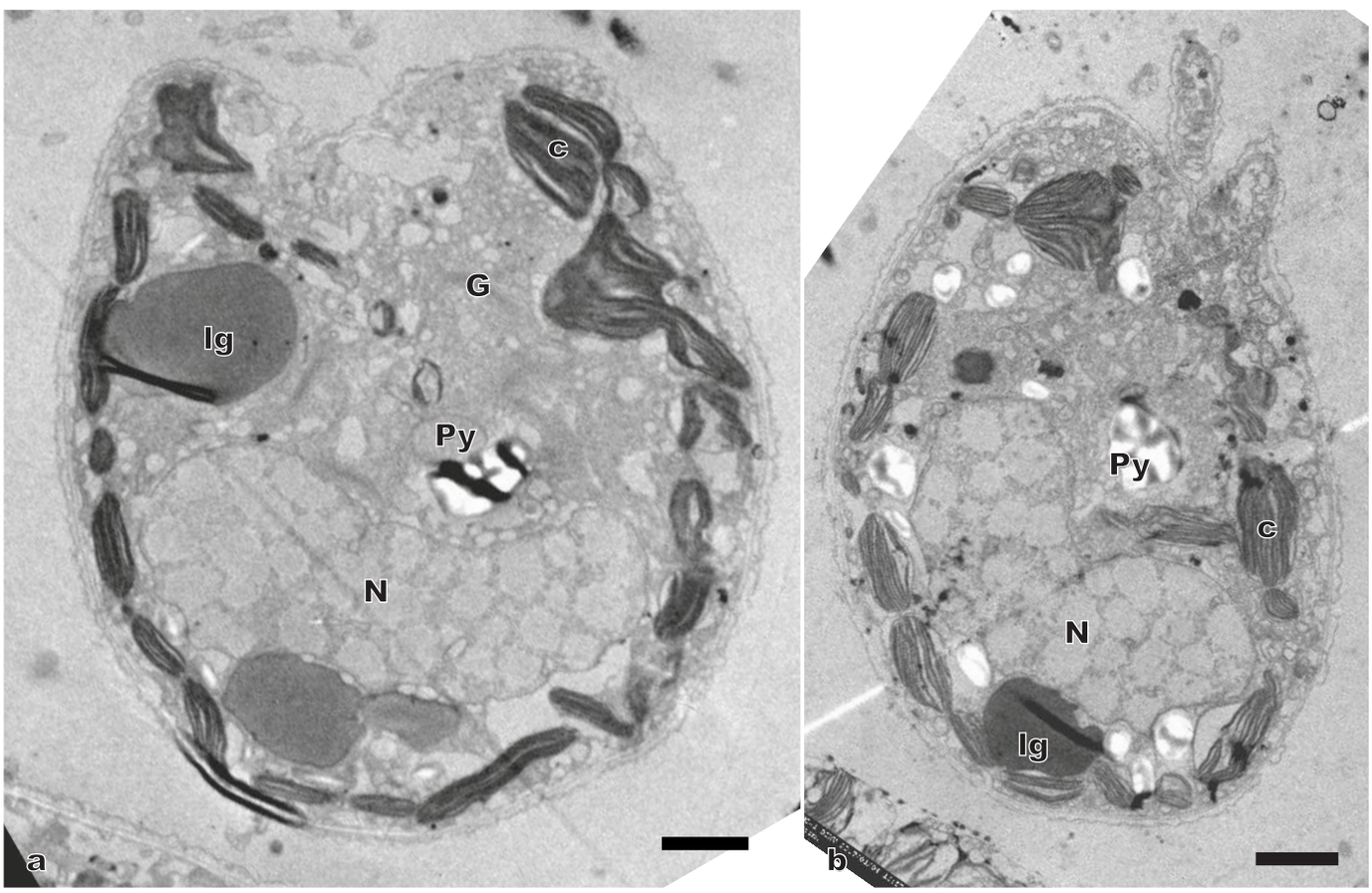


Fig. 30. *Testudodinium* cf. *maedaense* HG276. Transmission electron micrographs.
a. Longitudinal section in a lateral plane. The pyrenoid (Py) is central, the nucleus (N) is posterior, the chloroplasts (c) are peripheral. Lipid granules (lg) are distributed throughout the cell. Golgi apparatus (G) are found above the pyrenoid.
b. Longitudinal section in an angled plane. The nucleus (N) is posterior, the pyrenoid (Py) central and the chloroplasts (c) peripheral. A lipid granule (lg) is present.
Scale bar = 2 µm.

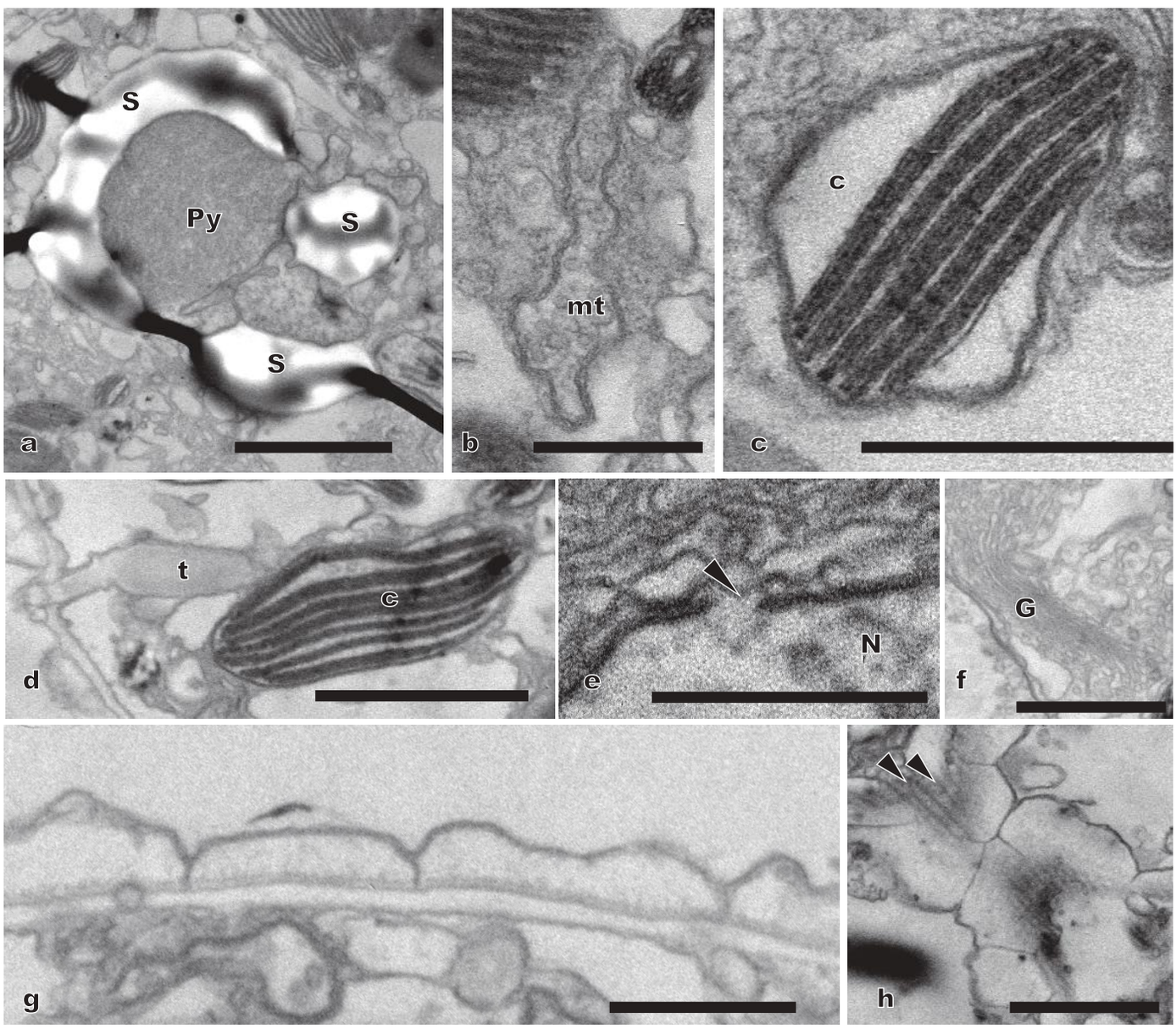


Fig. 31. *Testudodinium* cf. *maedaense* HG276. Transmission electron micrographs.
a. Pyrenoid complex (Py) composed of discrete pyrenoid profiles, surrounded by a discontinuous starch sheath (S). Scale bar = 2 µm.
b. Mitochondrion (mt). Scale bar = 500 nm.
c. Atypical chloroplast (c) showing lamellae with three thylakoid bands. Scale bar = 500 nm.
d. Trichocyst (t) and typical elongate chloroplast (c). Scale bar = 1 µm.
e. Simple nuclear pore (arrowhead) in the nuclear membrane. N: nucleus. Scale bar = 500 nm.
f. Golgi appartus (G). Scale bar = 1 µm.
g. Amphiesma. The amphiesmal vesicles are underlain by a continuous electron-transparent layer. The vesicles themselves are filled with a fibrous content.
h. Amphiesmal vesicles in tranvse view. The vesicles are polygonal. Microtubules (arrowheads) are associated with the ampiesma. Scale bar = 1 µm.

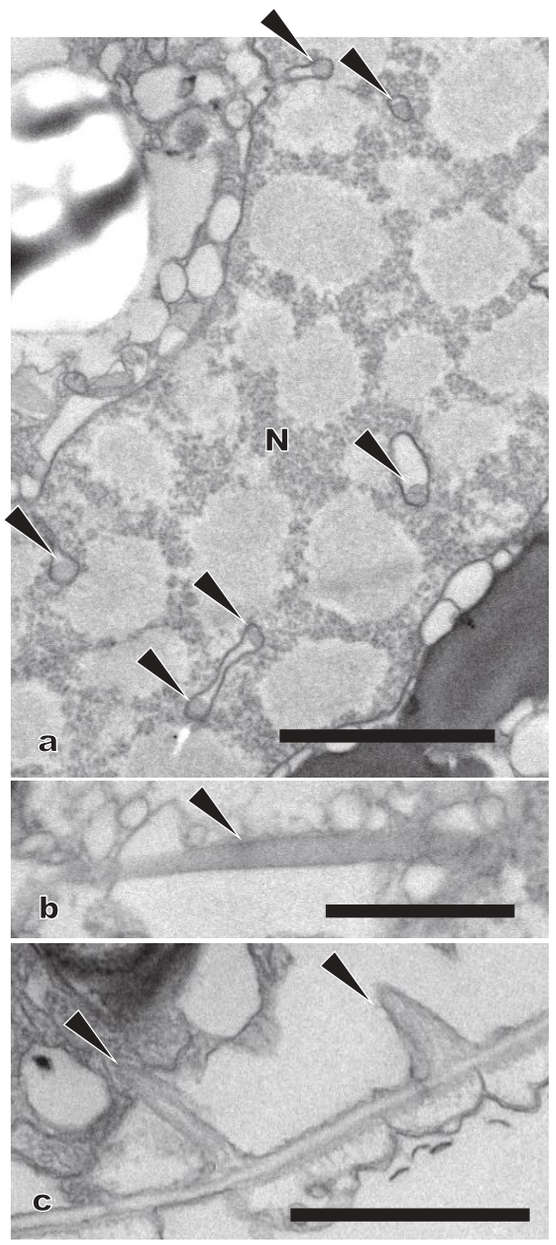


Fig. 32. *Testudodinium* cf. *maedaense* HG276. Transmission electron micrographs.
a. Portion of the nucleus (N) showing the props (arrowheads) that pass through it. Scale bar = 2 μm.
b. Portion of an internal prop (arrowhead). Scale bar = 1μm.
c. Bases of the internal props (arrowheads). They are separated from the basal layer by a distinction. Scale bar = 1 μm.

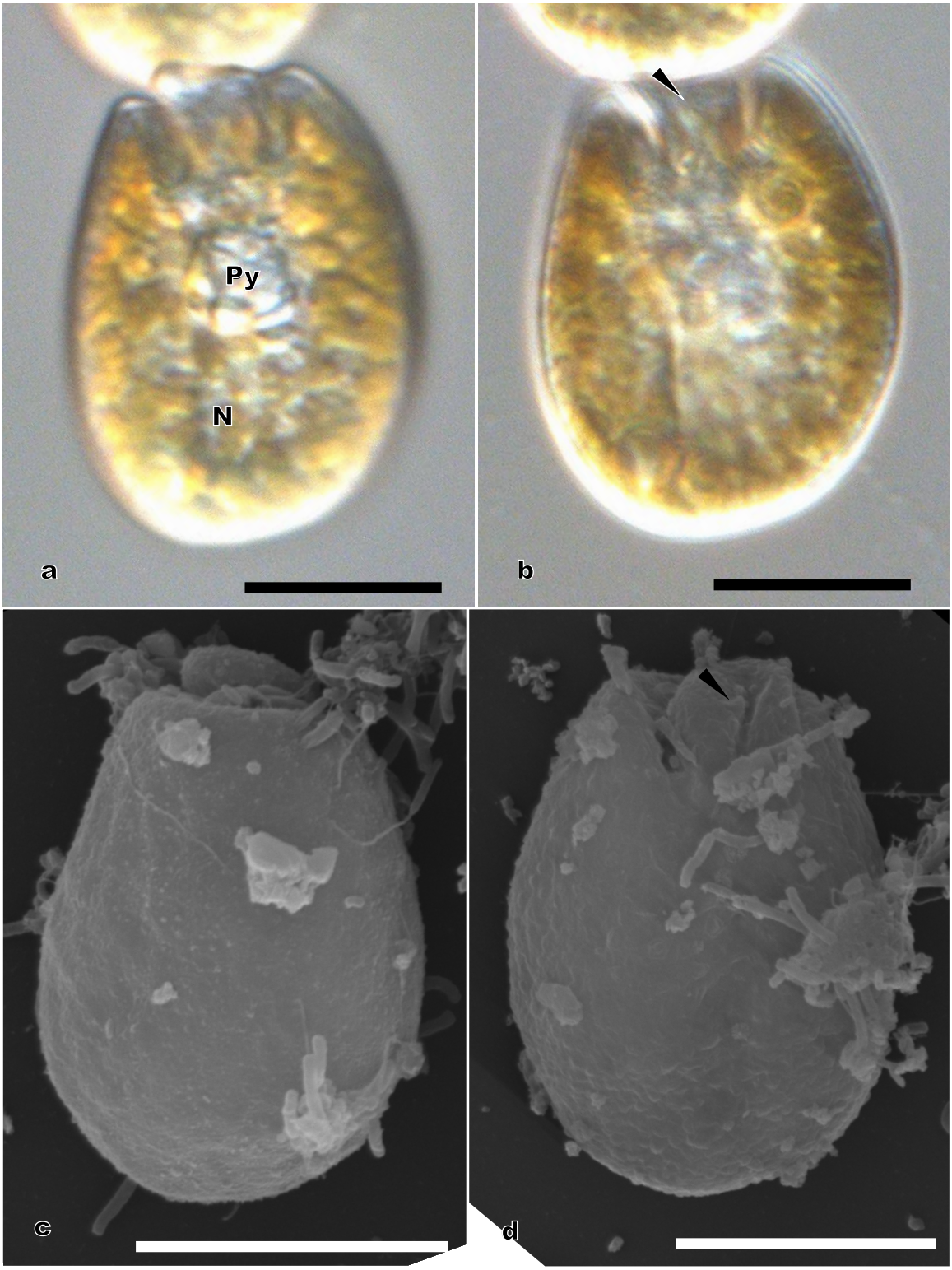


Fig. 33. *Testudodinium* cf. *maedaense* HG278. Light and scanning electron micrography.
a. Dorsal view. The pyrenoid (Py) is central and the nucleus (N) is posterior. The dorsal surface of the hyposome is smooth.
b. Ventral view. The episome possesses the ventral furrow (arrowhead) that is typical of the genus.
c. Dorsal view. The dorsal surface of the hyposome is smooth and the sac-like shape of the cell is typical of the maedaense sub-clade.
d. Ventral view. The episome possess the ventral furrow (arrowhead) that is typical of the genus. The sulcus is present but indistinct.
Scale bar = 10 μm.

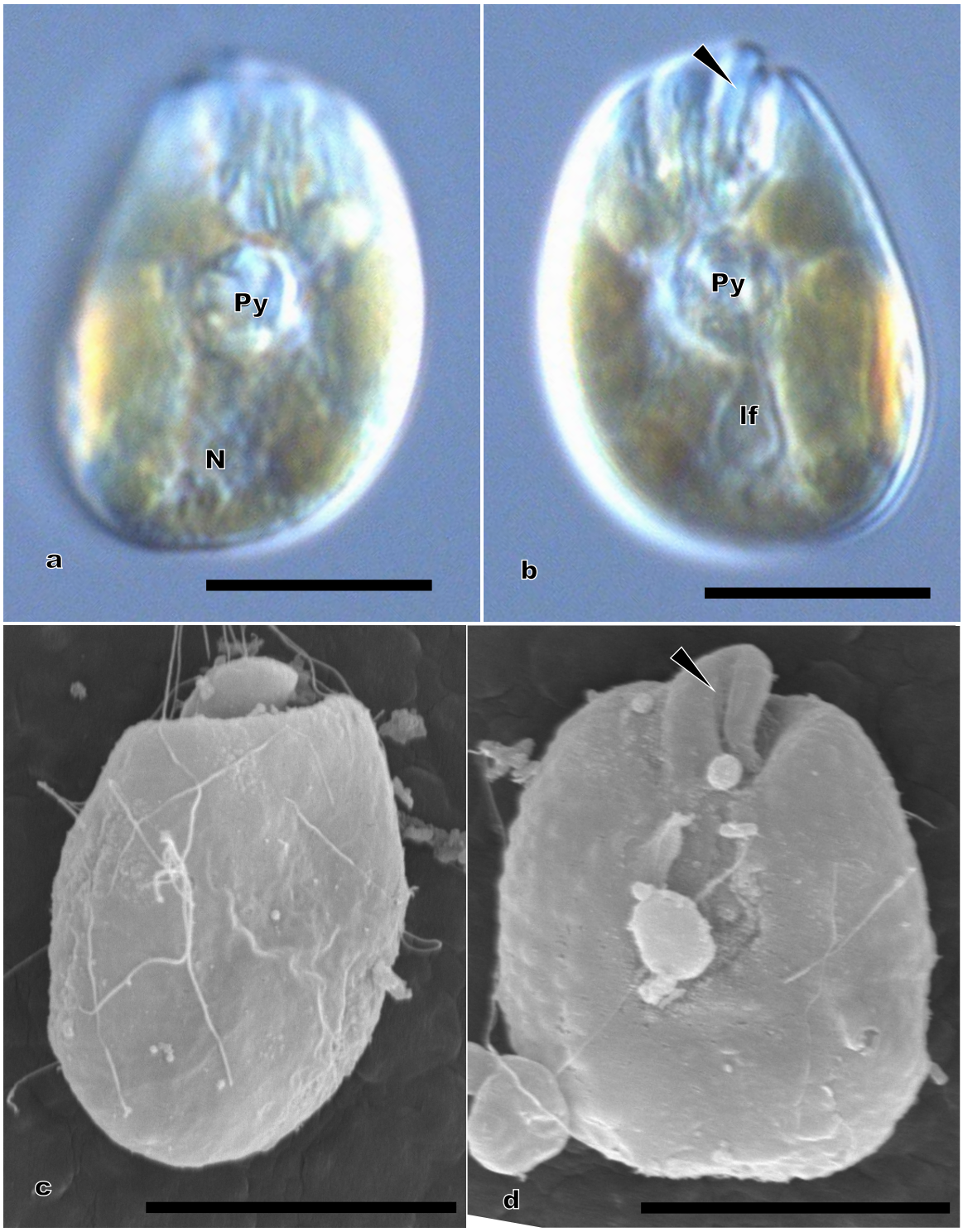


Fig. 34. *Testudodinium* cf. *maedaense* HG288. Light and scanning electron micrography.
a. Dorsal view. The pyrenoid (Py) is central and the nucleus (N) is posterior. The dorsal surface of the hyposome is smooth.
b. Ventral view. The episome possesses the ventral furrow (arrowhead) that is typical of the genus. The longitudinal flagellum (lf) is present in a broad sulcus.
c. Dorsal view. The dorsal surface of the hyposome is smooth and the sac-like shape of the cell is typical of the maedaense sub-clade.
d. Ventral view. The episome possess the ventral furrow (arrowhead) that is typical of the genus.
Scale bar = 10 μm.

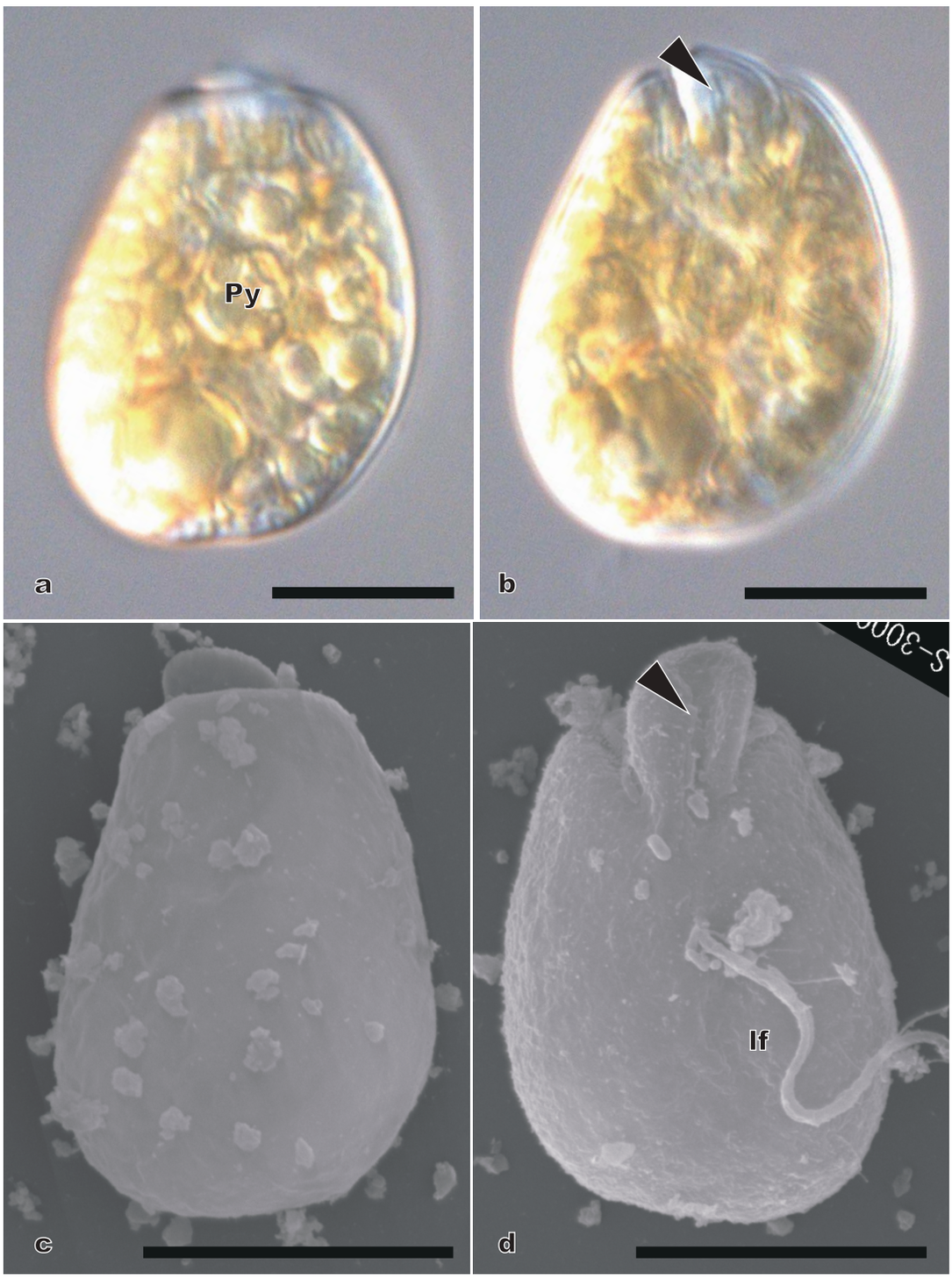


Fig. 35. *Testudodinium* cf. *maedaense* HG291. Light and scanning electron micrography.
a. Dorsal view. The pyrenoid (Py) is central. The nucleus is not visible. The dorsal surface of the hyposome is smooth.
b. Ventral view. The episome possesses the ventral furrow (arrowhead) that is typical of the genus.
c. Dorsal view. The dorsal surface of the hyposome is smooth and the sac-like shape of the cell is typical of the maedaense sub-clade.
d. Ventral view. The episome possess teshe ventral furrow (arrowhead) that is typical of the genus. The longitudinal flagellum (lf) is also present and arises from the centre of the cell.
Scale bar = 10 µm.

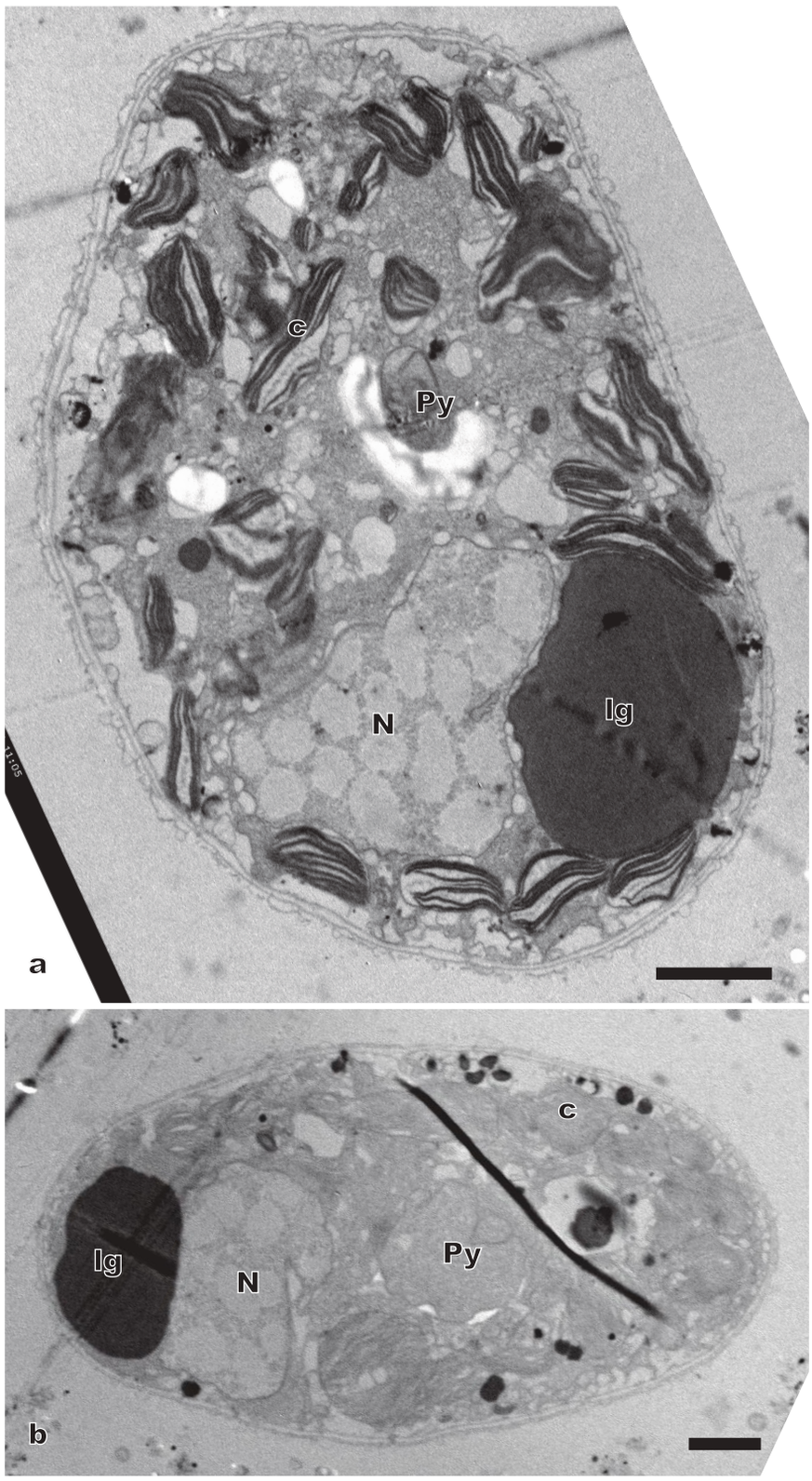


Fig. 36. *Testudodinium* cf. *maedaense* HG291. Transmission electron micrography.
a. Longitudinal section in a lateral plane. The pyrenoid (Py) is central, the nucleus (N) is posterior, the chloroplasts (c) are distributed throughout the cell. Lipid granules (lg) are adjacent to the nucleus.
b. Longitudinal section in an angled plane. The nucleus (N) is posterior, the pyrenoid (Py) central and the chlroplasts (c) peripheral. A lipid granule (lg) is present adjacent to the nucleus.
Scale bar = 2 μm.

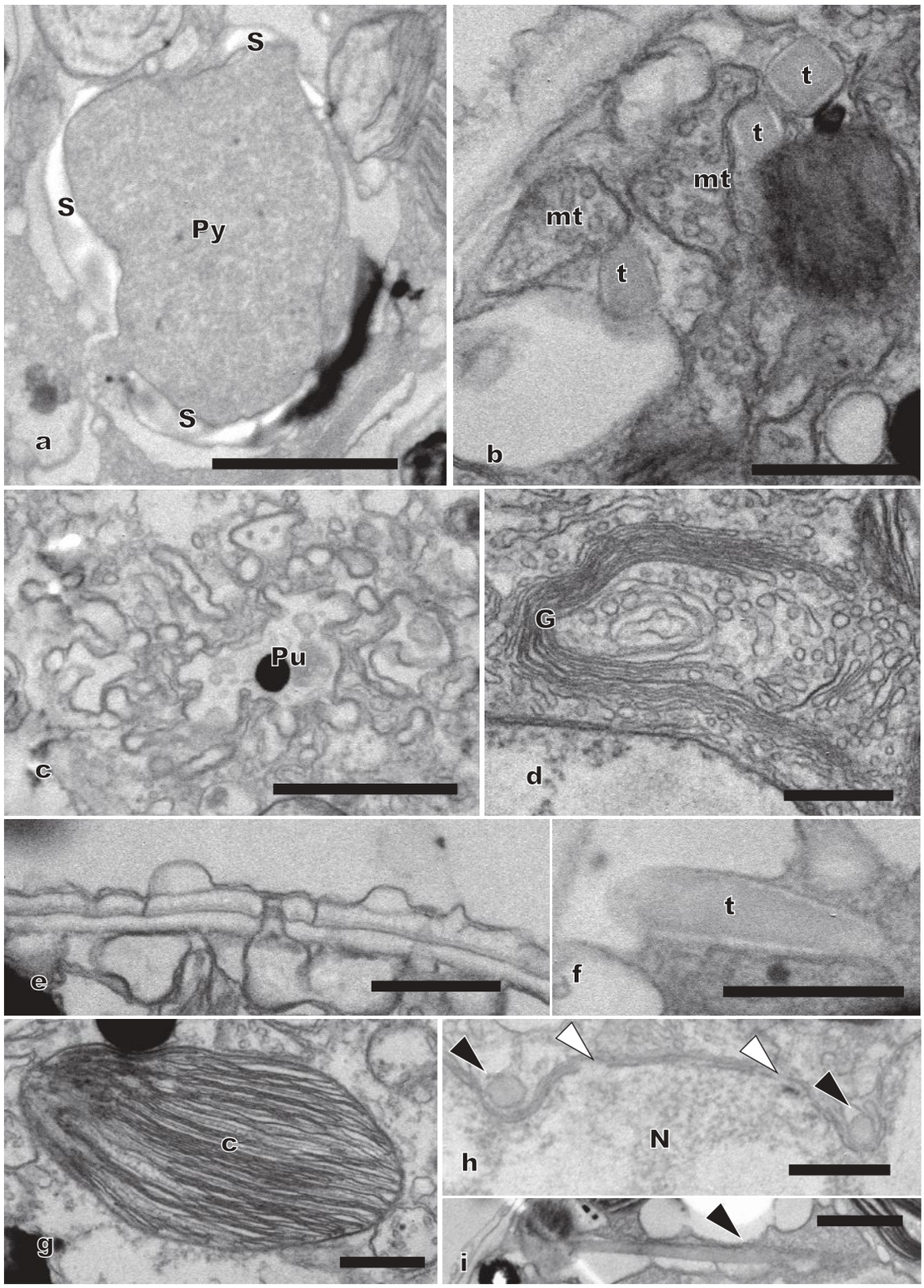


Fig. 37. *Testudodinium* cf. *maedaense* HG291. Transmission electron micrographs.
a. Pyrenoid complex (Py) surrounded by a discontinuous starch sheath (S). Scale bar = 2 µm.
b. Mitochondria (mt) and trichocysts (t). Scale bar = 500 nm.
c. Pusule (Pu) with a central tubule and collecting vesicles. Scale bar = 1 µm.
d. Golgi apparatus (G). Scale bar = 1 µm.
e. Amphiesma. The amphiesmal vesicles are underlain by a continuous electron-transparent layer. The vesicles themselves are filled with a fibrous content. Scale bar = 500 nm.
f. Trichocyst (t). Scale bar = 500 nm.
g. Elongate chloroplast (c) with thylakoids with three lamellae.
h. Portion of the nucleus (N) showing the simple nuclear pores (open arrowheads) and the props (arrowheads) around the nucleus. Scale bar = 1 µm.
i. Portion of an internal prop (arrowhead). Base of the prop is separated from the basal layer by a distinction. Scale bar = 1 µm.

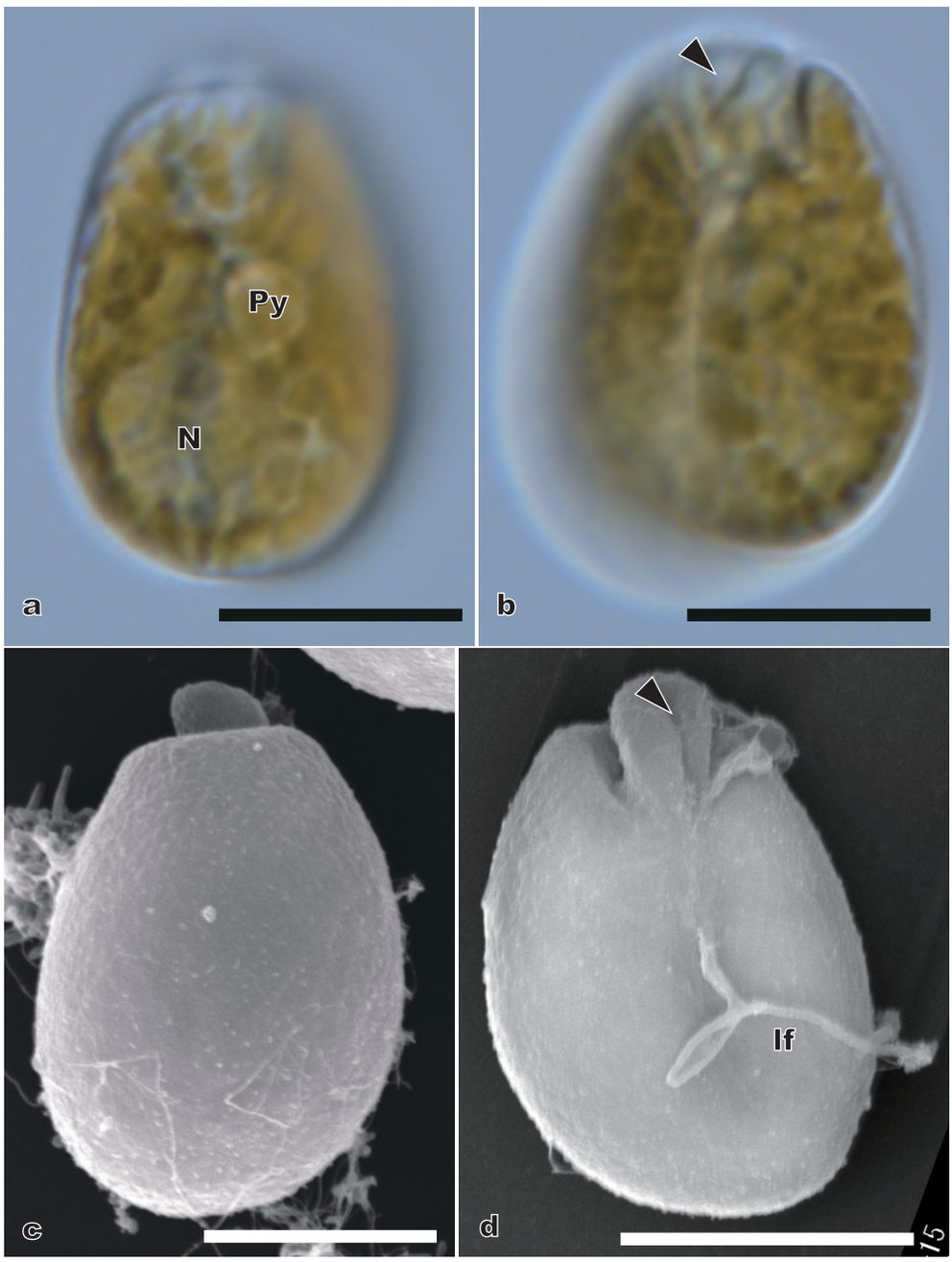


Fig. 38. *Testudodinium* cf. *maedaense* HG297. Light and scanning electron micrography.
a. Dorsal view. The pyrenoid (Py) is central and the nucleus (N) is posterior. The dorsal surface of the hyposome is smooth.
b. Ventral view. The episome possesses the ventral furrow (arrowhead) that is typical of the genus.
c. Dorsal view. The dorsal surface of the hyposome is smooth and the sac-like shape of the cell is typical of the maedaense sub-clade.
d. Ventral view. The episome possesses the ventral furrow (arrowhead) that is typical of the genus. The longitudinal flagellum (lf) arises from the centre of the cell..
Scale bar = 10 µm.

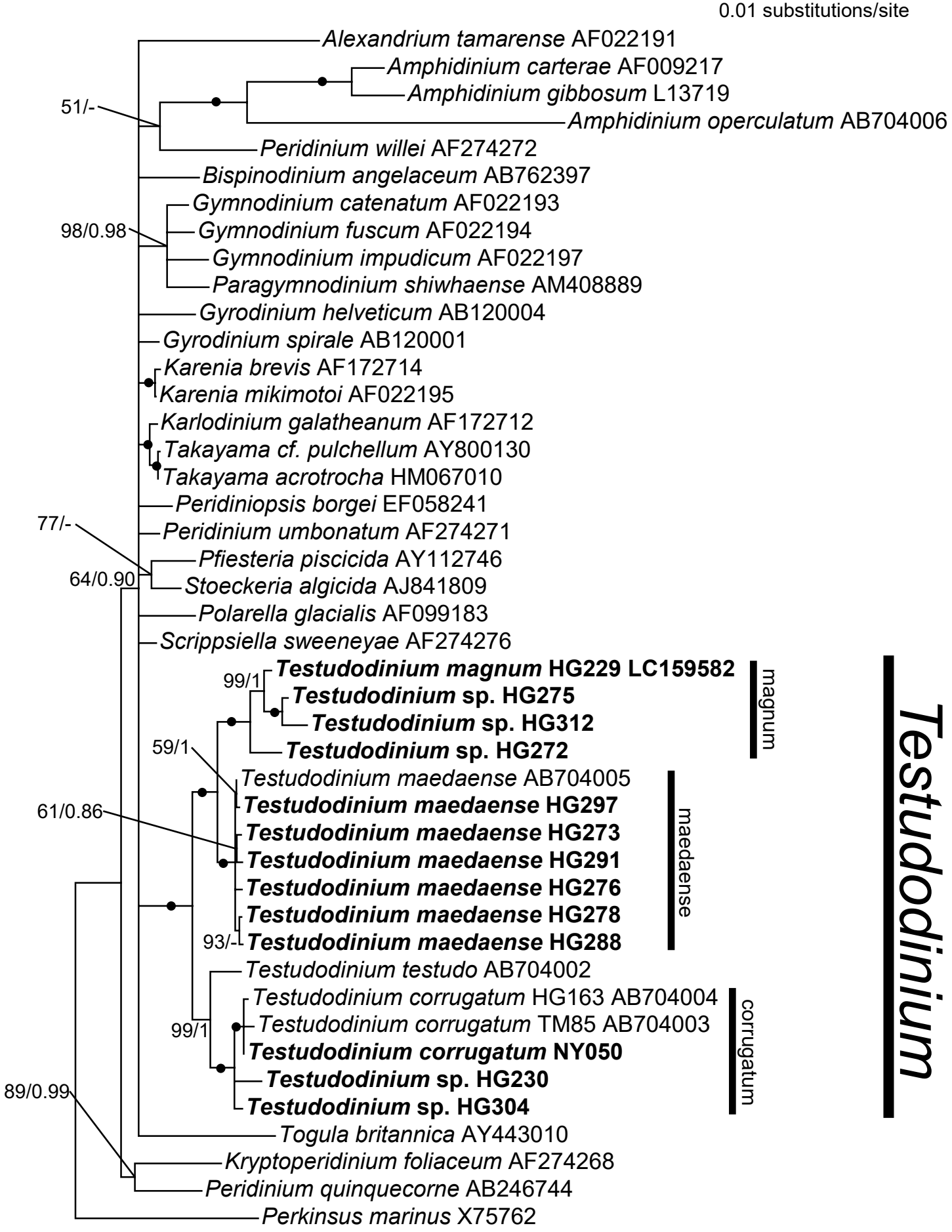


Fig. 39. Maximum likelihood phylogenetic tree inferred from partial SSU DNA sequences. ML bootstrap (>50%) and Bayesian PPI values (>0.8) are indicated. Solid circles represent nodes with a 100% ML bootstrap and Bayesian PPI of 1.

KEY
1. ventral furrow on the epitheca.
2. rugose dorsal hypotheca
3. smooth dorsal hypotheca
4. corrugated dorsal hypotheca
    a. clearly defined ribs
    b. faintly defined ribs
5. hyaline girdle encircling cell
6. internal props
    a. present
    b. absent
7. Pyrenoid
    a. Pyrenoid complex
    b. Single
    c. Single/complex - membranous structures in matrix
    d. circular
    e. matrix traversed by thylakoids
    f. matrix homogenous
    g. matrix invaded by cytoplasmic tubules
    h. no starch sheath
    i. aggregation of globular pyrenoids
    j. asymmetric

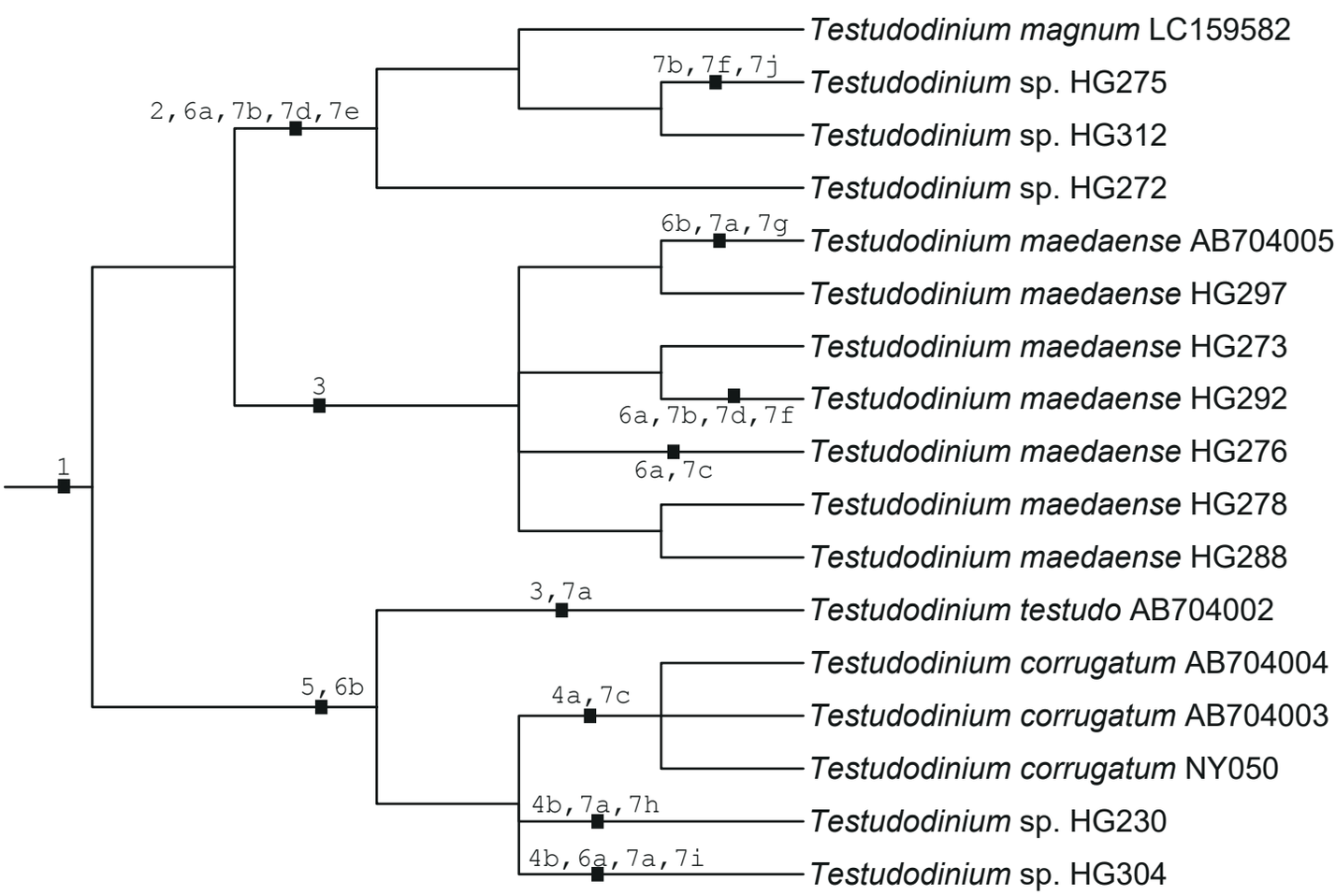


Fig. 40. Schematic representation of character evolution in the genus *Testudodinium*. The points of divergence are indicated on the cladogram, and the specific characters are listed in the key above the cladogram. See also Table 3.

Table 3. Morphological comparison of the *Testudodinium* spp.

Group	Species	Length (µm)	Width (µm)	Hyposome	Internal props	Pyrenoid ultrastructure
Testudo group	*T. testudo*	20 – 30	ND	Colourless band encircling body	ND	ND
	T. testudo	27.5 – 35.0	20.0 – 27.5	Smooth surface; colourless band encircling body	Absent	Pyrenoid complex
Magnum group	*T. magnum*	37.5 – 55.5	27.5 – 52.5	Rugose; numerous nodules	Present	Single, circular; matrix traversed by thylakoids
	T. sp. HG272	20 – 32.5	16.5 – 32.5	Rugose; many nodules	Present	Single, circular; matrix traversed by thylakoids
	T. sp. HG275	20 – 27.5	13.75 – 21.25	Rugose; numerous tiny nodules	Present	Single, asymmetrical; matrix homogeneous
	T. sp. HG312	22.5 – 30	20 – 27.5	Rugose; numerous nodules	Present	Single, circular; matrix traversed by thylakoids
Corrugatum group	*T. corrugatum*	28 – 35	22 – 32	Corrugated; 7 dorsal ribs	Absent	ND
	T. corrugatum	25.0 – 32.5	15.0 – 29.0	Corrugated; 6-8/10-11 dorsal ribs	Absent	Single (maybe complex); matrix traversed by membranous structures
	T. corrugatum NY050	22.5 – 31.25	17.5 – 30	Corrugated; 6-8 dorsal ribs	Absent	ND
	T. sp. HG230	22.5 – 32.5	15 – 27.5	Corrugated; 6-8 dorsal ribs	Absent	Pyrenoid complex; no starch sheath
	T. sp. HG304	23.75 – 27.5	17.5 – 25	Corrugated; 10-14 dorsal ribs	Present	Pyrenoid complex; aggregation of globular pyrenoids
Maedaense group	*T. maedaense*	20.0 – 27.5	15.0 – 20.0	Smooth surface	Absent	Single; matrix invaded by cytoplasmic tubules
	T. maedaense HG273	16.25 – 27.5	11.25 – 21.25	Smooth surface	ND	ND
	T. maedaense HG276	17.5 – 27.5	12.5 – 22.5	Smooth surface	Present	Single (maybe complex); matrix traversed by membranous structures
	T. maedaense HG278	17.5 – 22.5	12.5 – 17.5	Smooth surface	ND	ND
	T. maedaense HG288	20 – 25	13.75 – 22.5	Smooth surface	ND	ND

T. maedaense HG291	17.5 – 27.5	13.75 – 21.25	Smooth surface	Present	Single, circular; matrix homogeneous
T. maedaense HG297	20 – 27.5	15 – 20	Smooth surface	ND	ND

Chapter 2

Testudodinium-like species – convergent evolution?

Introduction

Amphidinium Claparède and Lachmann 1859 is a genus of athecate dinoflagellates. The type species is *Amphidinium operculatum* Claparède and Lachmann; by the early 2000s, the genus had grown to encompass approximately 200 species. The genus was described as consisting of athecate dinoflagellates with an episome that is one-third or less of the total cell length in size, with the cingulum being near the apex (Claparède and Lachmann, 1859; Kofoid and Swezy, 1921; Steidinger and Tangen, 1997). This definition is very broad, resulting in a morphologically diverse and polyphyletic collection of species. An exhaustive cladistic analysis of morphological and structural features combined with the analysis of partial LSU D1-D6 rDNA sequences led to the redefinition of *Amphidinium sensu stricto* (Flø Jørgensen *et al.*, 2004a), leading to a much more stringent definition of the genus. The number of species in *Amphidinium sensu stricto* numbers approximately 20; they possess a primary defining character of a minute, left-deflected episome (Flø Jørgensen *et al.*, 2004a).

While this resolved the issue of the polyphyletic and diverse nature of *Amphidinium*, it also resulted in over 150 species which needed to be taxonomically re-examined. A further proposal in the work that established *Amphidinium sensu stricto* was to transfer the remainder of the species to *Amphidinium sensu lato*, until they could be concretely identified (Flø Jørgensen *et al.*, 2004a). In the ensuing decade, numerous investigations have either led to the establishment of a number of new genera such as *Togula* Flø Jorgensen, Shauna Murray & N. Daugbjerg (Flø Jørgensen *et al.*, 2004b), *Prosoaulax* A.J.Calado & Moestrup (Calado and Moestrup, 2005), *Ankistrodinium* M. Hoppenrath, S. Murray, S. F. Sparmann & B. S. Leander (Hoppenrath et al., 2012), *Testudodinium* T. Horiguchi, M. Tamura, K. Katsumata & A. Yamaguchi (Horiguchi *et al.*, 2012), or to the reclassification of *Amphidinium sensu lato* species into recognised genera, with examples such as *Balechina pachydermata* (Kofoid & Swezy) A. R. Loeblich Jr. & A. R. Loeblich III (formerly *A.*

vasculum) (Gómez *et al.*, 2015; Loeblich and Loeblich, 1968) and *Gymnodinium venator* Flø Jørgensen & Murray (formerly *A. pellucidum* Herdman) (Flø Jørgensen *et al.*, 2004a).

Among the species that were assigned to *Amphidinium sensu stricto*, *A. corrugatum* and *A. testudo* were included only on the basis of morphological characters. These species were later transferred to the genus *Testudodinium* (Horiguchi *et al.*, 2012). It was also shown that the *Amphidinium sensu stricto* is polyphyletic based on the analysis of SSU DNA sequences.

In this chapter I shall describe two new species that are similar to *Testudodinium*, thus falling in the *Amphidinium sensu lato*; moreover, I shall endeavour to make the case for convergent evolution to account for the morphological similarity.

Materials and methods

Sampling and culture

Sand samples were collected from the sea floor at a depths between 25–35 m, off Mageshima Island, Kagoshima Prefecture, Japan on 30. July 2013 and 19. August 2014 (Table 1; Fig. 3) using a Smith-McIntyre bottom sampler (Rigosha, Tokyo, Japan). The sand samples were sent to the laboratory of Phycology at Faculty of Science, Hokkaido University, where dinoflagellate cells were isolated. A spoonful of the sand sample was taken in a plastic cup containing autoclaved seawater supplemented with Daigo IMK medium (Nihon Pharmaceutical Co., Tokyo, Japan) for enrichment. 0.1% Germanium dioxide (Sigma-Aldrich Japan, Tokyo) was also added to prevent growth of diatoms. This was cultured at 25°C at an irradiance of 50 µmol photons m^{-2} s^{-1} with a 16:8 light:dark regime. Dinoflagellate cells found were isolated using drawn capillary Pasteur pipettes with an inverted microscope (Olympus CX41, Tokyo, Japan) and clonal cultures were established. The culture strains (strain number HG310 and HG345, Table 1) were maintained in IMK-supplemented seawater under the same conditions described above.

Light microscopy and scanning electron microscopy

For light microscopic observations, living cells were observed using a Carl Zeiss Axioskop 2 microscope equipped with Nomarski interference optics (Carl Zeiss Japan, Tokyo); fluorescent microscopic observations were made using the same microscope with filter set No. 15. Photographs were taken using a Leica MC-120HD camera (Leica Microsystems, Germany). For scanning electron microscopy, the cells were fixed dehydrated and critically point dried according to the protocol described by Yamada *et al*. (2013). Cells were collected by centrifugation (2000 rpm) and the cell pellet was fixed in 1% OsO_4 made up in culture medium for 20 min at room temperature. After rinsing first in sterilized filtered seawater and then twice in distilled water, for 10 min in each wash, a drop of water containing cells was placed on a poly-L-lysine coated SEM glass plate and the cells were allowed to settle for 10 min. The cells were then gradually dehydrated by introducing the SEM plate to each of an increasing series of ethanol concentrations (25%, 30%, 50%, 70%, 80%, 90% and 95%) for 10 min each, followed by two washes in 100% ethanol, each for 30min. Finally critical-point dried (HITACHI HCP-2, Tokyo, Japan) samples were sputter-coated with gold for 180 seconds at 40 mA (HITACHI E-1045) and viewed with a SEM (S-3000N, HITACHI). Contrast of the images was edited using Adobe Photoshop CS5.

Transmission electron microscopy

After removing excess culture medium, the attached cells at the bottom of a Petri dish were gathered by sweeping gently with a sterilized paint brush. These cells were transferred into 15 ml plastic tubes and centrifuged at 40 × g for 10 min. The cell pellet was re-suspended in 150 µl culture medium, and 50 µl of 4% OsO_4 made up in distilled water was added for 1 h at room temperature. The following protocol was the same as chemical fixation protocol described by Yamada *et al*. (2013) except that fixation was made only with 1% osmium tetroxide (OsO_4) instead

of a cocktail of glutaraldehyde and OsO_4. Sections were cut using a diamond knife on an ultramicrotome (LEICA EM UC6, Germany). Sections were picked up on formvar coated one-slot grids and these were viewed with a transmission electron microscope (H-7650, HITACHI, Tokyo). Contrast of the images was adjusted using Adobe Photoshop CS5.

DNA extraction and Polymerase Chain Reaction (PCR) amplification

Approximately 10 cells from each culture were used to extract DNA using the QuickExtract™ FFPE DNA extraction kit (Epicentre, Tokyo, Japan) according to the recommended protocol. SSU DNA and LSU DNA were separately amplified by nested PCR. Primers used for amplification are given in Table 2.

The first round of amplification of SSU DNA was carried out using the primers SR1 and SR12b (Table 2). The thermocycling programme consisted of an initial denaturation step at 94°C for 5 minutes; followed by 35 cycles of denaturation at 94°C for 30 s, annealing at 55°C for 30 s and extension at 72°C for 120 s; and the final extension step at 72°C for 7 minutes. The second round of PCR was carried out using the primer pairs SR1 and SR4R or SR5TAK; SR2TAK and SR7TAK; SR4 and SR9; SR6 and SR11; and SR8TAK and SR12b. The conditions for PCR amplification were an initial denaturation step at 94°C for 5 minutes; followed by 25 cycles of denaturation at 94°C for 30 s, annealing at 51°C for 30 s and extension at 72°C for 90 s; and the final extension step at 72°C for 7 minutes.

The first round of amplification of LSU DNA was carried out using the primers D1RF1 and 28-1483R. The thermocycling programme consisted of an initial denaturation step at 94°C for 5 minutes; followed by 35 cycles of denaturation at 94°C for 30 s, annealing at 51°C for 30 s and extension at 72°C for 120 s; and the final extension step at 72°C for 7 minutes. The second round of PCR was carried out using the primer pairs D1RF1 and 25R1*; 305F-27 and 852R-70; and D3A and 28-1483R. The conditions for PCR amplification were an initial denaturation step at 94°C for 5

minutes; followed by 25 cycles of denaturation at 94°C for 30 s, annealing at 50°C for 30 s and extension at 72°C for 90 s; and the final extension step at 72°C for 7 minutes.

The PCR products were purified and sequenced with ABI PRISM Big Dye Terminator (Perkin-Elmer, USA). The purified sequence reaction products were run on a DNA autosequencer ABI PRISM310 Genetic Analyser (Perkin-Elmer). Both sense and anti-sense strands were sequenced.

Sequence analyses

The SSU and LSU sequences were aligned with sequences acquired from Genbank. The aligned sequences were analysed by the ML method using PAUP* version 4.0a152 (Swofford, 2001) and the Bayesian method using MrBayes 3.2.1 (Huelsenbeck and Ronquist, 2001; Ronquist and Huelsenbeck, 2003).

3041 aligned sites were used for the analyses of SSU DNA. The selected best fit model was the GTR + I + G model. The heuristic search for the ML analysis was performed with the following options: a TBR branch-swapping algorithm and the Kimura 2-parameter NJ tree as the starting tree. The parameters used for the analysis were as follows: assumed nucleotide frequencies A = 0.25221, C = 0.18773, G = 0.25343, and T = 0.30703; substitution rate matrix with A<>C = 1.45037, A<>G = 4.37974, A<>T = 1.41967, C<>G = 0.879106, C<>T = 9.21137, G<>T = 1.00000; proportion of sites assumed to be invariable = 0.344429; rates for variable sites assumed to follow a gamma distribution with shape parameter = 0.538888, and number of rate categories = 4. For the Bayesian analysis, GTR + I + G was selected as the best evolutionary model by MrModeltest 2.3 (Nylander *et al.*, 2004). Markov chain Monte Carlo iterations were carried out until 16,500,000 generations, when the average standard deviations of split frequencies fell below 0.01, indicating the convergence of the iterations.

1600 aligned sites were used for the analyses of LSU DNA. The selected best fit model was TIM3 + I + G model. The heuristic search for the ML analysis was performed with the following options: a TBR branch-swapping algorithm and the Kimura 2-parameter NJ tree as the starting tree. The parameters used for the analysis were as follows: assumed nucleotide frequencies A = 0.27394, C = 0.20127, G = 0.27350, and T = 0.25129; substitution rate matrix with A<>C = 0.734679, A<>G = 2.28391, A<>T = 1.00000, C<>G = 0.734679, C<>T = 5.27875, G<>T = 1.00000; proportion of sites assumed to be invariable = 0.174892; rates for variable sites assumed to follow a gamma distribution with shape parameter = 0.558779, and number of rate categories = 4. For the Bayesian analysis, SYM + I + G was selected as the best evolutionary model by MrModeltest 2.3 (Nylander *et al.*, 2004). Markov chain Monte Carlo iterations were carried out until 4,500,000 generations, when the average standard deviations of split frequencies fell below 0.01, indicating the convergence of the iterations.

Results

Species descriptions

A*mphidinium* sp. *sensu lato* HG310

(Figs 41 – 43)

Diagnosis: Cell dorso-ventrally compressed, ovoid in ventral view, 30 – 42.5 µm long, 25 – 37.5 µm wide; minute episome with a furrow on the ventral surface; ovoid to ellipsoid hyposome with a groove on the dorsal surface and an asymmetric posterior end. Chloroplasts many, yellow-brown, elongated, concentrated in the margins; pyrenoid absent. Sulcus indistinguishable. Pyrenoid absent. Nucleus large and posterior.

Locality: Sand sediment from a depth of 34 m; off Mageshima, Kagoshima, Japan.

Light and scanning electron microscopy

The cell was dorsoventrally flattened and ovoid in ventral view (Fig. 41). The cells were 30 – 42.5 µm in length (mean = 36.5 ± 3.07 µm, *n* = 50) and 25 – 37.5 µm in width (mean = 32.15 ± 3.35 µm, *n* = 50). The episome was small and slightly asymmetric (Fig. 41), and possessed a distinct furrow on its ventral surface (Fig. 41 b, e). The tip of the episome was marginally widened and was slightly asymmetric in dorsal view (Fig. 41 b, e). The hyposome was large and ovoid to ellipsoid (Fig. 41). It possessed a longitudinal dorsal groove in its centre (Fig. 41 a, d) and it spanned almost 2/3 of hyposome length. The sulcus was indistinguishable (Fig. 41 b, e). The chloroplasts were yellow-brown (Fig. 41 a, b) and elongated (Fig. 41 c). They were spread throughout the cells, but were concentrated in the centre of and in the margins of the hyposome (Fig. 41 a-c). The pyrenoid was absent. The nucleus was large and posteriorly located (Fig. 41 b). The anterior part of the cell possessed accumulation bodies on either side of the groove (Fig. 41 a, b). Their number, size and exact position was variable.

Transmission electron microscopy

Figure 42 shows the arrangement of organelles with a single cell. A large, typical dinokaryotic nucleus containing many thick chromosomes was present at the posterior of the cell (Fig. 42). Typical Golgi apparatus (Fig. 43 c) and mitochondria (Fig. 43 e) were observed. The chloroplasts were elongated (Fig. 43 a) and distributed around the centre and in the periphery of the cell (Fig. 42). They possessed lamellae with three thylakoids bands (Fig. 43 b) which are typical to dinoflagellates. There was no pyrenoid. The pusule consisted of an elongated tube-like chamber and surrounding variously shaped pusular vesicles (Fig. 43 f): It was a pusule with a collecting chamber. Trichocysts typical of dinoflagellates were observed (Fig. 43 d). Accumulation bodies (Fig. 43 g) were also observed. The amphiesmal vesicles were small, polygonal and contained a fibrous material (Fig. 43 h, i). The amphiesma was underlain by a continuous electron translucent layer similar to the layer underlying the amphiesma in *T. magnum* (Chapter 1).

Amphidinium sp. *sensu lato* HG345

(Figs 44-47)

Diagnosis: Cell dorso-ventrally compressed, ovoid in ventral view, 27.5 – 45 µm long, 22.5 – 32.5 µm wide; small triangular episome with a narrow base and expanded tip protruding from the hyposome; ovoid hyposome with a rounded posterior end. Chloroplasts many, yellow-brown, elongated; pyrenoid absent. Sulcus shallow and broad. Nucleus large, spherical to ellipsoid, and central.

Locality: Sand sediment from a depth of 25.5 m; off Mageshima, Kagoshima, Japan.

Light and scanning electron microscopy

The cell was dorso-ventrally flattened and ovoid in ventral view (Fig. 44). The cells were 27.5 – 45 µm long (mean = 36.5 ± 5.00 µm, *n* = 20) and 22.5 – 32.5 µm wide (mean = 27 ± 3.34 µm, *n* = 20). The episome was small and triangular or fan-shaped in outline in LM (Fig. 44 b, c, f). The base of the episome was narrow and continuous with hyposome (Fig. 44 f); its tip was widened and protruded from under the hyposome (Fig. 44 a, e, f) The hyposome was large, ellipsoid, and had a rounded, slightly asymmetric posterior end (Fig. 44). No furrows were observed either on episome or on hyposome (Fig. 44). The sulcus was broad and shallow (Fig. 44 b, c). The longitudinal flagellum arose from the centre of the cell (Fig. 44 b, c, f); the transverse flagellum arose from the base of the incomplete cingulum on the left side of the cell (Fig. 44 f). The chloroplasts were yellow-brown and globular to elongated (Fig. 44 a-d). The nucleus was central displaced slightly to the posterior (Fig. 44 a), and was spherical to ellipsoid in shape; when ellipsoid, it occasionally appeared to from two lobes.

Transmission electron microscopy

Figure 45 shows the arrangement of organelles with a single cell. A large, typical dinokaryotic nucleus containing many thick chromosomes (Fig. 46 a) was present at the centre of the cell, displaced towards the posterior (Fig. 45). Typical mitochondria (Fig. 46 f) were observed. The chloroplasts were elongated (Fig. 46 c) and distributed around the periphery of the cell (Fig. 45). They possessed lamellae with three thylakoids bands (Fig. 46 d) which are typical to dinoflagellates. There was no pyrenoid. Trichocysts typical of dinoflagellates were observed (Fig. 46 b). Electron opaque cell inclusions that might be lipid granules were also observed (Fig. 45). The amphiesmal vesicles were small and contained a fibrous material (Fig. 46 e). The amphiesma was underlain by a continuous electron translucent layer similar to the layer underlying the amphiesma in *T. magnum* (Chapter 1).

Internal props were present in this species (Fig. 47), distributed throughout the cell. They appear to span the thickness of the cell. The props passed through the protoplasm and the nucleus (Fig. 47). They maintained an even thickness throughout their span, flaring slightly where they attach to the continuous layer underneath the amphiesma (Fig. 47 c). The prop is composed of a homogeneous, electron opaque substance (Fig 47). The demarcation between the base of the prop and the basal layer is distinct (Fig. 47 c).

Phylogenetic analysis

The ML phylogenetic tree (Fig. 48) and the Bayesian consensus tree (Fig. 50) based on the SSU DNA sequences were incongruent. The ML tree provided no indication whatsoever of the relationships of HG310 and HG345, either to each or to *A. herdmanii* or *A. mootonorum*. The addition of a sequence from a strain identified as *Amphidinium* cf. *herdmanii* (isolated by our lab) did not help in the resolution of the relationships. The Bayesian consensus tree was more helpful: while relationships between HG310, HG345, *A. herdmanni*, *A. mootonorum* and *A.* cf. *herdmanii*

were unresolved, they were part of a clade that included the genera *Karenia* and *Testudodinium*. This clade was supported with a PPI of 0.95.

The ML phylogenetic tree based on the LSU D1 – D3 DNA sequences (Fig. 49) was congruent with the Bayesian consensus tree. In this dataset, the position of HG310 was still unresolved, but HG345 was grouped in the same clade as *A. mootonorum* GU295205. However, the sequences *A. herdmanii* AY455675, *A. herdmanii* AY455595 and *A. mootonorum* AY455676 fall within the *Amphidinium* sensu stricto clade with complete support. These position of these two clades relative to one another was unresolved.

Discussion

From a morphological viewpoint HG310 is most similar to *T. maedanese*, and can easily be misidentified for the latter in LM observations. The shapes of the cells of the two species are similar, and the distinguishing feature – the furrow on the ventral surface of the episome (Horiguchi *et al.*, 2012) – is present in both species (Table 4). Possible difference that can be detected under light microscope is the presence (in *T. maedaense*) or absence (HG310) of pyrenoid. A careful study of the SEM images of the HG310 and *T. maedanse* shows that there may be some differences in the exact structure of the furrow: the ventral furrow on *T. maedaense* (and the other members of *Testudodinium*) appears to be formed by the clockwise curling of the episome; in HG310, the furrow appears to be caused by a depression on the ventral surface of the episome. The most noticeable differences are the absence of a pyrenoid and the presence of a dorsal groove in HG310, which are, respectively, present and absent in *T. maedaense* (Hoppenrath *et al.*, 2014; Horiguchi *et al.*, 2012). The general shape of the cell also differs between the two (Table 4). Therefore, it is concluded that HG310 is a novel species.

HG345 is most similar to *A. herdmannii* (Hoppenrath *et al.*, 2014; Kofoid and Swezy, 1921) and *A. mootonorum* (Murray and Patterson, 2002) from a morphological viewpoint. These three

species all share the triangular episome with a narrow base and expanded tip (Hoppenrath *et al.*, 2014) – in the species diagnosis of *A. mootonorum*, the episome is not described as triangular, but an examination of the LM plates shows that it is roughly triangular. Additionally, the nucleus is centrally located in HG345 and in *A. mootonorum*, and both lack pyrenoids (Murray and Patterson, 2002); *A. herdmanii* possesses a pyrenoid-like structure which is occasionally visible in the centre of the cell (Hoppenrath *et al.*, 2014). HG345 can be distinguished from *A. mootonorum* in the shape of the nucleus, i.e. spherical in the former, while elongate-oval in the latter. In summary, HG345 appears to possess characters that are intermediate between *A. herdmanii* and *A. mootonorum*, with the cell shape being more similar to *A. herdmanii*, and the locations of internal structures being more similar to *A. mootonorum* (Table 4), but the species can be clearly distinguished from these described species and HG345 can be identified as a new species.

The phylogenetic analyses provide the greatest obstacle to the resolution of the relationships of these two novel species. In the phylogenetic tree derived from the LSU data (Fig. 49), the position of HG310 is completely unresolved, but probably not closely related to *Amphidinium sensu stricto* (= true *Amphidinium*). HG345 is grouped with *A. mootonorum* GU295205 (Hoppenrath and Leander, 2010), lending some support to the case from the morphological similarities; however, the LSU sequence *A. mootonorum* AY455676 (Flø Jørgensen *et al.*, 2004a) was placed within the *Amphidinium sensu stricto* clade along with both two sequences from *A. herdmanii*. On the other hand, the SSU sequences of *A. mootonorum* and *A. herdmanii* are shown to be different from those of *Amphidinium sensu stricto*. The same result was obtained by Horiguchi *et al.* (Horiguchi *et al.*, 2012). In their phylogenetic tree, *A. mootonorum* and *A. herdmanii* formed a strongly supported clade, but their position was far from that of *Amphidinium* sensu stricto. Although it is not known the cause for the differences between LSU and SSU phylogenetic trees, my result also revealed that *A. mootonorum* and *A. herdmanii* are both different from *Amphidinium* sensu stricto both in SSU and LSU trees. Therefore, it is likely that previously reported LSU data for *A. mootonorum* and *A.*

herdmanii are possibly due to misidentification. In the ML tree derived from the SSU sequences (Fig. 48), the relationships of HG310 and HG345 are unresolved, as are those of *A. mootonorum* and *A. herdmanii*; in the Bayesian consensus tree (Fig. 50), there is robust support for the inclusion of all these species in a single clade (that also includes *Karenia* and *Testudodinium*); however, the exact relationships between each species is unresolved. Also sequenced was a strain identified from morphology as *Amphidinium* cf. *herdmanii*; this strain was unresolved in the ML tree and fell in the *mootonorum-herdmanii* clade in the Bayesian consensus tree. Thus the phylogenetic tree fails to provide any insights into the relationships of HG310 and may also confound the interpretation of the relationships of *A. mootonorum*.

The species identified here as *Amphidinium* sp. *sensu lato* HG310 and *Amphidinium* sp. *sensu lato* HG345 are both new, highly interesting and quite difficult to definitively identify at the generic level. A cursory examination under a light microscope indicates that they are share morphological similarities with members of *Testudodinium* and *Amphidinium sensu stricto* respectively. A comparison of key features is made in Table 4. It should be noted that prior to the redefinition of the genus *Amphidinium* (Flø Jørgensen *et al.*, 2004a), all these species would have been part of that genus. The similarity of their morphological characteristics combined with the lack of clear phylogenetic relationships points to the possibility of convergent evolution: the evolutionary pressure from the similar ecological niche – benthic and sand dwelling – may have led to these two species developing a morphology very similar to previously described species. As there are no reports about the function or benefits of this morphology, convergent evolution remains a hypothesis. From the data, I conclude that *Amphidinium* sp. *sensu lato* HG310 and *Amphidinium* sp. *sensu lato* HG345 are novel species whose relationship to other dinoflagellates is unresolved. These two species should be classified in their autonomous genera respectively, or in case the close affinities between the two species are resolved, these two species should be accommodated in a single novel genus. The elucidation of the relationship between these two species and *A.*

mootonorum and *A. herdmanii* awaits further phylogenetic information from authentic strains, as the type species are not available for this analysis. As a result, I have chosen to reserve naming these species until the necessary information for their taxonomic treatment is available.

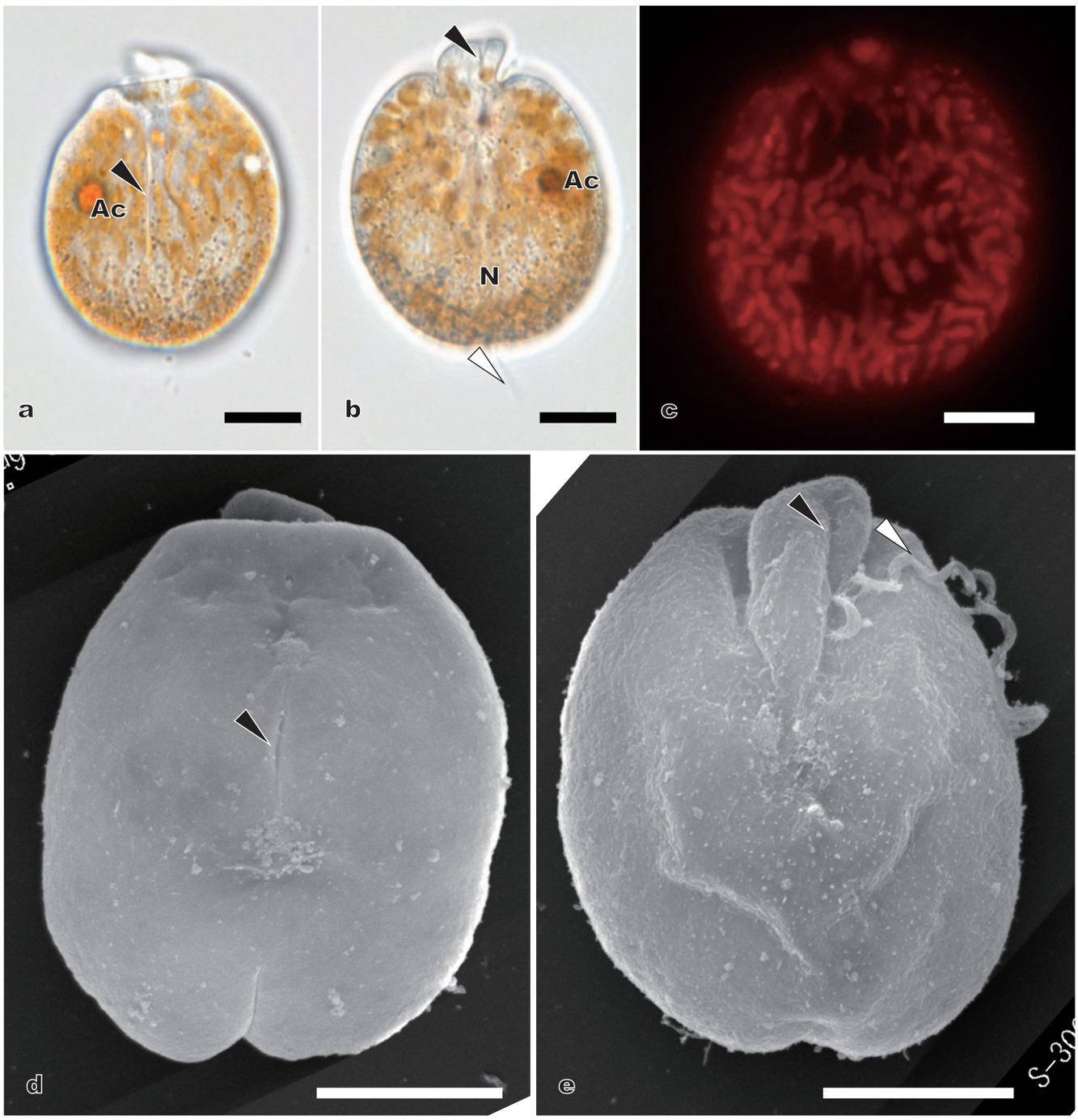


Fig. 41: *Amphidinium* sp. HG310. Light and scanning electron micrographs.
a. Dorsal view. The episome is asymmetric and a dorsal furrow is present in the centre of the hyposome (solid arrowhead). Accumulation body (Ac) is present.
b. Ventral view. The kidney-shaped nucleus (N) is posterior. A deep-red accumulation body (Ac) is present. The episome possesses a ventral groove (solid arrowhead) and the longitudinal flagellum is present (open arrowhead).
c. Fluorescence micrograph. The chloroplasts are multiple, discrete and elongated.
d. Dorsal view. The dorsal groove (solid arrowhead) is clearly visible.
e. Ventral view. The episome has a ventral furrow (solid arrowhead). The transverse flagellum (open arrowhead) arises from the left corner of the incomplete cingulum.
Scale bar = 10 µm.

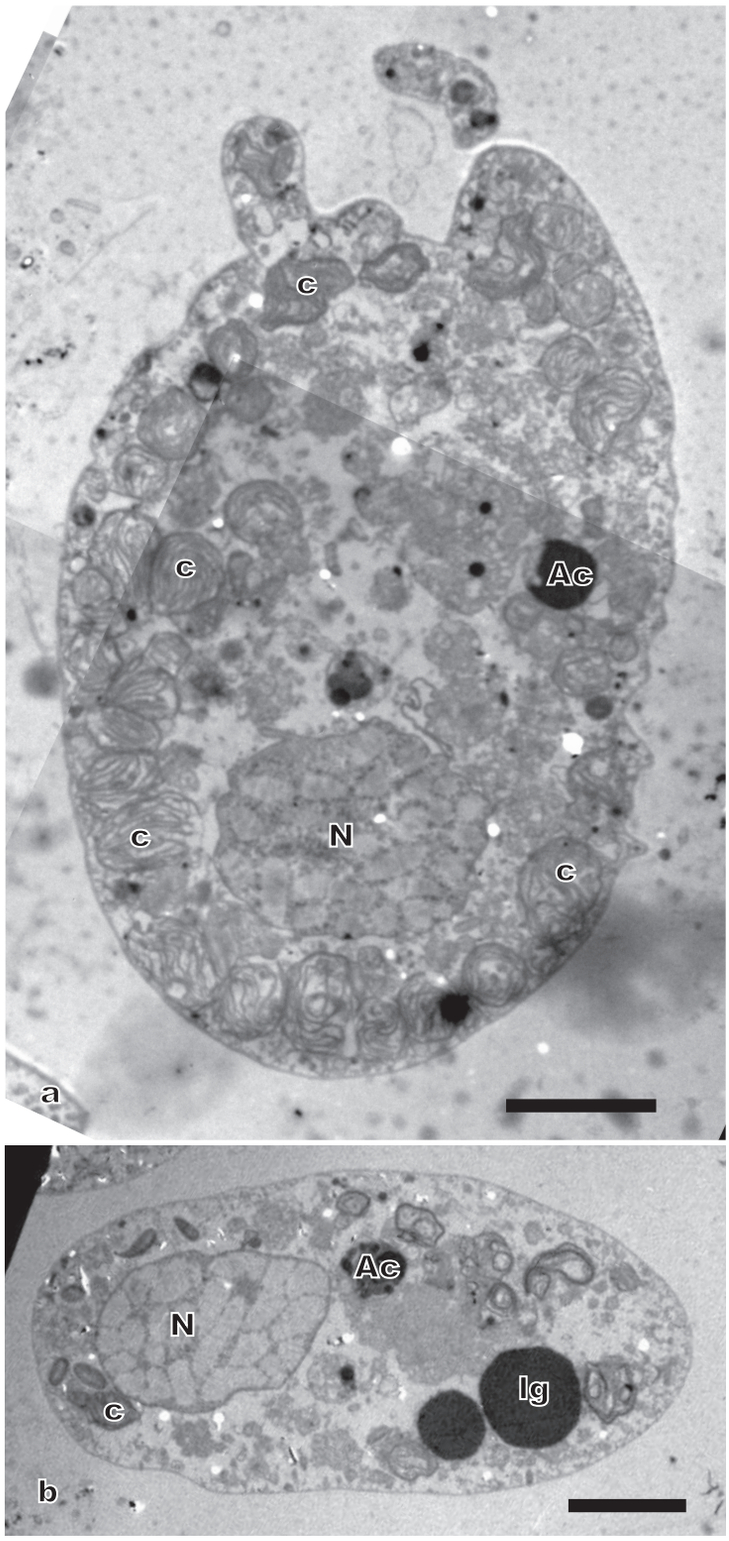


Fig. 42. *Amphidinium* sp. HG310. Transmission electron micrographs.
a. Longitudinal section at an angle. The nucleus (N) is posterior. The chloroplasts (c) are mostly distribuited throughout the periphery of the cell, including in the episome. An accumulation body (Ac) is present around the middle of the cell.
b. Longitudinal section in the dorso-ventral plane. The nucleus (N) is posterior, the chloroplasts (c) in the periphery and an accumulation body (Ac) in the middle of the cell. Electron opaque lipid granules (lg) are also present.
Scale bar = 5 µm.

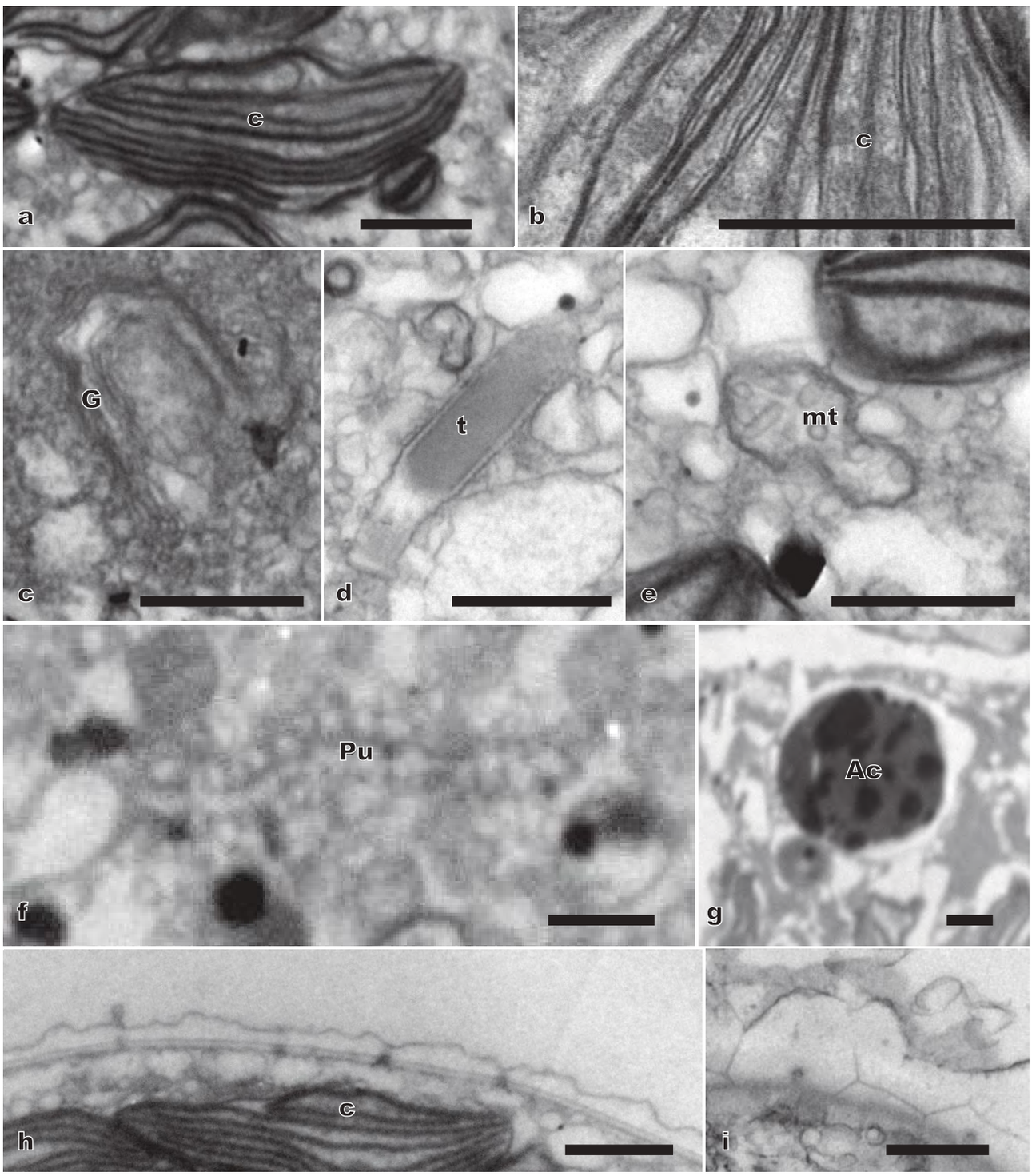


Fig. 43. *Amphidinium* sp. HG310. Transmission electron micrographs.
a. An elongate chloroplast (c). Scale bar = 1 μm.
b. Close-up of interior of a chloroplast (c), showing lamellae with three thylakoid bands. Scale bar = 1 μm.
c. Golgi apparatus (G). Scale bar = 1 μm.
d. Trichocyst (t). Scale bar = 500 nm.
e. Mitochondrion (m). Scale bar = 500 nm.
f. Pusule with central tubule and associated collecting vesicles. Scale bar = 1 μm.
g. Accumulation body (Ac). Scale bar = 1 μm.
h. Amphiesma. The amphiesmal vesicles are underlain by a continuous electron-translucent layer. The vesicles themselves contain a fibrous material. Scale bar = 1 μm
g. Amphiesma. Glancing section showing the polygonal shape of the ampiesmal vesicles. Scale bar = 500 nm.

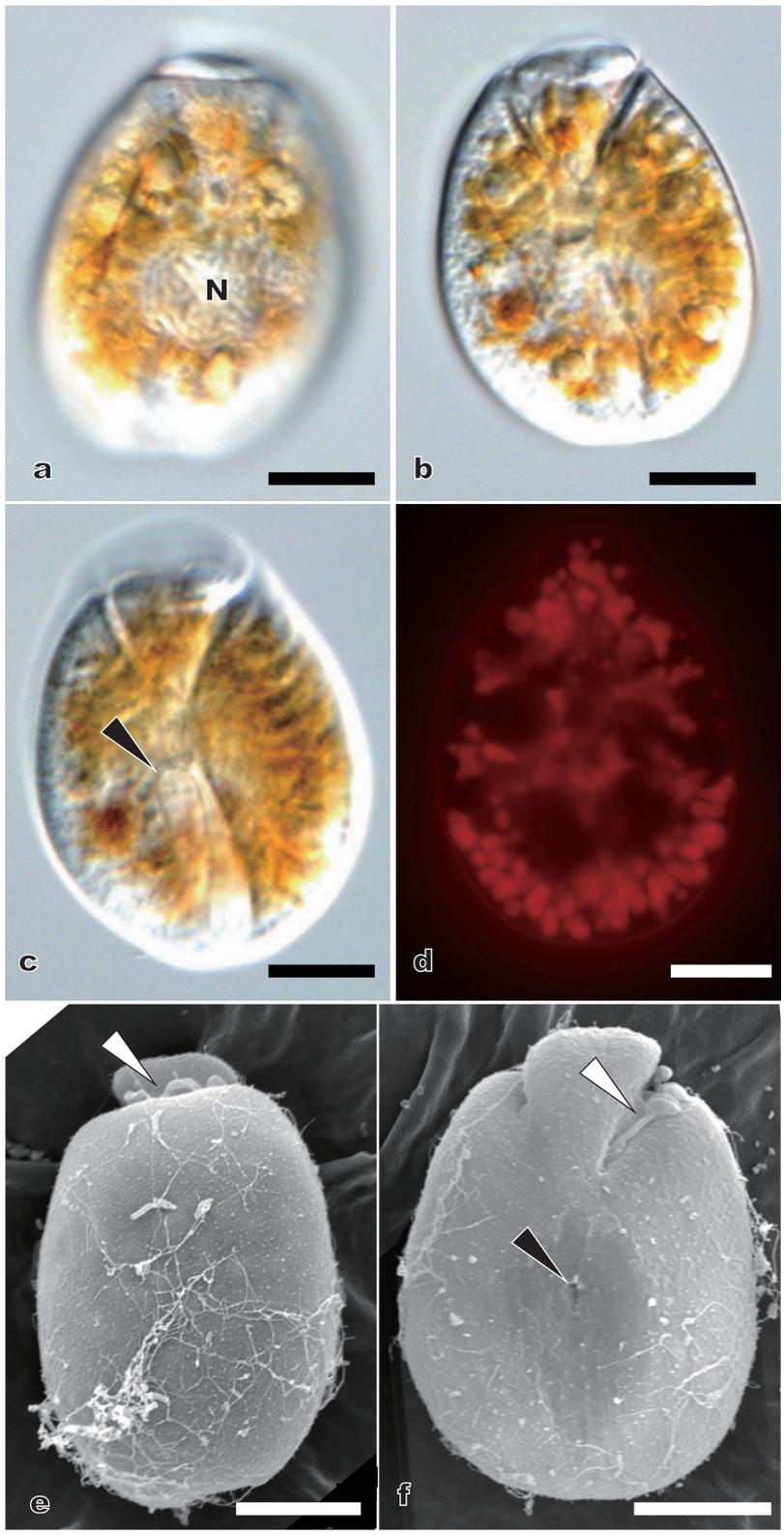


Fig. 44. *Amphidinium* sp. HG345. Light and scanning electron micrographs.
a. Dorsal view. The spherical nucleus (N) is central.
b. Ventral view. The episome is broadly triangular. The sulcus is broad and shallow.
c. Ventral view. The longitudinal flagellum (solid arrowhead) is visible.
d. Fluorescence micrograph. The chloroplasts are multiple, discrete and globular.
d. Dorsal view. The large hyposome is slightly asymmetric. The transverse flagellum is present within the cingulum.
e. Ventral view. The longitudinal flagellar pore is at centre of the cell. The transverse flagellum arises from the left corner of the of the incomplete cingulum.
Scale bar = 10 μm.

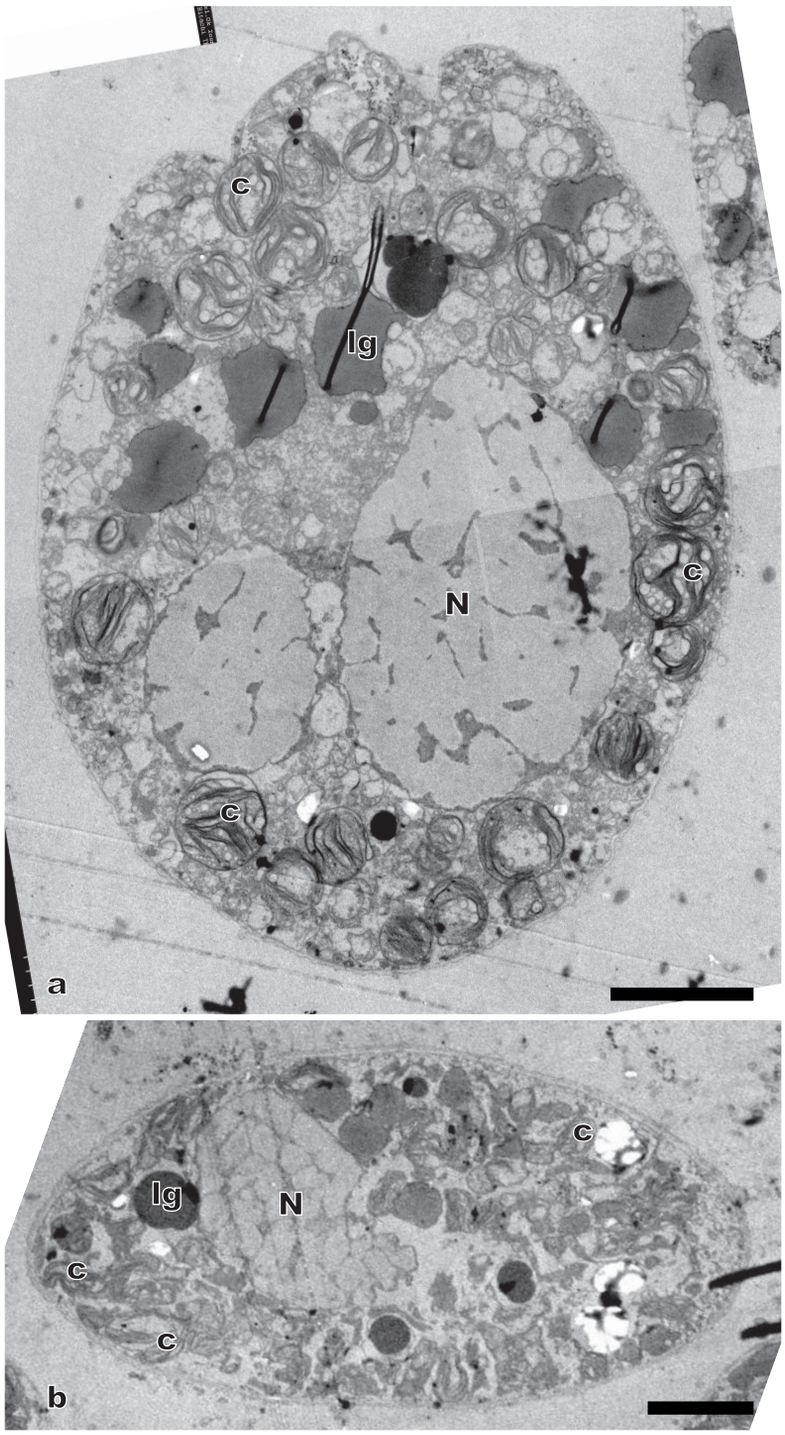


Fig. 45. *Amphidinium* sp. HG345. Transmission electron micrographs.
a. Longitudinal section in a dorsoventral plane. The nucleus (N) is slightly posterior, and is split. The chloroplasts (c) are distributed throughout the periphery of the cell; their appearance is an artefact of fixation. Electron-opaque lipid granules (lg) are present.
b. Longitudinal section in a lateral plane. The nucleus (N) is slightly posterior, and is towards the dorsum. The chloroplast (c) are peripheral. Lipid granules (lg) are present.
Scale bar = 5 µm

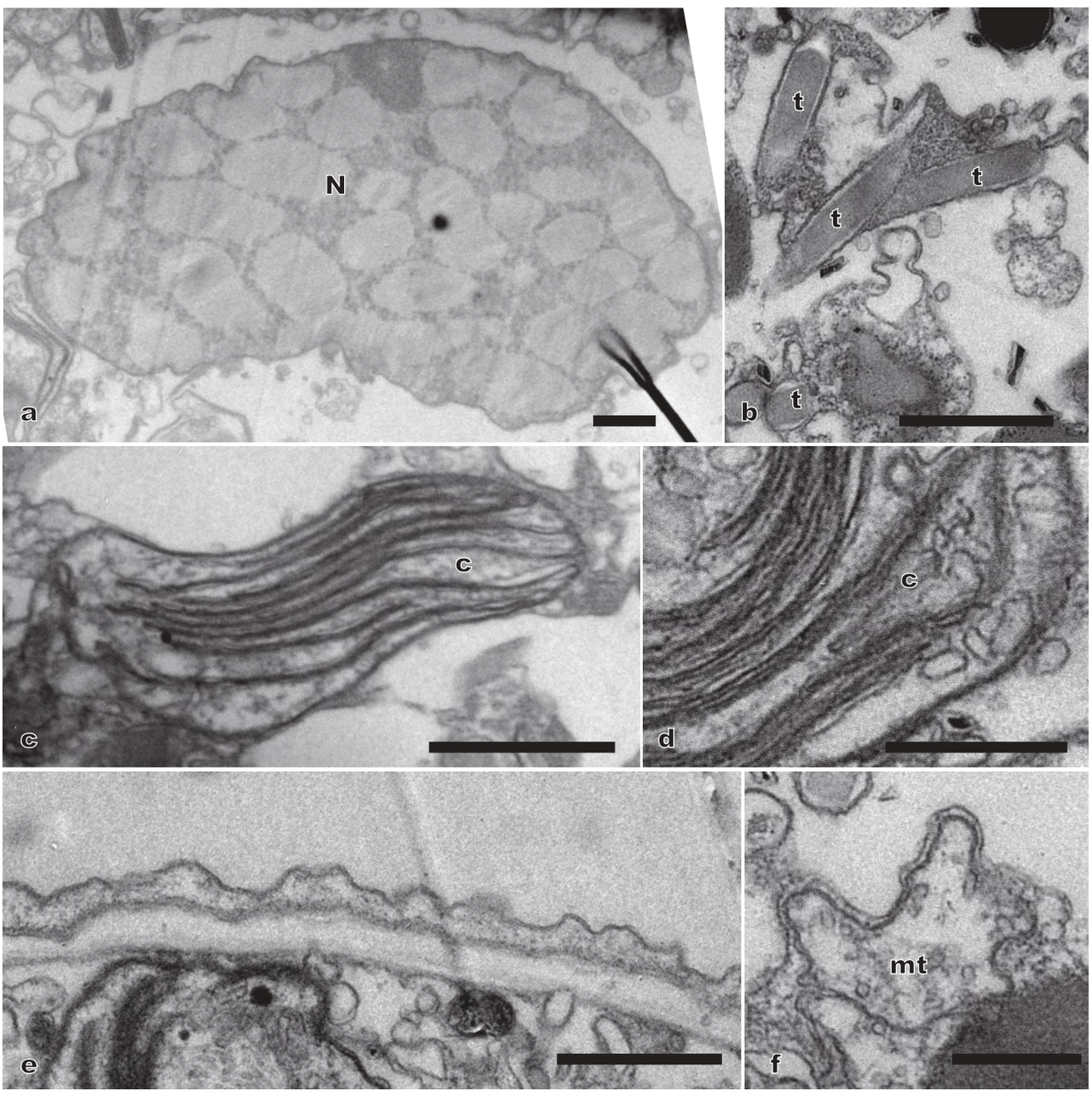


Fig. 46. *Amphidinium* sp. HG345. Transmission electron micrographs.
a. Typical dinoflagellate nucleus (N). Scale bar = 1 μm.
b. Trichocysts (t), in longitudinal and transverse sections. Scale bar = 1 μm.
c. Chloroplast (c). Scale bar = 1 μm
d. Interior of a chloroplast (c) showing lamellae with three thylakoid bands. Scale bar = 500 nm.
e. Amphiesma. The amphiesmal vesicles contain fibrous material. They are underlain by a thick, continuous, electron-transparent membrane. Scale bar = 1 μm.
f. Mitochondrion (mt). Scale bar = 500 nm.

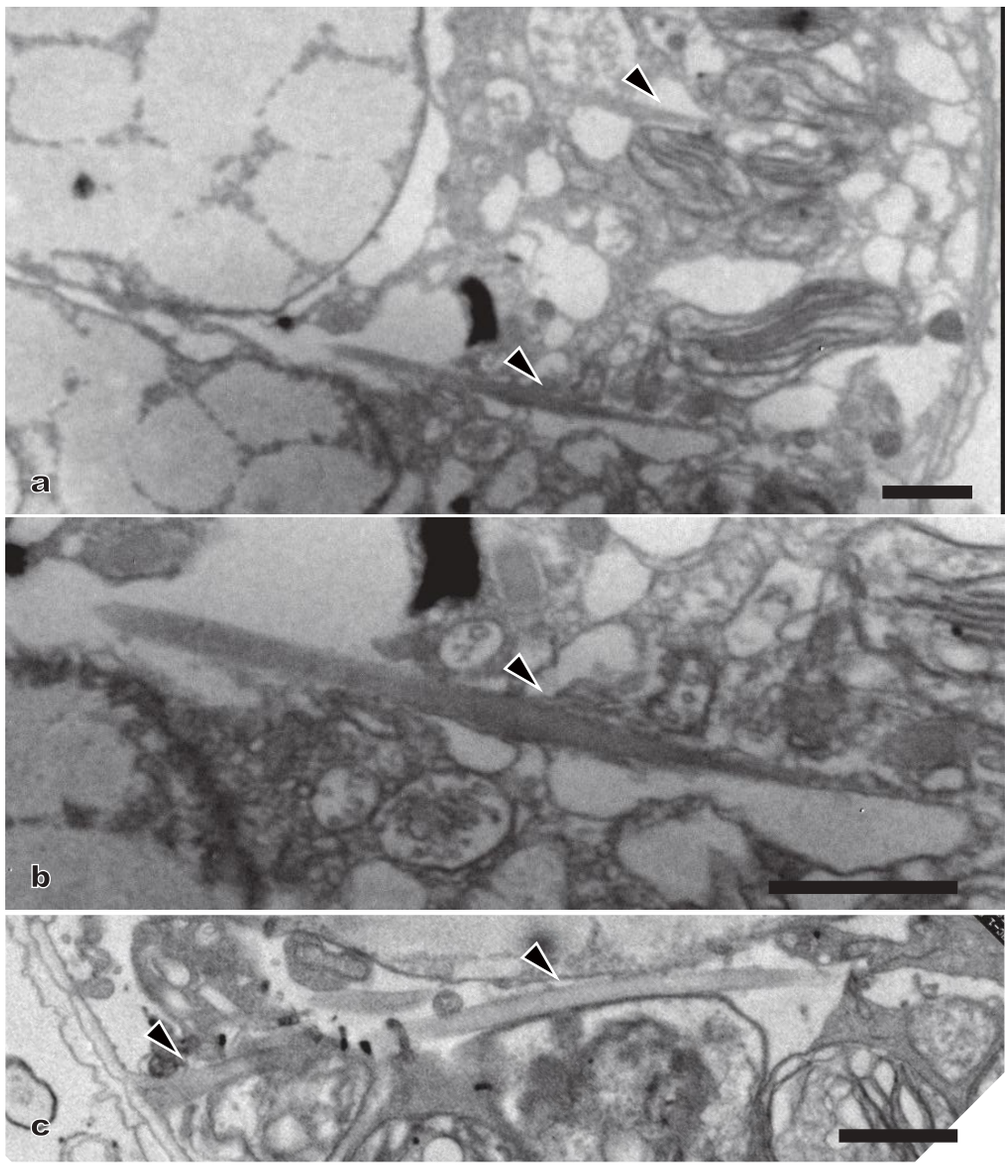


Fig. 47. *Amphidinium* sp. HG345. Transmission electron micrographs.
a. Portions of internal props (arrowheads). Scale bar = 1 μm.
b. Portion of a single internal prop (arrowhead). It is electron-opaque and is homogenous. Scale bar = 500 nm.
c. Portion of a single prop (arrowheads). It is attached to the basal layer, but is distinct from it (arrowhead). Scale bar = 1 μm.

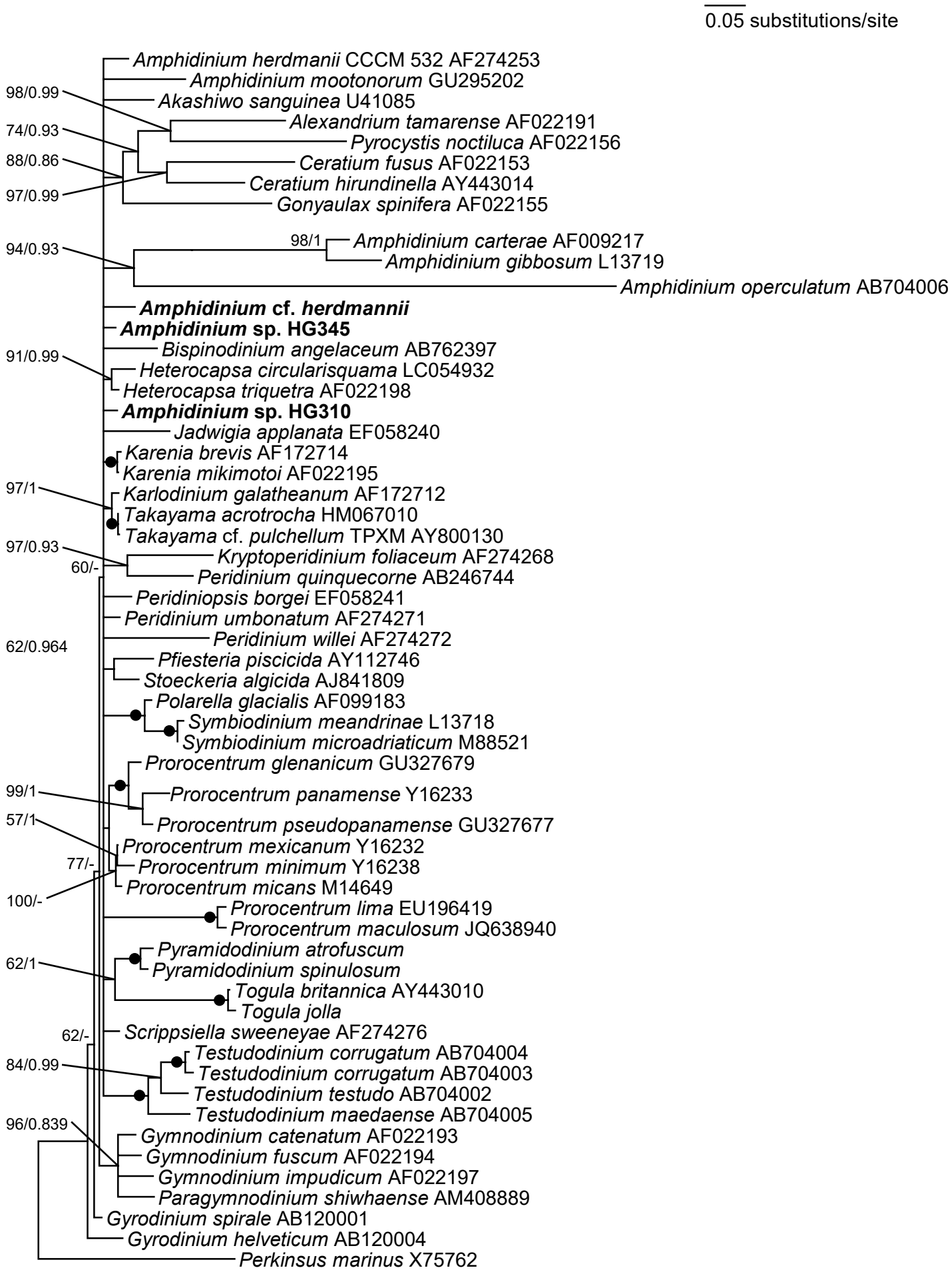


Fig. 48. Maximum likelihood phylogenetic tree tree inferred from partial SSU DNA sequences. ML bootstrap (>50%) and Bayesian PPI values (>0.8) are indicated. Solid circles represent nodes with a 100% ML bootstrap and Bayesian PPI of 1.

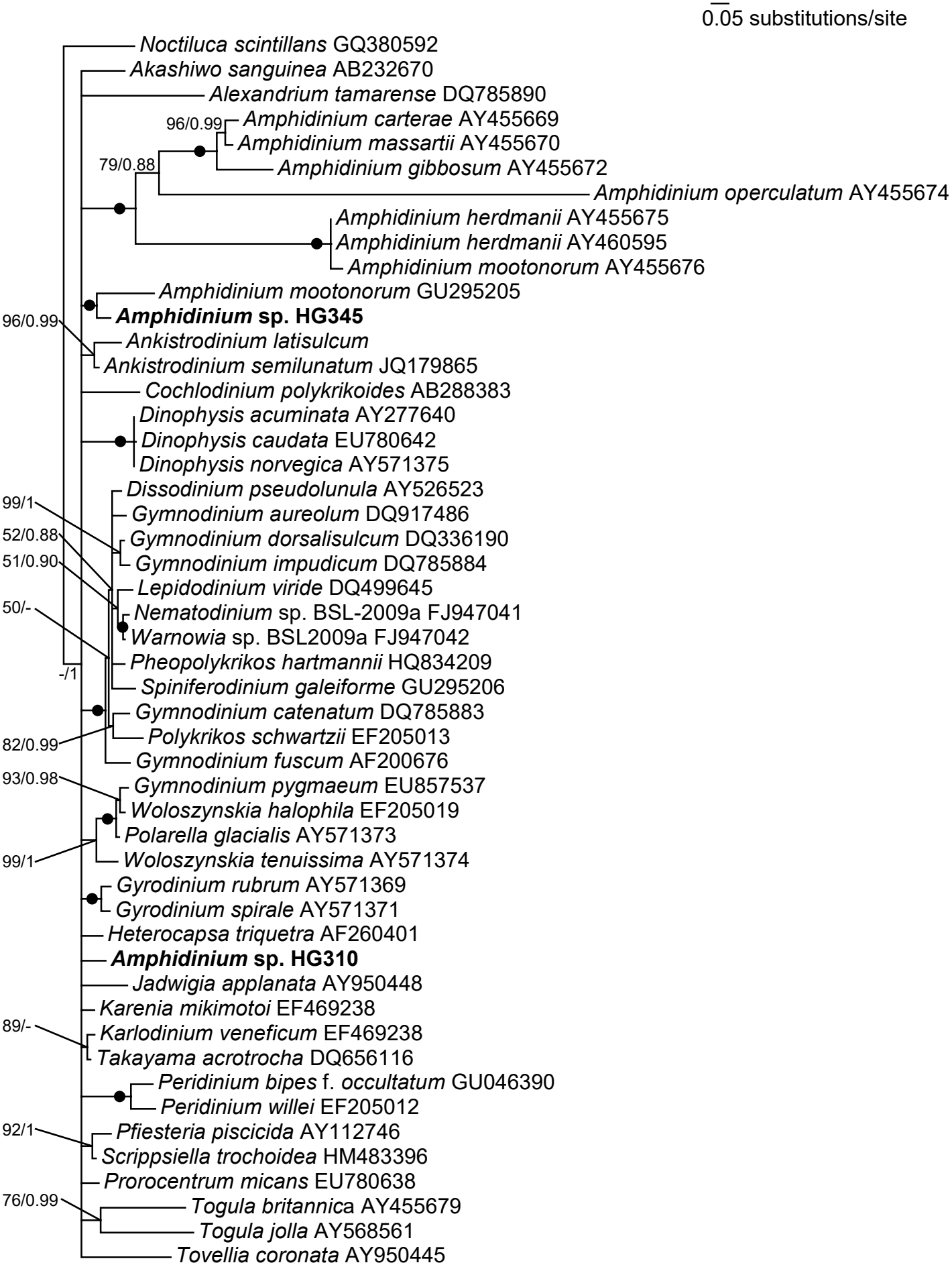


Fig. 49. Maximum likelihood phylogenetic tree tree inferred from partial LSU D1 - D3 DNA sequences. ML bootstrap (>50%) and Bayesian PPI values (>0.8) are indicated. Solid circles represent nodes with a 100% ML bootstrap and Bayesian PPI of 1.



Fig. 50. Bayesian PPI consensus phylogenetic tree inferred from partial SSU DNA sequences. The PPI values (>0.8) are indicated at the nodes. This tree is not congruent with the ML tree.

Table 4. HG310, HG345 and morphologically similar species

Species	Length (µm)	Width (µm)	Episome shape	Ventral furrow	Hyposome shape	Dorsal groove	Pyrenoid	Nucleus
Testudodinium maedaense[1,3]	20 – 28	15 – 20	very small, tongue-shaped	present	ellipsoidal, rounded posterior	absent	present	posterior, oval
Amphidinium herdmanii[2,3]	20 – 31	15 – 25	large triangle, apically flat	absent	Slightly asymmetrical, left longer than right	absent	present	posterior, crescent-shaped
Amphidinium mootonorum[2,3]	30 – 50	24 – 44	flattened anterior, slightly deflected to the left	absent	oval	absent	absent	central, elongate-oval
Amphidinium sp. HG310[4]	30 – 42.5	25 – 37.5	very small	present	ovoid to ellipsoid, asymmetric posterior end	present	absent	posterior, oval
Amphidinium sp. HG345[4]	27.5 – 45	22.5 – 32.5	small, triangular, expanded tip	absent	ovoid with rounded posterior	absent	absent	central, spherical or ellipsoidal

1 Horiguchi *et al.* (2012)
2 Murray and Patterson (2002)
3 Hoppenrath *et al.* (2014)
4 This work

Chapter 3:

Two new psammophilic species of the genus *Heterocapsa*

Introduction

Heterocapsa Stein 1883 is a cosmopolitan genus of thecate dinoflagellates, comprised of 18 recognised species and one sub-species (Guiry and Guiry, 2016; von Stein, 1883). The type species is *Heterocapsa triquetra* (Ehrenberg) Stein. The genus is of interest as some species form toxic algal blooms – notably *H. circularisquama* Horiguchi (Horiguchi, 1995a).

Members of *Heterocapsa* are small and free-living. They are thecate dinoflagellates, elliptical to ovoid in shape. The thecal plate formula is Po, cp, 5', 3a, 7", 6c, 5s, 5'", 0-1p, 2", with possible variations (Iwataki, 2002). Body scales are a characteristic of the genus: in *Heterocapsa*, the morphology of the body scales is considered as a diagnostic feature (Iwataki, 2002, 2008). All the species in the genus *Cachonina* (Loeblich, 1968) were later transferred to *Heterocapsa* following the re-examination of tabulation and noting the presence of body scales in the former (Morrill and Loeblich, 1981). The changes in tabulation patterns in the history of the description of *Heterocapsa* is partly due to the different systems for naming plates; the current system followed is the Kofoid system (Iwataki, 2002).

The taxonomy of *Heterocapsa* is currently dependent on a number of features accepted as diagnostic. These are the cell size, cell shape, thecal plate arrangement, relative positions of the nucleus and pyrenoid, nature of the pyrenoid matrix, and ultrastructure of the body scales. Of these, thecal plate arrangement, relative positions of nucleus and pyrenoid and the ultrastructure of the body scales are most significant. In addition to the thecal plate arrangement, the morphology of the second anterior intercalary plate is important in distinguishing between species. This and the relative positions of nucleus and pyrenoid are often helpful in distinguishing between otherwise similar species. The body scale ultrastructure is a key diagnostic characteristic: every species and sub-species has its own unique body scale, with the exception of *H. triquetra* and *H. pseudotriquetra*, whose body scales are highly similar (Iwataki, 2002, 2008). From a phylogenetic viewpoint, the ITS and 5.8S sequences are recognised as providing a good resolution of species

distinctions that correlates well with the delineations established from morphological data. The SSU data indicate that *Heterocapsa* is monophyletic within the Dinophyceae.

Heterocapsa psammophila Tamura, Iwataki et Horiguchi (Tamura *et al.*, 2005), is the first species of *Heterocapsa* that is known to be a true benthic dinoflagellate. All other species currently known are planktonic. In this chapter, I shall describe two novel benthic, psammophilic species of *Heterocapsa* and will provide morphological and phylogenetic evidence to support my case. In addition, I here, for the first time, report the ultrastructure *Heterocapsa* cysts.

Materials and methods

Sampling and culture

HG333 was isolated from sand samples collected on 30 April 2014 from the seafloor off Mageshima Island at a depth of 35 m; HG341 was isolated from samples collected on 19 August 2014 from the same area at a depth of 56 m (Table 1, Fig. 3). The samples were collected using a Smith-McIntyre grab sampler on collection cruises of the Nansei-maru. The sand samples were sent to the laboratory of Phycology at Faculty of Science, Hokkaido University, where dinoflagellate cells were isolated. A spoonful of the sand sample was taken in a plastic cup containing autoclaved seawater supplemented with Daigo IMK medium (Nihon Pharmaceutical Co., Tokyo, Japan) for enrichment. 0.1% Germanium dioxide was also added to prevent growth of diatoms. This was cultured at 25°C and with an illumination of 50 µmol photons m^{-2} s^{-1} with 16:8 light:dark regime. Dinoflagellate cells found were isolated using drawn capillary Pasteur pipettes under an inverted microscope (Olympus CX41, Tokyo, Japan) and a clonal culture was established. The culture strains) was maintained in IMK-supplemented seawater under the same conditions described above.

Light microscopy and scanning electron microscopy

For light microscopic observations, living cells were observed using a Carl Zeiss Axioskop 2 microscope equipped with Nomarski interference optics (Carl Zeiss Japan, Tokyo) and the fluorescent microscopic observations were made using the same microscope with filter set 15. Photographs were taken using a Leica MC-120HD digital camera (Leica Microsystems, Germany). For scanning electron microscopy, the cells were fixed for one hour in a solution of 0.1% Lugol's iodine made up with culture medium, and thereafter dehydrated and critically point dried according to the protocol described by Yamada *et al*. (2013). Critically point dried (HITACHI HCP-2, Tokyo, Japan) samples were sputter-coated with gold for 180 seconds at 30 mA (HITACHI E-1045) and viewed with a SEM (S-3000N, HITACHI). Contrast of the images was edited using Adobe Photoshop CS5.

Transmission electron microscopy

To collect cells, after removing excess culture medium, the attached cells at the bottom of Petri dish were harvested by sweeping gently by a sterilized paint brush. The collected cells were transferred into 15 ml plastic tubes and centrifuged at 40 × g for 10 min. The cell pellet was re-suspended in 150 µl culture medium and 50 µl of 4% OsO_4 made up in distilled water was added and fixed for 1 hour at room temperature. The following protocol was the same as chemical fixation protocol described by Yamada *et al*. (2013) except that fixation was made only with 1% osmium tetroxide (OsO_4) instead of a cocktail of glutaraldehyde and OsO_4. Sections were cut using a diamond knife on an ultra-microtome (LEICA EM UC6, Germany). Sections were picked up on formvar coated one-slot grids and these were viewed with a transmission electron microscope (H-7650, HITACHI, Tokyo). Whole mounts of cells were were negative stained for the oservation of body scales according to the protocol described by Iwataki (2002), but EM stain (Nisshin EM company, Tokyo) was used to stain the whole mounts in place of uranyl acetate.

DNA extraction and Polymerase Chain Reaction (PCR) amplification

Approximately 10 cells from the HG277 culture were used to extract DNA using the QuickExtract™ FFPE DNA extraction kit (Epicentre, Tokyo, Japan) according to the recommended protocol. SSU rDNA and LSU rDNA were separately amplified by nested PCR. Primers used for amplification are given in Table 1.

Both rounds of amplification of ITS DNA were carried out using the primers SR12cF and 25F1R. The thermocycling programme consisted of an initial denaturation step at 94°C for 5 minutes; followed by 35 cycles of denaturation at 94°C for 30 s, annealing at 55°C for 30 s and extension at 72°C for 120 s; and the final extension step at 72°C for 7 minutes. The conditions for the second round of PCR amplification were an initial denaturation step at 94°C for 5 minutes; followed by 25 cycles of denaturation at 94°C for 30 s, annealing at 51°C for 30 s and extension at 72°C for 90 s; and the final extension step at 72°C for 7 minutes. The PCR products were purified and sequenced with ABI PRISM Big Dye Terminator (Perkin-Elmer, USA). The purified sequence reaction products were run on a DNA autosequencer ABI PRISM310 Genetic Analyser (Perkin-Elmer). Both sense and anti-sense strands were sequenced.

Sequence analyses

The ITS r DNA sequences were aligned with the respective sequences from a number of other *Heterocapsa* species. The aligned sequences were analysed by the ML method using PAUP* version 4.0b10 (Swofford, 2001) and the Bayesian method using MrBayes 3.2.1 (Huelsenbeck and Ronquist, 2001; Ronquist and Huelsenbeck, 2003). The programme jModelTest version 2.1.4 (Darriba *et al.*, 2012; Guindon and Gascuel, 2003) was used to calculate the evolutionary model that was the best fit for ML analysis of the dataset.

Five hundred and sixty aligned sites were used for the analyses of ITS. The selected best fit model was the GTR + G model. The heuristic search for the ML analysis was performed with the

following options: a TBR branch-swapping algorithm and the Kimura 2-parameter NJ tree as the starting tree. The parameters used for the analysis were as follows: assumed nucleotide frequencies A = 0.2517, C = 0.2025, G = 0.2690, and T = 0.2768; substitution rate matrix with A<>C = 1.2448, A<>G = 4.1200, A<>T = 1.1780, C<>G = 0.4411, C<>T = 9.1462, G<>T = 1.0000; proportion of sites assumed to be invariable = 0.5280; rates for variable sites assumed to follow a gamma distribution with shape parameter = 0.696, and number of rate categories = 4. For the Bayesian analysis, GTR + G was also selected as the best evolutionary model by MrModeltest 2.3 (Nylander *et al*., 2004). Markov chain Monte Carlo iterations were carried out until 500,000 generations, when the average standard deviations of split frequencies fell below 0.01, indicating the convergence of the iterations.

Results

Species Descriptions

Heterocapsa sp. HG333

(Figures 51 – 57)

Diagnosis: Photosynthetic armoured dinoflagellate; cells ellipsoidal; 19.2 – 22.5 µm long, 13.8 – 18.0 µm wide; thecal plate arrangement Po, cp, 5', 3a, 7'', 6c, 5s, 5''', 2'''; dinokaryotic nucleus spherical, anterior, in epitheca; pyrenoid with cytoplasmic invaginations, surrounded by starch sheath, below nucleus; chloroplasts yellow-brown, elongated, peripheral; body scale triangular; forms cysts. Cysts spherical; 20 – 30 µm in diameter; vacuoles9 clearly visible.

Type locality: N30°41.153 E130°50.826; Sandy sediment on sea floor, depth 36.5 m, off Mageshima, Kagoshima, Japan.

Light microscopy

The motile cell was ellipsoid (Fig. 51 b, c), 19.2 – 22.5 µm (mean = 20.9 ± 1.14 µm, *n* = 15) long and 13.8 – 18.0 µm (mean = 16.1 ± 1.51 µm, *n* = 15) wide, with a length/width ratio between 1.12 – 1.45. The epitheca was slightly larger than the hypotheca (Fig. 51 b). The cingulum was equatorial, and was displaced about one time its width on the ventral surface (Fig. 51 c). The sulcus was wide, extending toward the antapex (Fig. 51 c). A large spherical dinokaryotic nucleus was located in the epitheca, occupying most of the volume (Fig. 51 b). A single, large starch-sheathed pyrenoid was present immediately below the nucleus, in the region of the cingulum (Fig. 51 b). The chloroplasts were yellow-brown (Fig. 51 b, c).

The thecal plate arrangement of this species was apical pore plate (Po), canal plate (cp), five apical plates (5'), three anterior intercalary plates (3a), seven pre-cingular plates (7"), six cingular plates (6c), five sulcal plates (5s), five post-cingular plates (5'"), and two antapical plates (2'"") (Figs 52, 53). The second anterior intercalary plate is heptagonal. It is quite large compared to the surrounding plates and abuts the 3', 4', 1a, 3a, 3", 4" and 5" plates.. The body scales in this species were either scarce or delicate, as none were observed in the SEM, even within the sulcus or cingulum.

The cells of this species also formed cysts (Fig. 51 a) in cultures older than a week, with the number of cysts increasing as the culture aged. Cysts were 20 – 30 µm in diameter and were spherical (Fig. 51 a, d, e). They were easily distigushed from and much larger than motile cells. Organelles could not easily be distinguished, but yellow-brown chloroplasts were present (Fig. 51 d, e). The cyst is highly vacuolated and a few vacuoles were observed within the cyst cytoplasm (Fig. 51 d, e). They were visibly distinct from the motile cells, and occupied a larger volume (Fig. 51 d, e). Motile cells were observed to emerge from the some cysts; however, the cysts were quite delicate and the shape of opening (archeopyle) was not confirmed.

Transmission electron microscopy

Figure 54 shows the arrangement of organelles. A large, typical dinokaryotic nucleus containing many thick chromosomes was present in the epitheca, taking up most of the volume (Fig. 54 a, b). Typical mitochondria were observed. The chloroplasts were elongated (Fig. 55 c), radiating outwards from the pyrenoid and distributed around the periphery of the cell (Fig. 54 a, b). They possessed lamellae with three thylakoid bands (Fig. 55 c) which are typical to dinoflagellates. The pyrenoid was large, angular, and surrounded by a starch sheath (Fig. 54); the pyrenoid matrix possessed cytoplasmic invaginations (Fig. 54 c, d). Electron opaque cell inclusions that might be lipid granules were also observed (Fig. 54 a, b). The thecal plates are present just below the plasmalemma; the plates themselves appear electron transparent (Fig. 55 a).

Only a few body scales were observed by negative staining TEM (Fig. 55 c-e). The scales were triangular in shape at the base plate, and a tri-radiate structure arose from it, possessing a number of spines (Fig. 55 c-e).

Figure 56 shows the arrangement of organelles within a cyst. The central part of the cysts is filled with vacuolar region which is filled with numerous granular materials. The nucleus was the only organelle that is similar to that in a motile cell (Fig. 56). The chloroplast profiles were completely different in outline: while a few elongate chloroplast profiles were seen, most of the profiles were large and asymmetrical (Fig. 57 a). The connection between the pyrenoid and the chloroplast was clearly visible; there were multiple instances of lamellae with multiple thylakoid bands – structures that appear similar to the grana in higher plants (Fig. 57 a). The chloroplasts themselves are much larger than those in the motile cells (Fig 57. a, b). Some of the chloroplast profiles also exhibited large thylakoid-free areas – stroma – that occupied up to half the volume of the chloroplast (Fig. 57 b). There are instances of multiple interconnected pyrenoids (Fig. 57 c), though the pyrenoids are surrounded by starch granules (Fig. 57 a, c). Thecal plates are absent in the cysts; there is a thick pellicle surrounding each cyst (Fig. 57 d). Large accumulation bodies are also present (Fig. 57 e) in all cysts.

Heterocapsa sp. HG341

(Figures 58 – 61)

Diagnosis: Photosynthetic armoured dinoflagellate; cells ellipsoidal; 17.5 – 27.5 µm long, 12.5 – 17.5 µm wide; thecal plate arrangement Po, cp, 5', 3a, 7", ?c, ?(2+)s, 5"', 2""; dinokaryotic nucleus spherical, anterior, in epitheca; large pyrenoid with cytoplasmic invaginations and starch sheath, below nucleus; chloroplast yellow-brown, elongated, reticulate; body scale triangular.

Type locality: N30°37.223 E130°51.067; Sandy sediment on sea floor, depth 56.4 m, off Mageshima, Kagoshima, Japan.

Light and Scanning electron microscopy

The motile cell was ellipsoid (Figs 58, 59), 17.5 – 30.0 µm (mean = 22.95 ± 3.26 µm, n = 50) long and 12.5 – 20.0 µm (mean = 16.0 ± 2.47 µm, n = 50) wide, with a length/width ratio between 1.125 – 1.67. The epitheca was slightly smaller than the hypotheca (Fig. 58 a, b; Fig. 59 a, b). The cingulum was equatorial, and was displaced about 0.5 times its width on the ventral surface (Fig. 59 a, b). The sulcus was wide, extending toward the antapex (Fig. 59 a). A large dinokaryotic nucleus was located in the epitheca, occupying most of the volume (Fig. 58 b). A single, large starch-sheathed pyrenoid was present immediately below the nucleus (Fig. 58 b). The chloroplasts were yellow-brown and were reticulate (Fig. 58).

The thecal plate arrangement of this species is apical pore plate (Po), canal plate (cp), five apical plates (5'), three anterior intercalary plates (3a), seven pre-cingular plates (7"), ? cingular plates (?c), 2+ sulcal plates (?s), five post-cingular plates (5"'), and two antapical plates (2"") (Fig. 59). The body scales in this species are abundant and adhere tightly to the cell: in order to detach them the cells were shaken thoroughly; even after vigorous agitation, a large number of scales remained in the sulcus and cingulum (Fig. 59 a, b).

Transmission electron microscopy

Figure 60 shows the arrangement of organelles. A large, typical dinokaryotic nucleus containing many thick chromosomes was present in the epitheca that occupies (Fig. 60). Typical mitochondria (Fig. 61 a) were observed. The chloroplast profiles were elongated (Fig. 61 b); they were interconnected, radiating outwards from the pyrenoid and spread across the periphery of the cell (Fig. 60). They possessed lamellae with three thylakoids bands (Fig. 61 a) which are typical to dinoflagellates. The pyrenoid was roughly triangular in shape, surrounded by starch granules; its matrix was penetrated by cytoplasmic invaginations (Fig. 61 c). A pusule was present, composed of a number of circular vesicles that were irregularly arranged (Fig 61 b).

The body scales possessed a circular base plate (Fig 61 d, e); the elevated portions were tri-radiate, supported by six uprights and possessed a total of nine spines (Fig. 61 d – f). There was no apparent hole in the middle of the base plate of the scale (Fig. 61 d, e).

Phylogenetic analysis

The phylogenetic tree based on ITS sequence data is shown in Figure 62. *Heterocapsa* sp. HG333 was positioned in the triquetra-pseudotriquetra sub-clade, closest to *H. pseudotriquetra*. *Heterocapsa* sp. HG341 was identical to *H. ovata* Iwataki et Fukuyo. Both these relationships had robust support from both the maximum likelihood bootstrap and the Bayesian posterior probability indices – 98% for HG333 from ML and Bayesian approaches; for HG341, the support from ML was 90.41 and that from the Bayesian approach was 95%.

Discussion

In this chapter, I describe two novel benthic species of *Heterocapsa*. In the description of the first benthic *Heterocapsa* species, *H. psammophila*, culture experiments with sterile sand were

conducted to ensure that the species was truly benthic (Tamura *et al.*, 2005). In the two species I have described, this approach was not taken; however, observations of both species in culture revealed that they adhered to the surface of the Petri dishes; when motile, they are mostly found close to the surface of the Petri dishes and very rarely at the surface of the culture medium.

A list of similarities and differences between all described species of *Heterocapsa* including the two novel species is presented in Table 5. It can be established that neither of the two novel species are similar to *H. psammophila*, beyond the diagnostic features of the genus.

The most similar species to HG333 is *H. pseudotriquetra*, with which shares a number of morphological similarities. HG333 is difficult to distinguish from it on the basis of gross morphological characters: under light microscopy, the only noticeable difference is the position of the pyrenoid. The cells of *H. pseudotriquetra* are described as spherical (Iwataki *et al.*, 2004) as opposed to ellipsoid cells in HG333; but the cell dimensions overlap: the average length:width ratio was 1.29 for both species. The second apical intercalary plate (2a) reveals some differences. In both species, it is heptagonal, abutting 3', 4', 1a, 3a, 3", 4" and 5". The 2a plate is larger in HG333 when compared to that of *H. pseudotriquetra*, but the value of this feature as a reliable diagnostic feature is debatable. Both HG333 and *H. pseudotriquetra* form cysts in culture. The pyrenoid matrices of HG333 and *H. pseudotriquetra* are penetrated by cytoplasmic invaginations. The pyrenoids themselves are angular in both species, but the starch sheath in *H. pseudotriquetra* is composed of much thicker starch granules (Iwataki, 2002) than that of HG333. The body scales of HG333 are similar to that of *H. pseudotriquetra* in possessing a triangular base; however, as only three were observed – due to the paucity of body scale in HG333 – no further conclusions could be established. It is possible that the body scales are indistinguishable from each other as this is a feature of the triquetra-pseudotriquetra sub-clade (Iwataki, 2002, 2008). While cysts have been reported from *H. pseudotriquetra*, not much is known beyond the fact they are formed (Iwataki *et al.*, 2004). In this chapter I describe the ultrastructural features of the cysts. Most notable are the oddly shaped

multiple pyrenoids (Fig. 57 c) and the large chloroplasts that contain grana-like regions, which are quite different from those of vegetative motile cells. While grana-like regions are rare in dinoflagellates, they are not completely unknown (see Horiguchi and Sukigara, 2005). In conclusion, the morphological data suggests that HG333 is indeed a new species in *Heterocapsa*, closely related to *H. pseudotriquetra*; the position of HG333 in the phylogenetic three and the production of cysts support this conclusion. It should be noted that *H. pseudotriquetra* is a planktonic species, while HG333 is a benthic species isolated from a depth of 56 m.

In terms of cell dimensions, HG341 is similar to *H. triqutera*, *H. orientalis*, and *H. circularisquama* (Table 5). However, there are distinct differences in the shape and position of the nucleus and the position of the pyrenoid that delineate them; most importantly, the body scales of all four species are completely different. In HG341, the nucleus is spherical and anterior, the pyrenoid is posterior with invaginations in the pyrenoid matrix, and the body scale has a circular base plate. In *H. circularisquama*, the nucleus is ellipsoid and lateral, being located both in epi- and hyposome, the pyrenoid is central and the pyrenoid matrix does not have invaginations, and the body scale has a circular base plate. *H. orientalis* has a spherical, posterior nucleus, an anterior, invaginated pyrenoid, and body scales with a triangular base plate; *H. triquetra* has a spherical, anterior nucleus, a posterior, invaginated pyrenoid, and body scales with a triangular base plate. The body scale of HG341 is best described as possessing a base plate similar to *H. circularisquama* and upright, horizontal bars and spines similar in arrangement to *H. triquetra*. Curiously, the phylogenetic study, however, indicates that HG341 possesses identical ITS sequence with that of *H. ovata*. This is surprising, as HG341 does not morphologically resemble *H. ovata*. *H. ovata* is larger than HG341, with hemispherical epitheca and hypotheca, a cingulum that is descends about 0.5 to 1 times its width and body scales with a triangular base plate (Iwataki *et al.*, 2003), as opposed to the conical epitheca and hemispherical hypotheca of HG341, along with a cingulum that descends 0.5 times its width and body scales with a circular base plate. Identical ITS sequences shared by

different species are not without precedent, as in macro algae, there have been instances of morphologically diverse species sharing identical ITS2 sequences (Stiger *et al.*, 2003). I conclude that HG341 is also a novel species of *Heterocapsa*.

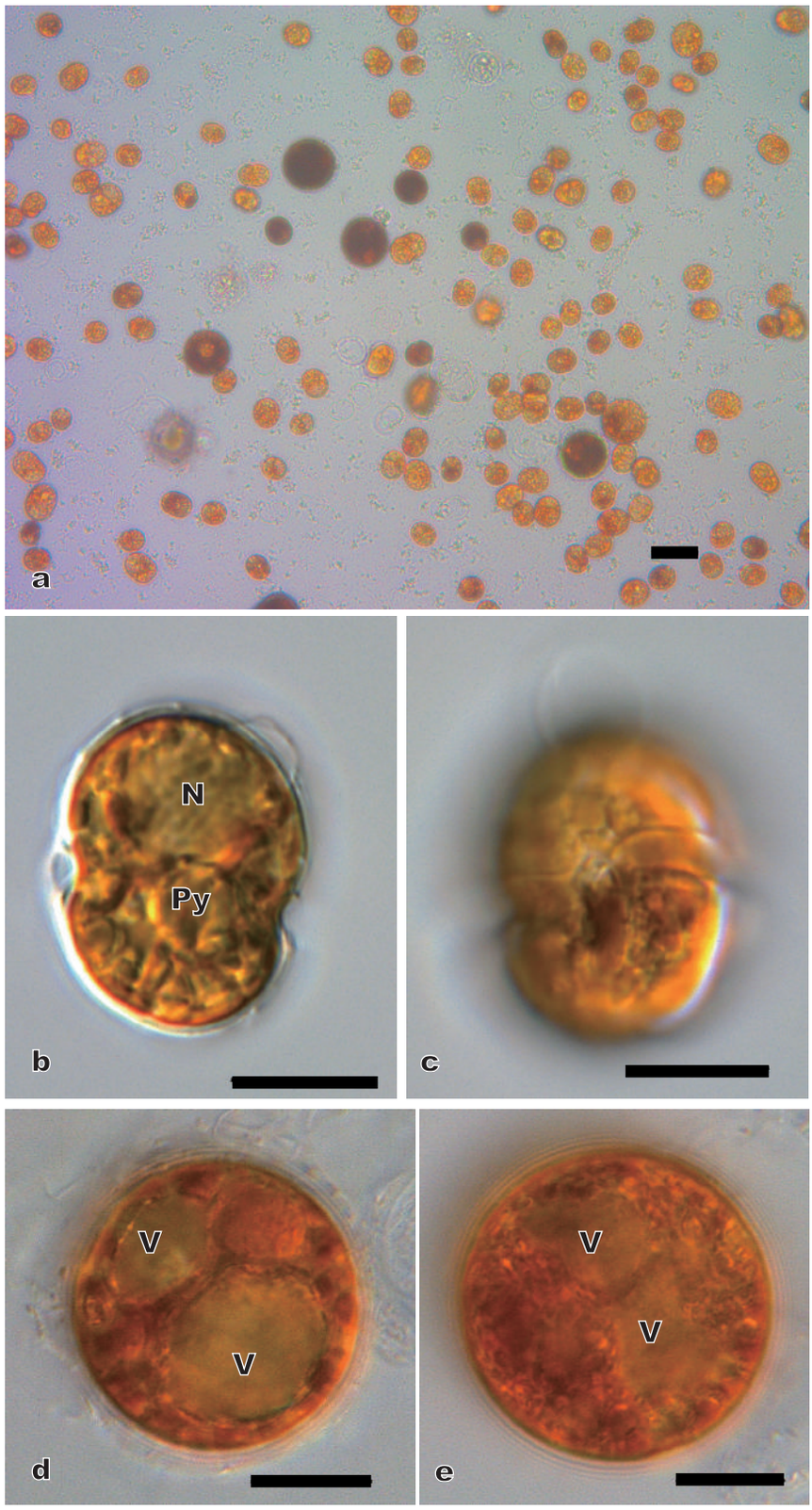


Fig. 51. *Heterocapsa* sp. HG333. Light micrographs.
a. Motile cells and cysts in culture.
b. Motile cell. The nucleus (N) is anterior and the pyrenoid (Py) is immediately below it.
c. Motile cell. The cingulum drops about one time its width on the ventral side of the cell. The sulcus is also visible.
d, e. Cysts. They are spherical and possess large vacuoles (V).
Scale bar = 10 µm.

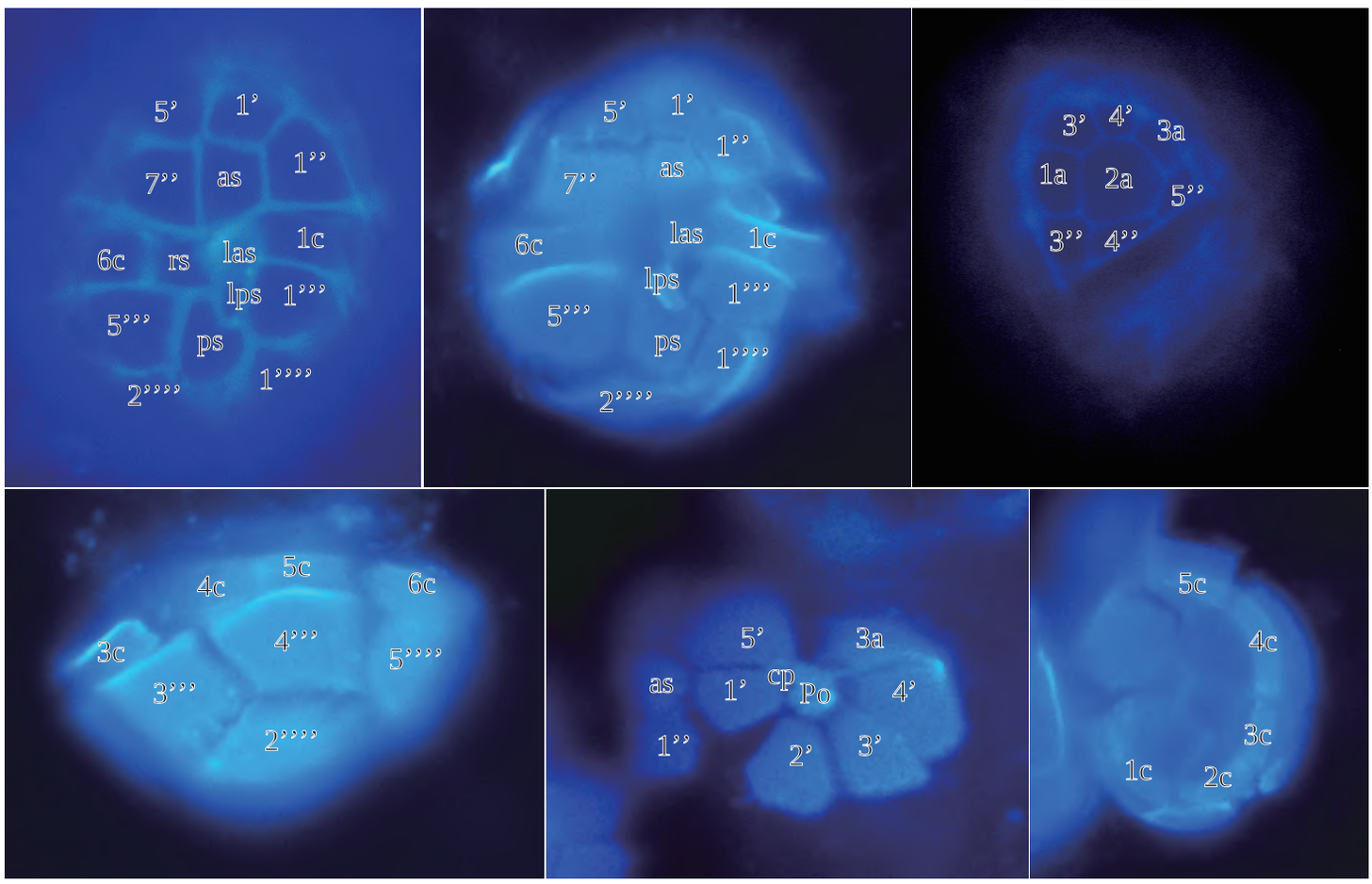


Fig. 52. *Heterocapsa* sp. HG333. Fluorescence light micrographs. Thecal plate arrangement in *Heterocapsa* HG333.

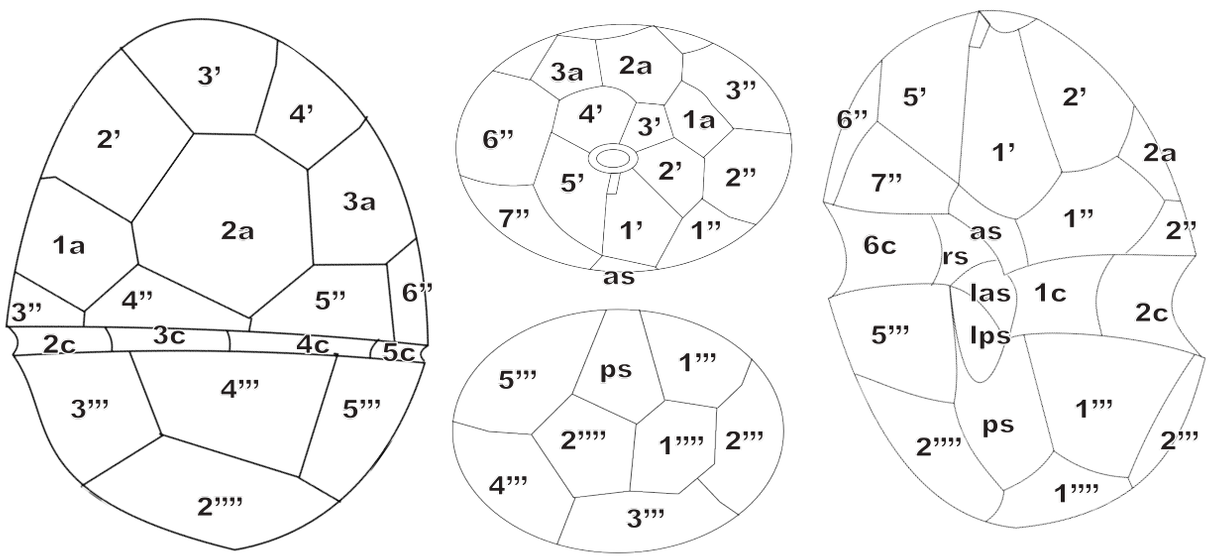


Fig. 53. Schematic representation of the thecal plate pattern in Heterocapsa sp. HG333

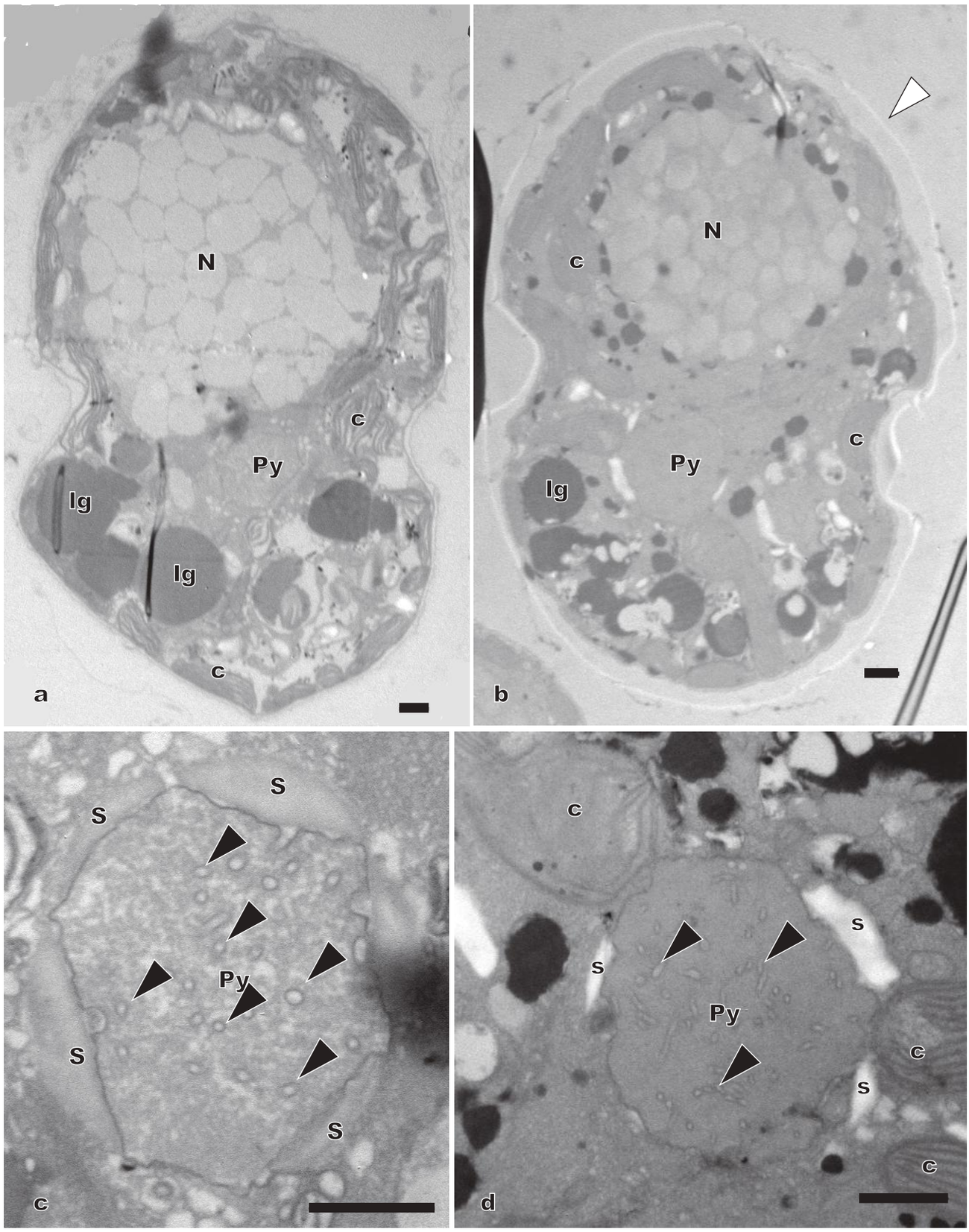


Fig. 54. *Heterocapsa* sp. HG333. Transmission electron micrographs.
a. Longitudinal section of a motile cell. The nucleus (N) occupies a large portion of the epitheca. The pyrenoid (Py) is immediately beneath it. The chloroplasts (c) are peripheral and radiate outwards from the pyrenoid. A large number of electron opaque lipid granules (lg) are also present.
b. Longitudinal sections of a cell entering encystment. The nucleus (N) occupies a large portion of the epitheca. The pyrenoid (Py) is central. The chloroplasts (c) are peripheral and radiate outwards from the pyrenoid. A large number of electron opaque lipid bodies are also present. The protplasm is detached from the thecal layer (open arrowhead).
c, d. Pyrenoid (Py). Cytoplasmic invaginations (soild arrowheads) are present in the matrix. They are surrounded by starch granules (S). Chloroplasts (c) radiate outward from the pyrenoid.
Scale bar = 1 μm

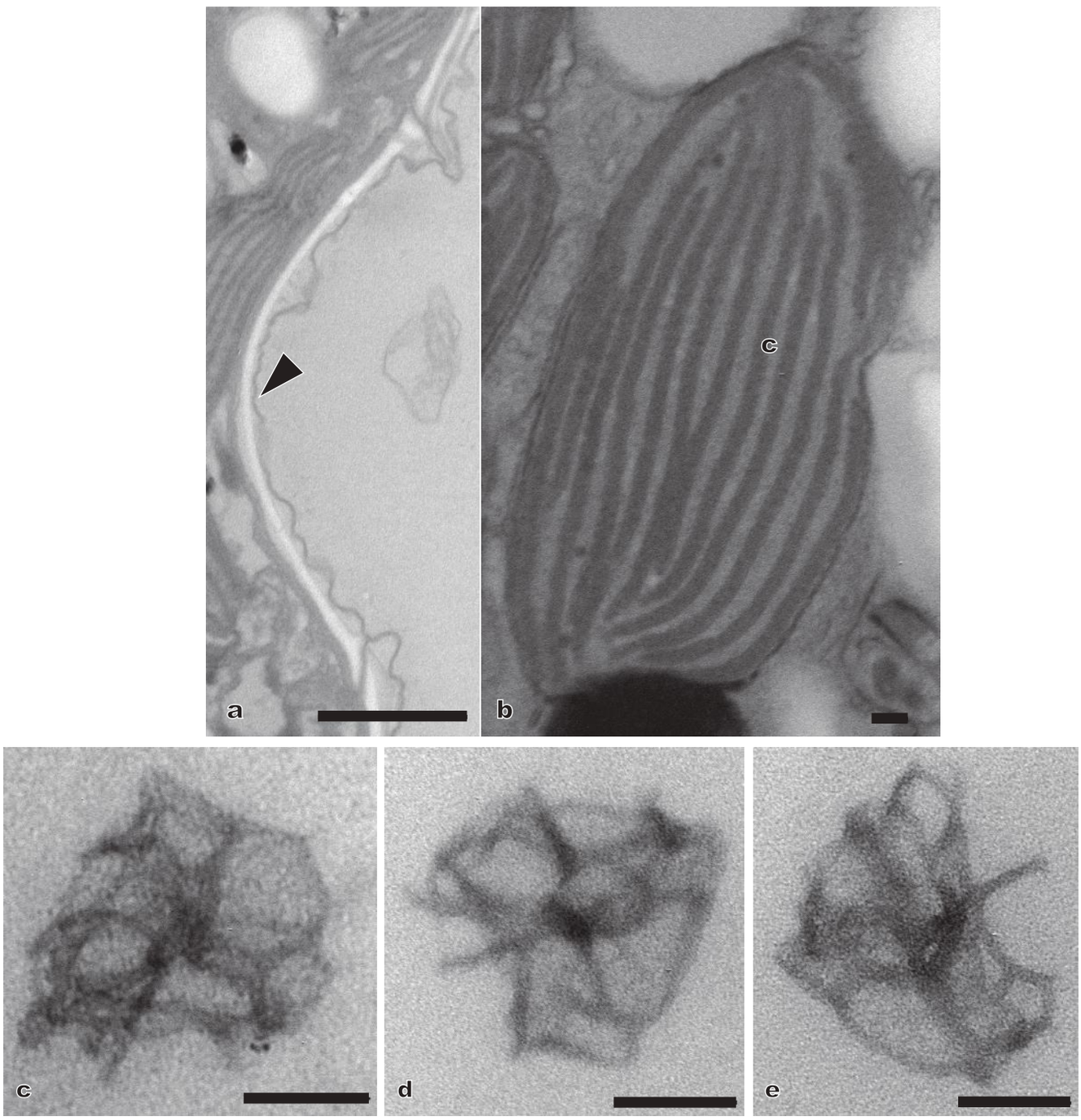


Fig. 55. *Heterocapsa* sp. HG333. Transmission electron micrographs
a. Thecal plates (amphiesma); a cingular plate (arrowhead) in the centre clearly separated from the pre- and post-cingular plates. Scale bar = 1 μm
b. Typical elongate chloroplast. Scale bar = 1 μm
c - e. Negative staining of body scales. The scales are triangular in outline, and appear to possess one to three spines in the centre. Scale bar = 100 nm.

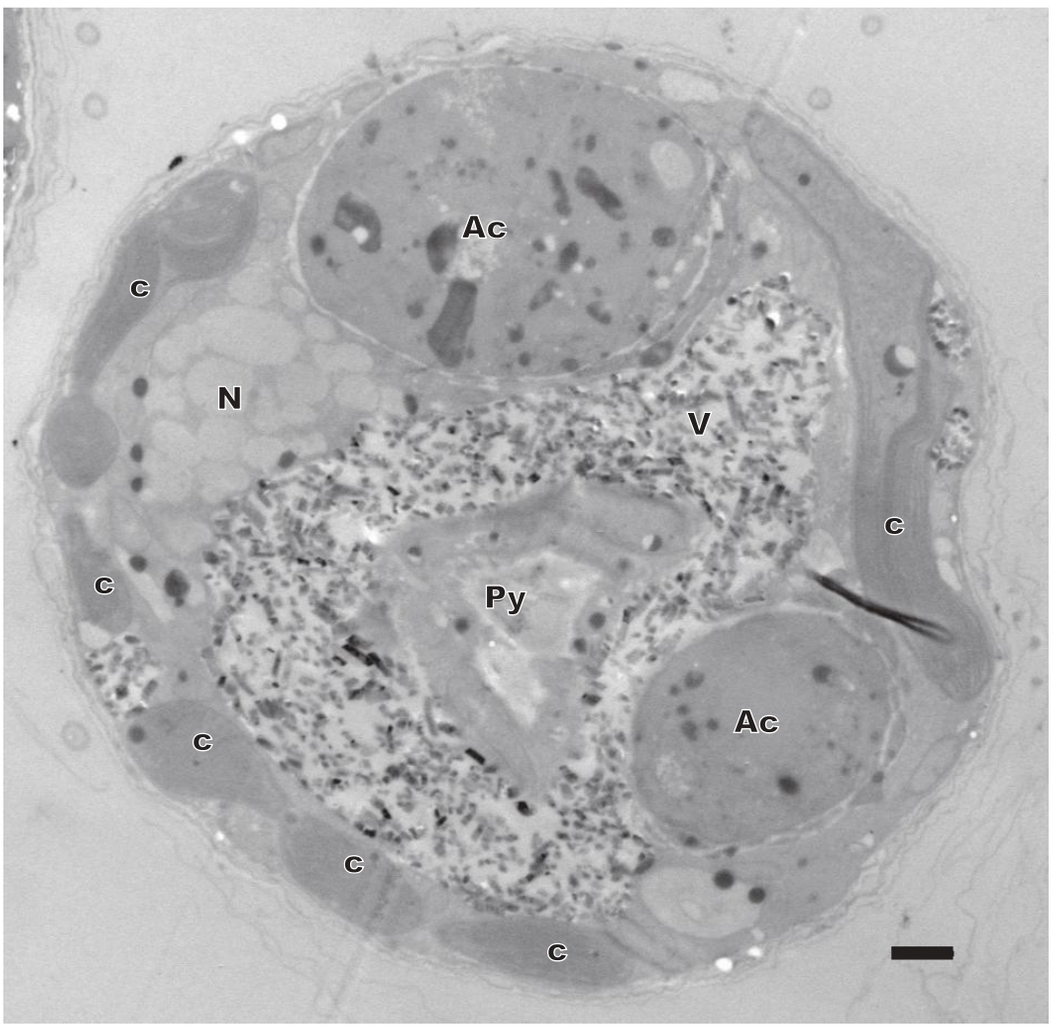


Fig. 56. *Heterocapsa* sp. HG333. Transmission electron micrograph.
Cyst. The nucleus (N) is tyipcally dinoflagellate, albeit reduced. The Pyrenoid (Py) is central and complety different from that of the motile cell. It is encircled by a vacuole (V) containing crystalline inclusions. The chloroplasts (c) are peripheral and elongated. Acuumulation bodies (Ac) are also present. Scale bar = 1 μm.

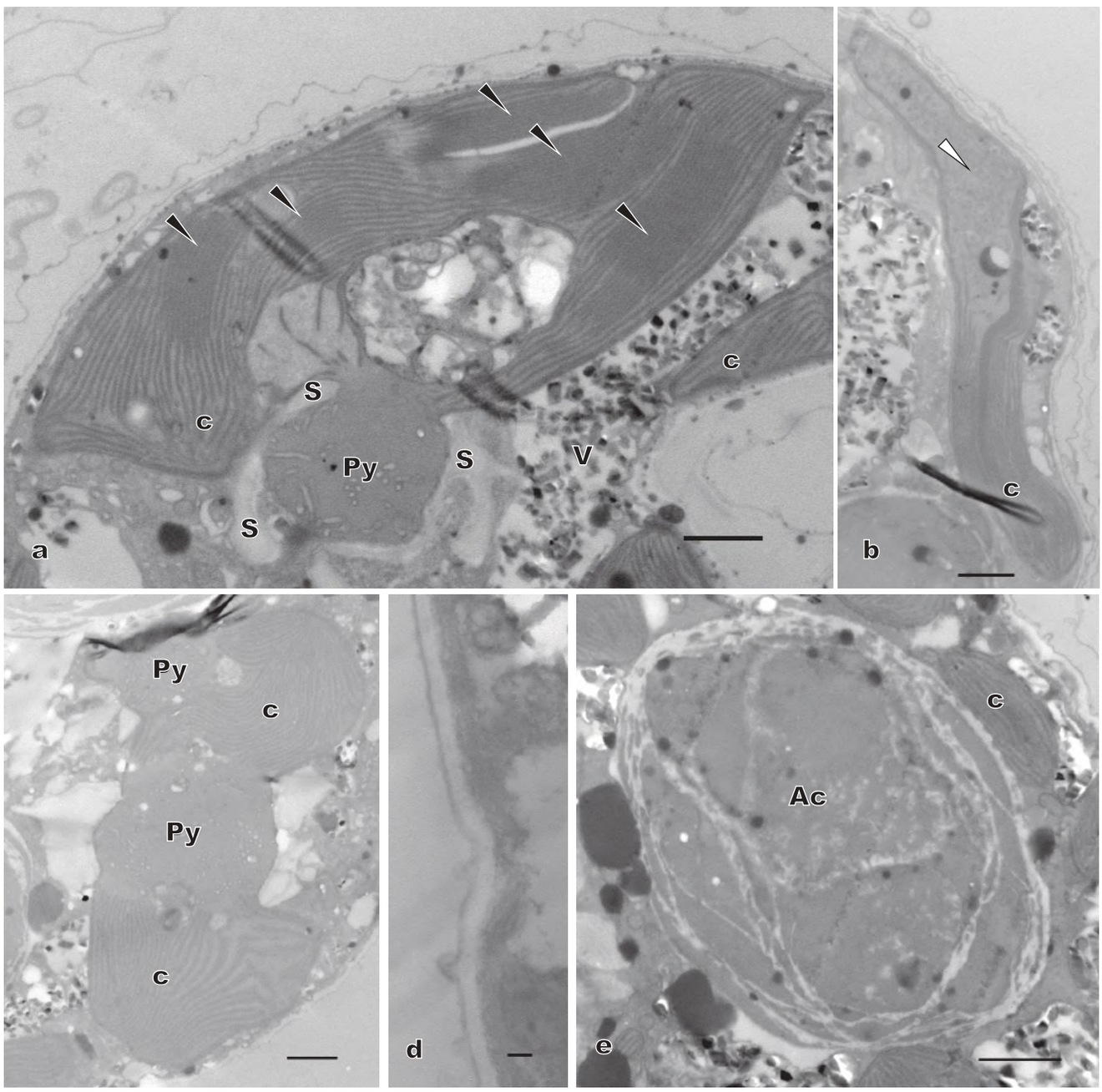


Fig. 57. *Heterocapsa* sp. HG333. Transmission electron micrographs of a cyst.
a. large chloroplast (c) with multiple instances lamellae comprised of numerous thylakoid bands -- grana-like lamellae (solid arrowheads).
b. a chloroplast (c) with a large stroma (open arrowhead).
c. a modified pyrenoid consisting of two regions of thylakoids (c) and two discrete pyrenoids (Py).
d. the surface of the cyst; the thecal plates are absent and in their place is a thick pellicle.
e. an accumulation body (Ac).
Scale bar = 1 μm.

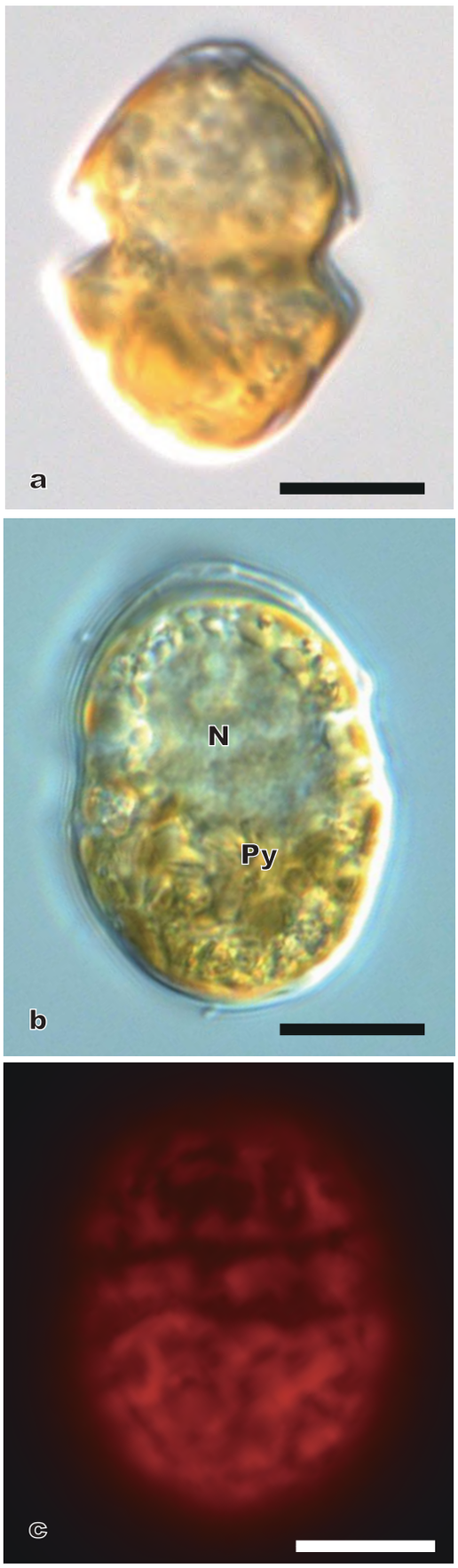


Fig. 58. *Heterocapsa* sp. HG341. Light micrographs.
a. Dorsal view of the cell.
b. Focal plane through the cell. The nucleus (N) and pyrenoid (Py) are visible.
c. Fluorescence light micrograph showing the reticulate chloroplast.
Scale bar = 10 µm

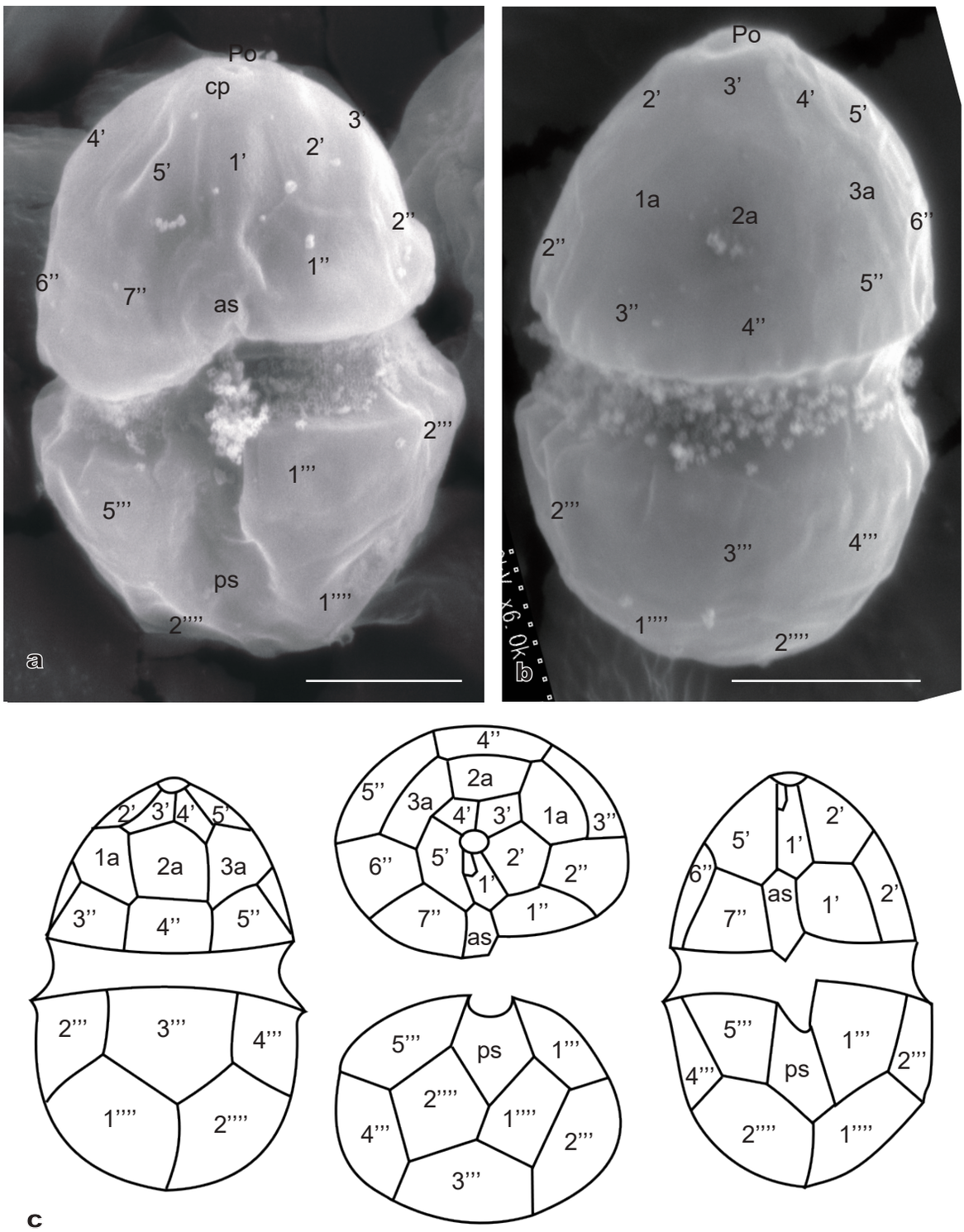


Fig. 59. Thecal plate arrangement in *Heterocapsa* sp. HG341. Scanning electron micrographs.
a. Ventral view and
b. Dorsal view of a cell showing the thecal plate arrangement.
c. Schematic illustrations of thecal plate arrangement.
Scale Bar = 10 μm.

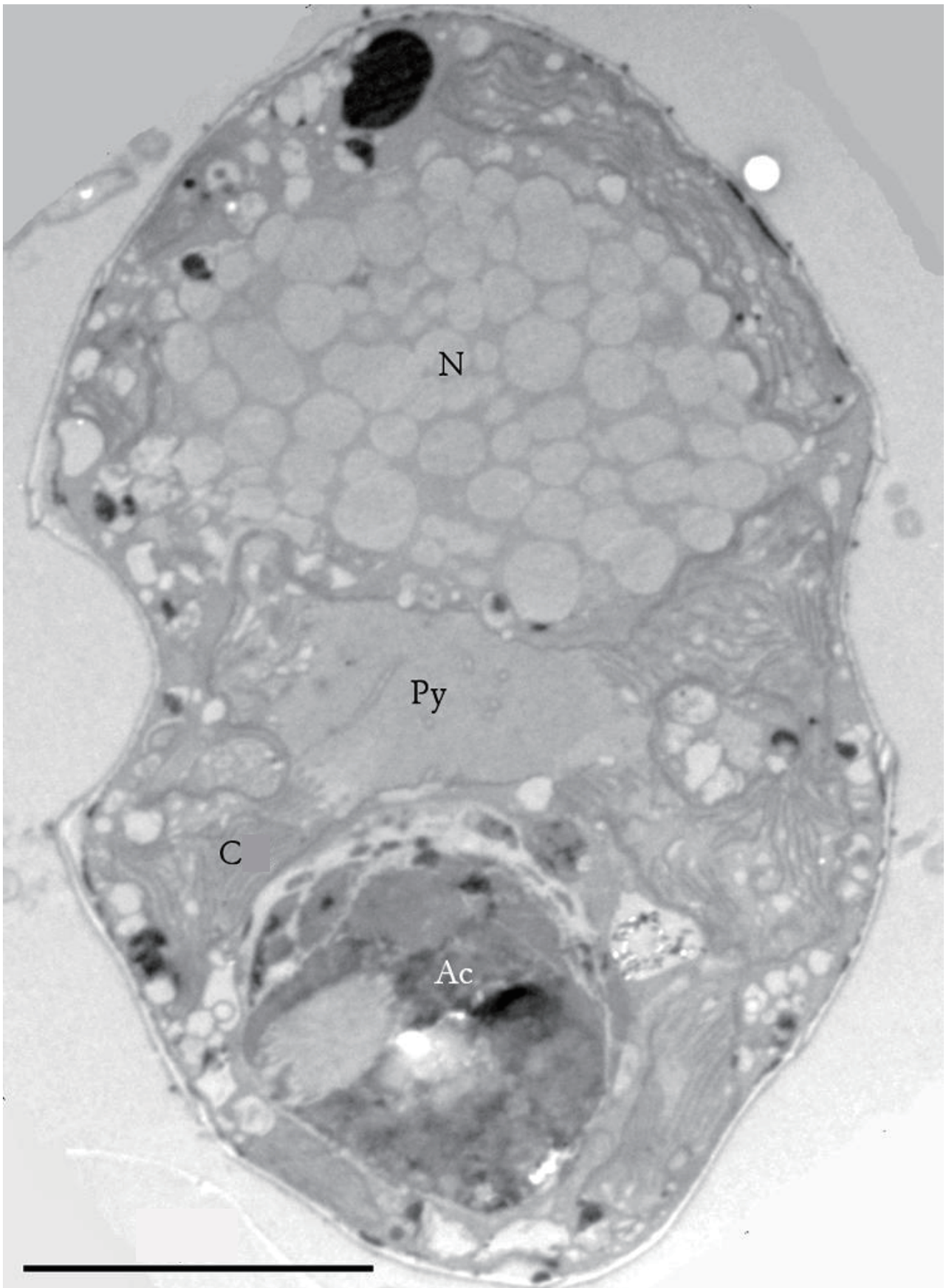


Fig. 60. *Heterocapsa* sp. HG341. Transmission electron micrograph.
Longitudinal section of entire cell. The nucleus (N) is anterior and the pyrenoid (Py) central. Chloroplasts (c) radiate outwards from the pyrenoid and are peripheral. An accumulation body (Ac) is present. Scale bar = 5 μm.

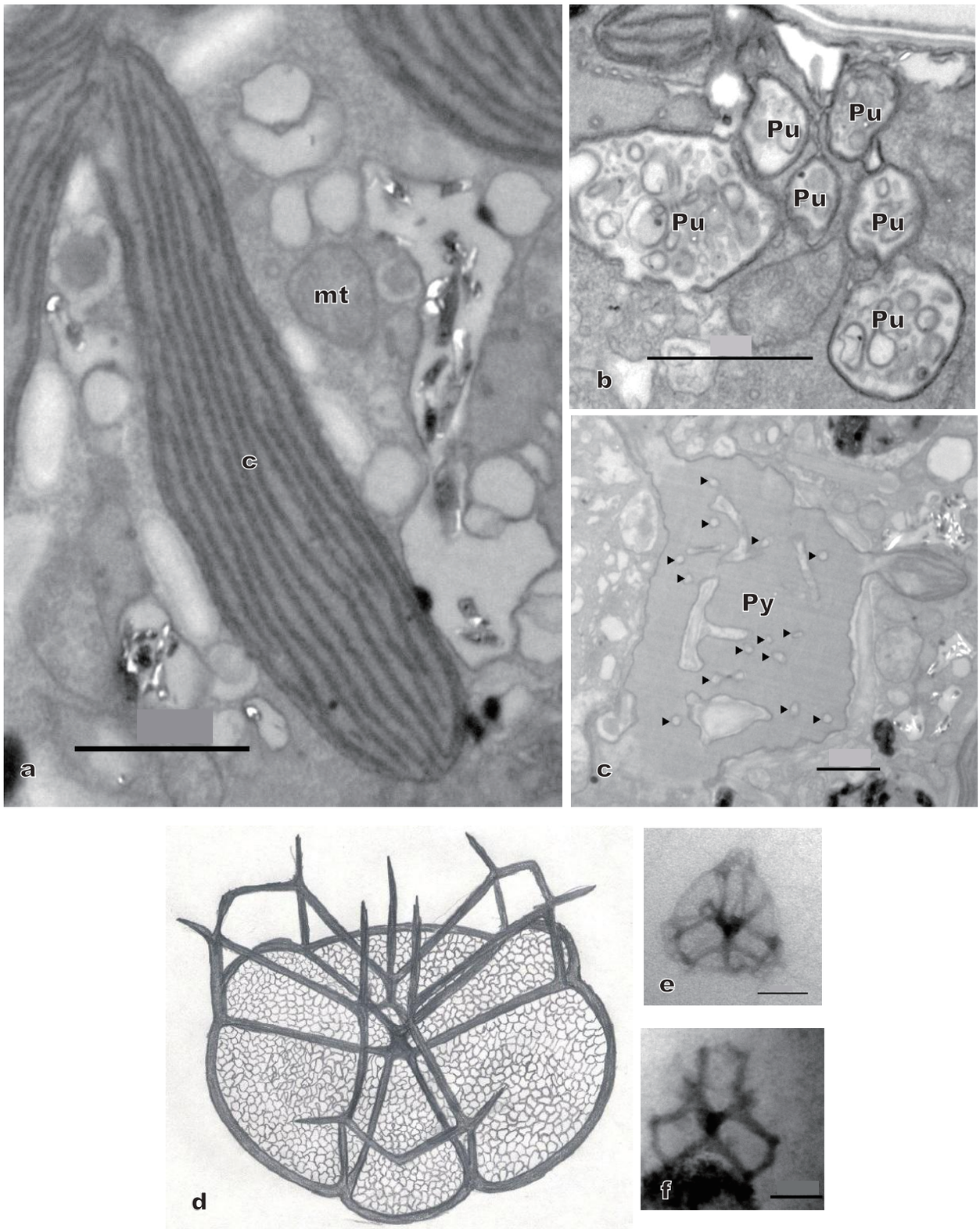


Fig. 61. *Heterocapsa* sp. HG341. Transmission electron micrograph.
a. Chloroplast (c) and mitochondrion (mt). Scale bar = 1 μm.
b. Pusule (Pu). Scale bar = 1 μm
c. Pyrenoid with cytoplasmic invaginations (arrowheads). Scale bar = 1 μm.
d. Line drawing of a body scale
e. Whole-mount transmission electron micrograph of a single body scale, possessing a circular base. Scale bar = 100 nm
f. Transmission electron micrograph of a body scale passing through the horizontal bars, showing three distinct sections. Scale bar = 100 nm.

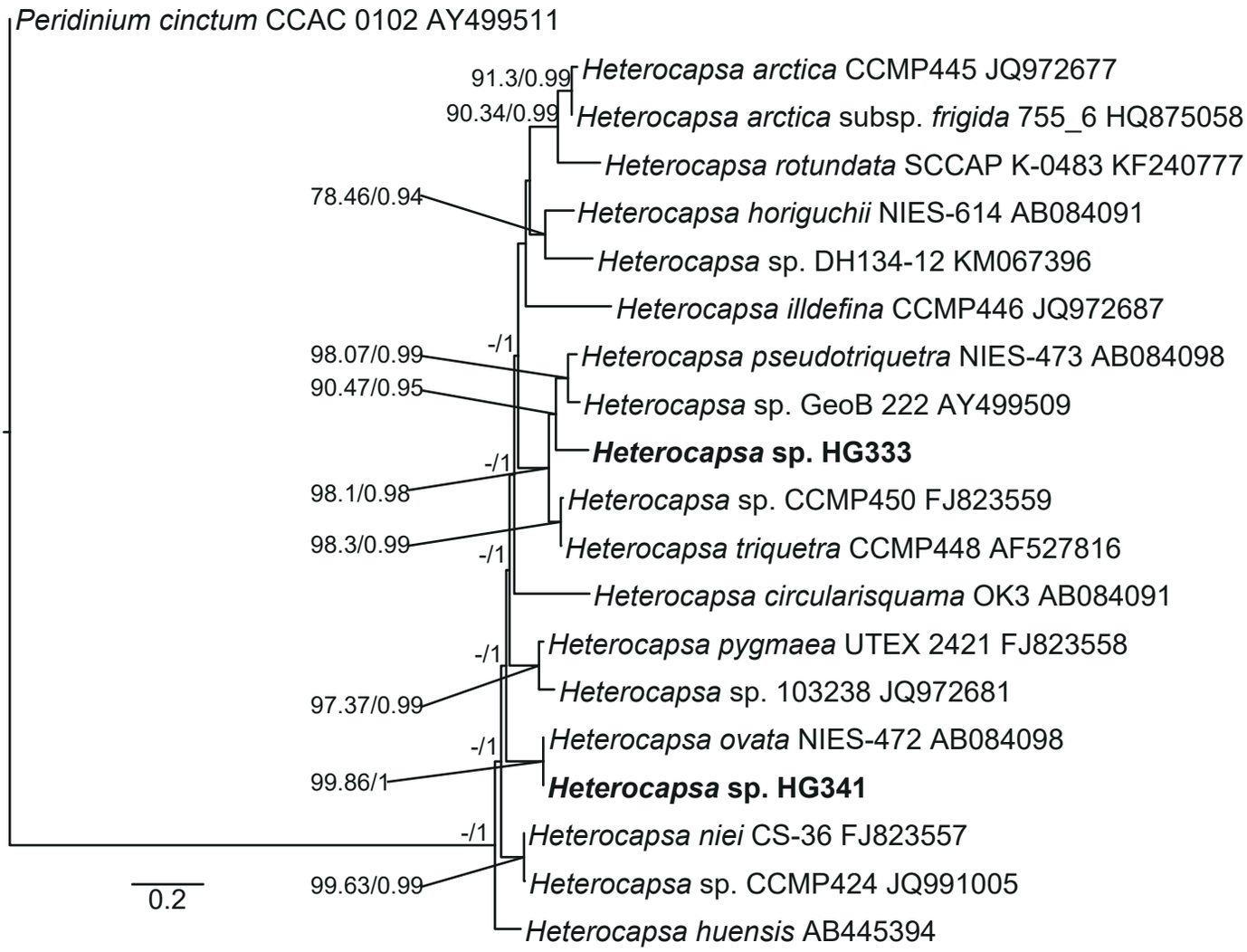


Fig. 62. Maximum likelihood tree constructed from ITS sequences. Sequences available from GenBank. Bootstrap values are given at the nodes as percentages; neighbour-joining (10000 replicates)/maximum-likelihood (100 pseudo-replicates).

Table 5. Morphological comparison of the *Heterocapsa* spp.

Species	Length, µm (mean)	Width, µm (mean)	Nucleus Shape	Nucleus position	Pyrenoid position	Pyrenoid Invaginations	Scale	Cysts
H. arctica	22.5-37.5 (29.5)	10.0-15.0 (11.6)	ellipsoid	middle	posterior	present	triangular	No
H. arctica subsp. *frigida*	12.0-19.0	7.5-12.5	ellipsoid	anterior	posterior	present	triangular	No
H. circularisquama	16.5-26.4 (23.7)	11.2-19.2 (15.5)	ellipsoid	middle	middle	absent	circular	No
H. horiguchii	13.2-20.8 (17.2)	10.0-13.6 (11.6)	spherical	anterior	posterior	absent	circular	No
H. huensis	13.6-22.4 (15.7)	9.6-16.8 (12.2)	spherical	posterior	middle	N.D.	triangular	No
H. illdefina	23.2-35.2 (29.2)	16.8-24.0 (19.8)	ellipsoid	middle	middle	present	triangular	No
H. lanceolata	16.4-25.0 (18.9)	10.0-15.0 (11.6)	ellipsoid	middle	anterior	absent	hexagonal	No
H. minima	10.0-13.0 (11.8)	6.9-9.1 (8.1)	ellipsoid ?	middle	anterior	N.D.	circular	No
H. orientalis	18.4-34.4 (25.7)	16.0-24.0 (19.6)	spherical	posterior	anterior	present	triangular	No
H. ovata	23.6-33.2 (26.9)	18.4-28.0 (21.4)	spherical	anterior	posterior	present	triangular	No
H. pacifica	45	30	N.D.	middle ?	N.D.	N.D.	N.D.	No
H. psammophila	9.0-12.0 (10.2)	6.0-9.0 (7.7)	spherical	posterior	middle	present	triangular	No
H. pseudotriquetra	18.4-27.2 (22.2)	14.4-21.6 (17.2)	spherical	anterior	posterior	present	triangular	Yes
H. pygmaea	12.0-18.4 (15.0)	9.6-12.8 (10.8)	spherical	posterior	anterior	absent	circular	No
H. rotundata	8.8-12.8 (10.4)	7.2-9.6 (8.5)	ellipsoid	middle	anterior	absent	triangular	No
H. triquetra	15.2-26.4 (22.1)	10.4-20.8 (15.0)	spherical	anterior	posterior	present	triangular	No
H. niei	18.4-27.2 (21.7)	12.0-19.2 (15.9)	spherical	posterior	anterior	absent	triangular	No
H. sp. HG333	19.2-22.5 (20.9)	13.8-18.0 (16.1)	spherical	anterior	middle	present	triangular	Yes
H. sp. HG341	17.5-27.5 (23.0)	12.5-17.5 (16.0)	spherical	anterior	posterior	present	circular	No

Chapter 4

Ultrastructure and phylogenetic position of a benthic marine dinoflagellate, *Prorocentrum* cf. *elegans* Faust

Introduction

The genus *Prorocentrum* is a member of the class Dinophyceae and possesses typical dinokaryotic nucleus and have both transverse and longitudinal flagella like other members of the typical dinoflagellates. However, the genus is unique in that they lack the cingulum and the sulcus. This type of cell morphology is called ‘prorocentroid’. Of the 81 currently accepted species in the genus (Guiry and Guiry, 2016), about thirty are recognised as benthic species (Hoppenrath *et al.*, 2013, 2014). Nine of these benthic species – *P. lima* (Ehrenberg) F. Stein, *P. hoffmannianum* M. A. Faust, *P. concavum* Y. Fukuyo, *P. faustiae* S. L. Morton, *P. rhathymum* A. R. Loeblich III, Sherley and Schmidt, *P. leve* M. A. Faust, M. W. Vandersea, S. R. Kibler, P. A. Tester and R. W. Litaker, *P. borbonicum* L. Ten-Hage, J. Turquet, J.-P. Quod, S. Puiseux-Dao and Couté, *P. maculosum* M. A. Faust, and *P. belizeanum* M. A. Faust – are known to produce toxins such as okadaic acid and its analogues, borbotoxin, prorocentrolide and many others (Hoppenrath *et al.*, 2014). Thus, benthic *Prorocentrum* species are of great interest, due to their potential toxicity.

The prorocentroid dinoflagellates are distinguished by their thecal plate pattern, which consists of two major plates termed valves separated by a sagittal suture. The typical dinoflagellate flagella (homologous to longitudinal and transverse flagella) arise from the apex of the cell. The peri-flagellar area has 5 to 14 tiny platelets. The difference between species are determined based on a combination of morphological characters such as valve ornamentation, platelet pattern, and pore pattern on the valves (Hoppenrath *et al.*, 2013).

I have isolated a number of benthic dinoflagellates from different sampling stations around Okinawa Island, Japan. Among these was a minute *Prorocentrum* species. Our morphological examinations and phylogenetic analyses of the SSU DNA and LSU DNA indicate that this species is closely related to *Prorocentrum elegans* Faust (1993a), although there are several discrepancies. Recently David *et al.* (2014) characterized *P. elegans* based on light and scanning electron microscopy together with phylogenetic analyses based on sequences of LSU rDNA and ITS region.

In this chapter, I will compare my strain, referred herein as *Prorocentrum* cf. *elegans*, with previous reports. This is also the first report of the ultrastructure of this species complex.

Materials and methods

Sampling and culture

Sand samples were collected from the shallow seafloor at a depth of 50 cm, at Bise, Okinawa Island, Japan on 23 May 2013 (Table 1, Fig. 3) using a 50 ml polypropylene Falcon tube (Becton Dickinson, NJ, U.S.A.). The sand samples were sent to the laboratory of Phycology at Faculty of Science, Hokkaido University, where dinoflagellate cells were isolated. A spoonful of the sand sample was taken in a plastic cup containing autoclaved seawater supplemented with Daigo IMK medium (Nihon Pharmaceutical Co., Tokyo, Japan) for enrichment. Germanium dioxide (Sigma-Aldrich Japan, Tokyo) was also added to prevent growth of diatoms. This was cultured at 25°C and with an illumination of 50 µmol photons m^{-2} s^{-1} with 16:8 light:dark regime. Dinoflagellate cells found were isolated using drawn capillary Pasteur pipettes under an inverted microscope (Olympus CX41, Tokyo, Japan) and a clonal culture was established. The culture strain (strain number HG277, Table 1) was maintained in IMK-supplemented seawater under the same conditions described above.

Light microscopy and scanning electron microscopy

For light microscopic observations, living cells were observed using a Carl Zeiss Axioskop 2 microscope equipped with Nomarski interference optics (Carl Zeiss Japan, Tokyo) and the fluorescent microscopic observations were made using the same microscope with filter set 15. Photographs were taken using a Leica MC-120HD digital camera (Leica Microsystems, Germany). For scanning electron microscopy, the cells were fixed for one hour in a solution of 0.1% Lugol's iodine made up with culture medium, and thereafter dehydrated and critically point dried according

to the protocol described by Yamada *et al*. (2013). Critically point dried (HITACHI HCP-2, Tokyo, Japan) samples were sputter-coated with gold for 180 seconds at 30 mA (HITACHI E-1045) and viewed with a SEM (S-3000N, HITACHI). Contrast of the images was edited using Adobe Photoshop CS5.

Transmission electron microscopy

To collect cells, after removing excess culture medium, the attached cells at the bottom of Petri dish were harvested by sweeping gently by a sterilized paint brush. The collected cells were transferred into 15 ml plastic tubes and centrifuged at 40 × g for 10 min. The cell pellet was re-suspended in 150 µl culture medium and 50 µl of 4% OsO_4 made up in distilled water was added and fixed for 1 hour at room temperature. The following protocol was the same as chemical fixation protocol described by Yamada *et al*. (2013) except that fixation was made only with 1% osmium tetroxide (OsO_4) instead of a cocktail of glutaraldehyde and OsO_4. Sections were cut using a diamond knife on an ultramicrotome (Diatome, Biel, Switzerland). Sections were picked up on formvar coated one-slot grids and these were viewed with a transmission electron microscope (H-7650, Hitachi, Tokyo).

DNA extraction and Polymerase Chain Reaction (PCR) amplification

Approximately 10 cells from the HG277 culture were used to extract DNA using the QuickExtract™ FFPE DNA extraction kit (Epicentre, Tokyo, Japan) according to the recommended protocol. SSU rDNA and LSU rDNA were separately amplified by nested PCR. Primers used for amplification are given in Table 2.

The first round of amplification of SSU rDNA was carried out using the primers SR1 and SR12b (Table 2). The thermocycling programme consisted of an initial denaturation step at 94°C for 5 minutes; followed by 35 cycles of denaturation at 94°C for 30 s, annealing at 55°C for 30 s and

extension at 72°C for 120 s; and the final extension step at 72°C for 7 minutes. The second round of PCR was carried out using the primer pairs SR1 and SR4R; SR2TAK and SR7TAK; SR4 and SR9; SR6 and SR11; and SR8TAK and SR12b (Table 2). The conditions for PCR amplification were an initial denaturation step at 94°C for 5 minutes; followed by 25 cycles of denaturation at 94°C for 30 s, annealing at 51°C for 30 s and extension at 72°C for 90 s; and the final extension step at 72°C for 7 minutes. The first round of amplification of LSU rDNA was carried out using the primers D1RF1 and 28-1483R. The thermocycling programme consisted of an initial denaturation step at 94°C for 5 minutes; followed by 35 cycles of denaturation at 94°C for 30 s, annealing at 51°C for 30 s and extension at 72°C for 120 s; and the final extension step at 72°C for 7 minutes. The second round of PCR was carried out using the primer pairs D1RF1 and 25R1*; 305F-27 and 852R-70; and D3A and 28-1483R (Table 2). The conditions for PCR amplification were an initial denaturation step at 94°C for 5 minutes; followed by 25 cycles of denaturation at 94°C for 30 s, annealing at 50°C for 30 s and extension at 72°C for 90 s; and the final extension step at 72°C for 7 minutes. The PCR products were purified and sequenced with ABI PRISM Big Dye Terminator (Perkin-Elmer, USA). The purified sequence reaction products were run on a DNA auto-sequencer ABI PRISM310 Genetic Analyser (Perkin-Elmer). Both sense and anti-sense strands were sequenced. The SSU DNA sequence obtained was 1575 bp in length and the LSU DNA was 1304 bp in length.

Sequence analyses

The SSU and LSU r DNA sequences were aligned with the respective sequences from a number of other *Prorocentrum* species, as listed in Saburova and Chomérat (Saburova and Chomérat, 2016). Although the sequence of LSU rDNA reported by David *et al.* (2014) is relatively short (452 bp), I have included in the alignment for the purpose of comparison. The aligned sequences were analysed by the ML method using PAUP* version 4.0b10 (Swofford, 2001) and the Bayesian method using MrBayes 3.2.1 (Huelsenbeck and Ronquist, 2001; Ronquist and Huelsenbeck, 2003).

1581 aligned sites were used for the analyses of SSU rDNA. The selected best fit model was the GTR + I + G model. The heuristic search for the ML analysis was performed with the following options: a TBR branch-swapping algorithm and the Kimura 2-parameter NJ tree as the starting tree. The parameters used for the analysis were as follows: assumed nucleotide frequencies A = 0.2517, C = 0.2025, G = 0.2690, and T = 0.2768; substitution rate matrix with A<>C = 1.2448, A<>G = 4.1200, A<>T = 1.1780, C<>G = 0.4411, C<>T = 9.1462, G<>T = 1.0000; proportion of sites assumed to be invariable = 0.5280; rates for variable sites assumed to follow a gamma distribution with shape parameter = 0.696, and number of rate categories = 4. For the Bayesian analysis, GTR + I + G was selected as the best evolutionary model by MrModeltest 2.3 (Nylander *et al.*, 2004). Markov chain Monte Carlo iterations were carried out until 500,000 generations, when the average standard deviations of split frequencies fell below 0.01, indicating the convergence of the iterations.

Nine hundred and eleven aligned sites were used for the analyses of LSU rDNA. The selected best fit model was TIM1 + I + G model. The heuristic search for the ML analysis was performed with the following options: a TBR branch-swapping algorithm and the Kimura 2-parameter NJ tree as the starting tree, with out-groups set manually. The parameters used for the analysis were as follows: assumed nucleotide frequencies A = 0.2461, C = 0.2102, G = 0.3006, and T = 0.2431; substitution rate matrix with A<>C = 1.0000, A<>G = 2.5748, A<>T = 0.7334, C<>G = 0.7334, C<>T = 7.3105, G<>T = 1.0000; proportion of sites assumed to be invariable = 0.112; rates for variable sites assumed to follow a gamma distribution with shape parameter = 0.699, and number of rate categories = 4. For the Bayesian analysis, GTR + G was selected as the best evolutionary model by MrModeltest 2.3 (Nylander *et al.*, 2004). Markov chain Monte Carlo iterations were carried out until 500,000 generations, when the average standard deviations of split frequencies fell below 0.01, indicating the convergence of the iterations.

Results

Prorocentrum cf. *elegans* Faust

(Figures 63 – 69)

Light and scanning electron microscopy

Cells were small, 13.75-17.5 µm (mean, 16.4 ± 1.02 µm, *n* = 50) long and 11.25-15 µm (mean, 13.1 ± 0.94 µm, *n* = 50) wide in lateral thecal view, with length to width ration varying from 1.08 to 1.42 (mean, 1.26 ± 0.08, *n* = 50). Cell shape was ovoid to oblong, rarely round, with a symmetrical apex (Fig. 63 a, b). The antapex was widely rounded (Fig. 63 a, b). The cells possessed two golden brown reticulate chloroplasts (Fig. 63 b, c) that were marginal and lay along the valves (Fig. 63 d). The nucleus was positioned posteriorly (Fig 63 a).

The valves were smooth, without ornamentation (Fig. 64); however, 10-17 (mean = 14.8 ± 2.28, *n* = 9) large pores were scattered across the valves in asymmetric patterns that were similar on both valves (Fig. 64 a, b). The right valve was convex (Fig. 64 b) to nearly flat in the centre (Fig. 64 c), while the left valve was convex (Fig. 64 a, d). Small pores were present, and were arranged asymmetrically (Fig. 64). The centre of both valves were devoid of pores (Fig. 64). Marginal pores were present on both valves; they were irregularly spaced on the most of the margin, but regularly spaced around the antapex (Fig. 64 a-c). The intercalary band possessed widely and slightly irregularly spaced transverse striations (Fig. 64 d).

The peri-flagellar area was small, V-shaped and located in an apical indentation on the right valve (Fig 64 b). The indentation was not visible in the left lateral thecal view (Fig. 64 a). There were 8 peri-flagellar platelets, 1, 2, 3, 4, 5, 6, 7, and 8 (Fig. 65). Platelet 1 possessed a wing (Fig. 65). The flagella pore was large, oval and surrounded by platelets 3, 5, 6 and 7 (Fig. 65). Platelets 1 2, 3, 4 and 6 were mostly smooth; platelet 5 had a raised border on the edge along the flagellar pore; and platelets 7 and 8 had raised borders on the edges along the accessory pore (Fig. 65).

Transmission electron microscopy

The observations of the ultrastructure of *P.* cf. *elegans* showed the general arrangement of organelles within the cell (Fig. 66). The nucleus was located in the anterior half of the cell (Fig. 66 a). The nuclear membrane was a double membrane with simple nuclear pores (Fig. 67 a). There were two chloroplasts, both marginal, situated along the valves (Fig. 66). Each chloroplast was associated with a hemispherical pyrenoid that lacked an apparent starch sheath (Fig. 67 b). The pyrenoid was projected into the cytoplasm and its matrix was homogeneous, bordered by thylakoids (Fig. 67 b). The lamellae in the chloroplasts generally consist of three thylakoids (Fig. 67 c); however, in greater than half the observed cells, grana-like structures were observed in portions of the chloroplasts (Fig. 66 a; Fig. 67 d). The cells contained few electron-opaque bodies that may be lipid granules (Fig. 66 b). The cells also contained typical mitochondria (Fig. 67 e), Golgi apparatuses (Fig. 67 b), which were arranged more or less circular fashion (Fig. 66), trichocysts (Fig. 67 g, h), pusule (Fig. 67 e) and starch grains (Fig. 67 h). The trichocysts are relatively large and measured up to 2.5 µm in length (Fig. 67 c). The pusule consists of central tubule and surrounding numerous narrow tubules (Fig. 67 e). The mucocysts were tear-drop shaped and contained fibrous materials and only a few of them were found to be located near the flagellar pore (Fig. 66).

Phylogenetic Analyses

Analyses of the SSU DNA sequences puts *Prorocentrum* cf. *elegans* as a sister species of *P. tsawwassenense* with support from ML bootstrap likelihood values, but lacking support from the Bayesian PP indices (Fig. 68). The position of both these species relative to their immediate relatives, however, has high support from ML bootstrap and robust support from Bayesian PP indices (Fig. 68).

The analyses of the LSU D1-D3 DNA sequence, *P.* cf. *elegans* from Japan formed a robust clade with *P. elegans* from David *et al.* (2014) and positioned at the base of the clade containing *P.*

mexicanum, *P. micans*, *P. minimum*, *P. dentatum*, *P. donghaiense*, and the clade consisting of *P. emarginatum*, *P. fukuyoi* is sister to above clade. *P. tsawwassenense* was positioned at the base of this clade with strong support from the ML bootstrap and robust support from Bayesian PP indices (Fig. 69). Although this slightly different from its position in the SSU tree, *P. elegans* is in the same clade in both trees (Figs 68, 69).

Discussion

The generic description of *Prorocentrum* records the size varying from 15-100 µm (Guiry and Guiry, 2016; Steidinger and Tangen, 1997) putting *P. elegans* among the smallest members of the genus. Benthic *Prorocentrum* species vary in length from 12 µm to 55 µm (Hoppenrath *et al.*, 2013), although size and shape of the cell are known to vary widely (Hoppenrath et al., 2013; Nagahama et al., 2011). Ornamentation of the valves is also a distinguishing characteristic (Hoppenrath *et al.*, 2013).

Among the previously reported benthic dinoflagellates, *P. sipadanense*, *P. borbonicum*, *P. norrisianum*, *P. elegans*, and *P. formosum* possess cell lengths that are in the same range as *P.* cf. *elegans*. Of these, *Prorocentrum elegans* is morphologically most similar to my strain. *P. elegans* was originally described as possessing an anterior nucleus (Faust, 1993a), in direct contrast to the posterior nucleus of my strain. However, a recent comprehensive review of benthic dinoflagellates states that the nucleus is posterior (Hoppenrath *et al.*, 2014). The recent observation by David *et al.* (2014) also clearly indicated that the nucleus is located in the posterior part of the cell. The chloroplasts of *P. elegans* were reported as lacking pyrenoids (Faust, 1993a) and David *et al.* (2014) also did not clearly state the presence of pyrenoid. However, in my strain, each chloroplast possesses a large central pyrenoid which can be observed in TEM. In the original description, it was reported that *P. elegans* possessed 22 ± 2.13 large pores on each valve arranged in a distinct pattern (Faust, 1993a); on the other hand, David *et al.* (2014) reported the presence of 18 – 22 large pores.

In my study, the 10 – 17 large pores were found. The pore patterns were described as asymmetric; the exact pattern of pores differs between the two previous reports (David *et al.*, 2014; Faust, 1993a). The pattern of pores on *P.* cf. *elegans* is similar to that reported by David *et al.* (2014). In the original description Faust (1993a) reported that the peri-flagellar area consists of 8 platelets and this coincides with my observation. David *et al.* (2014) failed to reveal the exact number of platelets in the peri-flagellar area and they reported existence of five platelets. By my molecular analysis, it was revealed that the species reported by David *et al.* (2014) and my strain are genetically different, although two species resemble each other. Also it should be pointed out that the sequence data are not available for the species used for original description from Belize (Faust, 1993a) and therefore, it is not possible to decide which of the two species is actually *P. elegans*. Or it is possible that all these three strains from Belize (Caribbean Sea) (Faust, 1993a), from Bay of Biscay (the Atlantic Ocean) (David *et al.*, 2014) and from Okinawa (the Pacific Ocean) are all different from each other. In conclusion, it is not possible to identify my strain from Okinawa, because the type sequence is not available and thus I would like to identify my strain at this stage as, *Prorocentrum* cf. *elegans*.

In my examination, it was revealed that cellular organization of *Prorocentrum* cf. *elegans* was mostly typical of dinoflagellates. The pyrenoids are hemispherical and bordered by several thylakoids. This type of pyrenoid has been reported for other benthic dinoflagellates, such as *Prorocentrum lima* (Zhou and Fritz, 1993). The difference between *P.* cf. *elegans* and the latter species is that the pyrenoid matrix is not surrounded apparent starch sheaths. The reason that Faust (1993a) and David *et al.* (2014) did not report the presence of pyrenoid is probably due to lack of starch sheaths, because without starch sheaths, it is difficult to locate the pyrenoid, unless observed by transmission electron microscopy. A somewhat unique feature that I found in this species was the presence of grana-like structure in portions of the chloroplasts. Although the existence of grana-like structure is extensive in *P.* cf. *elegans*, such a structure has previously been observed in the dinoflagellate *Pyramidodinium atrofuscum* (Horiguchi and Sukigara, 2005).

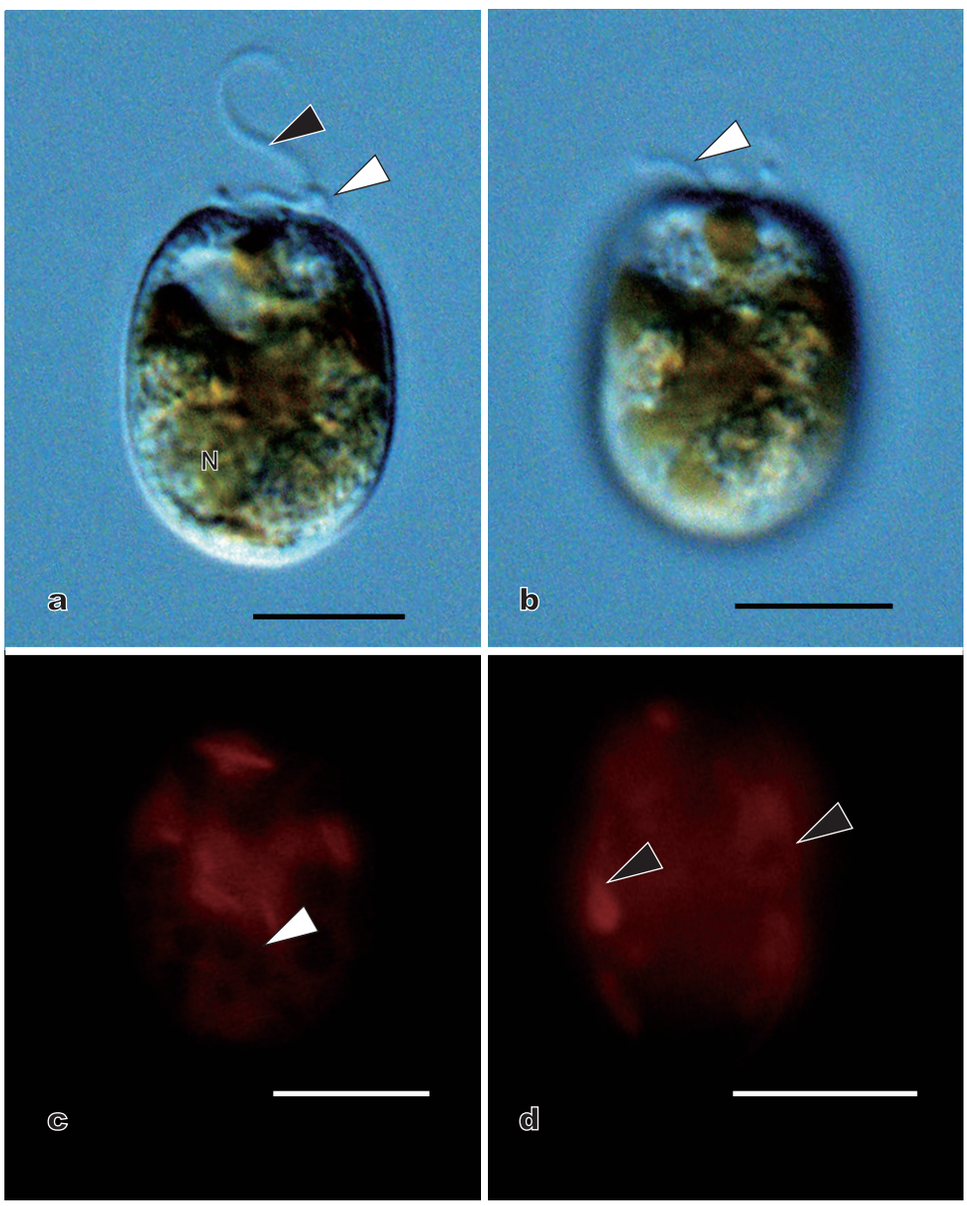


Fig. 63. *Prorocentrum* cf. *elegans*. Light micrographs.
a. Typical cell, ovoid to oblong, with nucleus (N) in antapical half of the cell; solid arrowhead, longitudinal flagellum; open arrowhead, transverse flagellum.
b. The same cell in a different focal plane; open arrowhead, transverse flagellum.
c. Reticulate choloroplast (open arrowhead)
d. Two marginal chloroplasts (solid arrowheads), along the valves.
Scale bars = 10 µm.

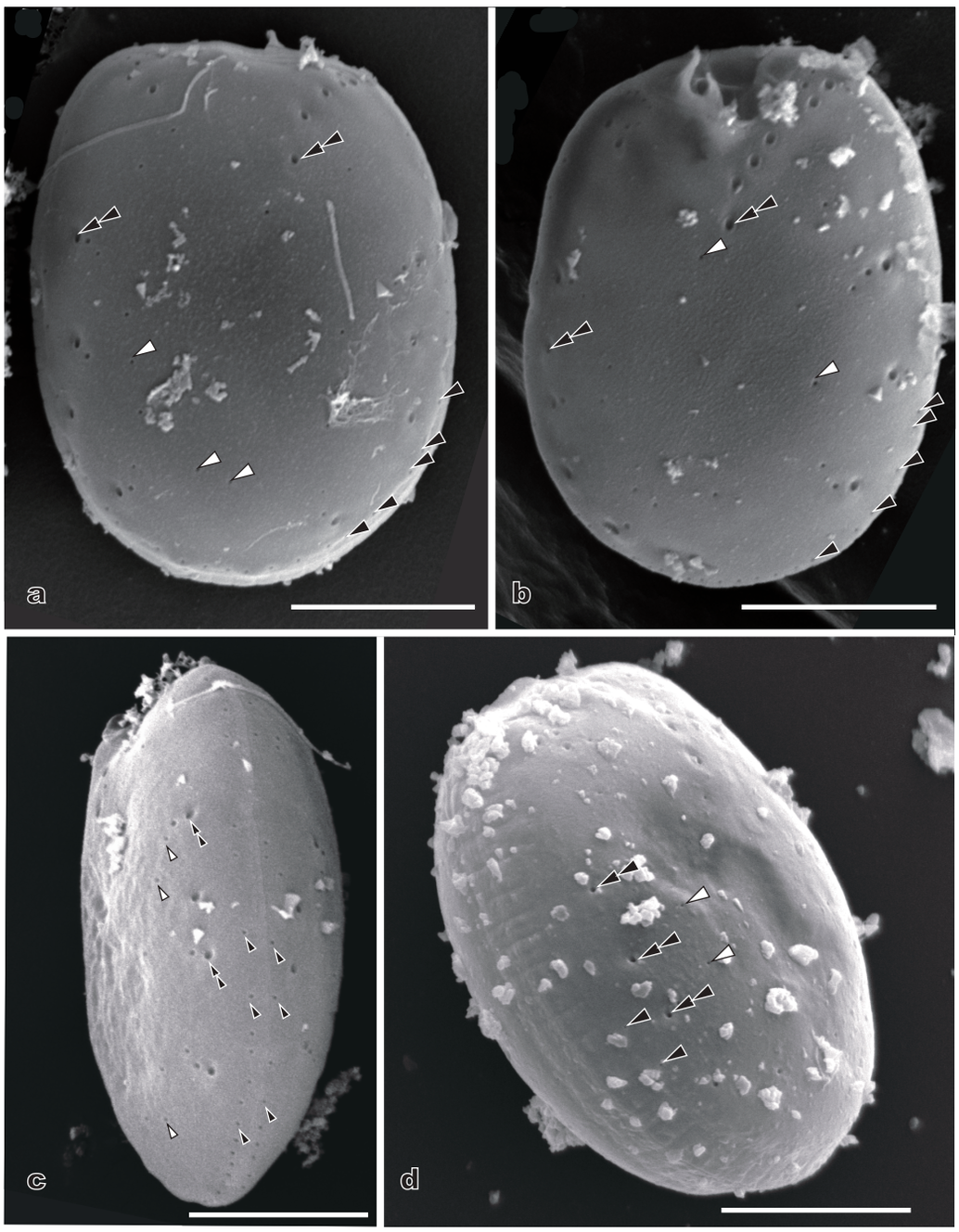


Fig. 64. *Prorocentrum* cf. *elegans*. Scanning electron micrographs.
a. Left thecal view, valve convex, asymmetric pattern of large pores (solid double arrowheads) on thecal surface clearly visible, small pores (open arrowheads) scattered on the valve, centre of valve devoid of pores, marginal pores (solid arrowheads) irregularly spaced on the most of the margin, but regularly spaced around the antapex, wing of platelet 1 visible;
b. Right thecal view, valve convex, pattern of large pores (solid double arrowheads) and of marginal pores (solid arrowheads) almost identical to left valve, periflagellar area in V-shaped depression, small pores (open arrowheads) scattered on the valve, centre of valve devoid of pores.
c. Dorsal antapical view, sagittal suture clearly visible, right valve flat in centre, left valve convex; open arrowheads, small pores; solid arrowheads, marginal pores; solid double arrowheads, large pores.
d. Ventral view, intercalary band with widely and slightly irregularly spaced sutures; open arrowheads, small pores; solid arrowheads, marginal pores; solid double arrowheads, large pores.
Scale bars = 5 µm.

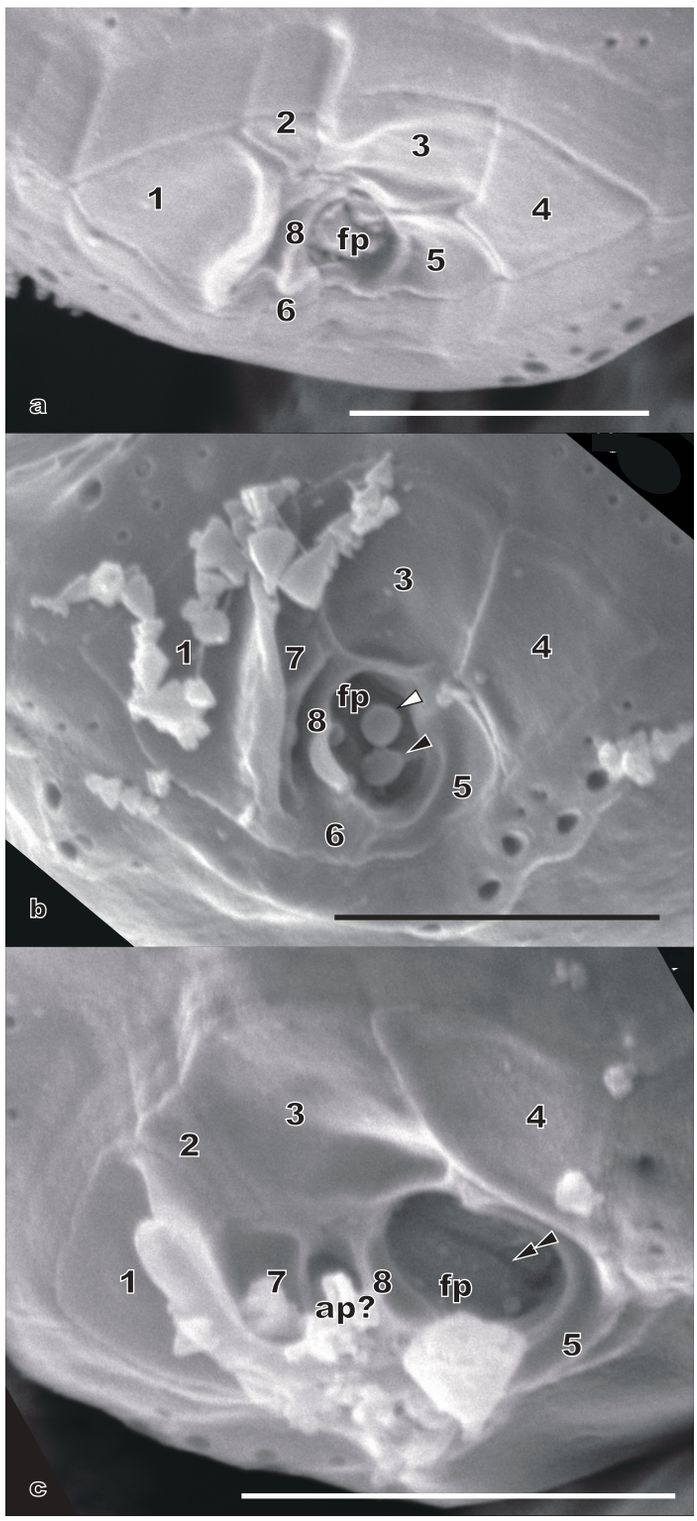


Fig. 65. *Prorocentrum* cf. *elegans.* Scanning electron micrographs showing the periflagellar area and the arrangement of the eight platelets, platelet 1 winged, platelets 1, 2, 3, 4, and 6 mostly smooth, platelets 5, 7 and 8 with raised borders, flagellar pore (fp) surrounded by platelets 3, 5, 6 and 7.

a. Platelet 8 obscured by wing of platelet 1, accessory pore appears to be absent.

b. Accessory pore appears to be absent, portions of the transverse flagellum (open arrowhead) and longitudinal flagellum (solid arrowhead) are visible in the flagellar pore (fp).

c. Accessory pore (ap) surrounded by platelets 7 and 8; flagellar pore (fp) closed by two lip-like structures.

Scale bars = 3 µm.

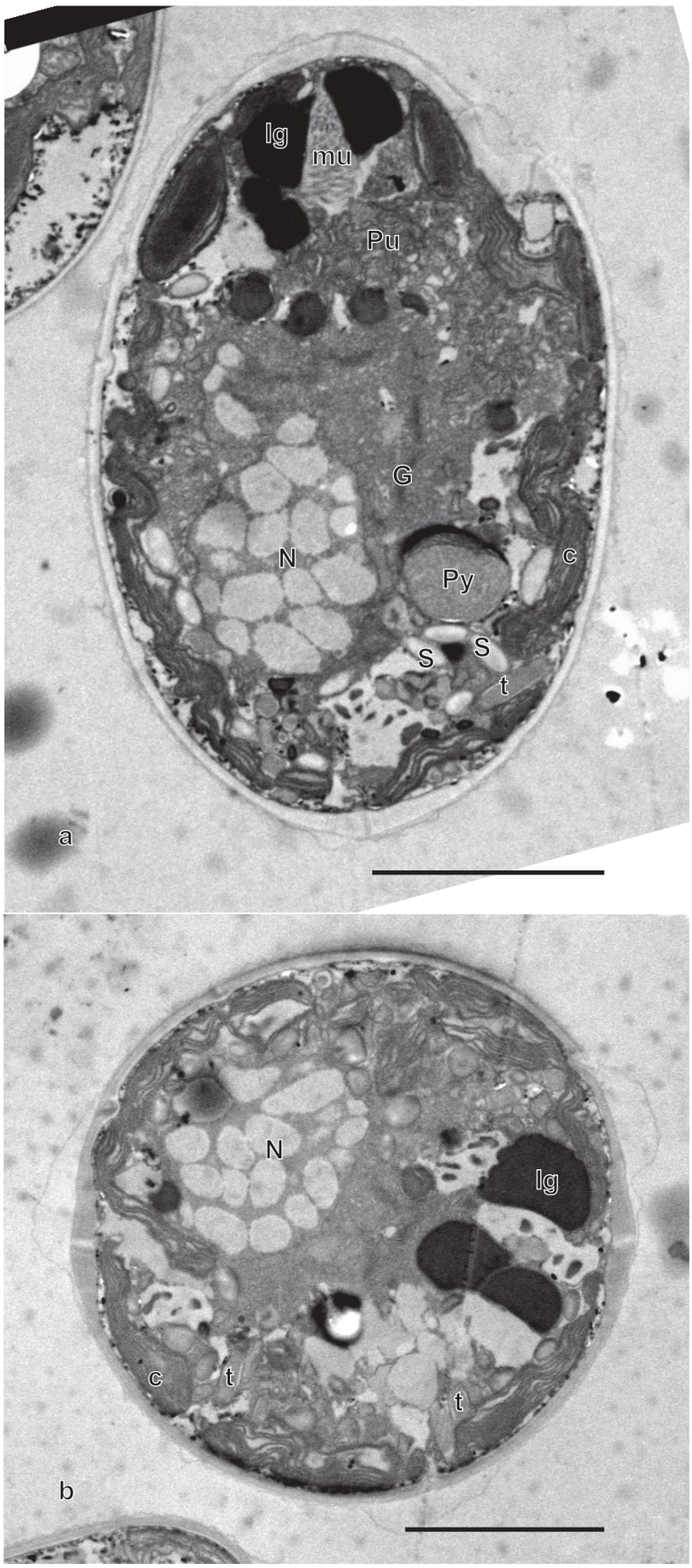


Fig. 66. *Prorocentrum* cf. *elegans*. Transmission electron micrographs of the ultrastructure of the cell.
a. Dorsal longitudinal section, showing nucleus (N) in the antapical half of the cell, large pyrenoid (Py), trichocyst (t), mucocysts (mu), two marginal chloroplasts (c), Golgi apparatus (G), pusule (Pu), lipid granules (lg) at the apex of the cell, and grana-like thylakoids in chloroplast portions near the apex of the cell. Scale bar = 5 µm.
b. Transverse section in dorso-ventral plane, showing a large nucleus (N), two chloroplasts (c), lipid granules (lg) and trichocysts (T). Scale bar = 5 µm

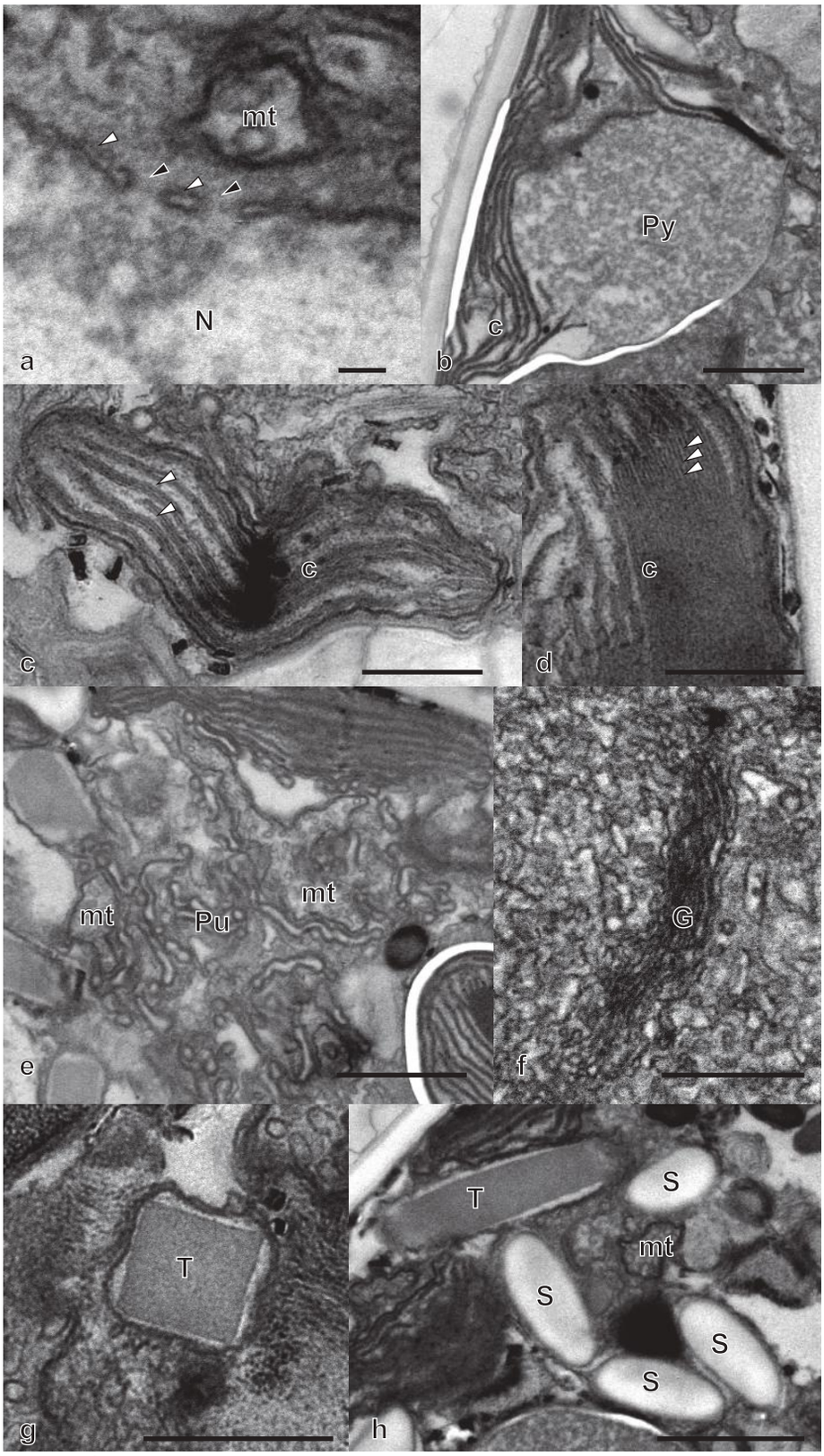


Fig. 67. *Prorocentrum* cf. *elegans*. Transmission electron micrographs showing detail of cellular organelles.

a. Nuclear double membrane (open arrowheads) and simple nuclear pores (solid arrowheads); N, nucleus; mt, mitochondrion. Scale bar = 100 nm.

b. Large pyrenoid (Py) with granular, homogeneous matrix, assocaited with chloroplast (c). Scale bar = 1 µm.

c. Portion of chloroplast (c) with trilamellar thylakoids (open arrowheads). Scale bar = 500 nm.

d. Portion of chloroplast (c) with numerous thylakoids (open arrowheads) forming a grana-like structure similar to that of higher plants. Scale bar = 500 nm.

e. Mitochondria (mt) and pusule (Pu). Scale bar = 1 µm.

f. Golgi apparatus (G). Scale bar = 500 nm.

g. Trichocyst (T) in cross-section. Scale bar = 500 nm.

h. Trichocysts (T) and mucocysts (mu). Scale bar = 1 µm.

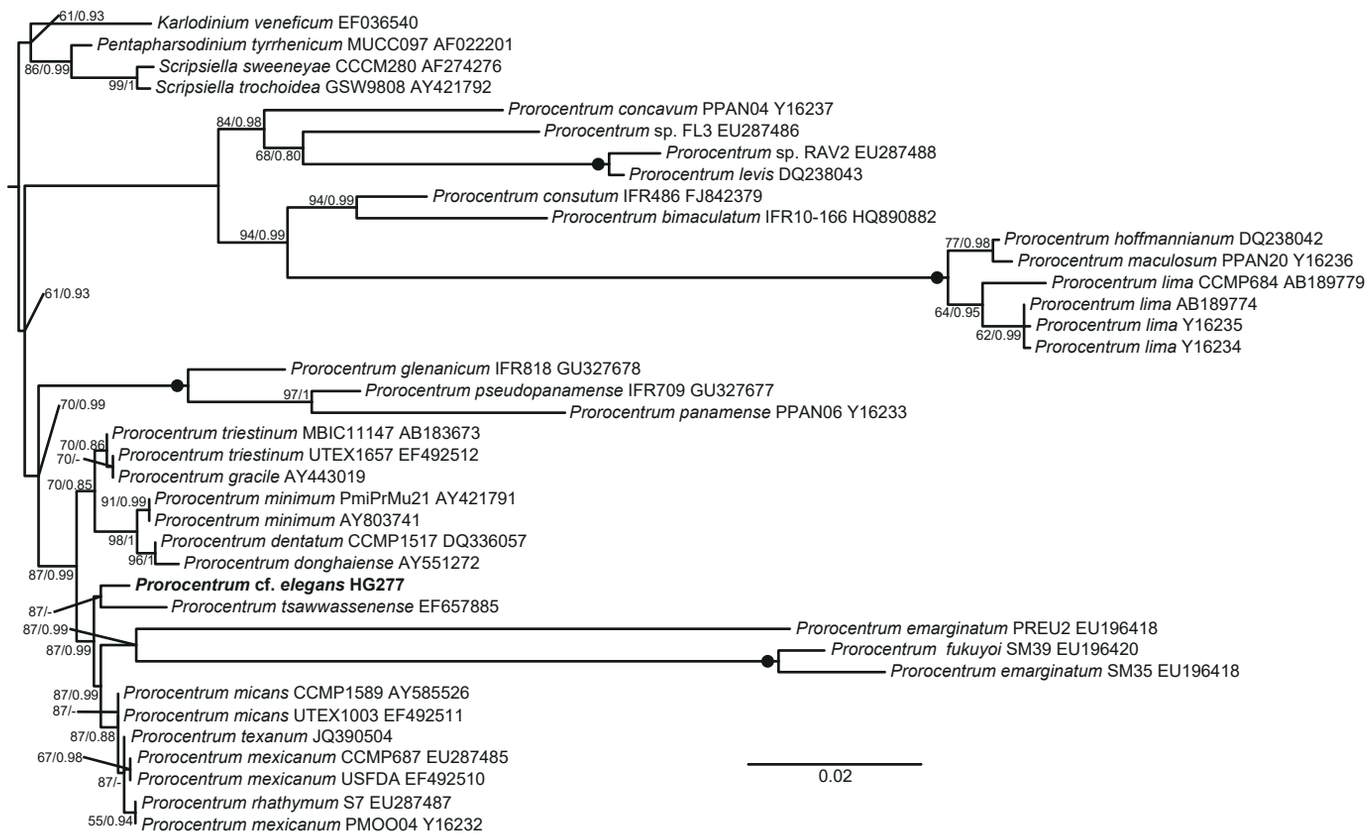


Fig. 68. Maximum likelihood (ML) phylogenetic tree inferred from partial small subunit (SSU) rDNA sequence alignment. Bootstrap support for ML analysis (100 pseudo-replicates) and Bayesian posterior probability (>50% and >0.8, respectively) are indicated. Nodes with a filled circle indicate a 100% bootstrap support for ML analysis and a Bayesian posterior probability of 1. Sequences obtained in this study are indicated in boldface; sequences from GenBank are followed by the accession numbers.

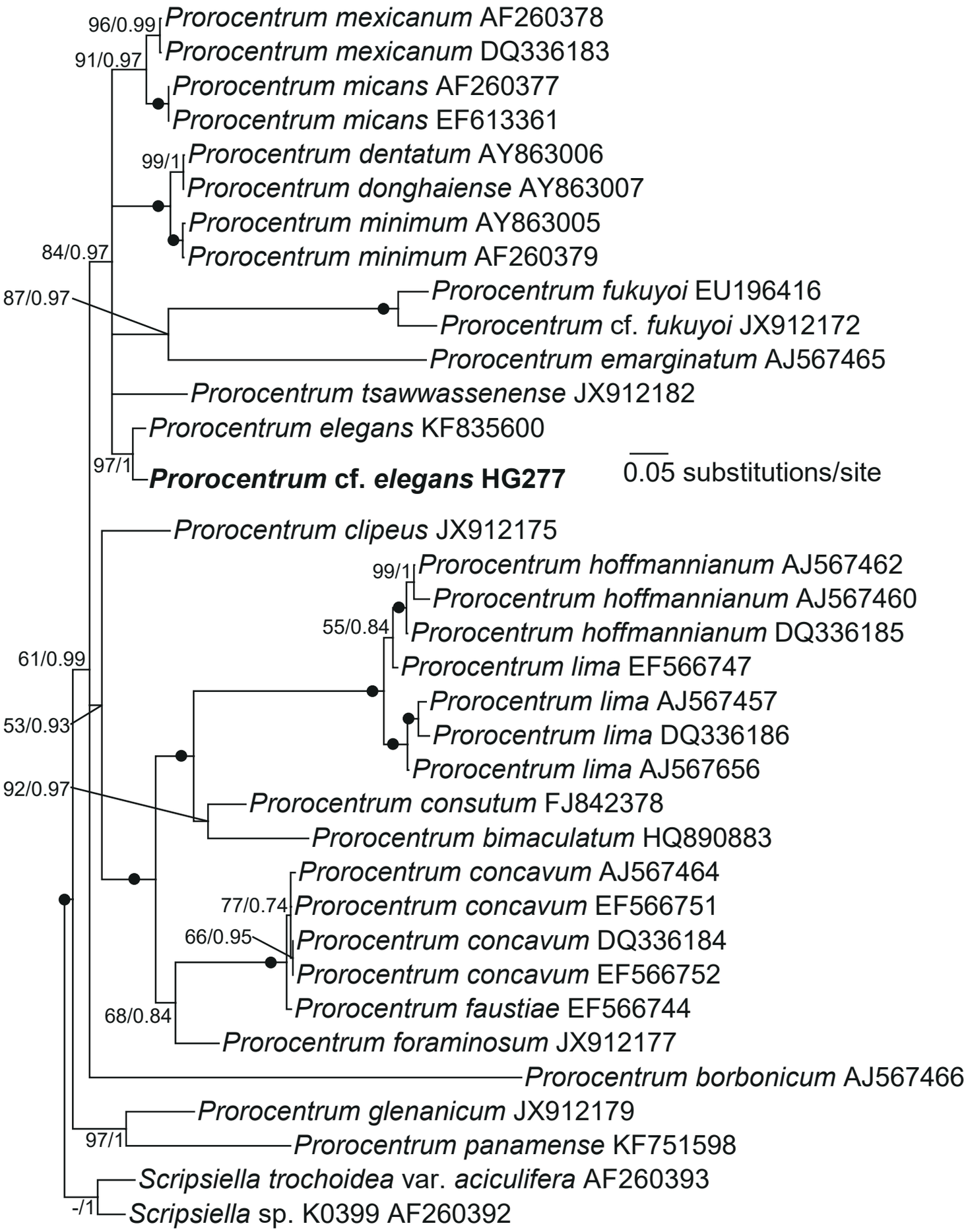


Fig. 69. Maximum likelihood (ML) phylogenetic tree inferred from partial large subunit (LSU) rDNA D1 - D3 sequence alignment. Bootstrap support for ML analysis (100 pseudo-replicates) and Bayesian posterior probability (>50% and >0.8, respectively) are indicated. Nodes with a filled circle indicate a 100% bootstrap support for ML analysis and a Bayesian posterior probability of 1. Sequences obtained in this study are indicated in boldface; sequences from GenBank are followed by the accession numbers.

Table 6. Morphological comparison of *Prorocentrum elegans* and *Prorocentrum* cf. *elegans*

	P. elegans (Faust, 1993)	*P. elegans* (David et al., 2014)	*P.* cf. *elegans* (this work)
Cell Shape	oval asymmetric	ovate	ovoid or oblong
Cell size			
Length	15-20 µm	14.78-21.51 µm	13.75-17.5 µm
Width	10-14 µm	12.49-18.02 µm	11.25-15 µm
Periflagellar area			
Shape	wide, v-shaped	large, shallow, triangular	wide, v-shaped
Collar on the left plate	No	?	N.D.
Wing-shaped spine	yes	yes	yes
Protrusions	No?	?	?
Platelet lists	No?	?	yes
No. of platelets	8	5 easily distinguished	8
Flagellar pore	yes	yes	yes
Accessory pore	yes	yes	yes
Thecal ornamentation	Smooth	smooth	Smooth
Pore pattern	yes; apical row	yes, apical row	yes, apical row and peripheral pattern
Marginal pores	No?	yes	yes
Plate centre	devoid	devoid	devoid
Large pores	22 ± 2.13 per valve, 0.6 µm dia.	18-22 per valve, 0.21-0.31 µm dia.	N.D.
Small pores	0.12µm dia.	80-91 per valve, 0.09-0.16 µm dia.	N.D.
Intercalary band	smooth, transversely striated	smooth, transversely striated	smooth, transversely striated
Pyrenoid	no	no	yes (in TEM, but not LM)
Nucleus	anterior	posterior	Posterior
Trichocysts	?	N.D.	yes, large
Mucocysts	?	N.D.	yes

Chapter 5

A taxonomic study on a new marine benthic thecate peridiniod dinoflagellate

Introduction

The genera *Peridinium* Ehrenberg and *Peridiniopsis* Lemmermann are morphologically similar thecate dinoflagellates and two major genera commonly found in freshwater habitats. They are characterised by a hypotheca that possesses five postcingular and two antapical plates and a complete cingulum (Popovský and Pfiester, 1990). Traditionally, the major difference between the two genera is in the plate formulae of the epitheca. *Peridinium* has a plate formula of 4', (2a – 3a), 7'', 5''', 2''''; while that of *Peridiniopsis* is (3 – 5)', (0a – 1a), (6 – 8)'', 5''', 2'''' (Popovský and Pfiester, 1990). Thus, the most notable difference between the two genera is in the number of apical intercalary plates.

Peridinium is a large genus with 67 recognised species (Guiry and Guiry, 2016). While morphologically similar, it has been determined that this group is in fact polyphyletic (Daugbjerg *et al.*, 2000) For example, it has been demonstrated that *Peridinium palatinum* is only distantly related to the type species of the genus *Peridinium*, *P. cinctum* and thus has been transferred to its own genus, *Palatinus* (Craveiro *et al.*, 2009). Likewise, another freshwater representative, *Peridinium lomnickii* was moved to its own new genus, *Chimonodinium* (Craveiro *et al.*, 2011), as was *Peridinium umbonatum* transferred to *Parvodinium umbonatum* (Carty, 2008). It is apparent that the vigorous revisions of *Peridinium* and its related dinoflagellates are needed. In terms of habitat, *Peridinium* is cosmopolitan, being present in freshwater, brackish, and marine environments. The species *Peridinium quinquecorne* Abé, for example, is known as a marine species ((Abé, 1927; Horiguchi and Pienaar, 1991), but its phylogenetic position indicates that this is not closely related to the type species of *Peridinium*, *P. cinctum* (Horiguchi and Takano, 2006) and thus requires taxonomic revision (Hoppenrath *et al.*, 2014).

Peridiniopsis is a somewhat smaller genus, with 31 recognised species (Guiry and Guiry, 2016). The genus is predominantly freshwater, with a handful of species recorded inhabiting brackish estuarine waters. No marine species have been reported, although *Peridinopsis salina*

Trigueros has been recorded inhabiting highly saline waters near a wastewater treatment plant (Trigueros, 2000).

A peridiniod dinoflagellate has been isolated from the shallow seafloor at Odo, Okinawa Island. It is morphologically similar to *Perdinium/Peridiniopsis*, although the phylogenetic analysis provides only moderate support for a relationship with *Peridiniopsis borgei*, the type species of the genus. In this chapter, I shall describe this novel species, and compare it with *Peridiniopsis borgei* and some related species.

Materials and Methods

Sampling and culture

Sand samples were collected from the shallow seafloor at a depth of 50 cm, at Odo, Okinawa Island, Japan on 11 April 2011 (Table 1, Fig. 3) using a 50 ml polypropylene Falcon tube (Becton Dickinson, NJ, U.S.A.). The sand samples were sent to the laboratory of Phycology at Faculty of Science, Hokkaido University, where dinoflagellate cells were isolated. A spoonful of the sand sample was taken in a plastic cup containing autoclaved seawater supplemented with Daigo IMK medium (Nihon Pharmaceutical Co., Tokyo, Japan) for enrichment. Germanium dioxide (Sigma-Aldrich Japan, Tokyo) was also added to prevent growth of diatoms. This was cultured at 25°C and with an illumination of 50 µmol photons m^{-2} s^{-1} with 16:8 light:dark regime. Dinoflagellate cells found were isolated using drawn capillary Pasteur pipettes under an inverted microscope (Olympus CX41, Tokyo, Japan) and a clonal culture was established. The culture strain (strain number HG152, Table 1) was maintained in IMK-supplemented seawater under the same conditions described above.

Light microscopy and scanning electron microscopy

For light microscopic observations, living cells were observed using a Carl Zeiss Axioskop 2 microscope equipped with Nomarski interference optics (Carl Zeiss Japan, Tokyo) and the fluorescent microscopic observations were made using the same microscope with filter set 15. Photographs were taken using a Leica MC-120HD digital camera (Leica Microsystems, Germany). For scanning electron microscopy, the cells were fixed for one hour in a solution of 0.1% Lugol's iodine made up with culture medium, and thereafter dehydrated and critically point dried according to the protocol described by Yamada *et al*. (2013). Critically point dried (HITACHI HCP-2, Tokyo, Japan) samples were sputter-coated with gold for 180 seconds at 30 mA (HITACHI E-1045) and viewed with a SEM (S-3000N, HITACHI). Contrast of the images was edited using Adobe Photoshop CS5.

Transmission electron microscopy

To collect cells, after removing excess culture medium, the attached cells at the bottom of Petri dish were harvested by sweeping gently by a sterilized paint brush. The collected cells were transferred into 15 ml plastic tubes and centrifuged at 40 × g for 10 min. The cell pellet was re-suspended in 150 µl culture medium and 50 µl of 4% OsO_4 made up in distilled water was added and fixed for 1 hour at room temperature. The following protocol was the same as chemical fixation protocol described by Yamada *et al*. (2013) except that fixation was made only with 1% osmium tetroxide (OsO_4) instead of a cocktail of glutaraldehyde and OsO_4. Sections were cut using a diamond knife on an ultramicrotome (Diatome, Biel, Switzerland). Sections were picked up on formvar coated one-slot grids and these were viewed with a transmission electron microscope (H-7650, Hitachi, Tokyo).

DNA extraction and Polymerase Chain Reaction (PCR) amplification

Approximately 10 cells from the HG152 culture were used to extract DNA using the QuickExtract™ FFPE DNA extraction kit (Epicentre, Tokyo, Japan) according to the recommended protocol. SSU rDNA and LSU rDNA were separately amplified by nested PCR. Primers used for amplification are given in Table 2.

The first round of amplification of SSU rDNA was carried out using the primers SR1 and SR12b (Table 2). The thermocycling programme consisted of an initial denaturation step at 94°C for 5 minutes; followed by 35 cycles of denaturation at 94°C for 30 s, annealing at 55°C for 30 s and extension at 72°C for 120 s; and the final extension step at 72°C for 7 minutes. The second round of PCR was carried out using the primer pairs SR1 and SR4R; SR2TAK and SR7TAK; SR4 and SR9; SR6 and SR11; and SR8TAK and SR12b (Table 2). The conditions for PCR amplification were an initial denaturation step at 94°C for 5 minutes; followed by 25 cycles of denaturation at 94°C for 30 s, annealing at 51°C for 30 s and extension at 72°C for 90 s; and the final extension step at 72°C for 7 minutes. The first round of amplification of LSU rDNA was carried out using the primers D1RF1 and 28-1483R. The thermocycling programme consisted of an initial denaturation step at 94°C for 5 minutes; followed by 35 cycles of denaturation at 94°C for 30 s, annealing at 51°C for 30 s and extension at 72°C for 120 s; and the final extension step at 72°C for 7 minutes. The second round of PCR was carried out using the primer pairs D1RF1 and 25R1*; 305F-27 and 852R-70; and D3A and 28-1483R (Table 2). The conditions for PCR amplification were an initial denaturation step at 94°C for 5 minutes; followed by 25 cycles of denaturation at 94°C for 30 s, annealing at 50°C for 30 s and extension at 72°C for 90 s; and the final extension step at 72°C for 7 minutes. The PCR products were purified and sequenced with ABI PRISM Big Dye Terminator (Perkin-Elmer, USA). The purified sequence reaction products were run on a DNA autosequencer ABI PRISM310 Genetic Analyser (Perkin-Elmer). The sequences fragments were assembled in Geneious R10 (www.geneious.com, Kearse *et al.*, 2012). Both sense and anti-sense strands were sequenced. The SSU DNA sequence obtained was 2050 bp in length and the LSU DNA was 1455 bp in length.

Sequence analyses

The assembled sequences were manually aligned with a number of other dinoflagellate sequences obtained from GenBank to reflect the secondary structure of the RNA. The aligned sequences were analysed by the ML method using PAUP* version 4.0a152 (Swofford, 2001) and by the RAxML BlackBox (Stamatakis *et al.*, 2008); and the Bayesian method using MrBayes 3.2.1 (Huelsenbeck and Ronquist, 2001; Ronquist and Huelsenbeck, 2003).

3041 aligned sites were used for the analyses of SSU rDNA. The selected best fit model was the TIM2 + I + G model. The heuristic search for the ML analysis was performed with the following options: a TBR branch-swapping algorithm and the Kimura 2-parameter NJ tree as the starting tree. The parameters used for the analysis were as follows: assumed nucleotide frequencies A = 0.25456, C = 0.18418, G = 0.25865, and T = 0.30261; substitution rate matrix with A<>C = 1.5337, A<>G = 4.49574, A<>T = 1.5337, C<>G = 1.0000, C<>T = 10.4154, G<>T = 1.0000; proportion of sites assumed to be invariable = 0.339066; rates for variable sites assumed to follow a gamma distribution with shape parameter = 0.541643, and number of rate categories = 4. For the Bayesian analysis, GTR + I + G was selected as the best evolutionary model by MrModeltest 2.3 (Nylander *et al.*, 2004). Markov chain Monte Carlo iterations were carried out until 4,000,000 generations, when the average standard deviations of split frequencies fell below 0.01, indicating the convergence of the iterations.

1601 aligned sites were used for the analyses of LSU rDNA. The selected best fit model was TIM3 + I + G model. The heuristic search for the ML analysis was performed with the following options: a TBR branch-swapping algorithm and the Kimura 2-parameter NJ tree as the starting tree, with out-groups set maually. The parameters used for the analysis were as follows: assumed nucleotide frequencies A = 0.28205, C = 0.19922, G = 0.27196, and T = 0.24677; substitution rate matrix with A<>C = 0.737965, A<>G = 2.14016, A<>T = 1.0000, C<>G = 0.737965, C<>T =

5.09095, G<>T = 1.0000; proportion of sites assumed to be invariable = 0.118274; rates for variable sites assumed to follow a gamma distribution with shape parameter = 0.503955, and number of rate categories = 4. For the Bayesian analysis, GTR + I + G was selected as the best evolutionary model by MrModeltest 2.3 (Nylander *et al.*, 2004). Markov chain Monte Carlo iterations were carried out until 5,000,000 generations, when the average standard deviations of split frequencies fell below 0.01, indicating the convergence of the iterations.

Results

Peridinioid dinoflagellate HG152

(Figures 70 – 74)

Diagnosis: Photosynthetic armoured dinoflagellate; cells ellipsoidal; 13.5 – 20.0 µm long, 10.5 – 17.5 µm wide; thecal plate arrangement Po, cp, 4', 2a, 6'', 5c, 5s, 5''', 2''''; epitheca larger than hypotheca; dinokaryotic nucleus spherical, posterior, in hypotheca; pyrenoid surrounded by starch sheath, above nucleus; chloroplasts yellow-brown, elongated, reticulate.

Type locality: 26.090055N 127.708909E; Sandy sediment on intertidal region; Odo, Okinawa, Japan.

Light and scanning electron microscopy

The cell was spherical (Fig. 70 a, b) to ellipsoidal (Fig 71), 13.5 – 20.0 µm (mean = 14.9 ± 3.05 µm, *n* = 15) long and 10.5 – 17.5 µm (mean = 12.3 ± 3.21 µm, *n* = 15) wide. The epitheca was conical, slightly larger than the hypotheca, which was hemispherical in shape (Fig. 71). The cingulum was sub-equatorial, and was displaced about 0.5 times its width on the ventral surface (Fig. 71). The sulcus was wide towards the antapex (Fig. 71). The nucleus was spherical and posterior in position. A single, large starch-sheathed pyrenoid was present in the epitheca (Fig. 70 b). The chloroplast was yellow-brown (Fig. 70 a, b) and was reticulate (Fig 70 c, d). An eyespot was clearly visible in the

hypotheca near the sulcus, and was also clearly visible under fluorescent microscopy (Fig. 70). The dinoflagellate showed characteristic swimming movement. The motile cells did not swim in straight line, but they often swam in circular fashion. Before cell division, the motile cells settled and transformed to non-motile phase. In this phase, the movement of organelles took place and as a result, the nucleus was positioned in the epitheca, while the pyrenoid was in the hypotheca.

The thecal plate arrangement of this species was apical pore plate (Po), canal plate (cp), four apical plates (4'), 2 anterior intercalary plates (2a), six pre-cingular plates (6''), five cingular plates (5c), five sulcal plates (5s), five post-cingular plates (5'''), and two antapical plates (2'''') (Figs 71, 72). The first anterior intercalary plate was hexagonal, abutting the 2', 3', 2a, 2'', 3'' and 4'' plates. The apical pore complex and the canal plate were present. There are two anterior intercalary plates; 1a plate was hexagonal, while 2a plate was pentagonal and these are almost the same in size (Fig. 71). The arrangement of hypothecal plates was almost symmetrical. The surface ornamentation of thecal plates was almost smooth, and the sutures were smooth and raised (Fig. 71).

Transmission electron microscopy

Figure 73 shows the arrangement of organelles within a single non-motile cell. The position of organelles were shifted, so the position of nucleus and pyrenoid is reversed compared to that of motile vegetative cells (Fig. 70). The typical dinoflagellate nucleus with condensed chromosomes was large and occupies the epitheca (Fig 73). The nuclear membrane was a double-membrane (Fig. 74 a) with simple nuclear pores (Fig. 74 b). The pyrenoid was circular to oval in outline (Fig 73). The pyrenoid was surrounded by two cup-shaped starch sheaths (Fig. 73 c). The pyrenoid was connected to the chloroplasts (Fig. 73 d); the chloroplast profiles were elongated (Fig. 73 e) and they formed a reticulate network radiating outward from the pyrenoid and occupying the periphery of the cell (Fig. 73 e; Fig 72). A simple eyespot was present in the hypotheca; it was formed of a double layer of pigment globules within a functioning chloroplast (Fig. 74 f). No crystalline

structures were not observed outside the eyespot (Fig. 74f). Typical trichocysts (Fig. 74 g) and mitochondria (Fig. 74 h) were observed. the cells depicted in Figs 73 and 74 are non-motile cells and the thecal plates were underlain by continuous pellicular layer (Figs 73, Fig. 74 e, i). The thecal plates were thin and electron-transparent. As mentioned in the light microscopy section, the position of nucleus and pyrenoid was reversed compared to that of motile cells.

Discussion

From the gross external morphology, HG152 is similar to small peridinoid dinoflagellates such as *Peridiniopsis borgei*, *Parvodinium umbonatum* and *Palatinus apiculatus*. *Peridiniopsis borgei* is a freshwater dinoflagellate with a plate formula of APC, 3', 1a, 6", 6c, 5s, 5"', 2"" (Calado and Moestrup, 2002; Popovský and Pfiester, 1990). This is a clear difference from HG152, which has a plate formula of Po, cp, 4', 2a, 6", 5c, 5s, 5"', 2"" - that is, it possesses a clearly defined pore plate and canal plate, one more each of the apical plates and pre-cingular plates, and one less cingular plate. *Parvodinium umbonatum* is another freshwater peridiniod dinoflagellate, which has a Po, cp, 4', 2a, 7", 6c, 5s, 5"', 2""; with a wide, sub-median cingulum, a hypotheca smaller than an epitheca a sulcus that spreads to the antapex (Carty, 2008). While most of the characters are shared with HG152, there is clear difference in the plate formula – HG152 has one less each of pre-cingular and cingular plates. *Palatinus apiculatus* is yet another freshwater peridiniod dinoflagellate, however it has a distinctly different plate formula of 4', 2a, 7", 6c, 5s, 5"', 2"" lacking an apical pore (Craveiro *et al.*, 2009). This is a very clear difference from HG152, which does have an apical pore, a pore complex and a canal plate. Furthermore, all of these three species are freshwater representatives and different from the habitat of HG 152 which is marine. From these data, it can be concluded that HG152 is a novel species.

The phylogenetic tree based on the LSU sequences does not indicate any of the relationships of HG152. The phylogenetic tree based on the SSU data does lend moderate support to the

relationship between *Peridiniopsis borgei*, the type species of *Peridiniopsis*, and HG152. This warrants further examination to determine whether HG152 is a novel genus distinct from *Peridiniopsis* or not.

The ultrastructure of *Peridiniopsis borgei* has been examined in great detail (Calado and Moestrup, 2002). The external morphology reveals a plate formula of APC, 3', 1a, 6'', 6c, 5s, 5''', 2''''. In comparison, HG152 has a plate formula of Po, cp, 4', 2a, 6'', 5c, 5s, 5''', 2'''': the apical pore plate and the canal plate are well-defined, and there is one more apical plate and one more apical intercalary plate than *Peridinopsis borgei*. The ornamentation on the plates also differs, with *Peridiniopsis borgei* having a reticulate ornamentaion on the thecal plates and flanges bordering the cingulum and part of the sulcus, while HG152 has somewhat smooth thecal plates and no flanges. The most significant difference is that *P.. borgei* possesses 6 cingular plates, while HG152 has only 5 cingular plates.

The ultrastructure of *Peridiniopsis borgei* reveals a large pyrenoid connected to a reticulate chloroplast. HG152 also possesses a large pyrenoid connected to a reticulate chloroplast; however the chloroplast occupies a larger area cell compared to *Peridiniopsis borgei*. There is also a major difference in the structure of the eyespots of the two species: *Peridiniopsis borgei* possess an eyespot is under the sulcus, that inconspicuous in LM. It consists of up to six rows of pigment globules, occasionally separated by thylakoid lamellae, within a chloroplast lobe, arranged parallel to the cell surface; the eyespot was associated with crystal-like bodies – in short, it was a Type II eyespot (Hoppenrath, 2016). In HG152, the eyespot was also associated with the sulcus, but it was clearly visible in LM. About 2 µm long in TEM, it consists of two rows of pigment globules in a functional chloroplast lobe, arranged parallel to the cell surface – it was most similar to the Type I eyespot (Hoppenrath, 2016).

The aggregation of all these differing characteristics lead me to conclude that HG152 is a small peridiniod dinoflagellate belonging to a novel genus and species that is closely related to *Peridiniopsis borgei*.

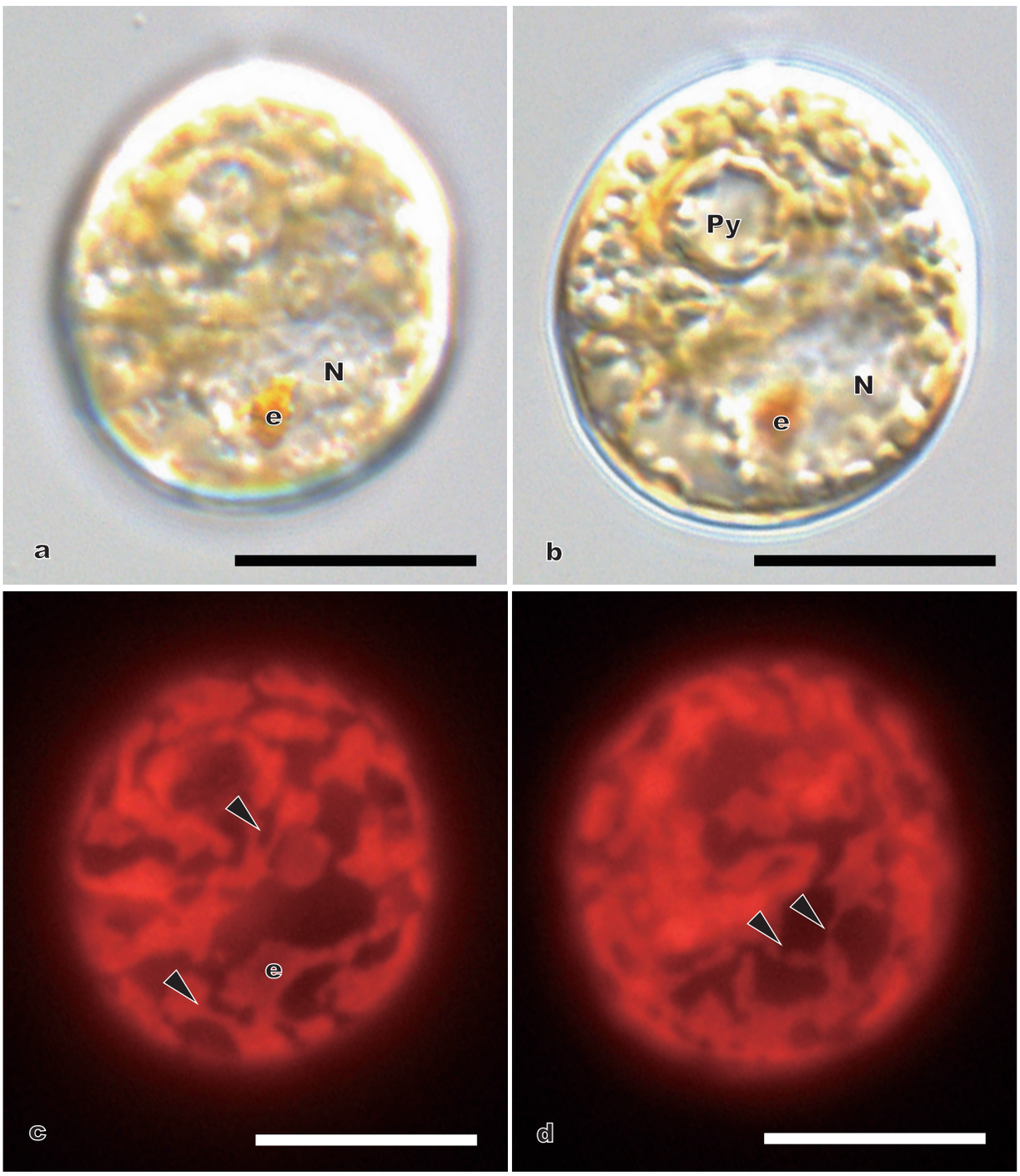


Fig .70. HG152. Light and fluorescence micrographs of a single cell.
a. Surface view. The nucleus (N) is anterior and the eyespot (e) is clearly visible.
b. Focal plane within a cell. The nucleus (N), pyrenoid (Py) and eyespot (e) are visible.
c. The chloroplasts are elongated and reticulate. The eyespot (e) also fluoresces.
d. Chloroplasts in a different focal plane. Arrowheads indicate the connections that form the reticulations.
Scale bar = 10 µm.

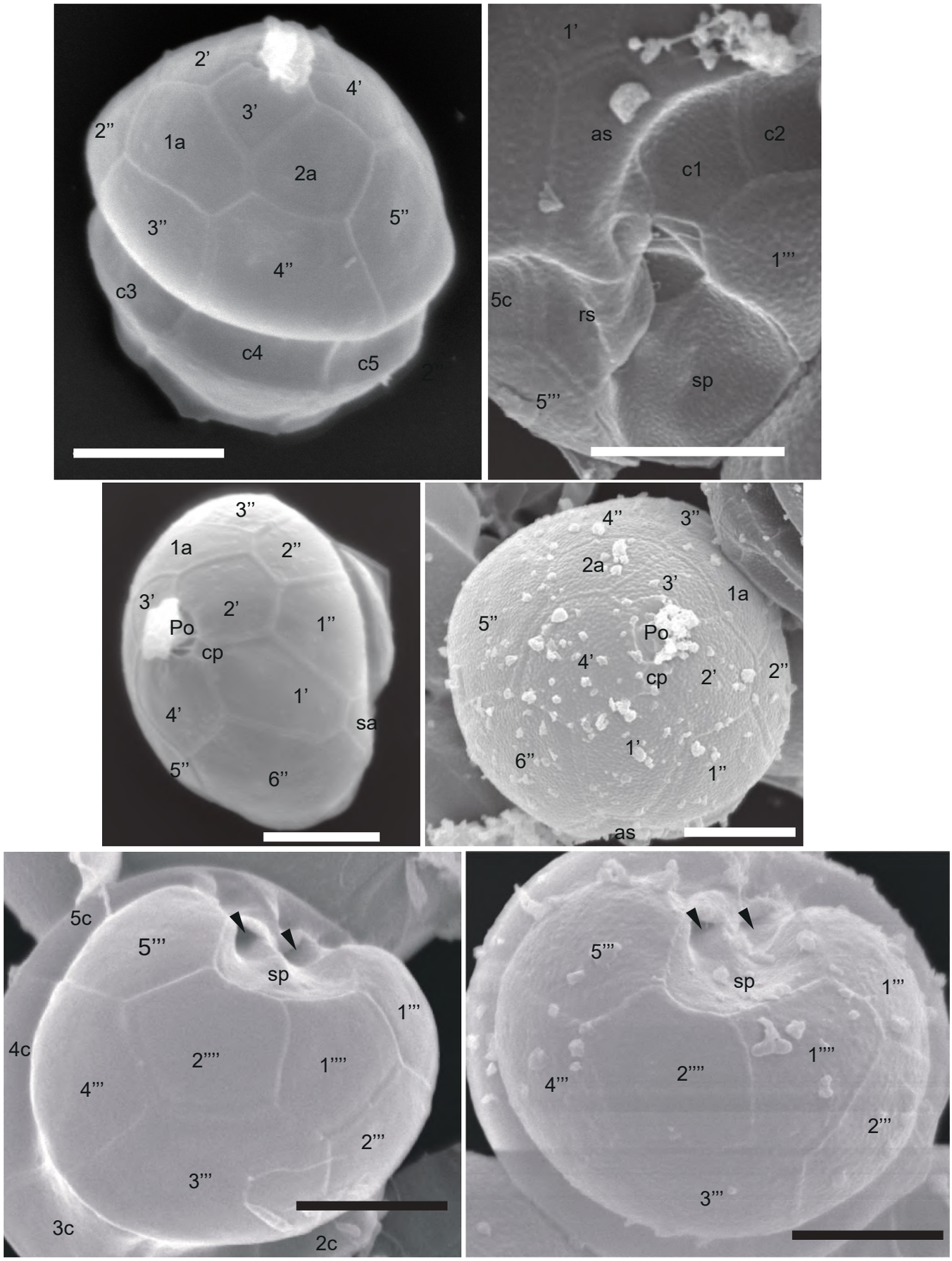


Fig. 71. HG152. Thecal plate arrangement. The Thecal plate formula is Po, cp, 4’ , 2a, 5", 5c, ?(5)s, 5"', 2"". The solid arrowheads indicate the flagellar pores rising from the sulcus. Scale bars = 5 µm

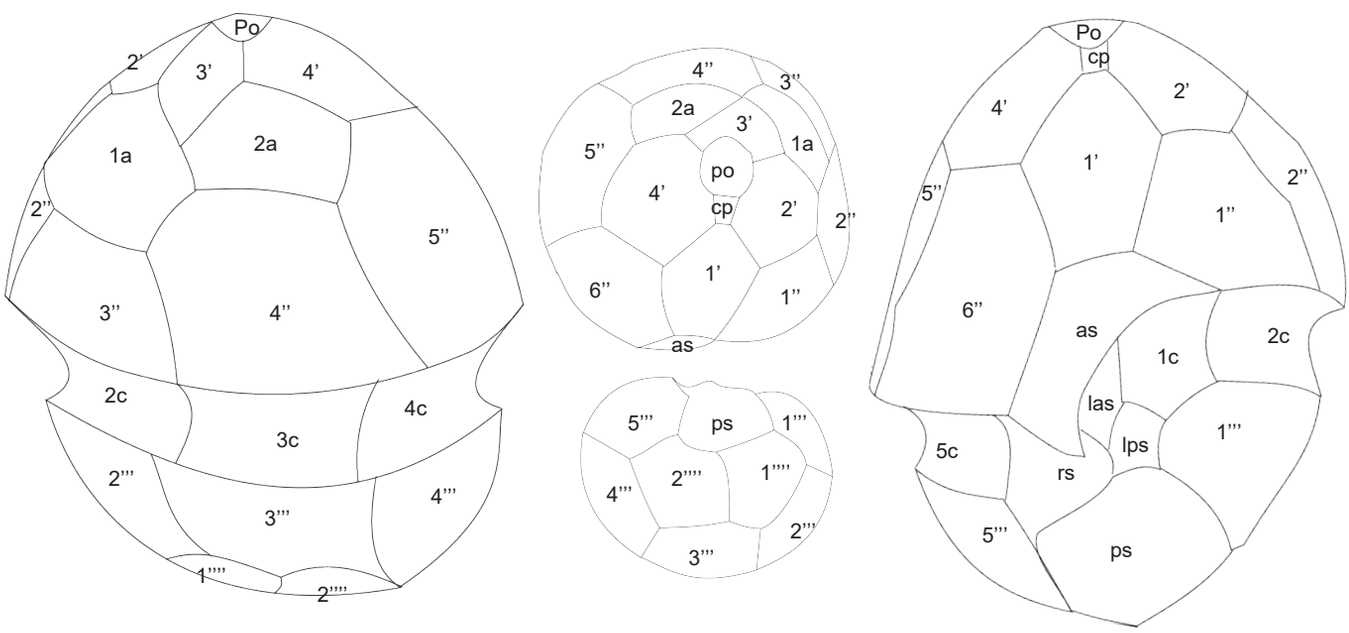


Fig. 72. HG152. Schematic illustration of thecal plate pattern.

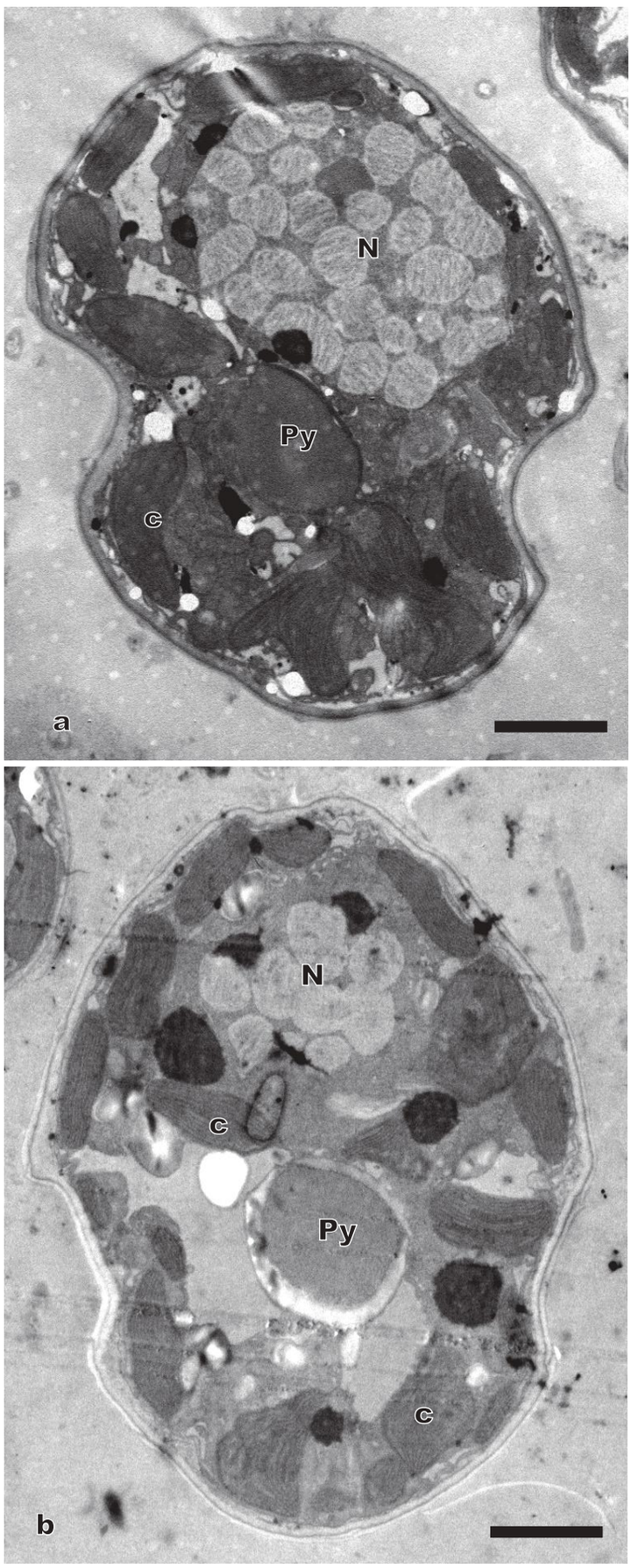


Fig. 73. HG152. Transmission electron micrographs. Non-motile cells.
a, b. Longitudinal sections of the cell. The nucleus (N) is in the epitheca. The pyrenoid (Py) is in the region of the cingulum, surrounded by two starch granules. The elongated chloroplasts (c) radiate outwards from the pyrenoid and occupy the periphery of the cell. Scale bar = 2 μm.

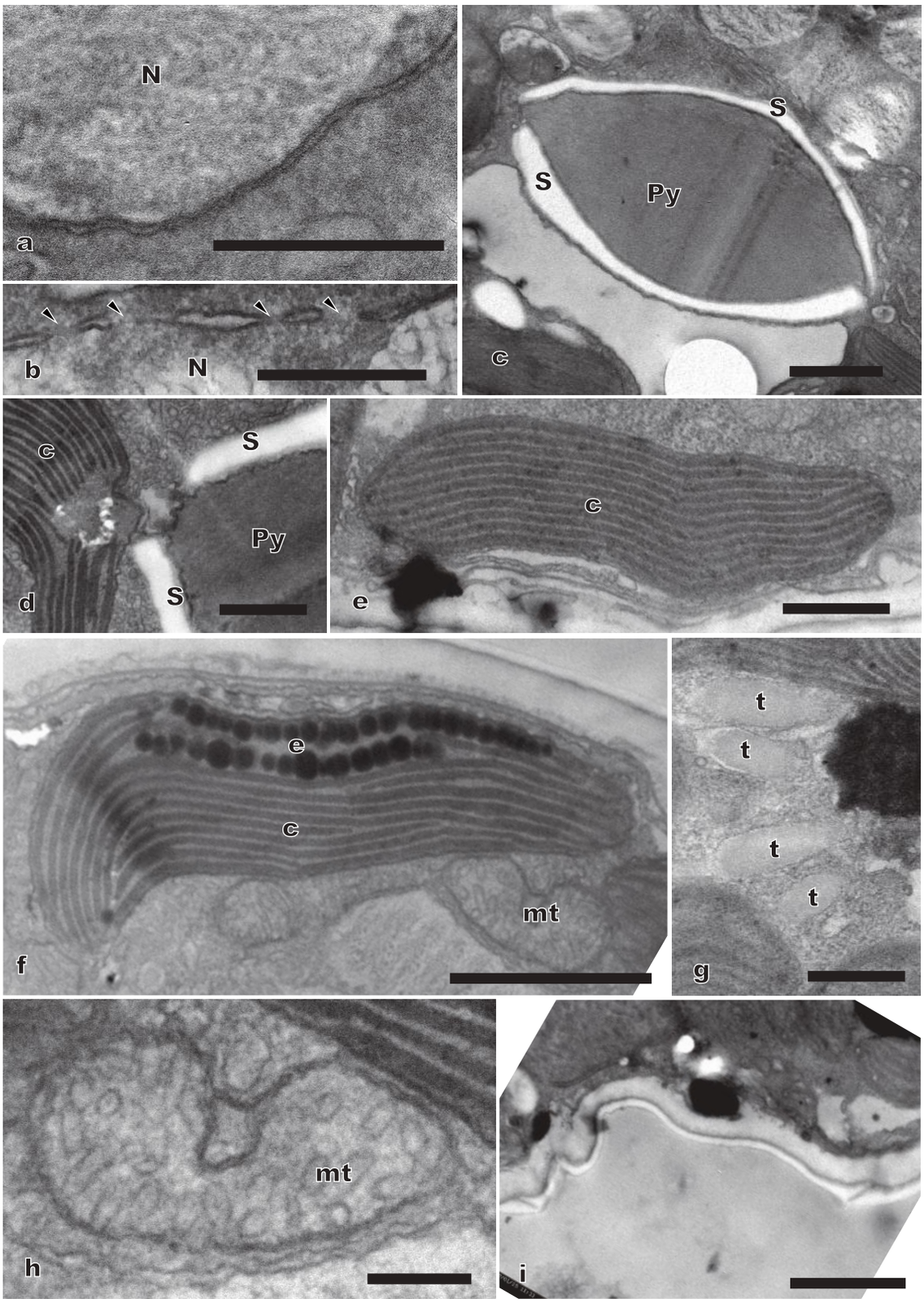


Fig. 74. HG152. Transmission electron microscopy.
a. Double-membrane surrounding the nucleus (N). Scale bar = 500 nm.
b. Simple nuclear pores (arrowheads) in the nuclear membrane. Scale bar = 500 nm.
c. Typical biconvex pyrenoid (Py) surrounded by two starch granules (S), connected to the adjacent chloroplasts. Scale bar = 1 μm.
d. The junction between starch- sheathed (S) pyrenoid (Py) and adjacent chloroplast (c). Scale bar = 500 nm.
e. Elongate chloroplast (c). Scale bar = 500 nm.
f. Simple eyespot (e) within a functional chloroplast (c). Scale bar = 1 μm.
g. Trichocysts (t). Scale bar = 500 nm.
h. Mitochondrion (mt). Scale ber = 200 nm.
i. Section of a thecal plate. Scale bar = 1 μm.

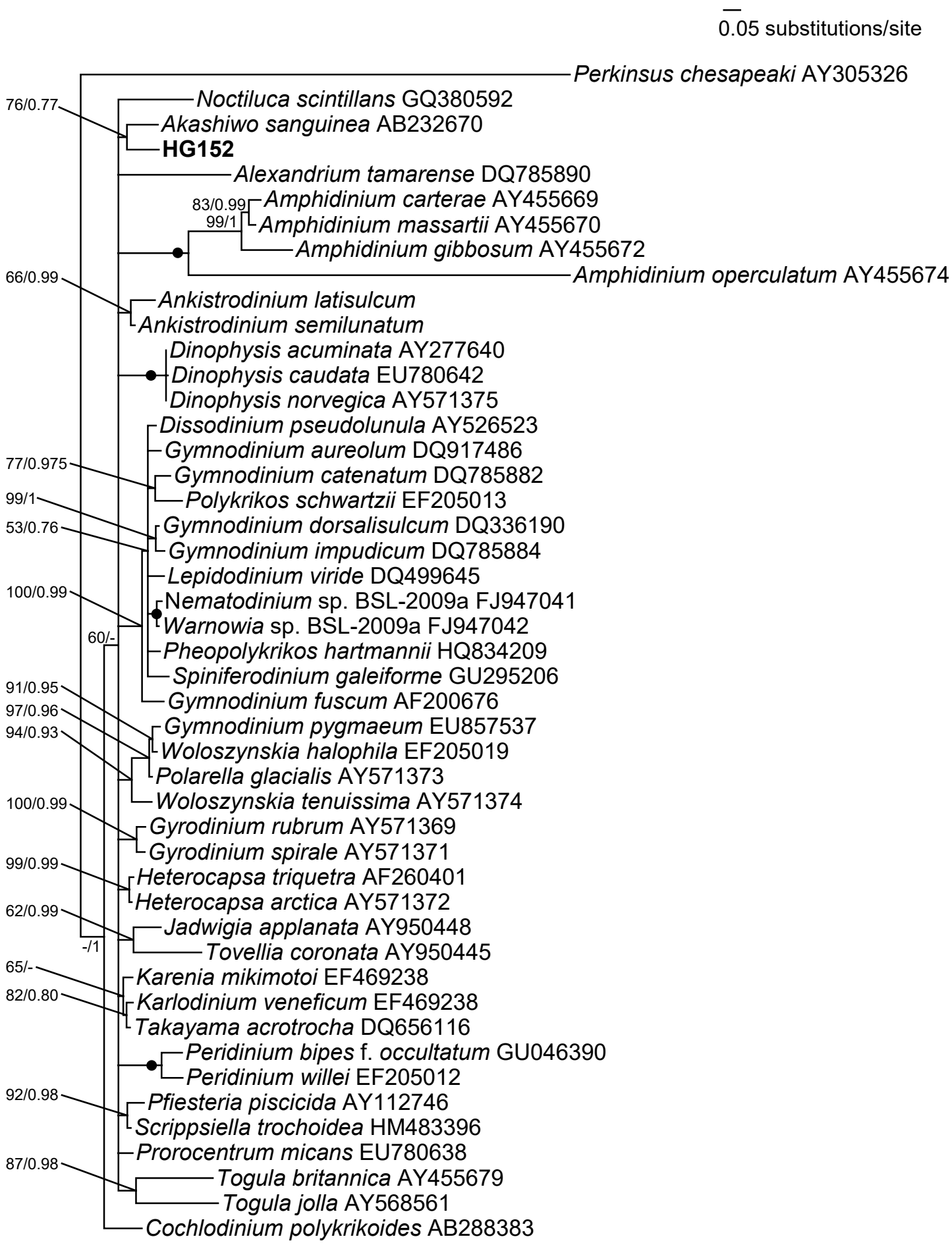


Fig. 75. Maximum likelihood (ML) phylogenetic tree inferred from partial large subunit (LSU) rDNA D1-D3 sequence alignment. Bootstrap support for ML analysis (100 pseudo-replicates) and Bayesian posterior probability (>50% and >0.8, respectively) are indicated. Nodes with a filled circle indicate a 100% bootstrap support for ML analysis and a Bayesian posterior probability of 1. Sequences obtained in this study are indicated in boldface; sequences from GenBank are followed by the accession numbers.

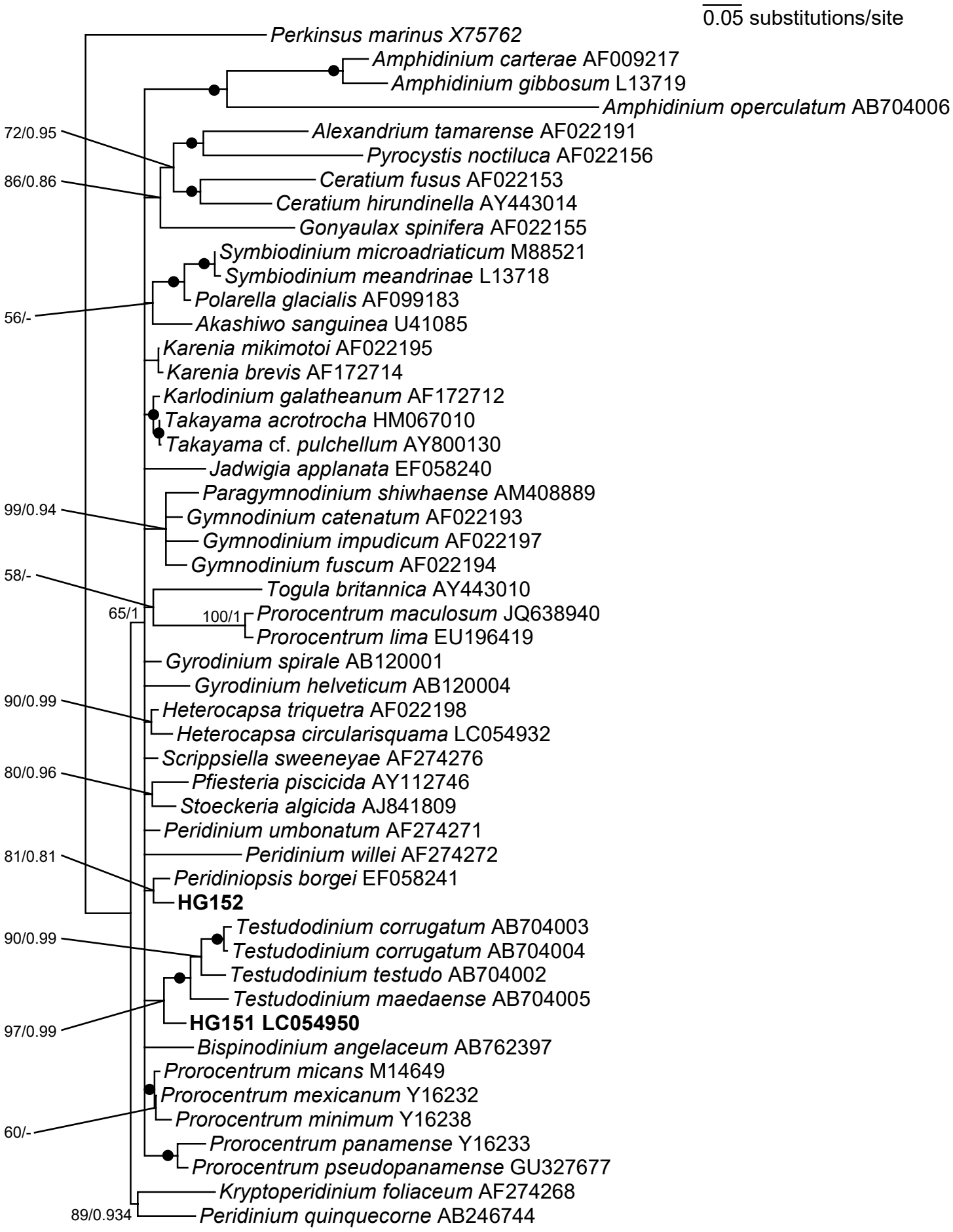


Fig. 76. Maximum likelihood (ML) phylogenetic tree inferred from partial SSU rDNA sequence alignment. Bootstrap support for ML analysis (100 pseudo-replicates) and Bayesian posterior probability (>50% and >0.8, respectively) are indicated. Nodes with a filled circle indicate a 100% bootstrap support for ML analysis and a Bayesian posterior probability of 1. Sequences obtained in this study are indicated in boldface; sequences from GenBank are followed by the accession numbers.

References

Abé, T.H. (1927). Report of the biological survey of Mutsu Bay. 3. Notes on the protozoan fauna of Mutsu Bay. I. Peridiniales. Sci. Rep. Tohoku Imp. Univ. *II*.

Adl, S.M., Simpson, A.G.B., Lane, C.E., Lukeš, J., Bass, D., Bowser, S.S., Brown, M.W., Burki, F., Dunthorn, M., Hampl, V., et al. (2012). The Revised Classification of Eukaryotes. J. Eukaryot. Microbiol. *59*, 429–514.

Al-Has, A., and Mohammad Noor, N. (2011). Identification of marine sand-dwelling dinoflagellates in Dinawan Island, Sabah. Borneo Sci. *28*, 37–45.

Aligizaki, K., Nikolaidis, G., Katikou, P., Baxevanis, A.D., and Abatzopoulos, T.J. (2009). Potentially toxic epiphytic *Prorocentrum* (Dinophyceae) species in Greek coastal waters. Harmful Algae *8*, 299–311.

Bagnis, R., Chanteau, S., Chungue, E., Hurtel, J.M., Yasumoto, T., and Inoue, A. (1980). Origins of ciguatera fish poisoning: a new dinoflagellate, *Gambierdiscus toxicus* Adachi and Fukuyo, definitively involved as a causal agent. Toxicon *18*, 199–208.

Baker, A.C. (2003). Flexibility and Specificity in Coral-Algal Symbiosis: Diversity, Ecology, and Biogeography of *Symbiodinium*. Annu. Rev. Ecol. Evol. Syst. *34*, 661–689.

Balech, E. (1956). Etude des dinoflagelles du sable de Roscoff. Rev Algol *2*, 29–52.

Calado, A.J., and Moestrup, Ø. (2002). Ultrastructural study of the type species of *Peridiniopsis, Peridiniopsis borgei* (Dinophyceae), with special reference to the peduncle and flagellar apparatus. Phycologia *41*, 567–584.

Calado, A.J., and Moestrup, Ø. (2005). On the freshwater dinoflagellates presently included in the genus *Amphidinium*, with a description of *Prosoaulax* gen. nov. Phycologia *44*, 112–119.

Carty, S. (2008). *Parvodinium* gen. nov. for the *Umbonatum* Group of *Peridinium* (Dinophyceae). Ohio J. Sci. Columb. *108*, 103–107.

Chomérat, N., and Couté, A. (2008). *Protoperidinium bolmonense* sp. nov. (Peridiniales, Dinophyceae), a small dinoflagellate from a brackish hypereutrophic lagoon (South of France). Phycologia *47*, 392–403.

Chomérat, N., Loir, M., and Nézan, E. (2009). *Sinophysis verruculosa* sp. nov. (Dinophysiales, Dinophyceae), a new sand-dwelling dinoflagellate from South Brittany, northwestern France. Bot. Mar. *52*, 69–79.

Chomérat, N., Zentz, F., Boulben, S., Bilien, G., van Wormhoudt, A., and Nézan, E. (2011). *Prorocentrum glenanicum* sp. nov. and *Prorocentrum pseudopanamense* sp. nov. (Prorocentrales, Dinophyceae), two new benthic dinoflagellate species from South Brittany (northwestern France). Phycologia *50*, 202–214.

Claparède, E., and Lachmann, J. (1859). Études sur les infusoires et les rhizopodes. Mém. Inst. Natl. Genev. *6*, 261–482.

Clark, R.B. (1968). Biological Causes and Effects of Paralytic Shellfish Poisoning. The Lancet *292*, 770–772.

Craveiro, S.C., Calado, A.J., Daugbjerg, N., and Moestrup, Ø. (2009). Ultrastructure and LSU rDNA-based revision of *Peridinium* Group Palatinum (Dinophyceae) with the description of *Palatinus* gen. nov. J. Phycol. *45*, 1175–1194.

Craveiro, S.C., Calado, A.J., Daugbjerg, N., Hansen, G., and Moestrup, Ø. (2011). Ultrastructure and LSU rDNA-based Phylogeny of *Peridinium lomnickii* and Description of *Chimonodinium* gen. nov. (Dinophyceae). Protist *162*, 590–615.

Dale, B., and Yentsch, C.M. (1978). Red Tide and Paralytic Shellfish Poisoning. ResearchGate *21*.

Darriba, D., Taboada, G.L., Doallo, R., and Posada, D. (2012). jModelTest 2: more models, new heuristics and parallel computing. Nat. Methods *9*, 772–772.

Daugbjerg, N., Hansen, G., Larsen, J., and Moestrup, Ø. (2000). Phylogeny of some of the major genera of dinoflagellates based on ultrastructure and partial LSU rDNA sequence data, including the erection of three new genera of unarmoured dinoflagellates. Phycologia *39*, 302–317.

David, H., Laza-Martínez, A., García-Etxebarria, K., Riobó, P., and Orive, E. (2014). Characterization of *Prorocentrum elegans* and *Prorocentrum levis* (Dinophyceae) from the southeastern Bay of Biscay by morphology and molecular phylogeny. J. Phycol. *50*, 718–726.

Dodge, J.D. (1971). Fine structure of the pyrrophyta. Bot. Rev. *37*, 481–508.

Dodge, J.D. (1972). The ultrastructure of the dinoflagellate pusule: A unique osmo-regulatory organelle. Protoplasma *75*, 285–302.

Dodge, J.D. (1984). The functional and phylogenetic significance of dinoflagellate eyespots. Biosystems *16*, 259–267.

Dodge, J.D., and Crawford, R.M. (1969). Observations on the Fine Structure of the Eyespot and Associated Organelles in the Dinoflagellate *Glenodinium foliaceum*. J. Cell Sci. *5*, 479–493.

Dodge, J.D., and Crawford, R.M. (1971). A fine-structural survey of dinoflagellate pyrenoids and food-reserves. Bot. J. Linn. Soc. *64*, 105–115.

Ehrenberg, C.G. (1830). Beiträge zur Kenntnis der Organisation der Infusorien und ihrer geographischen Verbreitung, besonders in Sibirien. Abh. K. Akad. Wiss. Zu Berl. 1–88.

Ehrenberg, C.G. (1834). Dritter Beitrag zur Erkenntnis großer Organisation in der Richtung des kleinsten Raumes. Phys. Abh. K. Akad. Wiss. Zu Berl. 145–336, pl.1–11.

Faust, M.A. (1993a). *Prorocentrum belizeanum*, *Prorocentrum elegans* and *Prorocentrum caribbaeum*, three new benthic species (Dinophyceae) from a mangrove island, Twin Cays, Belize. J. Phycol. *29*, 100–107.

Faust, M.A. (1993b). Three new benthic species of *Prorocentrum* (Dinophyceae) from Twin Cays, Belize: *P. maculosum* sp. nov., *P. foraminosum* sp. nov. and *P. formosum* sp. nov. Phycologia *32*, 410–418.

Faust, M.A. (1997). Three new species of *Prorocentrum* (Dinophyceae) from Belize: *P. norrisianum* sp. nov., *P. tropicalis* sp. nov., and *P. reticulatum* sp. nov. J. Phycol. *33*, 851–858.

Faust, M.A., Vandersea, M.W., Kibler, S.R., Tester, P.A., and Litaker, R.W. (2008). *Prorocentrum levis*, a New Benthic Species (Dinophyceae) from a Mangrove Island, Twin Cays, Belize. J. Phycol. *44*, 232–240.

Fensome, R.A., Taylor, F.J.R., Norris, G., Sarjeant, W.A.S., Wharton, D.I., and Williams, G.L. (1993). A classification of living and fossil dinoflagellates (Salem, Massachusetts: American Museum of Natural History).

Fløe Jørgensen, M., Murray, S., and Daugbjerg, N. (2004a). *Amphidinium* Revisited. I. Redefinition of *Amphidinium* (Dinophyceae) Based on Cladistic and Molecular Phylogenetic Analyses. J. Phycol. *40*, 351–365.

Fløe Jørgensen, M., Murray, S., and Daugbjerg, N. (2004b). A new genus of athecate interstitial dinoflagellates, *Togula* gen. nov., previously encompassed within *Amphidinium* sensu lato: Inferred

from light and electron microscopy and phylogenetic analyses of partial large subunit ribosomal DNA sequences. Phycol. Res. *52*, 284–299.

Gavelis, G.S., Hayakawa, S., White Iii, R.A., Gojobori, T., Suttle, C.A., Keeling, P.J., and Leander, B.S. (2015). Eye-like ocelloids are built from different endosymbiotically acquired components. Nature *523*, 204–207.

Gómez, F. (2008). *Dicroerisma* (Actiniscales, Dinophyceae) in the open Pacific Ocean, a gymnodinioid dinoflagellate with an endoskeleton. Chin. J. Oceanol. Limnol. *26*, 116–120.

Gómez, F. (2012). A checklist and classification of living dinoflagellates (Dinoflagellata, Alveolata). CICIMAR Oceánides *27*, 65–140.

Gómez, F., López-García, P., Takayama, H., and Moreira, D. (2015). *Balechina* and the new genus *Cucumeridinium* gen. nov. (Dinophyceae), unarmored dinoflagellates with thick cell coverings. J. Phycol. *51*, 1088–1105.

Guindon, S., and Gascuel, O. (2003). A simple, fast and accurate method to estimate large phylogenies by maximum-likelihood. Syst. Biol. *52*, 696–704.

Guiry, M.D., and Guiry, G.M. (2016). AlgaeBase. World-wide electronic publication, National University of Ireland, Galway.

Hallegraeff, G.M. (1993). A review of harmful algal blooms and their apparent global increase. Phycologia *32*, 79–99.

Hansen, G. (1993). Light and Electron Microscopical Observations of the Dinoflagellate *Actimscus pentasterias* (Dinophyceae). J. Phycol. *29*, 486–499.

Hansen, G., and Daugbjerg, N. (2009). *Symbiodinium natans* sp. nov.: A “free-Living” Dinoflagellate from Tenerife (northeast-Atlantic Ocean). J. Phycol. *45*, 251–263.

Hayakawa, S., Takaku, Y., Hwang, J.S., Horiguchi, T., Suga, H., Gehring, W., Ikeo, K., and Gojobori, T. (2015). Function and Evolutionary Origin of Unicellular Camera-Type Eye Structure. PLOS ONE *10*, e0118415.

Herdman, E.C. (1924). Notes on dinoflagellates and other organisms causing discolouration of the sand at Port Erin. IV. In Proceedings and Transactions of the Liverpool Biological Society, (Liverpool: C. Tinling & Co.), pp. 75–84.

Hoppenrath, M. (2002). Taxonomische und ökologische Untersuchungen von Flagellaten mariner Sande. Doctoral Thesis. University of Hamburg.

Hoppenrath, M. (2016). Dinoflagellate taxonomy — a review and proposal of a revised classification. Mar. Biodivers. 1–23.

Hoppenrath, M., and Saldarriaga, J.F. (2012). Dinoflagellates. Version 15 December 2012 (under construction).

Hoppenrath, M., Saldarriaga, J.F., Schweikert, M., Elbrächter, M., and Taylor, F.J.R. (2004). Description of *Thecadinium mucosum* sp. nov. (Dinophyceae), a New Sand-Dwelling Marine Dinoflagellate, and an Emended Description of *Thecadinium inclinatum* Balech. J. Phycol. *40*, 946–961.

Hoppenrath, M., Bachvaroff, T.R., Handy, S.M., Delwiche, C.F., and Leander, B.S. (2009). Molecular phylogeny of ocelloid-bearing dinoflagellates (Warnowiaceae) as inferred from SSU and LSU rDNA sequences. BMC Evol. Biol. *9*, 116.

Hoppenrath, M., Murray, S., Sparmann, S.F., and Leander, B.S. (2012). Morphology and Molecular Phylogeny of *Ankistrodinium* gen. nov. (Dinophyceae), a New Genus of Marine Sand-Dwelling Dinoflagellates Formerly Classified Within *Amphidinium*. J. Phycol. *48*, 1143–1152.

Hoppenrath, M., Chomérat, N., Horiguchi, T., Schweikert, M., Nagahama, Y., and Murray, S. (2013). Taxonomy and phylogeny of the benthic *Prorocentrum* species (Dinophyceae)—A proposal and review. Harmful Algae *27*, 1–28.

Hoppenrath, M., Murray, S.A., Chomérat, N., and Horiguchi, T. (2014). Marine benthic dinoflagellates – unveiling their worldwide biodiversity (Stuttgart: Schweizerbart'sche Verlagsbuchhandlung).

Horiguchi, T. (1995a). *Heterocapsa circularisquama* sp. nov. (Peridiniales, Dinophyceae): A new marine dinoflagellate causing mass mortality of bivalves in Japan. Phycol. Res. *43*, 129–136.

Horiguchi, T. (1995b). *Amphidiniella sedentaria* gen. et sp. nov. (Dinophyceae), a new sand-dwelling dinoflagellate from Japan. Phycol. Res. *43*, 93–99.

Horiguchi, T. (2015). Diversity and Phylogeny of Marine Parasitic Dinoflagellates. In Marine Protists, S. Ohtsuka, T. Suzaki, T. Horiguchi, N. Suzuki, and F. Not, eds. (Springer Japan), pp. 397–419.

Horiguchi, T., and Kubo, F. (1997). *Roscoffia minor* sp. nov. (Peridiniales, Dinophyceae): A new, sand-dwelling, armored dinoflagellate from Hokkaido, Japan. Phycol. Res. *45*, 65–69.

Horiguchi, T., and Pienaar, R.N. (1988). Ultrastructure of a New Sand-Dwelling Dinoflagellate, *Scrippsiella arenicola* sp. nov. J. Phycol. *24*, 426–438.

Horiguchi, T., and Pienaar, R.N. (1991). Ultrastructure of a Marine Dinoflagellate, *Peridinium quinquecorne* Abé (Peridiniales) from South Africa with Particular Reference to its Chrysophyte Endosymbiont. Bot. Mar. *34*, 123–132.

Horiguchi, T., and Pienaar, R.N. (1994a). Ultrastructure and ontogeny of a new type of eyespot in dinoflagellates. Protoplasma *179*, 142–150.

Horiguchi, T., and Pienaar, R.N. (1994b). Ultrastructure of a new marine sand-dwelling dinoflagellate, *Gymnodinium quadrilobatum* sp. nov. (Dinophyceae) with special reference to its endosymbiotic alga. Eur. J. Phycol. *29*, 237–245.

Horiguchi, T., and Sukigara, C. (2005). *Pyramidodinium* atrofuscum gen. et sp. nov. (Dinophyceae), a new marine sand-dwelling coccoid dinoflagellate from tropical waters. Phycol. Res. *53*, 247–254.

Horiguchi, T., and Takano, Y. (2006). Serial replacement of a diatom endosymbiont in the marine dinoflagellate *Peridinium quinquecorne* (Peridiniales, Dinophyceae). Phycol. Res. *54*, 193–200.

Horiguchi, T., Tamura, M., Katsumata, K., and Yamaguchi, A. (2012). *Testudodinium* gen. nov. (Dinophyceae), a new genus of sand-dwelling dinoflagellates formerly classified in the genus *Amphidinium*. Phycol. Res. *60*, 137–149.

Huelsenbeck, J.P., and Ronquist, F. (2001). MRBAYES: Bayesian inference of phylogenetic trees. Bioinformatics *17*, 754–755.

Iwataki, M. (2002). Taxonomic study on the genus *Heterocapsa* (Peridinales, Dinophyceae). Doctoral Thesis. The University of Tokyo.

Iwataki, M. (2008). Taxonomy and identification of the armored dinoflagellate genus *Heterocapsa* (Peridiniales, Dinophyceae). Plankton Benthos Res. *3*, 135–142.

Iwataki, M., Botes, L., Sawaguchi, T., Sekiguchi, K., and Fukuyo, Y. (2003). Cellular and body scale structure of *Heterocapsa ovata* sp. nov. and *Heterocapsa orientalis* sp. nov. (Peridiniales, Dinophyceae). Phycologia *42*, 629–637.

Iwataki, M., Hansen, G., Sawaguchi, T., Hiroishi, S., and Fukuyo, Y. (2004). Investigations of body scales in twelve *Heterocapsa* species (Peridiniales, Dinophyceae), including a new species *H. pseudotriquetra* sp. nov. Phycologia *43*, 394–403.

Janouškovec, J., Gavelis, G.S., Burki, F., Dinh, D., Bachvaroff, T.R., Gornik, S.G., Bright, K.J., Imanian, B., Strom, S.L., Delwiche, C.F., et al. (2017). Major transitions in dinoflagellate evolution unveiled by phylotranscriptomics. Proc. Natl. Acad. Sci. *114*, E171–E180.

Kearse, M., Moir, R., Wilson, A., Stones-Havas, S., Cheung, M., Sturrock, S., Buxton, S., Cooper, A., Markowitz, S., Duran, C., et al. (2012). Geneious Basic: An integrated and extendable desktop software platform for the organization and analysis of sequence data. Bioinformatics *28*, 1647–1649.

Kofoid, C.A., and Swezy, O. (1921). The free-living unarmored dinoflagellata (Berkeley, Calif.: University of California Press).

LaJeunesse, T.C., and Thornhill, D.J. (2011). Improved Resolution of Reef-Coral Endosymbiont (*Symbiodinium*) Species Diversity, Ecology, and Evolution through psbA Non-Coding Region Genotyping. PLOS ONE *6*, e29013.

Larsen, J., and Patterson, D.J. (1990). Some flagellates (Protista) from tropical marine sediments. J. Nat. Hist. *24*, 801–937.

Lebour, M.V. (1917). The Peridiniales of Plymouth Sound from the Region beyond the Breakwater. J. Mar. Biol. Assoc. U. K. *11*, 183–200.

Loeblich, A.R. (1968). A new marine dinoflagellate genus, *Cachonina*, in axenic culture from the Salton Sea, California with remarks on the genus *Peridinium*. Proc. Biol. Soc. Wash. *81*, 91–96.

Loeblich, A.R., and Loeblich, A.R. (1968). Index to the genera, subgenera, and sections of the Pyrrhophyta, [Part] 2. J. Paleontol. *42*, 210–213.

Morrill, L.C., and Loeblich, A.R. (1981). A survey for body scales in dinoflagellates and a revision of *Cachonina* and *Heterocapsa* (Pyrrhophyta). J. Plankton Res. *3*, 53–65.

Murray, S., and Patterson, D.J. (2002). The benthic dinoflagellate genus *Amphidinium* in south-eastern Australian waters, including three new species. Eur. J. Phycol. *37*, 279–298.

Murray, S., Flø Jørgensen, M., Daugbjerg, N., and Rhodes, L. (2004). *Amphidinium* Revisited. II. Resolving Species Boundaries in the Amphidinium operculatum Species Complex (Dinophyceae), Including the Descriptions of *Amphidinium trulla* sp. nov. and *Amphidinium gibbosum*. comb. nov. J. Phycol. *40*, 366–382.

Nagahama, Y., Murray, S., Tomaru, A., and Fukuyo, Y. (2011). Species Boundaries in the Toxic Dinoflagellate *Prorocentrum lima* (Dinophyceae, Prorocentrales), Based on Morphological and Phylogenetic Characters. J. Phycol. *47*, 178–189.

Nakayama, T., Watanabe, S., Mitsui, K., Uchida, H., and Inouye, I. (1996). The phylogenetic relationship between the Chlamydomonadales and Chlorococcales inferred from 18SrDNA sequence data. Phycol. Res. *44*, 47–55.

Nézan, E., and Chomérat, N. (2011). *Vulcanodinium rugosum* gen. et sp. nov. (Dinophyceae), un Nouveau Dinoflagellé Marin de la Côte Méditerranéenne Française. Cryptogam. Algol. *32*, 3–18.

Nylander, J.A.A., Ronquist, F., Huelsenbeck, J.P., and Nieves-Aldrey, J. (2004). Bayesian Phylogenetic Analysis of Combined Data. Syst. Biol. *53*, 47–67.

Penna, A., Battocchi, C., Capellacci, S., Fraga, S., Aligizaki, K., Lemée, R., and Vernesi, C. (2014). Mitochondrial, but not rDNA, genes fail to discriminate dinoflagellate species in the genus *Ostreopsis*. Harmful Algae *40*, 40–50.

Pinto, S.K., Terada, R., and Horiguchi, T. (2016). *Testudodinium magnum* sp. nov. (Dinophyceae), a novel marine sand-dwelling dinoflagellate from subtropical Japan. Phycologia *56*, 136–146.

Popovský, J., and Pfiester, L.A. (1990). Süßwasserflora von Mitteleuropa 6: Dinophyceae (Dinoflagellida) (Jena: Gustav Fischer Verlag).

Ronquist, F., and Huelsenbeck, J.P. (2003). MrBayes 3: Bayesian phylogenetic inference under mixed models. Bioinformatics *19*, 1572–1574.

Rouzé, H., Lecellier, G.J., Saulnier, D., Planes, S., Gueguen, Y., Wirshing, H.H., and Berteaux-Lecellier, V. (2017). An updated assessment of *Symbiodinium* spp. that associate with common scleractinian corals from Moorea (French Polynesia) reveals high diversity among background symbionts and a novel finding of clade B. PeerJ *5*, e2856.

Saburova, M., and Chomérat, N. (2016). An emended description and phylogeny of the little-known *Prorocentrum sipadanense* Mohammad-Noor, Daugbjerg & Moestrup (Prorocentrales, Dinophyceae) from the Indian Ocean, Oman. Eur. J. Phycol. *0*, 1–12.

Saunders, R.D., and Dodge, J.D. (1984). An SEM study and taxonomic revision of some armoured sand-dwelling marine dinoflagellates. Protistologica *20*, 271–283.

Schnepf, E., and Elbrächter, M. (1999). Dinophyte chloroplasts and phylogeny – A review. Grana *38*, 81–97.

Sparmann, S.F., Leander, B.S., and Hoppenrath, M. (2008). Comparative Morphology and Molecular Phylogeny of *Apicoporus* n. gen.: A New Genus of Marine Benthic Dinoflagellates Formerly Classified within *Amphidinium*. Protist *159*, 383–399.

Stamatakis, A., Hoover, P., Rougemont, J., and Renner, S. (2008). A Rapid Bootstrap Algorithm for the RAxML Web Servers. Syst. Biol. *57*, 758–771.

Steidinger, K.A., and Tangen, K. (1997). Chapter 3 – Dinoflagellates. In Identifying Marine Phytoplankton, C.R. Tomas, ed. (San Diego: Academic Press), pp. 387–584.

von Stein, F.R. (1883). Der Organismus der Arthrodelen Flagellaten nach eigenen forschungen in systematischere Reihenfolge bearbeitet (Leipzig: Wilhelm Engelmann).

Stiger, V., Horiguchi, T., Yoshida, T., Coleman, A.W., and Masuda, M. (2003). Phylogenetic relationships within the genus *Sargassum* (Fucales, Phaeophyceae), inferred from ITS-2 nrDNA, with an emphasis on the taxonomic subdivision of the genus. Phycol. Res. *51*, 1–10.

Swofford, D.L. (2001). PAUP*: Phylogenetic Analysis Using Parsimony (and other methods) 4.0.a152.

Takano, Y., and Horiguchi, T. (2004). Surface ultrastructure and molecular phylogenetics of four unarmored heterotrophic dinoflagellates, including the type species of the genus *Gyrodinium* (Dinophyceae). Phycol. Res. *52*, 107–116.

Takano, Y., and Horiguchi, T. (2005). Acquiring Scanning Electron Microscopical, Light Microscopical and Multiple Gene Sequence Data from a Single Dinoflagellate Cell. J. Phycol. *42*, 251–256.

Tamura, M., Iwataki, M., and Horiguchi, T. (2005). *Heterocapsa psammophila* sp. nov. (Peridiniales, Dinophyceae), a new sand-dwelling marine dinoflagellate. Phycol. Res. *53*, 303–311.

Taylor, F.J.R. (1985). The biology of dinoflagellates (London: Blackwell).

Taylor, F.J.R., Hoppenrath, M., and Saldarriaga, J.F. (2007). Dinoflagellate diversity and distribution. Biodivers. Conserv. *17*, 407–418.

Tester, P.A., Vandersea, M.W., Buckel, C.A., Kibler, S.R., Holland, W.C., Davenport, E.D., Clark, R.D., Edwards, K.F., Taylor, J.C., Pluym, J.L.V., et al. (2013). *Gambierdiscus* (Dinophyceae) species diversity in the Flower Garden Banks National Marine Sanctuary, Northern Gulf of Mexico, USA. Harmful Algae *29*, 1–9.

Trigueros, J.M. (2000). *Peridiniopsis salina* (Peridiniales, Dinophyceae), a new species of brackish dinoflagellate from Urdaibai estuary, North Spain. Phycologia *39*, 126–133.

Watanabe, K., Miyoshi, Y., Kubo, F., Onuma, R., Murray, S., and Horiguchi, T. (2014). *Ankistrodinium armigerum* sp. nov. (Dinophyceae), a new species of heterotrophic marine sand-dwelling dinoflagellate from Japan and Australia. Phycol. Res. *62*, 125–135.

Yamada, N., Terada, R., Tanaka, A., and Horiguchi, T. (2013). *Bispinodinium angelaceum* gen. et sp. nov. (Dinophyceae), a new sand-dwelling dinoflagellate from the seafloor off Mageshima Island, Japan. J. Phycol. *49*, 555–569.

Yentsch, C.M. (1984). Paralytic Shellfish Poisoning. In Seafood Toxins, (American Chemical Society), pp. 9–23.

Zhou, J., and Fritz, L. (1993). Ultrastructure of two toxic marine dinoflagellates, *Prorocentrum lima* and *Prorocentrum maculosum*. Phycologia *32*, 444–450.